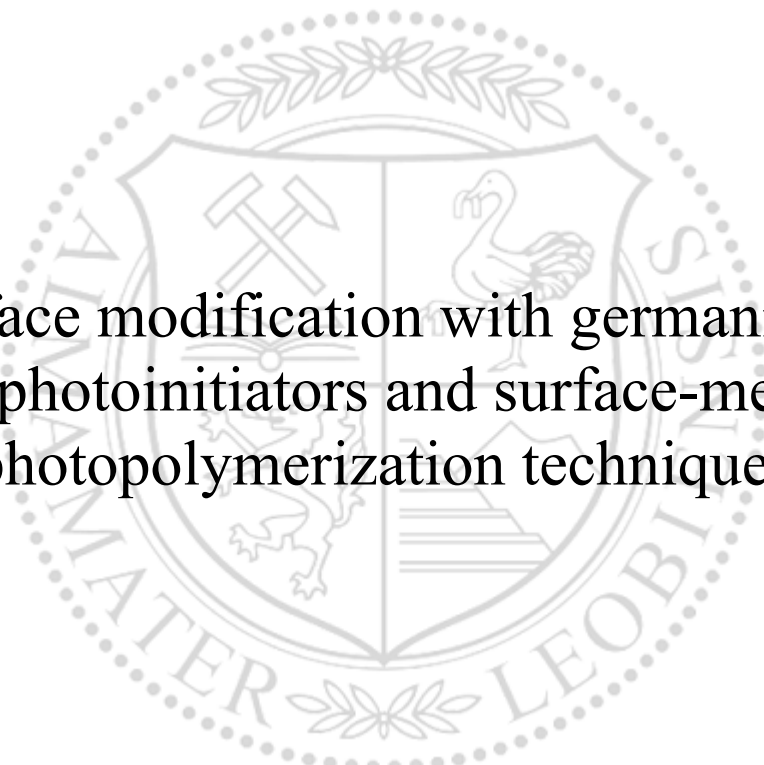




Chair of Chemistry of Polymeric Materials

Doctoral Thesis



Surface modification with germanium-  
based photoinitiators and surface-mediated  
photopolymerization techniques

Dipl.-Ing. Matthias Wolfgang Müller, BSc

July 2024



**AFFIDAVIT**

I declare on oath that I wrote this thesis independently, did not use any sources and aids other than those specified, have fully and truthfully reported the use of generative methods and models of artificial intelligence, and did not otherwise use any other unauthorized aids.

I declare that I have read, understood and complied with the "Good Scientific Practice" of the Montanuniversität Leoben.

Furthermore, I declare that the electronic and printed versions of the submitted thesis are identical in form and content.

Date 17.07.2024

A handwritten signature in black ink, appearing to read 'M. Müller', written over a horizontal line.

Signature Author  
Matthias Wolfgang Müller

## Danksagung

Zu Beginn meiner Dissertation dachte ich, dass drei Jahre für die Fertigstellung eine lange Zeit sei. Nun da ich am Ende dieses Abschnitts stehe frage ich mich, warum alles so schnell vorbei war. „Die Zeit verfliegt, wenn wir Spaß haben“ ist ein allseits bekanntes Motto, mit dem sich auch Forscher aus dem medizinischen Bereich beschäftigen. Die Hypothese lautet, dass Zeit, die schnell verstreicht, im Nachhinein als spannend und positiv empfunden wird. Wohingegen Zeit, die langsam verstreicht, als schleppend, lustlos und frustrierend angesehen wird. Ich kann ganz ehrlich sagen, dass ich fast immer viel Freude und Spaß an der Arbeit im Labor und an der Forschung hatte, auch wenn es zwischendurch Phasen gegeben hat, in denen sich die Chemie als Wissenschaft von ihrer gnadenlosen, grausamen und „funktioniert nicht“- Seite gezeigt hat. Daher möchte ich zu aller erst **Prof. Wolfgang Kern** danken, der mir nicht nur die Dissertation ermöglicht, sondern auch immer alle Freiheit gegeben hat. Keine Chemikalie war zu teuer, keine Idee wurde abgelehnt und jede Analysemethode wurde bewilligt. Vielen, vielen Dank! Natürlich darf man bei all dem auch **Dr. Christine Bandl** nicht vergessen, die mir gerade zu Beginn meiner Dissertation (und auch schon davor) strukturiertes Arbeiten, wissenschaftliche Herangehensweisen und nicht zuletzt wissenschaftliches Schreiben von Grund auf beigebracht hat. Auch hierfür ein herzliches Dankeschön!

Den Lehrstuhl für Chemie der Kunststoffe zu verlassen fällt mir sehr schwer, vor allem da ich bereits viele Kollegen ins Herz geschlossen habe und als meine Freunde bezeichnen kann. Obwohl die meisten Witze auf meine Kosten gingen, bin ich mir sicher, dass ich auch in Zukunft etwas zu lachen habe, wenn ich an meine Zeit mit Euch zurückdenke. Vielen Dank **Heike, Katja (Kitty), Michelle, Rocki** und **Theresa**. Außerdem möchte ich **Claudia Wieser** und **Mike Koinigg** für die organisatorische Hilfe in zahlreichen Anliegen und Problemstellungen danken.

Zu guter Letzt gilt mein größter Dank natürlich meiner Familie, **Markus, Mama, Lisa, Leopold, Johanna, Elisabeth, Lukas, Florian, Arthur, Elisa**, und **Großeltern**. Ich kann gar nicht aufzählen wofür ich Euch alles danken möchte, denn das würde die Länge dieser Dissertation wahrscheinlich verdoppeln. Ich möchte nur sagen ich bin so froh, dass ich euch alle habe!

## Cooperation

The results of this thesis were obtained not least through beneficial working relationships with the following scientific organisations.

- Technical university of Graz, institute of inorganic chemistry and institute of physical and theoretical chemistry, Stremayrgasse 9, 8010 Graz, AUT. **Michael Haas** and **Manfred Drusgala** both have contributed by synthesizing the employed germanium-based photoinitiators. **Georg Gescheidt** and **Max Schmallegger** performed several photo-bleaching experiments.



- University of Leoben, Chair in chemistry of polymeric materials, Otto-Glöckelstraße 2, 8700 Leoben AUT. Essential experimental work was performed by **Zizheng Zhang** as part of his PhD-Thesis. **Lisa Reisinger**, **Benjamin Holter**, **Amelie Krug**, **Bujon Zhao**, **Leonie Wenk**, **Benjamin Sydor**, **Yijin Wang**, **Yansen Tang** and **Leonie Wenk** all successfully completed their bachelor and diploma theses within this research, respectively. XPS measurements and data analysis were kindly performed by **Christine Bandl**.



## Abstract

Over the last decades, surface science has witnessed an ever more increasing interest in surface-modification and functionalization techniques across academic and industrial sectors. Especially the grafting-from approach, giving access to smart materials and surfaces, continues to drive innovation also in biomedical fields, in terms of drug release systems, tissue engineering, wound healing, diagnostics, protein binding and many more. This technique relies on the covalent attachment of an initiating species at a surface, which is then utilized to deliver reactive sides like radicals or ions, upon heat or light exposure. This is then followed by surface-initiated polymerization reactions, resulting in a fixed polymer brush system. Among those methods, especially light induced processes have received much attention due to the fast reaction rates, low cost as well as the spatial and temporal controllability. Hence, huge progress has been made so far in order to introduce type I and type II photoinitiators or other photo-sensitive molecules to different material surfaces.

In order to provide new perspectives in the field of grafting-from techniques, especially for usage in biomedical applications, a highly efficient, low-toxic and visible light sensitive class of photoinitiators, based on germanium (trisacylgermanes), were immobilized onto inorganic surfaces, including silicon wafers, optically polished quartz plates and spherically shaped silica nanoparticles. Those moieties were then exploited to initiate a radical chain-growth reaction from those surfaces via visible light illumination. By choice of functional monomers, polymer brushes with anti-adhesive, hydrophilic and fluorescent features were produced onto silicon wafers and quartz plates, also in spatially resolved and combined manners. The derived polymer monolayers were then investigated in respect to certain properties and brush-thicknesses using a set of characterization methods, including spectroscopic ellipsometry, XPS, UV-Vis, contact angle -and fluorescence measurements. Taking photo-initiator functionalized nanoparticles into account, hybrid organic-inorganic nanomaterials were synthesized, comprising a 6 to 12 nm thick polymeric shell around the SiO<sub>2</sub>-core. Moreover, the polymer content, the grafting-yield as well as the initiator and polymer grafting-density will be discussed in detail herein.

Another highlight in this thesis is the presentation of the first example of a so-called surface-initiated radical promoted cationic photopolymerization, which was achieved via the oxidation of photoinitiator formed radicals by iodonium salts. The derived germanium centred cation allowed then to remove the restriction to radically polymerizable monomers by expanding the selection with cationic polymerizable counterparts, like vinyl ethers and epoxides, hence opening up new perspective for grafting-from processes. For this method, the emphasis was placed on the overall prove of principle.

## Kurzfassung

In den vergangenen Jahrzehnten rückte die Wissenschaft der Oberflächenmodifizierung und Funktionalisierung immer mehr ins Interesse der akademischen und industriellen Forschungsbereiche. Insbesondere der sogenannte „grafting-from“ Ansatz, mit dessen Hilfe smarte Materialein und Oberflächen erzeugt werden können, ist auch in der Biomedizin eine vielversprechende und weit verbreitete Methode für zahlreiche Innovationen. Beispielhaft kommen Oberflächen-funktionalisierte Materialien und Substrate oftmals in Wirkstofffreisetzungssystemen, der Geweberegeneration, Wundheilung, Diagnostik, Proteinanbindung und in vielen anderen Gebieten, zum Einsatz. Die „grafting-from“- Technik beruht prinzipiell auf der kovalenten Koppelung eines Initiators an eine Oberfläche, der anschließend genutzt wird, um hoch reaktive Teilchen wie Radikale oder Ionen unter Einwirkung von Temperatur oder Licht zu erzeugen. Diese Teilchen initiieren Kettenwachstumsreaktionen für die Synthese polymerer Makromoleküle, welche somit an der Oberfläche in kovalent gebundener Form vorliegen („polymer-brushes“). In diesem Kontext sind vor allem lichtinduzierte Prozesse von großem Interesse aufgrund ihrer schnellen Reaktionsraten, niedrigen Kosten sowie ihrer räumlichen und zeitlichen Kontrollierbarkeit. Daher wurden bisher zahlreiche Fortschritte gemacht, um verschiedene Photoinitiatoren vom Typ I und Typ II an verschiedene Materialoberflächen anzubinden.

Um die Perspektiven im Bereich der "Grafting-From"-Techniken zu erweitern, insbesondere für den Einsatz in biomedizinischen Anwendungen, wurde ein hoch effizienter und physiologisch unbedenklicher Photoinitiator, basierend auf Germanium, an anorganischen Oberflächen einschließlich Siliziumwafer, optisch polierte Quarzplatten und sphärisch geformte SiO<sub>2</sub>-Nanopartikel angekoppelt. Die immobilisierten Verbindungen wurden anschließend genutzt, um radikalische Kettenwachstumsreaktionen von den Oberflächen durch sichtbares Licht anzuregen. Durch die Wahl funktionaler Monomere wurden Polymere bzw. „polymer-brushes“ mit anti-adhäsiven, hydrophilen und fluoreszierenden Eigenschaften auf Siliziumwafern und Quarzplatten erzeugt, sowie auch in räumlich aufgelösten und kombinierten Varianten hergestellt. Die Polymerschichten wurden hinsichtlich ihrer Eigenschaften und Schichtdicken unter Verwendung zahlreicher Charakterisierungsmethoden untersucht. Hierfür kamen spektroskopische Ellipsometrie, XPS, UV-Vis, Kontaktwinkel- und Fluoreszenzmessungen zum Einsatz. Im Hinblick auf Photoinitiator-funktionalisierte Nanopartikel wurden organisch-anorganische Nanomaterialien synthetisiert, deren SiO<sub>2</sub>-Kern mit einer 6 bis 12 nm dicken polymeren Schicht umhüllt vorlagen. Darüber hinaus werden der prozentuelle Polymergehalt, die „grafting-Ausbeute“ sowie die Initiator- und Polymermoleküldichte („grafting-density“) im Detail diskutiert.

Weiters wird in dieser Dissertation erstmalig eine oberflächeninitiierte kationische Polymerisation vorgestellt. Dies wurde durch die Oxidation von Photoinitiator-radikalen durch Iodoniumsalze erreicht. Das gebildete, Germanium-zentrierte Kation ermöglichte dann, die Bildung kationischer Polymerisate aus Vinylethern und Epoxiden, welche gekoppelt an der Oberfläche vorlagen. Bei dieser Methode lag der Schwerpunkt auf dem Beweis der Funktionalität.

# Table of Content

<b>1</b>	<b>General Introduction .....</b>	<b>1</b>
1.1	<i>Surface-modification techniques.....</i>	1
1.2	<i>Germanium-based photoinitiators.....</i>	4
1.3	<i>Motivation.....</i>	5
<b>2</b>	<b>Theoretical Part.....</b>	<b>6</b>
2.1	<i>Immobilization of light-sensitive molecules for surface-initiated photopolymerizations</i>	6
2.1.1	Type I and type II photoinitiators .....	6
2.1.2	Coupling of type I photoinitiators to surfaces.....	7
2.1.3	Coupled type II photoinitiators .....	15
2.1.4	Surface immobilization of synergists for benzophenone and thioxanthone .....	24
2.2	<i>Light mediated controlled polymerization from surfaces .....</i>	30
2.2.1	Surface-initiated photoiniferter-mediated polymerization (SI-PIMP) .....	30
2.2.2	Surface-initiated atom transfer radical polymerization (SI-ATRP) .....	36
2.2.3	Surface-initiated photoinduced electron/energy transfer reversible addition-fragmentation chain transfer polymerization (SI-PET-RAFT) .....	39
2.2.4	Coupled photoacids and photoacid generators .....	44
2.3	<i>Immobilization of light-sensitive molecules for coupling reactions.....</i>	47
2.3.1	Coupled azides.....	47
2.3.2	Surface-attached tetrazoles .....	53
2.3.3	Immobilized diazirines.....	54
2.4	<i>Summary .....</i>	55
<b>3</b>	<b>Experimental Part.....</b>	<b>56</b>
3.1	<i>Materials .....</i>	56
3.2	<i>Methods .....</i>	57
3.2.1	Surface functionalization of silica nanoparticles with bromo-tris(2,4,6-trimethylbenzoyl)germane (compound 1) .....	57



## Table of Content

---

3.2.2	Surface-initiated photopolymerization of 1H,1H,2H,2H-perfluorodecylacrylate (PFACr) and styrene from silica nanoparticles.....	57
3.2.3	Surface-initiated radical promoted cationic polymerization (SI-RPCP) of n-propyl vinyl ether (nPVE) and cyclohexane oxide (CHO).....	58
3.2.4	De-grafting of polystyrene with hydrofluoric acid .....	59
3.2.5	Calculation of the polymer content as well as initiator and polymer grafting density.....	60
3.2.6	Surface functionalization of silicon substrates and quartz plates with bromo-tris(2,4,6-trimethylbenzoyl)germane (compound 1).....	62
3.2.7	Surface-initiated photopolymerization of fluorescent monomers from 1-functionalized quartz plates .....	62
3.2.8	Surface-initiated photopolymerization of non-polar and polar monomers from 1-functionalized silicon wafers .....	63
3.2.9	Spatially resolved photopolymerization of 1H,1H,2H,2H-perfluorodecyl-acrylate and acrylamide from 1-modified silicon wafers .....	63
3.3	<i>Characterization methods</i> .....	65
3.3.1	FT-IR Spectroscopy .....	65
3.3.2	XPS Spectroscopy .....	65
3.3.3	UV-Vis Spectroscopy.....	65
3.3.4	Fluorescence Spectroscopy .....	66
3.3.5	Contact angle measurements.....	66
3.3.6	Spectroscopic ellipsometry .....	67
3.3.7	Thermogravimetric analysis (TGA) .....	67
3.3.8	Photo differential scanning calorimetry (photo-DSC) .....	67
3.4	<i>Scanning electron microscopy (SEM)</i> .....	69
3.5	<i>Size exclusion chromatography (SEC)</i> .....	69
3.6	<i>Time-of-flight secondary ion mass spectrometry (TOF-SIMS)</i> .....	69
<b>4</b>	<b>Results and Discussion</b> .....	<b>70</b>
4.1	<i>Surface-initiated radical photopolymerization, mediated by photoinitiator-functionalized silica nanoparticles</i> .....	70
4.1.1	Surface-functionalization of silica nanoparticles with light sensitive units .....	71

## Table of Content

---

4.1.2	Surface-initiated photopolymerization (SIPP) from silica nanoparticles and characterization of the polymeric shell .....	75
4.1.3	Visualization of polymer covered silica nanoparticles .....	87
4.1.4	Evaluation of the grafting yield and calculation of the grafting density .....	91
4.1.5	Conclusion on surface-initiated photopolymerization mediated by photoinitiator-functionalized silica nanoparticles .....	95
4.2	<i>Surface modification of silicon substrates and quartz plates with light sensitive moieties and subsequent grafting-from photopolymerization</i> .....	97
4.2.1	Immobilization of the photo-initiating species derived from compound 1 .....	98
4.2.2	Surface-initiated photopolymerization from 1-funtionalized silicon wafer and quartz plate surfaces .....	100
4.2.3	Spatially resolved surface-initiated photopolymerization .....	105
4.2.4	Conclusion with respect to grafting-from techniques using planar surfaces functionalized with initiator 1 .....	110
4.3	<i>Free radical promoted cationic photopolymerzation with acylgermanes</i> .....	111
4.3.1	Capability of acylgermanes for curing epoxide resins.....	111
4.3.2	Results on surface-initiated, free radical promoted cationic photopolymerization (SI-RPCP) .....	116
4.3.3	Investigation on the potential living character of SI-RPCP.....	126
4.3.4	Conclusion on surface-initiated radical-promoted cationic photopolymerization with functionalized nanoparticles .....	128
<b>5</b>	<b>Summary and Outlook</b> .....	<b>129</b>
<b>6</b>	<b>Bibliography</b> .....	<b>131</b>
<b>7</b>	<b>Abbreviations</b> .....	<b>151</b>
<b>8</b>	<b>List of Figures</b> .....	<b>155</b>
<b>9</b>	<b>List of Tables</b> .....	<b>160</b>

# 1 General Introduction

## *Disclaimer*

This chapter is reproduced for the most part from the original articles i) “Nanoparticles bearing germanium based photoinitiators at their surface: Preparation and use in grafting-from photopolymerization reactions”. DOI: <https://doi.org/10.1016/j.apsusc.2024.160035>; ii) “Surface-Initiated Polymerizations Mediated by Novel Germanium-Based Photoinitiators”. DOI: <https://doi.org/10.1021/acsami.3c05528>; iii) “Surface-Immobilized Photoinitiators for Light Induced Polymerization and Coupling Reactions” DOI: <https://doi.org/10.3390/polym14030608>.

All research articles are open-access, distributed under the terms and conditions of the Creative Commons Attribution (CC BY) license. I affirm, under penalty of perjury, that I retain the rights to reuse these publications in their entirety for this dissertation and hereby explicitly declare this intention.

## 1.1 Surface-modification techniques

In the last decades surface modification techniques have witnessed an ever more increasing interest in the academic field as well as in the industrial sector. In most cases, surface modification and functionalization aim to create a certain functionality, developing smart surfaces, which are able to interact with other media, materials and components or respond to external stimuli like light, temperature, electric/ magnetic fields, or pH value variations.<sup>1</sup> To give some examples, those functionalities include the control of adhesion,<sup>2</sup> wettability,<sup>3,4</sup> adsorption<sup>5</sup> and self-cleaning properties,<sup>6</sup> anti-corrosive<sup>7</sup> or anti-fouling<sup>8</sup> behaviour and many more. Considering this wide range of applications, great effort has also been made in the biomedical field. Among others, functionalized surfaces continue to drive innovation in nanodrug delivery systems, circulation times, loading capacity, enhanced accuracy of targeting infectious sites, enhance cellular penetration and implant design.<sup>9,10</sup>

Surface modification, being the major key to open up those possibilities, can be done in various ways, reaching from etching with highly reactive species, e.g., ozone or oxygen plasma, over silanization and vapor deposition methods up to (spatially resolved) polymer coatings for high end applications. Overviews of different surface modification techniques applicable for various materials and even enzymes, are given in the literature.<sup>11–14</sup> Among all these surface modification methods, (nanometre scale) coatings based on polymers are used in different applications and industries, as they provide a huge number of diverse functionalities for the underlying substrates.<sup>15</sup>

In general, surface modification with polymeric layers can be done by both physical and chemical modification, whereas physical modification suffers from severe limitations including low thermal stability, the inability to withstand high shear forces and the fact that the applied layers can be easily removed by appropriate solvents.<sup>11</sup> Chemical modification, on the other

hand, is more desirable because it leads to more stable systems due to covalent linkage. This technique is mainly carried out via “grafting-from” or “grafting-to” reactions. A schematic representation of both processes is depicted in Figure 1. The “grafting-to” approach, where preformed polymeric macromolecules are attached to the surface, is achieved by exploiting a chemical reaction between two functional groups, one of which is already tethered to the surface and the other one is part of the macromolecule. Furthermore, using surface-coupled photosensitive species, such as phenyl azides, light triggered (cyclo) addition or insertion reactions with other molecules can also be employed for the “grafting to” approach. The “grafting from” technique, which - in comparison to the “grafting to” counterpart - leads to more densely packed polymer brushes and layer thicknesses, directly initiates and therefore starts a polymerization from the surface. This is based on the formation of highly reactive species such as radicals or ions, derived from surface tethered initiators upon heat exposure or irradiation.<sup>11,16</sup> Therefore, an initiating species, which is covalently coupled to the surface is mandatory. In the past, much progress has been made to covalently couple (photo)-initiating species to different surfaces. An overview of these reactions, including numerous initiating species and coupling strategies, will be given in the theoretical part of this thesis.

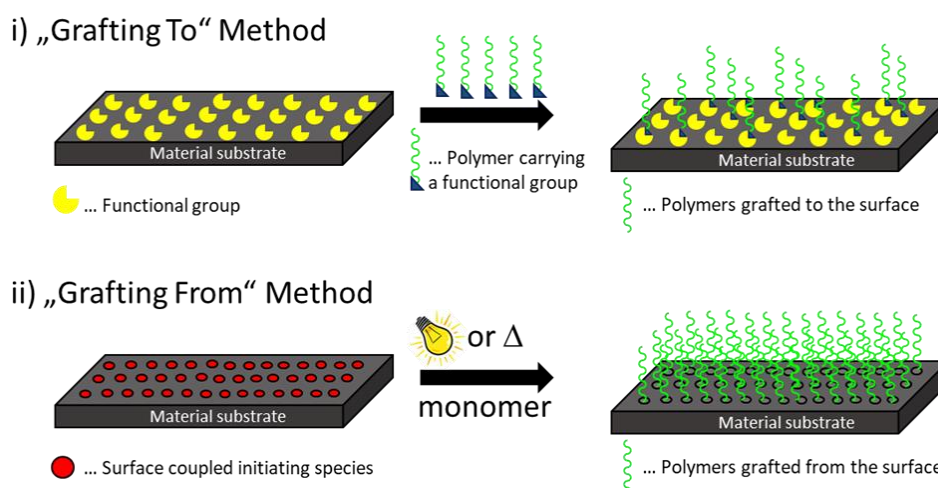


Figure 1: Schematic illustration of surface modification using “grafting-to” and “grafting-from” techniques.

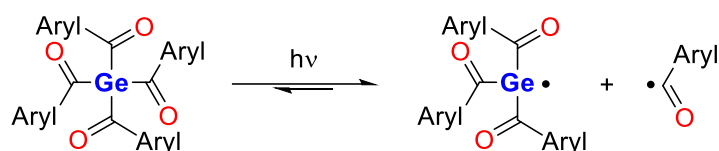
While the “grafting-to” method requires the usage of a preformed polymer, numerous surface-initiated polymerization reactions are available for the “grafting-from” method, including, for example, simple non-controlled radical polymerization, surface-initiated photoiniferter-mediated polymerization (SI-PIMP),<sup>17,18</sup> surface-initiated atom-transfer radical polymerization (SI-ATRP)<sup>19</sup> as well as surface-initiated photoinduced electron/energy transfer reversible addition-fragmentation chain transfer polymerization (SI-PET-RAFT).<sup>20–22</sup>

Among numerous polymerization techniques, especially light induced processes have received much interest in the last couple of years, because they exhibit pronounced

advantages compared to thermal initiation. The high reaction rate, low process cost and the energy-efficiency make light triggered polymerization processes also desirable for industrial applications. However, first and foremost, the possibility to spatially and temporally control the polymerization, simply by switching on and off the light, is the most outstanding feature of this method. <sup>11,16,23</sup>

## 1.2 Germanium-based photoinitiators

Germanium-based photoinitiators, or more precisely acylgermanes, are representatives of typical Type I photoinitiators, but with unique and exceptional characteristics. Looking at their history, the photolysis of aromatic germyl ketones was originally reported by Mochida et al.<sup>24</sup> in 1985. But to whatever reason, less attention was paid originally to these compounds. The picture then changed when Ganster et al. firstly presented two novel germanium-based photoinitiators in 2007, leaving the state-of-the-art photoinitiators of that time left behind in terms of quantum yield, photo-bleaching and visible light absorption.<sup>25</sup> Since then, Ge-based photoinitiators have emerged to act as promising and efficient platforms for numerous radical photopolymerization reactions. The radical generation pathway on the example of a tetra-acylgermane is shown in Scheme 1. Similar to other Type I photoinitiators those compounds cleave via a Norrish I pathway (cleavage of Ge-C(O) bond) resulting in highly reactive germanium centred radicals (germyl radicals), which readily add to monomeric double bonds, and therefore start a polymerization reaction.<sup>26–28</sup>



Scheme 1: Photolytic cleavage of acylgermanes following Norrish type 1 pathway.

As mentioned above, germanium based photoinitiators exhibit unique and outstanding features when compared to other widely used Type I photoinitiators. Many conventional photoinitiators exhibit either no or poor absorption of visible light, whereas acylgermanium derivatives are characterized by strong light absorption in this range extending well into the visible light spectrum, up to 500 nm.<sup>29</sup> Apart from that, these Ge-based photoinitiators are frequently described as minimal or even non-cytotoxic.<sup>30</sup> Especially these two characteristics render them particularly desirable for biomedical applications. This has led to an extensive use of Ge-based photoinitiators in dental composites.<sup>30–34</sup> Moreover, in 2008 Yagci et al. demonstrated that acylgermanes cannot only serve as free radical photoinitiators but also as scaffolds for free radical promoted cationic photopolymerization of vinyl ethers and epoxides. This mechanism relies on the oxidation of the generated germyl radicals by diphenyliodonium salts, thus forming germanium centred cations for initiation.<sup>35</sup> Especially this twofold functionality highlights again the distinctive position of acylgermanes among Type I photoinitiators. However, there are also some drawbacks encountered with the use of acylgermanes as photoinitiators. These compounds are expensive and of limited commercial availability. This makes them not favourable for high-throughput and large-scale applications

in industry. Hence, it can be expected that the use of acylgermanes will be first and foremost related to specific biomedical and cutting-edge applications.

### **1.3 Motivation**

Putting together the outstanding advantages of germanium based photoinitiators with the numerous applications of grafting-from processes, we herein aim to provide a fundamental pathway to immobilize a Ge-based initiating species to surfaces for subsequent surface-initiated photopolymerization reactions. In the first task, the goal was to investigate whether a trifunctional Ge-based photoinitiator, equipped with a halogen unit can be covalently tethered to hydroxyl rich surfaces. Secondly, the goal was to prove that those species can be taken into account to induce a radical grafting-from reaction of different monomers including (meth)acrylates and vinyl compounds from the respective surfaces. The last step of this project comprised a preliminary examination of a so-called surface-initiated radical promoted cationic photopolymerization, a very unique and highly novel method for the synthesis of surface-attached cationic polymer grafts. Overall, this work is first and foremost addressed to polymer chemists, who are interested in the synthesis covalently coupled polymeric nanolayers for surface-modification and functionalization issues.

## 2 Theoretical Part

The theoretical part of the thesis is meant to guide the reader through the start-of-the-art in respect to the covalent attachment of light-sensitive molecules onto different material substrates. Also, it will be shown how those species can be used for surface-modification and functionalization by means light induced grafting-from polymerization or photo-coupling and click reactions. Moreover, and although not directly photoactive, covalently coupled synergists for light induced atom transfer radical and reversible addition fragmentation chain transfer polymerizations (ATR, -RAFT polymerization) will be presented as well.

### ***Disclaimer***

This section entirely reproduces the original article “Surface-Immobilized Photoinitiators for Light Induced Polymerization and Coupling Reactions”.

DOI: <https://doi.org/10.3390/polym14030608>

This review article is an open-access literature article, distributed under the terms and conditions of the Creative Commons Attribution (CC BY) license. I affirm, under penalty of perjury, that I retain the rights to reuse this publication in it’s entirety for this dissertation and hereby explicitly declare this intention.

## **2.1 Immobilization of light-sensitive molecules for surface-initiated photopolymerizations**

### **2.1.1 Type I and type II photoinitiators**

In general, photoinduced polymerization proceeds via a chain growth mechanism, which is based on the interaction between an active centre and a monomer. Therefore, the active centre can be a radical, cation or anion, which is generated via an initiating step. In terms of photoinduced radical polymerization the initiation step involves a photoinitiator, generating free radicals upon UV irradiation. In respect to this, the photophysical and photochemical process of radical generation can be divided into two main mechanisms: (i) photo-scission (type I photoinitiators) and (ii) hydrogen abstraction that requires a co-initiator (type II photoinitiators).<sup>23</sup> According to Figure 2, exposing a type I photoinitiator to UV light leads to homolytic cleavage processes, once the molecule has reached an excited singlet and triplet state via intersystem crossing. This cleavage commonly occurs at bonds such as C-C bonds in  $\alpha$  position to carbonyl groups ( $\alpha$ -cleavage), and creates two radicals via the Norrish type I reaction.<sup>23,36</sup> In contrast to that, the radical generation with a type II system (e.g., benzophenone/tertiary amine) is more complex and includes three steps: (i) intermolecular exciplex formation once the photoinitiator reached excited triplet state, (ii) fast electron and (iii) slow proton transfer. Notably, type II systems are less efficient because of bimolecular



processes, back electron transfer and solvent cage effect in aqueous solutions.<sup>23,37,38</sup> In the following chapters, surface coupled type I and type II photoinitiators and corresponding co-initiators will be reviewed. Photopolymerization from coupled initiators provide—in most cases—photopolymers covalently bound to the surface. On the other hand, the immobilization of photoinitiators to the surface of (nano)particles can serve the purpose of preventing unwanted migration and leaching of photoinitiators.

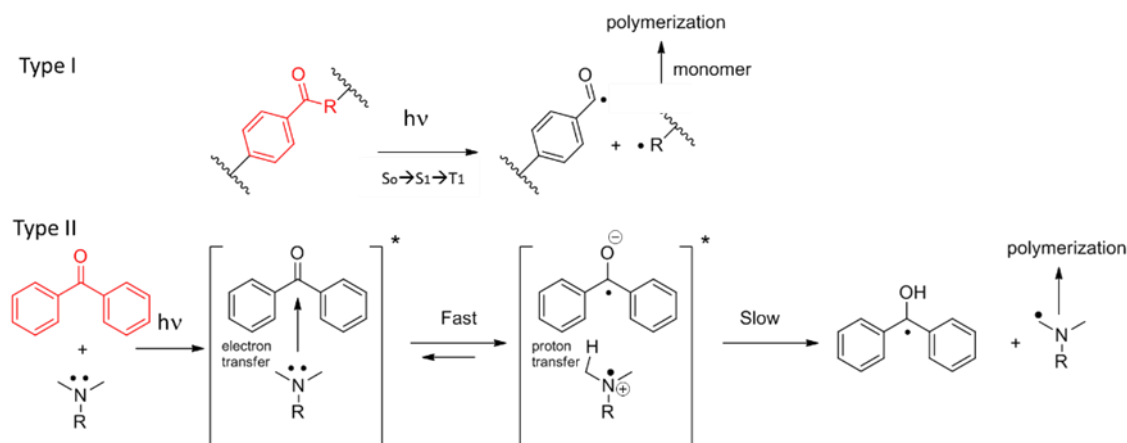


Figure 2: Radical generation of type I and II photoinitiators upon light irradiation.

### 2.1.2 Coupling of type I photoinitiators to surfaces

The earliest example of a surface coupled Norrish type I photoinitiator was given by Köhler and Ohngemach in 1990. They introduced triethoxysilyl and epoxy functionalities to a (2-hydroxy-2-propyl) phenone initiator originally bearing an allylic ether or a hydroxy group in para position, employing hydrosilylation with triethoxysilane and etherification with epichlorohydrin. They then used the silane derivative as a model for the “grafting from” approach and successfully photopolymerized undiluted monomers ((N-vinyl) pyrrolidone and 2-(dimethylaminoethyl) methacrylate (DMAEMA)) from silica surfaces. However, it was not possible to polymerize styrene, (2-hydroxyethyl) methacrylate (HEMA) and (2-hydroxyethyl) acrylate (HEA) under the applied conditions.<sup>39</sup> Twenty years later, Rühle and coworkers showed an example of assembling a monolayer of type I initiator on silica surfaces using two different approaches starting from commercially available 2-hydroxy-4-(2-hydroxyethoxy)-2-methylpropiophenone (Irgacure 2959, see Figure 3). One approach was to protect the hydroxy group before the introduction of the silyl anchor to the molecule by converting it into a methyl ester using several steps, while the second approach was without this protection. Gradient polymer brushes of poly (methyl methacrylate) (PMMA), poly (methacrylic acid) (PMAA) and poly(dimethylacrylamide) (PDMAA) were then generated on silicon substrates employing both photoinitiator systems.<sup>40</sup>

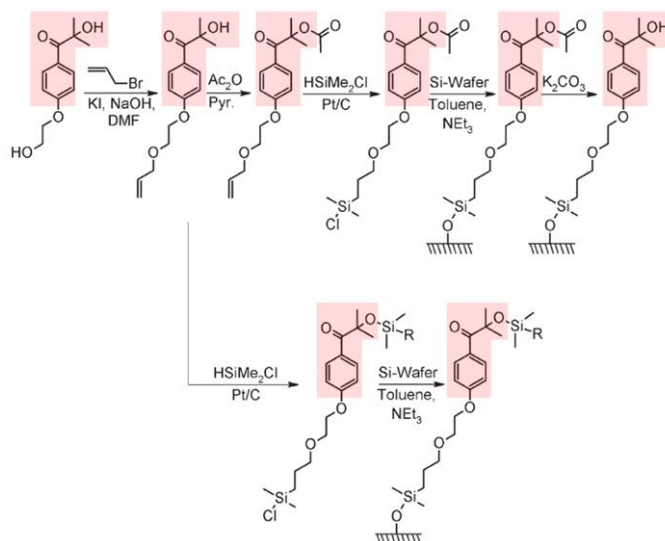


Figure 3: Two synthesis pathways to attach type I initiators onto silicon surfaces (slightly modified from reference [40]; the photosensitive moiety is labelled in red).

By using interference lithography (with a “Lloyd mirror”) the surface initiated photopolymerization yielded patterned structures. The optical arrangement (see Figure 4) included a parallel light beam, that was partly reflected from a mirror which was positioned vertically to the surface. This led to interference patterns with strong fluctuations of the light intensity irradiating the surface. Consequently, a periodical modulation of the thickness of the grafted polymer along the grating was achieved. The peak-to-valley distance was 155 nm (Figure 4 A), 700 nm (Figure 4 B) and 1500 nm (Figure 4 C), and the thickness of the photografted polymer was in the range from 8 to 45 nm.<sup>40</sup>

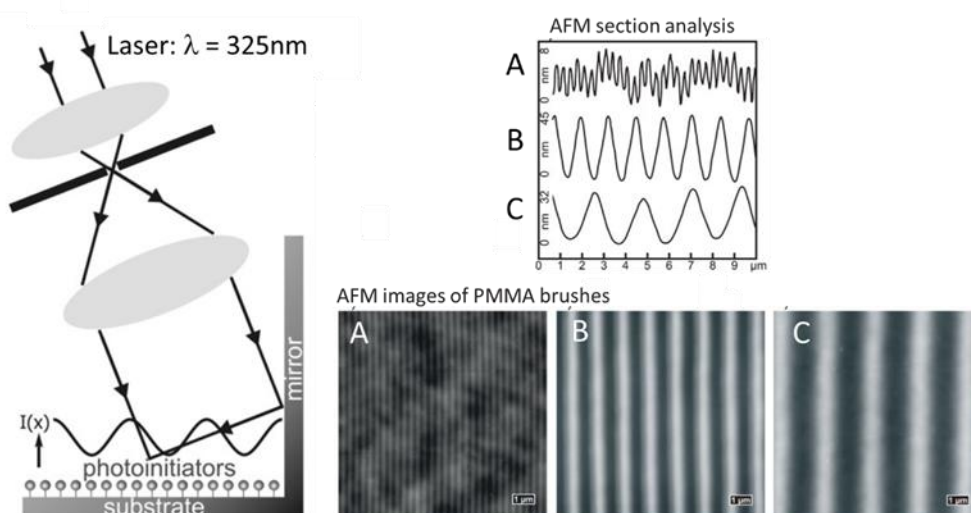


Figure 4: Setup for UV interference lithography and resulting polymer (PMMA) gratings (taken from reference [40]).

Patton and colleagues used the same synthesis pathway (with hydroxy group protection) to produce silicon surfaces functionalized with Irgacure 2959. They grew a polymer brush of previously synthesized trimethylsilane protected propargyl methacrylate which was further modified by well-known thiol-yne click chemistry after removing the trimethylsilane moiety by immersing it into a KOH solution.<sup>41</sup> Moreover, they extended these orthogonal click reactions with base catalyzed thiol-isocyanate, thiol-epoxy and thiol-bromo reactions preparing multifunctional polymer brushes.<sup>42</sup> More recently, Roszkowski et al., synthesized another compound bearing an Irgacure 2959 headgroup and a trialkoxysilyl unit (Figure 5 A), and studied its efficiency in curing acrylic and thiol-ene resin systems. When comparing the reactivity of the functionalized initiator to the parent initiator, it was proven that the initiator bearing the silane group was very reactive and even outperformed its parent initiator. Moreover, the same initiator coupled to silica nanopowder via well-known silanization reaction also turned out to be efficient in polymerizing acrylic monomers and thiol-ene resins.<sup>43</sup> Sahin et al. investigated the influence of the amount of photoreactive groups at the surface of silica nanoparticles on the efficiency in radical mediated thiol-ene photopolymerizations. The amount of photoreactive groups was varied by the reaction conditions of the silanization procedure. It was shown that the grafting method controls size, distribution and degree of modification of the photoreactive silica nanoparticles, and therefore has an impact on the reaction kinetics.<sup>44</sup>

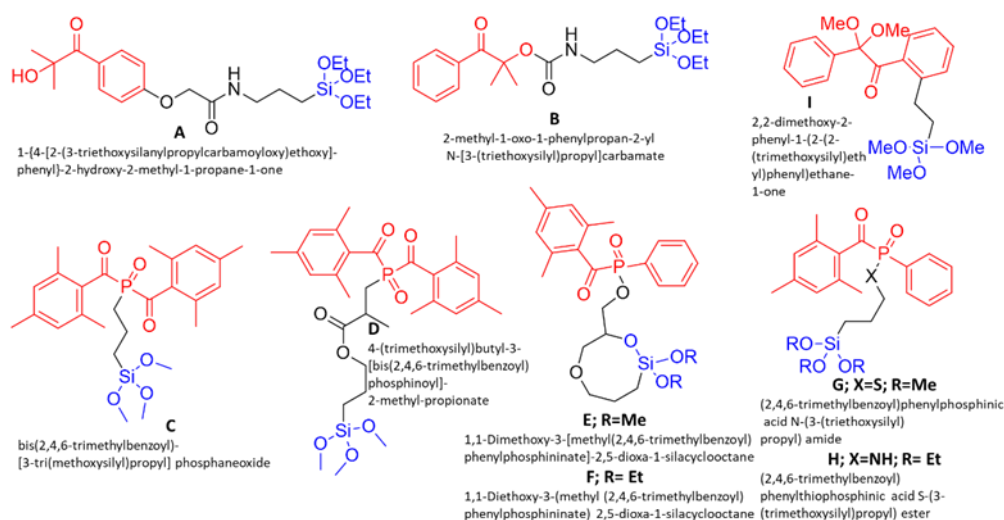


Figure 5: Type I photoinitiators (red) bearing a silane coupling unit (blue) for surface tethering.

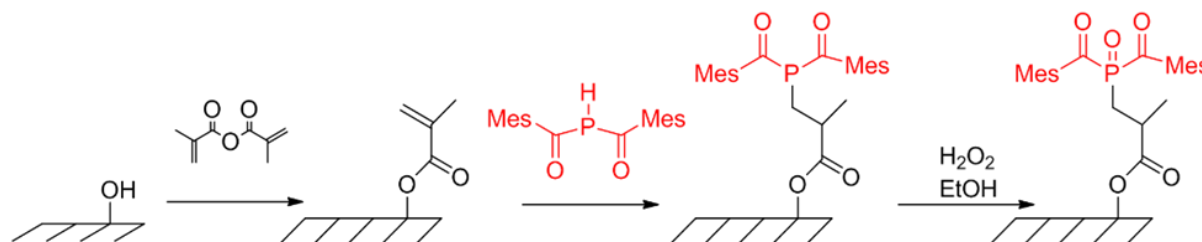
With respect to  $\alpha$ -hydroxyphenyl ketones such as Irgacure 2959, a hydroxypropyl radical and a benzoyl radical are formed after UV induced cleavage. The reactivity of the hydroxypropyl radical is significantly higher than that of the benzoyl radical. With regard to the so far presented photoinitiators, which were immobilized on inorganic surfaces, the less reactive radical remains immobilized on the surface. Thus, it is expected that the low molecular weight hydroxypropyl radical, which was released into the bulk, will mainly initiate photopolymerization.<sup>44</sup> To circumvent this, another photoinitiator with a trialkoxysilane anchor, was presented by Tan et al. in 2009. This compound was synthesized by the reaction of (3-isocyanatopropyl) triethoxysilane and 2-hydroxy-2-methyl-1-phenylpropane-1-one (Figure 5 B).<sup>45</sup>

Regarding bis(acyl)phosphane oxide (BAPO) modified surfaces, the higher reactive radical remained on the surface since the phosphinoyl radical was about 1000 times more reactive than the acyl one.<sup>46</sup> In addition, BAPO derivatives are frequently used because they are able to form more than one radical upon UV irradiation, have an extended absorption window ( $\lambda = 360\text{--}440\text{ nm}$ ) and show rapid photobleaching which enables deeper light penetration.<sup>47</sup> The first example of a BAPO based photoinitiator covalently coupled to surfaces was given by Huber et al. in 2012, who synthesized functionalized BAPO derivatives, including modification with a trimethoxy functionality (Figure 5 C), which was employed to react with hydroxy groups on the surface of a cellulose material. The authors reported a slightly yellowish colored substrate which was placed in an n-hexane solution of 1H,1H,2H,2H-perfluorodecylacrylate and irradiated for 60 min, leading to a hydro- and lipophobic coating.<sup>46</sup> Staying with alkoxy silane functionalized BAPO, Sangermano et al. published a straight forward synthesis for 4-(trimethoxysilyl)butyl-3-[bis(2,4,6-trimethylbenzoyl)phosphinoyl]-2-methyl-propionate (Figure 5 D) and successfully immobilized it on glass surfaces. Utilizing surface initiated photopolymerization they polymerized a fluorinated acrylate (1H,1H,2H,2H-perfluorooctyl acrylate) or a specifically synthesized polysiloxane to generate hydrophobic surfaces.<sup>16</sup> This

compound was also used to grow photo-active polymer brushes bearing o-nitrobenzyl ester chromophores onto silica microparticles. Upon UV radiation, carboxylic groups were generated, which were then used to immobilize a fluorescent Alexa-546 protein.<sup>48</sup> The same compound was also used for the preparation of Janus II or IV hairy polymer coronas made of hydrophilic polyethylene(glycol) methacrylic ester and a hydrophobic methacrylic monomer (bearing an alkyl side chain) onto silica particles.<sup>49</sup> Recently, Roszkowski et al., synthesized short- and long-wavelength absorbing photoinitiators bearing trialkoxysilyl moieties, including four different BAPO-type compounds (Figure 5 E–H), starting from commercially available materials. In respect to their photoreactivity, some of these initiators were compared to their parent compounds and showed comparable or even improved reactivity. However, when modifying silica nanopowder via typical silanization, it turned out that the nanopowder is a mediocre carrier for coupled photoinitiators. This is because of the low silanol content on the surface, the aggregated structure and the broad particle size distribution. Nevertheless, it was proven that photoactive nanoparticles were capable of polymerizing acrylic monomers (e.g., tetrahydrofurfuryl acrylate) and thiol-ene resins.<sup>43</sup> As an approach towards low extractable photoinitiators, Sahin<sup>47</sup> investigated silica nanoparticles bearing BAPO initiators (Figure 5 D) at their surface with respect to the initiation of thiol-ene photopolymerization. Migration of the filler bound photoinitiators was examined by extraction of thiol-ene photopolymers. An elemental analysis of the extracts (phosphorus content) showed that the content of extractable photoinitiator is below detection limit when the BAPO initiator is coupled onto particle surfaces.

Another example of a type I photoinitiator, which was attached to silica nanoparticles via silanization, was given by Moehrke et al. The silane functionalized initiator (Figure 5 I) was synthesized starting from the commercially available photoinitiator 2,2-dimethoxy-2-phenylacetophenon and was used to graft n-butyl methacrylate from silica surfaces to investigate the suitability of the SP-PLP-ESR (single-pulse–pulsed-laser polymerization–electron spin resonance) technique for examination of the termination kinetics of surface-tethered macroradicals. Photolysis of this grafted initiator generated a benzoyl-type radical covalently coupled to the surface and a free dimethoxybenzyl radical. The second one is not supposed to initiate polymerization and can be further cleaved into methyl benzoate and a methyl radical which is postulated to act as a terminating species due to its high reactivity and diffusivity.<sup>50</sup> An example of a macromolecular photoinitiator, which includes a benzoin (type I photoinitiator) and an anhydride moiety was given by Ohar et al. This molecule is a surface modifier for filler materials, such as TiO<sub>2</sub> and hydroxyapatite. Compared to the parent benzoin photoinitiator, the modified photoactive fillers showed a higher efficiency in curing resins and enhanced the surface hardness of the cured samples.<sup>51</sup> Besides coupling with organosilane chemistry, Wang et al. synthesized BAPO derivatives which are capable of covalently attaching to the surface of cellulose nanocrystals (CNC). In the first step, the cellulose, bearing hydroxyl groups at the surface, was treated with methacrylic anhydride yielding surface attached methacryloyl groups. These activated surface-coupled olefins readily reacted with bis(mesityl)phosphane in a phospho-Michael addition in the

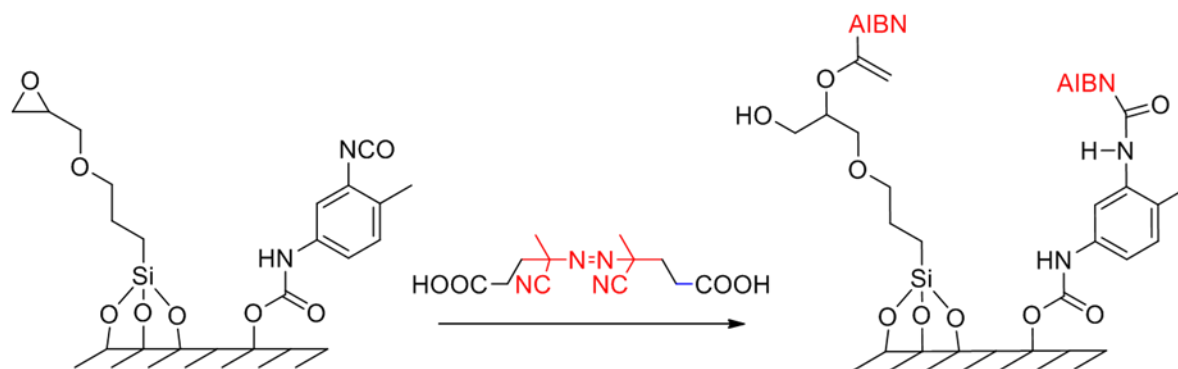
presence of catalytic amount of triethylamine. By oxidation with aqueous hydrogen peroxide the CNC-BAPO was generated (see Scheme 2), and confirmed by elemental analysis of the yellow powder. The photoactive substrate was then used to photopolymerize MMA, butyl acrylate, N-isopropylacrylamide (NIPAM) and HEA from the surface of the CNC.<sup>52</sup>



Scheme 2: Synthetic route to attach BAPO moieties (red) onto cellulose surfaces.

Another group of initiators for radical polymerization is based on azo initiator compounds, which can generally be activated by heat or UV radiation. The most frequently used azo initiators are 2,2-azobis(2-methylpropionitrile) (AIBN) and its derivatives, which are often used for surface modification via light induced grafting-from processes. However, these initiators cause long curing rates due to low absorbance and long decomposition half-life. Furthermore, AIBN initiators produce two radicals by splitting off molecular nitrogen. One of the two radicals remains tethered to the surface, and the other radical diffuses into the adjacent solution starting a (unwanted) homopolymerization in the bulk.<sup>23</sup>

One early example of an AIBN-type initiator, which was covalently coupled to surfaces, was given by Tsubokawa et al., who polymerized vinyl monomers (MMA, styrene (St), N-vinylcarbazole) from ultrafine inorganic particles such as silica, titanium oxide and ferrite. The attachment of azo groups onto the particle surface was achieved by the reaction of epoxy groups (introduced by silanization with 3-glycidoxypropyltrimethoxysilane) with commercially available 4,4'-azobis(4-cyanopentanoic acid) (ACPA, see Scheme 3).<sup>53</sup> Four years later, Tsubokawa et al. investigated the photopolymerization of azo-modified silica and titanium dioxide particles. Here, the azo groups were introduced to the surface via the reaction of ACPA with surface tethered isocyanate groups, which were generated in a previous step by the reaction between surface hydroxyl groups and toluene 2,4-diisocyanate (see Scheme 3). Compared to previous studies, the authors reported higher grafting efficiency of the photopolymerization compared to thermally induced polymerizations.<sup>54</sup>



Scheme 3: Introduction of AIBN moieties (red) onto pre-modified surfaces.

In several publications, Prucker and Rhe developed multiple step syntheses for azo-compounds with a chlorosilane head group (Figure 6 A–D). Moreover, these compounds contained a cleavable ester group in order to evaluate molar masses and molar mass distributions of the macromolecules (polystyrene PSt, PMMA) obtained after the polymerization from silica surfaces. Here, typical methods of polymer analysis, such as gel permeation chromatography and light scattering, were employed.<sup>55–58</sup> As mentioned above, AIBN-type initiators typically show rather low extinction coefficients for their  $n-\pi^*$  transition around 350 nm. To address this, the authors synthesized another azo compound, which can be immobilized on silicon oxide surfaces, the structure of which is also shown in Figure 6 E.<sup>59</sup> They also utilized a combination of photolithographic techniques with this “grafting from” photopolymerization method. By employing immobilized azo initiators, patterned layers of covalently attached PMMA, poly(hydroxyethyl methacrylate) (PHEMA),<sup>60</sup> PSt as well as PSt-fluorescence dye labelled methacrylate copolymer were created on silica surfaces.<sup>59</sup>

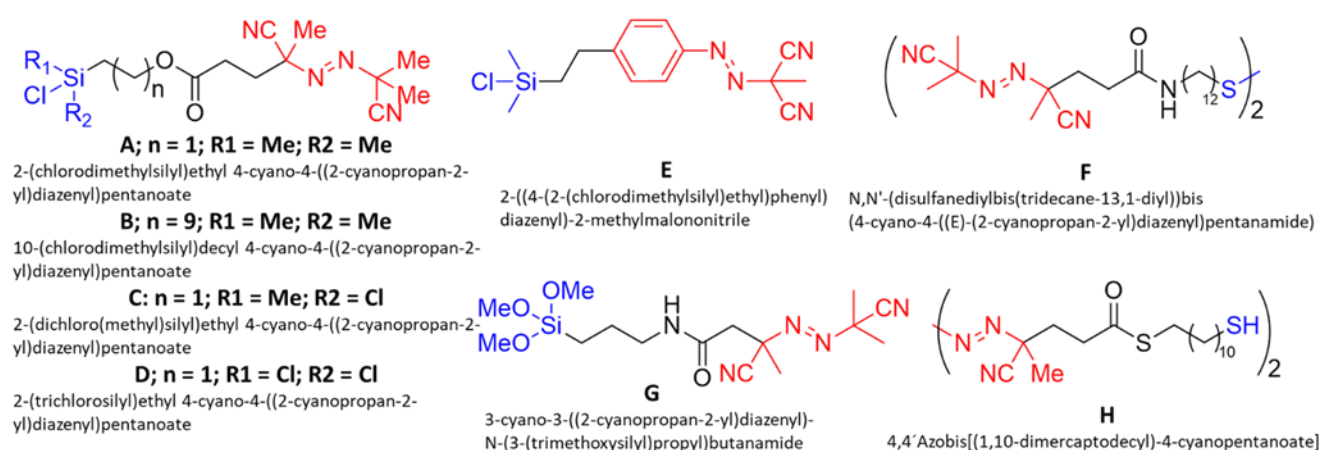
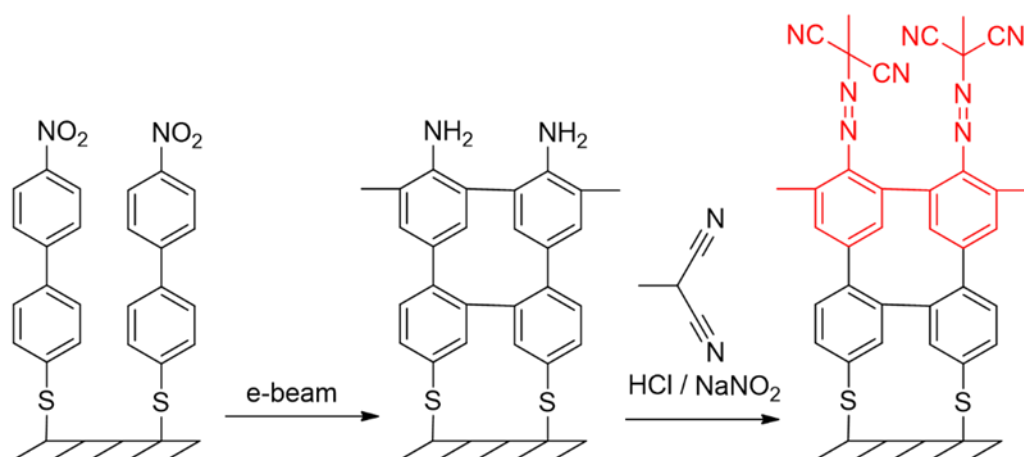


Figure 6: Photosensitive azo-compounds (red) with anchor moieties (blue).

To modify gold surfaces, the same authors synthesized an azo-based initiator with a disulfide moiety, bearing a long alkyl group (spacer) to avoid unwanted interactions with the radicals generated by the initiator and the sulfur moiety which is used for coupling to the gold surface (Figure 6 F).<sup>59</sup> To circumvent free radical accelerated desorption of thiols from gold surfaces, which can hinder polymerization due to chain transfer reactions, Huang et al. utilized a crosslinked adhesion layer for initiator attachment based on mercapto-propyltrimethoxysilane. In a subsequent step they introduced azo-moieties to the surface by using a synthesized trimethoxysilane substituted azo compound (Figure 6 G).<sup>61</sup> Apart from these contributions, Dyer and colleagues firstly synthesized an azo initiator bearing a thiol group (Figure 6 H) which was utilized for the photopolymerization of St, and mixed PMMA/PSt polymer brushes from gold surfaces. Moreover, they investigated the effect of monomer concentration and reaction on the layer thickness.<sup>62-64</sup> In a cooperation with Zauscher and colleagues, they presented a strategy to fabricate nano- and micropatterned polymer brush arrays made of pH- and salt-sensitive polyelectrolyte copolymers (e.g., poly(N-isopropylacrylamide-co-methacrylic acid)) using the same thiol based azo initiator.<sup>65</sup> Schmelmer et al. showed another interesting approach to couple azo groups to surfaces. In their work they used e-beam radiation to convert a self-assembled monolayer of 4'-nitro-1,1'-biphenyl-4-thiol on gold into a crosslinked 4'-amino-1,1'-biphenyl-4-thiol layer. The amino groups in terminal position were then diazotized and treated with methylmalonodinitrile to give a surface-bound monolayer of the 4'-azomethylmalonodinitrile-1,1'-biphenyl-4-thiol (see Scheme 4). Irradiation with UV light generated a highly reactive phenyl radical, which remained coupled to the surface, and a relatively stable free methylmalonodinitrile radical, which is not capable of initiating radical polymerization because of its resonance stabilization. With this approach nanopatterned polymer brushes with sub-50nm resolution and a brush height of approximately 10 nm were created.<sup>66</sup>



Scheme 4: Introduction of azo moieties (red) from coupled nitrobiphenyl units using e-beam radiation.

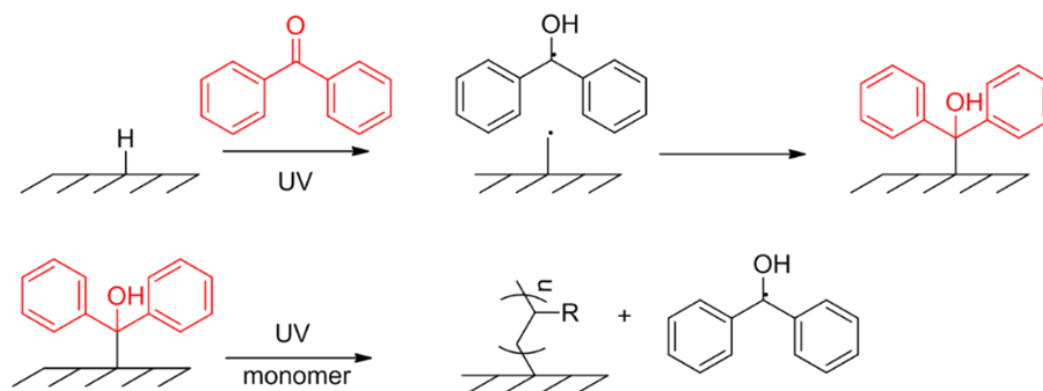


### 2.1.3 Coupled type II photoinitiators

In contrast to the type I photoinitiators, type II initiators do not spontaneously generate radicals upon excitation with UV light, but readily abstract hydrogen from a co-initiator or the environment. The co-initiator may also function as an electron donor with subsequent hydrogen abstraction. Benzophenone (BP) is certainly the most popular representative of a type II photoinitiator, due to its characteristics and low cost. Other important examples of this initiator class are anthraquinone, thioxanthone (TX) and camphorquinone.<sup>36</sup> This chapter is dedicated to type II initiators which are covalently coupled to surfaces of different materials, starting with BP.

#### Coupled Benzophenone (BP)

The earliest example for coupled BP initiators was given by Yang and Ranby in 1996 who suggested a living nature of the photopolymerization based on BP chemistry. A solution of BP and methacrylic acid (MAA) was placed between two low-density-polyethylene (LDPE) films using a micro syringe. As a consequence of irradiation for 1 min, BP abstracted hydrogen from the LDPE surface, generating reactive carbon centered radicals which initiated polymerization of MAA. In their earlier studies they found that termination reactions are mainly carried out by combination of the growing chain and the semipinacol radical. The same procedure was done with different monomers (St, MMA) leading to different end-capped polymers. Upon a second UV irradiation it was found that all these end groups, except for the one consisting of acrylic acid (AA) and benzophenone, could be reinitiated for polymerization of methacrylic acid.<sup>67</sup> A disadvantage of this method is the significant formation of homopolymers in the solution since BP also abstracts hydrogen from monomers (and solvent molecules). To circumvent this, Ma et al. suggested a two-step method (Scheme 5), in which the substrate was, firstly, immersed in a saturated solution of benzophenone, then washed and dried and subsequently irradiated with UV light. It was supposed that BP abstracts hydrogen from the substrate which then immediately recombines with the semipinacol radical in the absence of monomers in solution. In the second step the monomer solution was directly cast onto the substrate and exposed to UV light, reinitiating and starting the polymerization. With this sequential method, the authors grew PMAA and poly (ethylene glycol) mono methacrylate onto hydrophobic porous polypropylene (PP) membranes and reported a four times larger amount of grafted polymer in comparison to the method of Yang and Ranby.<sup>68</sup> Later they extended this method for application on different substrates (cellulose acetate, poly (vinylidene fluoride)). Furthermore, and for the first time, they provided direct evidence for the covalent coupling of the grafted polymer using GPC. For this, they dissolved low molecular weight PSt and BP in benzene and exposed a thin film of this solution to UV light, resulting into BP that is coupled to PSt. After washing with ethanol to remove unreacted BP, methacrylic monomers were photopolymerized onto BP-modified PSt macromolecules in solution. A comparative GPC study between modified and virgin PS, revealed a higher molar mass of the modified PSt and therefore evidenced covalent coupling.<sup>69</sup>



Scheme 5: Sequential method for photografting polymers using benzophenone (BP) as surface coupled photoinitiator (red). BP coupling comprises two steps: (i) UV triggered hydrogen abstraction with subsequent recombination, and (ii) reinitiation by UV light in the presence of monomers leading to grafted polymer chains.

Several groups then used this two-step “photo-grafting” method with surfaces which provide hydrogen for abstraction (for example polyethylene terephthalate, polylactic acid, etc.).<sup>70–74</sup> Castell et al. used BP and numerous BP derivatives to modify surface properties, more specifically the wettability and adhesion, of chemically inert PP films without subsequent polymerizations and performed a series of experiments to evaluate impact factors on the grafting reaction. Depending on the structure of the utilized BP derivative, the author reported an increase of the surface energy from 26 (pure PP) up to 36 mN/m and pointed out that oxygen might inhibit the photografting reaction. In a subsequent work, surface wettability and adhesion were further improved by photografting MAA, pentaerythritol triacrylate, and 2-hydroxyethyl acrylate from BP derivatized PP surfaces.<sup>75,76</sup> The two-step method, proposed by Ma et al., was also used for another type II initiator, namely, 1-hydroxycyclohexyl phenyl ketone, to increase the wettability of the negative tone photoresist SU-8, through photopolymerization of tetraethyleneglycol dimethacrylate and HEMA.<sup>77</sup>

As already described, the above-mentioned method is limited to surfaces, which provide hydrogen for abstraction in the course of the photo-grafting process. In contrast, the following section deals with non-hydrogen containing surfaces, which are modified with BP utilizing different coupling chemistries. Starting with well-known silanization, Prucker et al. developed a simple and high yield synthesis of a BP derivative bearing a silyl anchor to typically attach to oxidized surfaces such as silica (Figure 7 A). Performing a “grafting to” approach, they successfully grafted PSt and poly(ethyloxazoline) (PEOX) onto SiO<sub>2</sub> surfaces by illumination of the polymer layer which had been spincoated onto the surface modified with BP.<sup>78</sup> Based on this fundamental work, Kado et al. showed an impressive photolithographic patterning method using a combination of a photo-cross-linkable polymer bearing an acrylic functionality, which was sequentially deposited by the Langmuir–Blodgett method onto photoreactive BP-silica surfaces. The self-crosslinking and the photo-grafting upon UV radiation led to patterned multilayer polymer nanosheets which displayed interference coloring corresponding to

different film thicknesses.<sup>79</sup> One further example of an application was recently given by Braun et al., who functionalized indium tin oxide coated glass substrates with the same silane bearing BP derivative to assemble liquid crystal test cells. The test cells were filled with reactive mixtures of acrylate monomers and exposed to UV light in order to generate a surface grafted polymer network with enhanced electrooptic responses.<sup>80</sup> BP and its derivatives also found application in biochemistry because they can be manipulated by ambient light and activated by light in the range of 345–360 nm, avoiding protein damage at this region. Moreover, they react with comparatively inert C–H bonds in a broad range of different chemical environments and are more stable than diazo esters, aryl azides and diazirines. Therefore, the silane derivative of BP was used to immobilize biomolecules onto a fiberoptic silica surface<sup>81</sup>, to develop a polymer-tethered phospholipid bilayer consisting of a BP-derivatized glass surface, a polymer layer and a tethered phospholipid bilayer<sup>82</sup>, and to create a broad range of polymeric coatings for biomedical applications.<sup>83</sup>

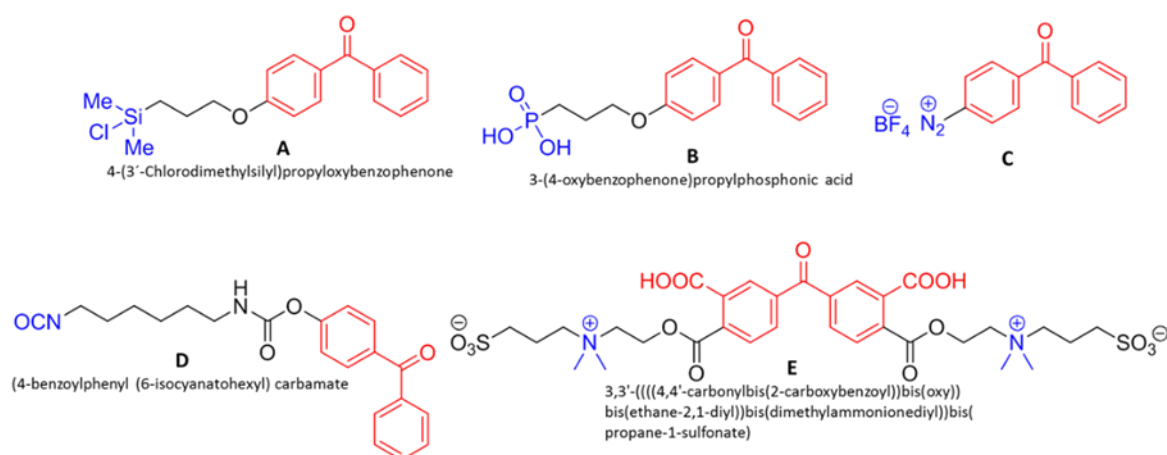
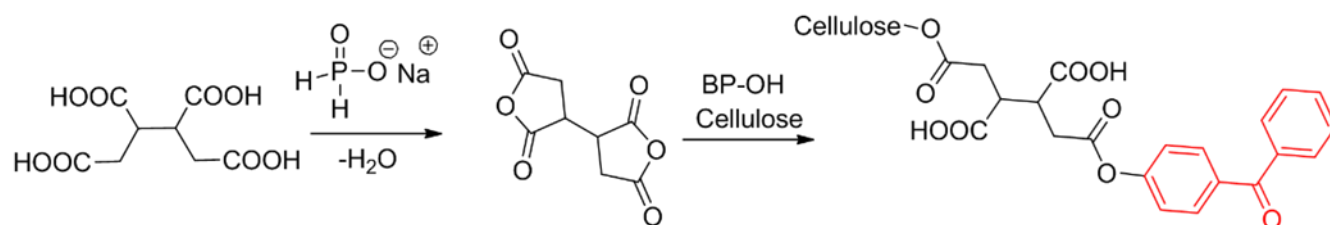


Figure 7: BP derivatives with different coupling units (photosensitive groups are labelled in red; anchor moieties are labelled in blue).

Staying with biochemical applications, Griep-Raming et al. used a phosphonic acid anchor to attach BP moieties onto the surface of titanium. In comparison to organosilanes, the hydrolytic stability of phosphonic acid monolayers on titanium is higher, which is important for long lasting implants. The BP-phosphonic acid compound (Figure 7 B) was synthesized in a three step synthesis in very good yields and was coupled to the surface by convenient depositing-heating-washing cycles. The authors then re-reported successful grafting of PHEMA and PSt and pointed out that phosphonic acid anchors can also be used to couple the initiator to tantalum, aluminium, mica, zirconium, silicon, steel, stainless steel, copper, brass, etc.<sup>84</sup> A slightly different coupling approach was shown by Raghuraman et al., who used a hydro silane for the attachment onto SiO<sub>2</sub> surfaces. Compared to chlorosilanes the hydrosilane does not need strict exclusion of moisture during self-assembly but can be applied under ambient conditions. With this, PSt was grafted to the surface using the BP route and also an ATRP

initiator was introduced with the same approach to the surface, followed with surface-initiated polymerization of tert-butyl acrylate.<sup>85</sup>

Leaving silanization chemistry, Gam-Derouich et al. showed the covalent coupling through electroreduction of the synthesized diazonium salt BP derivative (Figure 7 C) to different surfaces. The authors initiated photopolymerization of model monomers, namely, St, MMA and HEMA from gold-coated silicon substrates, which were previously electro-grafted with the BP diazonium salt (BP-DS).<sup>86</sup> In their following studies they grafted a superhydrophilic polymer onto BP-DS functionalized stainless steel and gold surfaces using surface-initiated photopolymerization for biomedical applications,<sup>87</sup> and extended this grafting-from method to different substrates (glassy carbon, indium tin oxide) and monomers (MAA, poly (4-vinyl pyridine)), also using dimethyl aniline as co-initiator.<sup>88</sup> Another impressive application was given by the same group, developing molecularly imprinted polymer grafts on gold or gold nanoparticles for the specific and selective detection of dopamine<sup>89</sup> and melamine.<sup>90</sup> Surface modification of cellulosic materials utilizing BP was demonstrated by Hong et al. The authors used butane tetracarboxylic acid which was reacted with sodium hydrophosphite resulting in the corresponding dianhydride. This bifunctional linker reacts with the hydroxy groups of the cellulosic material and the hydroxy group of 4-hydroxybenzophenone simultaneously (see Scheme 6). Upon UV irradiation the BP moiety abstracts hydrogen from the cellulosic material, thus generating two radicals which are both capable of photopolymerizing acrylamide (AAm). The so prepared cotton fabrics showed enhanced thermal stability and, through a chlorination process, excellent antibacterial properties were obtained.<sup>91</sup>



Scheme 6: Introduction of a benzophenone unit (red) to cellulose.

Another approach towards modified cellulose nanocrystals was recently shown by Biyani et al. They synthesized an isocyanate bearing BP derivative (Figure 7 D) which was reacted with cellulosic hydroxyl groups at elevated temperatures in the presence of a catalytic amount of dibutyltin dilaurate, forming a urethane group. The cellulose nanoparticles were incorporated into a polymer (ethylene oxide/epichlorohydrin copolymer) forming covalent bonds with the macromolecules of the matrix upon UV radiation. This led to a stiffness increase as well as reduced swelling and softening upon exposure to water.<sup>92</sup>

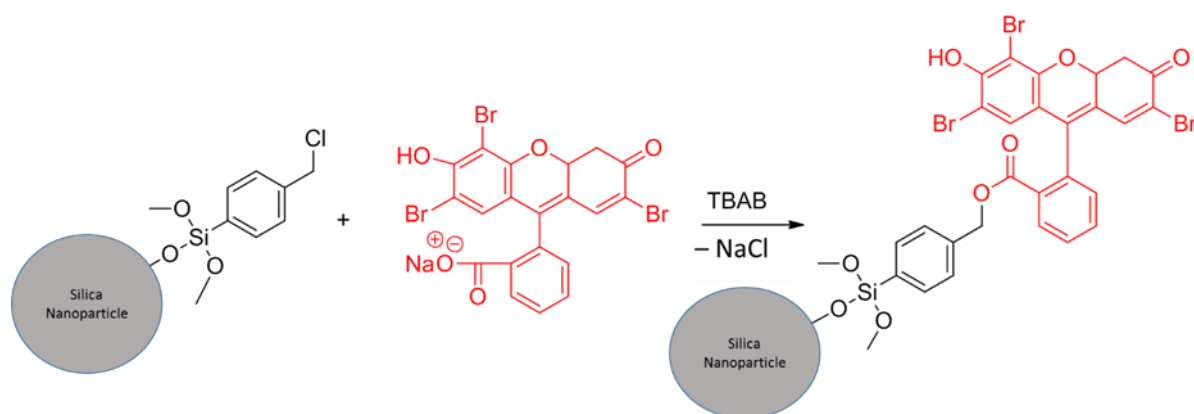
Photoinitiator-modified montmorillonite was recently reported by Melinte et al., who synthesized a novel initiator bearing a BP core and a quaternary ammonium unit, which was

capable of coupling to cloisite layers via a cationic exchange of  $\text{Na}^+$  (Figure 7 E). Furthermore, acrylic monomers (urethane dimethacrylates) were photo-crosslinked with modified montmorillonite as the initiating species without the use of solvents, leading to a hybrid nanocomposite coating.<sup>93</sup>

### Coupled Eosin

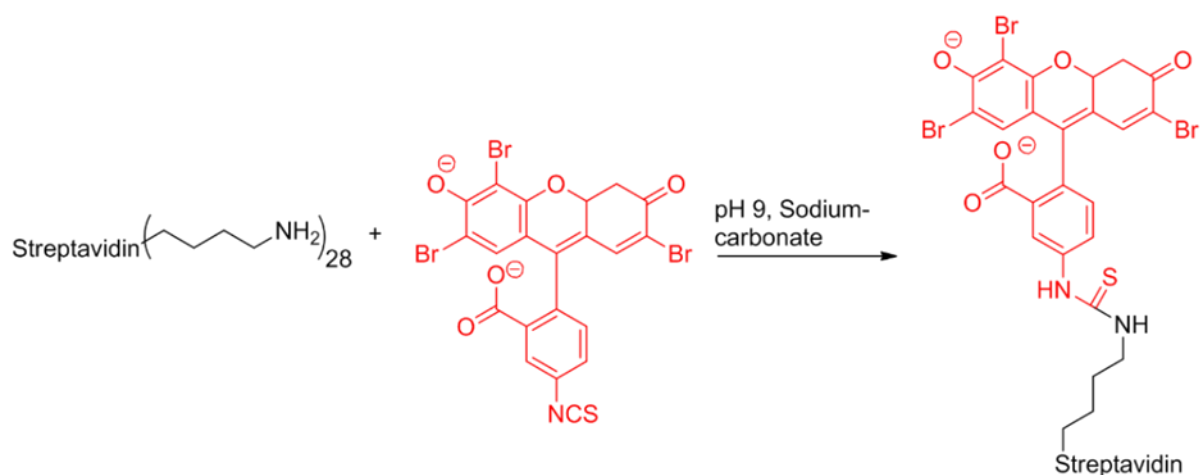
Furthermore, eosin is a well-known type II photoinitiator. This dye strongly absorbs light ( $\epsilon = 60800 \text{ L mol}^{-1} \text{ cm}^{-1}$  at 540 nm), and is then transferred into its singlet state followed by a rapid intersystem crossing (ISC) to the lowest energy triplet state, with a lifetime of 24  $\mu\text{s}$ . Electron transfer from the co-initiator (commonly tertiary amines) leads to a radical eosin anion and an amine radical cation, followed by a proton transfer generating an eosin radical and a more reactive  $\alpha$ -amino radical which is expected to start the polymerization. In terms of surface coupled eosin initiator, the subsequent photopolymerization is meant to be surface mediated since the reactive amino radical is generated in the vicinity of eosin, which is surface-tethered. Eosin is, because of visible light absorption, highly suitable for applications which require a high penetration depth and in which a high dose of UV light would destroy proteins or DNA. Furthermore, the use of visible light avoids unwanted bulk polymerization, which is often observed for irradiation with UV light.<sup>94–97</sup>

Satoh et al. reported eosin modified silica nanoparticles via the reaction between sodium carboxylate groups of eosin Y and benzyl chloride groups in the presence of a phase transfer catalyst (see Scheme 7). Subsequent photopolymerization of St, MMA, AA and acrylonitrile was carried out in the presence of oxygen and ascorbic acid as a reducing agent, and determined the wettability of the grafted silica nanoparticles.<sup>98</sup>



Scheme 7: Synthesis pathway towards silica nanoparticles modified with eosin (red). A phase transfer catalyst (tetrabutylammonium bromide; TBAB) was used.

Hansen and co-workers coupled eosin, which was functionalized with a streptavidin protein unit according to Scheme 8, to biochip glass surfaces, selectively carrying biotinylated oligonucleotides, through a biotin-streptavidin bond. Upon irradiation with visible light and being in contact with a monomer (polyethylene glycol (PEG) -diacrylate) containing a co-initiator, a hydrogel was exclusively grown at spots, where the photoinitiator was allocated. This served as a visible-light-polymerization-based-amplification for visual biotin detection. For this purpose, eosin-5-isothiocyanate was reacted with amino groups of streptavidin leading into the formation of a thiourea bond.<sup>97</sup> Streptavidin-eosin was further used to encapsulate mammalian cells by photopolymerization of hydrogel precursors from the cell surface in order to manipulate transport processes at the surface.<sup>99</sup> The same authors also showed that PEG coated cells are protected in harsh environments, for example, during antigen specific lysis, and proved a strong correlation between the density of surface immobilized streptavidin-eosin and the yield of intact cells during antigen specific lysis.<sup>100</sup>



Scheme 8: Synthesis of photo initiating eosin (red) species bearing a streptavidin anchor.

Cho et al., exploited the reaction between polyamines (polyethylenimine, spermine, polypeptide) and eosin-5-isothiocyanate to create eosin-bearing macromolecules, which build a polyplex with plasmid DNA. After surface initiated photopolymerization with water-degradable acrylic monomers an acid-degradable polyketal shell with the gene-carrying polyamine core was received. The polyketal shell of this gene delivery system was degraded in certain pH-defined environments exposing the DNA core to the targeted cell.<sup>101</sup>

Surface modification of cotton fabrics using eosin as a covalently bound photoinitiator was investigated by Stenava et al. The authors synthesized an eosin derivative bearing a pyridinium salt unit, which was added to the dye bath. Surface initiated photopolymerization of 4-propylamino-N-ethylmethacrylate-1,8-naphthalimide (synthesized by the authors) and N,N-methylenebisacrylamide in the presence of a co-initiator yielded a fluorescent and pH-responsive hydrogel layer.<sup>102</sup>

Kizilel et al. used amino-functionalized glass or silicon substrates, modified by silanization with

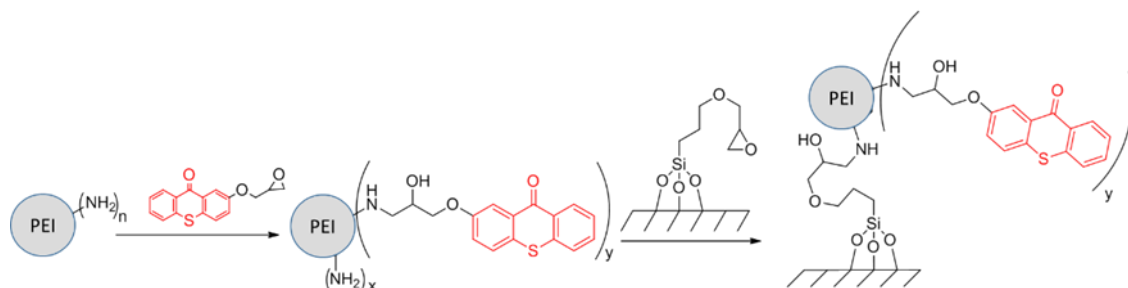
3-aminopropyltriethoxysilane APTES to introduce eosin moieties to the corresponding surface. Therefore, the carboxylic group of the eosin molecule was reacted with Woodward's Reagent K (WRK), and subsequently formed an amide bond with the amino-functionalized substrate. Photopolymerization of PEG-diacrylate and 1-vinyl-2-pyrrolidinone was carried out under mild conditions in the presence of triethanolamine, generating patterned hydrogels, which have tissue-like physical and mechanical properties.<sup>96</sup> In a subsequent contribution the same authors exploited the reaction between pendant amino groups and the carboxylic acid group of eosin (activated with WRK) to generate hydrogel multilayers using PEG amino acrylate along with other hydrogel precursors through sequential introduction of eosin Y and photopolymerization.<sup>103</sup>

### Coupled Thioxanthone

Thioxanthone (TX) is another widely used type II photoinitiator. The research goes back to 1981. Upon irradiation with UV light, TX reaches its triplet state via intersystem crossing. From its triplet state TX reacts with hydrogen donors, such as amines, forming a co-initiator radical and a TXH ketyl radical. The latter can dimerize, carry out disproportion reactions, terminate radical polymerization in some cases and react with molecular oxygen. A deeper look into TX photophysics and photochemistry can be obtained from the literature.<sup>104</sup>

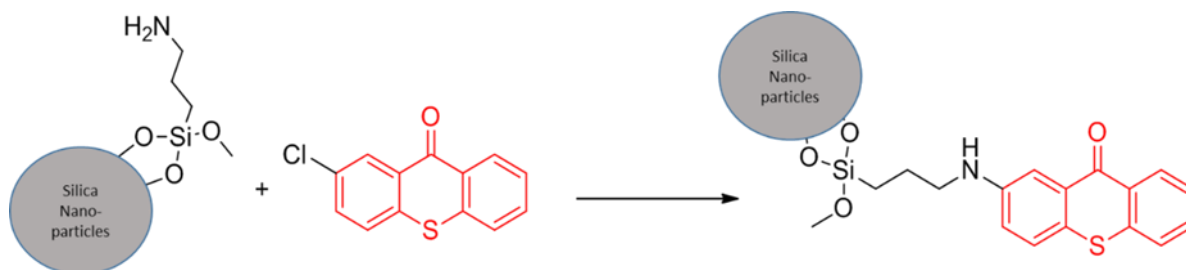
Water compatible photoinitiators derived from thioxanthone are widely used in printing inks, coatings, microelectronics and photoresists. For this purpose, Jiang and co-workers synthesized a hyperbranched TX derived macrophotoinitiator (HPTX, depicted in Scheme 9) using dendritic poly(propyleneimine) (PEI) which is a well-defined and highly branched molecule with a high density of amino groups. PEI is composed of tertiary amines in the core and of secondary as well as primary amines in the periphery, which can be easily utilized for the reaction with epoxides such as epoxy derivatives of TX. The resulting HPTX includes photoinitiating species as well as the co-initiator moiety in one molecule and shows photobleaching properties.<sup>105,106</sup> In a further contribution of the same group, HPTX was covalently attached to silica surfaces via nucleophilic addition reaction between surface tethered epoxy groups and amino groups of the initiator leading to a self-assembled monolayer. The epoxy groups at the silica surface were preliminary introduced via silanization with 3-glycidyloxypropyl trimethoxysilane. Through surface initiated photopolymerization of NIPAM, a coating with temperature responsive properties was gained.<sup>107</sup> Exploiting the photobleaching properties of HPTX, patterned binary polymer brushes were produced. HPTX was immobilized onto silica surfaces by the above-mentioned procedure. In the absence of monomers, the samples were exposed to UV light through a photomask in order to photo-bleach and therefore deactivate the initiator within a defined area. Subsequent photopolymerization of MMA created polymer brushes coupled to the non-bleached area. Binary brushes were then developed using a solution of St and free TX to grow PSt-brushes from the formerly bleached area, taking into account the remaining immobilized amino groups, which can still act as co-initiators for polymerization.<sup>108</sup> Chen and co-workers extended the scope of this technology to silica particles. TX derivatives are suitable for this application because of their excellent UV-

absorbance in the spectral region 365–400 nm, which is not affected by the shield of light caused by particles. The introduction of HPTX was, in a similar way to the above described method, based on the reaction between epoxy and amino functionalities. After surface initiated photopolymerization of MMA, the obtained particles were incorporated in a PMMA matrix to enhance thermal and mechanical properties.<sup>109</sup>



Scheme 9: Synthesis of the macroinitiator HPTX, and subsequent surface coupling (photosensitive TX moieties are labelled in red).

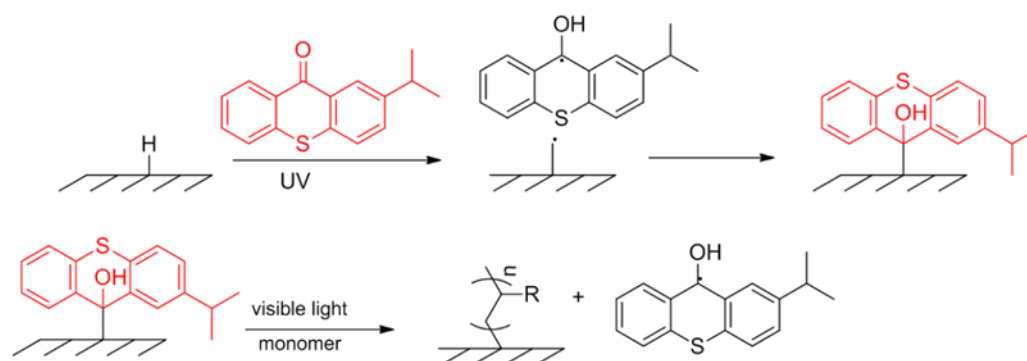
Recently, Li et al. introduced the TX moiety onto the surface of silica nanoparticles. Nanoparticles were firstly modified with APTES via silanization leading to surface anchored amino groups. These groups were converted with a TX derivative bearing a chlorine substituent, developing a covalent link between TX and silica nanoparticles as shown in Scheme 10. In a comparative study, these modified nanoparticles exhibited higher efficiency in photopolymerizations than the parent TX initiator and prominently showed good dispersibility in epoxy acrylate resins. Furthermore, cured samples with these modified nanoparticles had a significantly lower amount of extractable residual photoinitiator which offered advantages with respect to environmental issues.<sup>110</sup>



Scheme 10: Introduction of TX (red) onto silica nanoparticle surfaces.

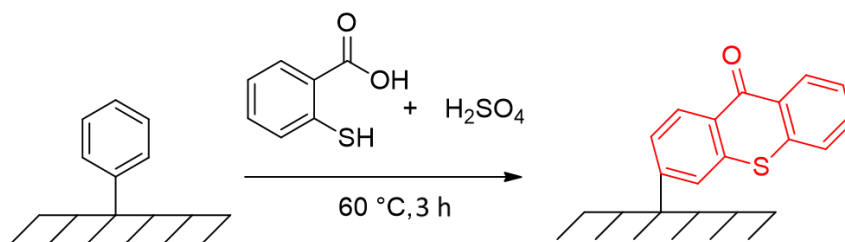
As was done with BP, a derivative of TX, namely, isopropyl-TX (ITX), was also coupled to polymer surfaces by Bai et al., using the two-stew method. UV illumination of ITX between two LDPE films leads to surface tethered isopropyl thioxanthone semipinacol through excitation, subsequent hydrogen abstraction and recombination (see Scheme 11)





Scheme 11: Two step method for thioxanthone immobilization and subsequent grafting-from reaction (photo-sensitive moieties are labelled in red).

The resulting “dormant” group exhibits light absorption in the visible light region, and was employed to graft glycidyl methacrylate (GMA) from the LDPE-surface via visible light induced photopolymerization. The authors also pointed out the “living” characteristics of this grafting polymerization since the thickness of the grafted layer was controlled by altering the irradiation time (linear increase of layer thickness versus irradiation time).<sup>111</sup> This technology found application in biomedicine where the “dormant” groups at the surface of LDPE were used to generate polymer brushes of poly(ethylene glycol) methyl methacrylate for antifouling properties. Furthermore, dormant ITX moieties at the end of the polymer brushes were again utilized for a crosslinking copolymerization of GMA and polyethylene glycol diacrylate (PEGDA), generating a layer which can bind proteins via epoxy-amine reactions onto the resulting microarray. Both photopolymerizations were carried out under visible light.<sup>112</sup> A technique which combines photolithography and visible light induced photopolymerization was shown by Zhao and co-workers. After coupling ITX onto LDPE surfaces, using the same procedure, PEGDA was grafted from the surface in a patterned manner using a photomask. To verify the living nature of this grafting polymerization, a second reinitiating illumination step was performed with a solution of PEGDA and sodium acrylate resulting in a 3D-patterned surface. Furthermore, a reactive two-layer 3D pattern of poly (acrylic acid) (PAA) and PEGDA with a morphology of lateral stripe on vertical stripe (for example) was prepared and employed to separately immobilize model biomolecules.<sup>113</sup> In an unconventional approach by Fukumori et al., the TX photoinitiator was directly formed on the surface of solid polystyrene. In this reaction thioxanthone was readily formed on the surface by utilizing phenyl groups of PSt in the presence of sulfuric acid and thiosalicylic acid (see Scheme 12). Surface initiated photopolymerization of poly(N-isopropylacrylamide) under visible light led to temperature responsive cell culture surfaces.<sup>114</sup>



Scheme 12: Introduction of the TX moiety (red) onto p(St) surfaces.

### Coupled Anthraquinone

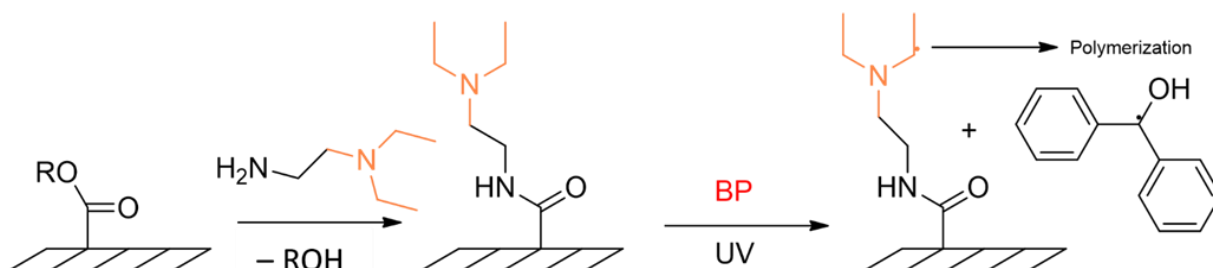
Another type II initiator, namely, anthraquinone, was also used for surface modification, but to a lesser extent when compared to above mentioned BP, eosin and TX. Liu et al. used water-soluble anthraquinone-2-sulfonate sodium as an acid dye to modify polyamide fibres via a simple dyeing process, which leads to ionic bond formation. Upon UV irradiation they grafted AA onto the fibres.<sup>115</sup> The same group produced self-cleaning cotton-fabrics with antimicrobial functions against both Gram negative and Gram-positive bacteria, using 2-anthraquinone carboxylic acid. This initiator was attached to the surface through a N,N-carbonyldiimidazole catalyzed esterification between the hydroxy groups of the cellulose material and the carboxyl groups of the initiator.<sup>116</sup>

#### **2.1.4 Surface immobilization of synergists for benzophenone and thioxanthone**

Another approach to use BP as a photoinitiator for surface-initiated polymerization is to immobilize the corresponding co-initiator (hydrogen donor). Commonly used co-initiators for BP are tertiary amines which form an exciplex with BP upon UV radiation. Immobilizing the synergist seems to be favourable, since the amino-substituted alkyl radical is highly reactive in initiating polymerizations.<sup>117</sup>

He et al. extensively studied BP synergist immobilization for the modification of polymeric membranes with different pore sizes. In their first publication in 2006 the tertiary amine was introduced through an aminolysis reaction between ester groups on the surface of hydrophilized PP and etched poly (ethylene terephthalate) (PET) membranes for microfiltration, and N,N-diethylethylenediamine according to Scheme 13. This coupling method was supposed to be possible for all polymers, which bear ester groups at their surface. With BP in solution the authors grafted a water swellable layer of poly (acrylamide) (PAAm) from the PET and PP surfaces and analyzed the grafting mechanism under variation of the irradiation time, monomer and BP concentration, as well as the synergist content on the surface. Intense UV irradiation accelerated the grafting process but led to a loss of surface selectivity. Furthermore, for ideal surface selectivity a low concentration of photoinitiator was required. The authors also pointed out that a potential competition between the monomer, which serves as a solvent, and the membrane could decrease the degree of grafting and the surface selectivity.<sup>117,118</sup> Using this well studied synergist immobilization method, the authors

prepared anion exchange membranes with different architectures of grafted layers,<sup>119</sup> and a protein selective copolymer layer on PET track-etched membranes.<sup>120</sup>



Scheme 13: The immobilization of amine synergists onto surfaces and subsequent type II photopolymerization (the co-initiating species is labelled in orange).

Dyer et al., designed a series of dimethylamino terminated thiols (Figure 9 A, B) and disulfides to graft polymer brushes from gold surfaces. When grafting PSt and PMMA from an amino functionalized Au surface, the authors surprisingly obtained a higher grafting degree in the absence of BP. They also compared an azo-initiator with this tertiary amine system, and reported much thicker films in about half the irradiation time in cases where the tertiary amine system is used.<sup>121</sup>

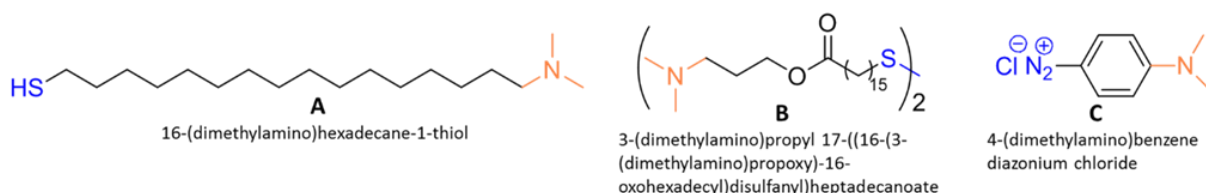
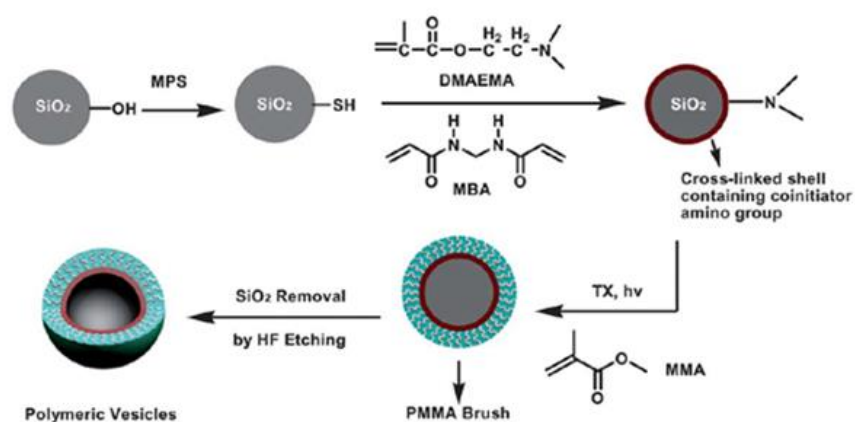


Figure 8: Examples for synergists bearing dimethylamine units (orange) and different coupling groups (blue).

To prepare bioactive polymer grafts, Gam-Derourich et al. electroreduced N,N-dimethylamino benzenediazonium chloride (Figure 8 C) to provide a 4-(dimethylamino)phenyl hydrogen donor layer on gold under nitrogen abstraction. Using free BP and HEMA in solution the group reported densely packed PHEMA layers which completely covered the gold substrate.<sup>122</sup> According to the study of Kim et al., BP is also able to abstract hydrogen from OH-groups at silica nanoparticle surfaces upon UV irradiation. The resulting oxygen radical initiated chain growth of MMA, leading into a covalent Si-O-C bonding as it was proven by FT-Raman analysis. The modified silica nanoparticles contained 31% of PMMA by weight and therefore showed improved monodispersity without agglomeration.<sup>123</sup>

Synergist immobilization was also examined by Chen et al. for TX creating polymer vesicles with well-defined PMMA brushes onto silica nanoparticles. The modification was done using

(3-mercaptopropyl) trimethoxysilane in order to introduce thiols onto the surface of synthesized silica nanoparticles (see Scheme 14). A crosslinked shell was then coupled onto the surface via free radical polymerization of 2-(dimethylamino)ethyl methacrylate, which bears the tertiary amine group, and N,N-methylenebis(acrylamide) as the crosslinking agent. The polymerization was carried out in solution at elevated temperatures using AIBN as a radical initiator. In this process the surface tethered thiol groups were expected to undergo transfer reactions with the propagating chains, therefore leading into the polymeric shell. Subsequent surface initiated photopolymerization of MMA, using TX in solution and the coupled amino group as the co-initiator, followed by removing the SiO<sub>2</sub> core with aqueous HF, yielded polymeric vesicles.<sup>124</sup>

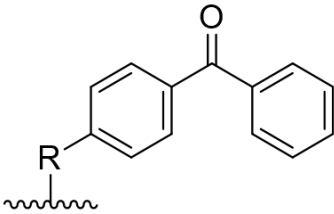
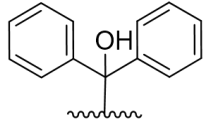
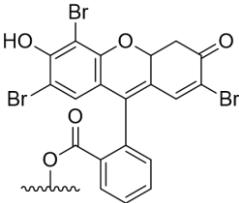
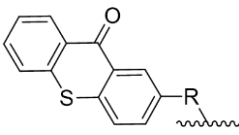


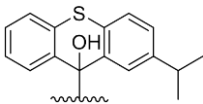
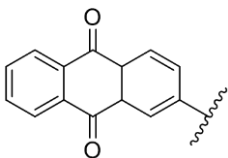
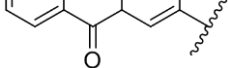
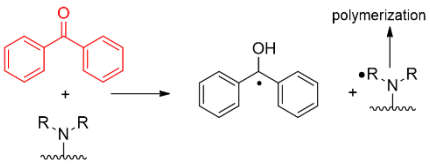
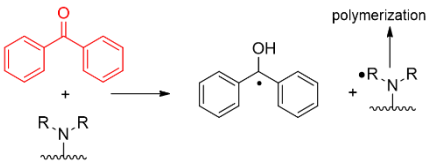
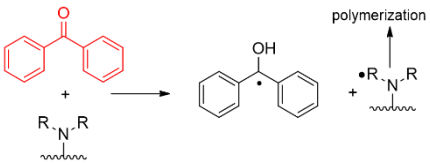
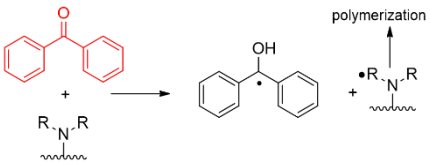
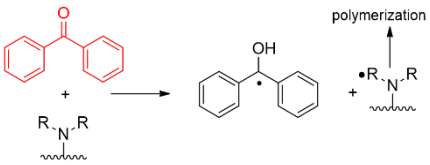
Scheme 14: Production of polymeric vesicles using a combination of conventional polymerization and subsequent grafting from photopolymerization utilizing thioxanthone photochemistry (taken from ref. [124]).

To provide a quick overview of this section, Table 1 summarizes the presented surface-coupled type I and II photoinitiators and co-initiators (synergist). In the first column the chemical structure of the corresponding compound is described. Thereby, the wavy line suggests the substrate surface to which the (co)-initiator is coupled. The second and third columns include the modified material and the corresponding reference, respectively.

Table 1: Summary of surface coupled photoinitiators and co-initiators.

Photoinitiator	Substrate	Reference
<i>Type I photoinitiators</i>		
	Silicon substrate	39–41
	Silica nanoparticles	43,44
	Silica nanoparticles	45
	Cellulosic material	46
	Cellulose nanocrystals	52
	Glass surface	16
	Silica microparticles	48
	Silica nanoparticles	44,47,49
	Silica nanoparticles	43
	Silica nanoparticles	50
	Titanium oxide, ferrite	53,54
	Ferrite	53
	Silica particles	53–55,57,58
	Silicon substrate	57,59,60
	Gold	59,61–65
	Silicon substrate	59
	Gold	66

<i>Type II photoinitiators</i>		
	Silicon substrate	78,79,85
	Indium tin oxide coated glass	80,88
	Silica fibers	81
	Glass substrate	82,83
	Gold	86–90
	Stainless steel	87,88
	Glassy carbon	88
	Cellulose	91
	Cellulose nanocrystals	92
	Sodium montmorillonite Cloisite Na+	93
	Polypropylene	68–70,75,76
	Cellulose acetate, poly(vinylidene)fluoride, polystyrene	69
	Poly(lactide acid)	72
	Poly(dimethylsiloxane)	71
<p>Derived from BP via hydrogen abstraction from the surface according to Scheme 5</p>	Silica nanoparticles	98
	Glass oligonucleotide biochip	97
	Cells	99,100
	Polyamine	101
	Cellulose	102
	Glass and silicon substrates	96,103
	Silicon substrate	107,108
	Silica nanoparticles	109,110
	Polystyrene	114

	LDPE	111-113
<p>Derived from thioxanthone via hydrogen abstraction from the surface according to Scheme 11</p>		
	Poly(amid) fibers	115
	Cellulose	116
<p>Synergist immobilization (tert. amine) for type II photoinitiators</p>		
	PP	118
	PET	120
	Hydrophilized PP	117,119
	Gold	121,122
	Silica nanoparticles	123,124

## 2.2 Light mediated controlled polymerization from surfaces

Among different controlled and living polymerization techniques, radical-based strategies are frequently used because of their compatibility with both aqueous and organic media as well as their high tolerance towards a wide range of functional groups. Controlled polymerization techniques for polymer brush synthesis include (i) surface-initiated reversible addition fragmentation chain transfer (SI-RAFT) polymerization, (ii) surface-initiated photoiniferter-mediated polymerization (SI-PIMP), (iii) surface-initiated atom transfer radical polymerization (SI-ATRP) and (iv) surface-initiated nitroxide-mediated polymerization (SI-NMP), whereas the latter is commonly conducted at high temperatures<sup>125</sup> and will not be further discussed in this contribution.<sup>125–127</sup> In terms of surface initiated photopolymerization the SI-PIMP concept will be discussed in detail since the photo-initiating species is directly coupled to different surfaces in the given examples below. In addition, some examples of surface initiated photopolymerizations based on the ATRP and the RAFT technique, in which the photo initiating species, or better to say the photoredox catalyst, is not coupled to surfaces, will also be presented.

### 2.2.1 Surface-initiated photoiniferter-mediated polymerization (SI-PIMP)

The concept of polymerization methods, which are mediated by photoiniferters was pioneered by Otsu et. al. in 1982.<sup>128</sup> Iniferters are molecules, which induce radical polymerization and simultaneously act as chain transfer and chain terminating agents. The controlled nature of the polymerization is based on the photolytic cleavage of the iniferter-molecule leading to a carbon centred radical, which readily undergoes addition reactions with monomers initiating the chain propagation, and a persistent dithiocarbamyl radical. Herein, the dithiocarbamyl radical does not initiate the polymerization but acts as a chain transfer agent and also induces reversible termination, yielding polymers with reactive chain ends, which can be reinitiated to form copolymers.<sup>126</sup> The mechanism of SI-PIMP, including photolytic cleavage of the iniferter molecule and subsequent “grafting from” (co)-polymerization of acrylic or vinyl monomers is summarized in Figure 9. Within this example, the iniferter molecule is coupled to an appropriate surface via silanization chemistry as an example. However, more detailed information about the iniferter concept, different iniferter molecules and living radical polymerization, can be found elsewhere.<sup>129,130</sup>



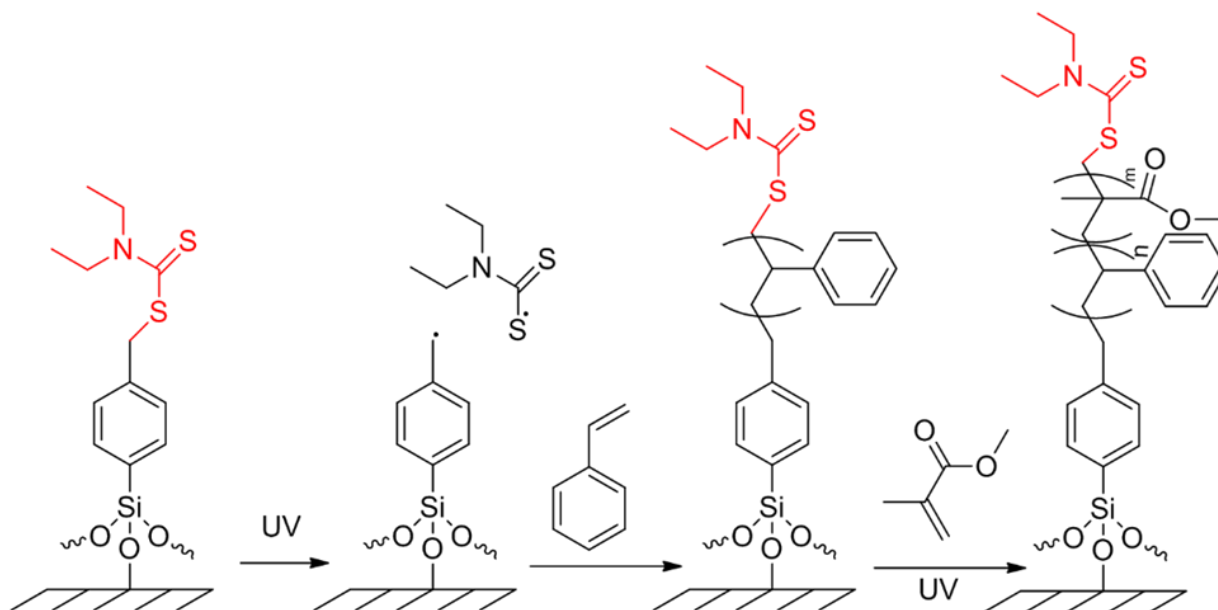
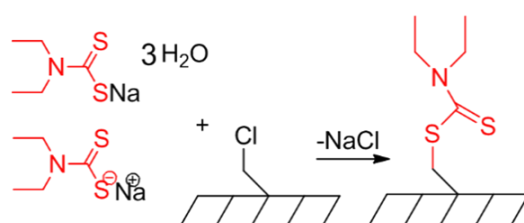


Figure 9: Exemplary preparation of copolymer brushes by SI-PIMP from a benzyl-N,N-diethyldithiocarbamate derivatized substrate (photosensitive group is labelled in red).

The SI-PIMP based grafting-from approach is a widely used method to prepare numerous polymer brushes and coatings on different surfaces.<sup>125</sup> This method provides the possibility to adjust chemical compositions, film thickness and grafting densities of the produced layers by regulating the monomer concentration and the UV exposure time. Moreover, it does not require any toxic catalysts making this technology suitable for biomedical applications.<sup>131,132</sup> Otsu et al. also reported the first example of SI-PIMP by coupling a N,N-diethyldithiocarbamate derivative onto PSt surfaces via hydrolysable ester bonds. The authors used polystyrene-divinylbenzene- copolymer beads, which were chloro-methylated and subsequently reacted with N,N-diethyldithiocarbamyl acetate yielding a photoreactive solid PSt (see Scheme 15). As a proof of concept, the authors grafted PMMA and PSt from the modified surface to synthesize PMMA-PSt-block copolymer brushes.<sup>133</sup>



Scheme 15: Coupling strategy to introduce a photoiniferter functionality (red) to chloromethylated surfaces using sodium N,N-diethyldithiocarbamate.

Matsuda and colleagues extended this concept using a PSt film which was crosslinked by  $\gamma$ -rays from a  $^{60}\text{Co}$  source in a preliminary step and subsequently immersed into a solution of

chloromethylethylether and  $\text{ZnCl}_2$ . The chloromethylated p(St) film was kept in a solution of sodium N,N diethyldithiocarbamate trihydrate (DC-H) to immobilize the photolabile group onto the PSt surface. Precise control of the molecular architectures of PDMAA, poly- N-[3-(dimethylamino)propyl]acrylamide, PMAA and PSt under UV radiation at room temperature was reported.<sup>134</sup> The same group later presented a two-step method for highly spatio-resolved graft-copolymerized surfaces, in which the stem and the branch design were comparatively well controlled using the photoiniferter concept. In an initial step they synthesized a photoactive glass surface using a well-known silanization approach with chloromethylphenylethylsilane. The chloromethylated glass was then converted into dithiocarbamate (DC) derivated glass using DC-H. After photopolymerization of chlorovinylstyrene, a second functionalization with DC-H was done leading to polymer chains with DC-derivatized side groups from which MAA, N,N-dimethylacrylamide (DMAAM), sodium methacrylate and poly(ethylene glycol) methacrylate (PEGMA) were photopolymerized.<sup>135</sup> In a further publication, Matsuda et al. used the same coupling strategy (chloromethylation and subsequent treatment with DC-H, Scheme 15) to develop DC-derivatized polyurethane surfaces, from which poly(PEGMA) and PDMAA were photografted in order to achieve highly water wettable surfaces.<sup>136</sup> The nucleophilic substitution of surface tethered chlorine units, which were covalently coupled to surfaces by commercially available DC-H via a  $\text{S}_{\text{N}}2$  mechanism,<sup>137</sup> was further exploited by many groups modifying cellulose membranes with MAA and ethylene glycol dimethacrylate,<sup>138</sup> inert cycloolefin polymer substrates with an upper PAA and a bottom poly (PEGMA) layer<sup>139</sup> and different silica microparticles with PMMA.<sup>137</sup> Ma et al. prepared iniferter functionalized magnetic microspheres which consisted of  $\text{Fe}_3\text{O}_4$ . An  $\text{SiO}_2$  layer prepared from tetraethyl orthosilicate improved the microsphere stability and provided the anchoring site for initiator-attachment using p-chloromethyl, phenyltrimethoxysilane and DC-H. After photopolymerization the resulting polymer brush showed antifouling and antibody immobilization properties.<sup>140</sup> A slightly different approach was shown by Ulbricht and colleagues, who modified hydrophilized PP microfiltration membranes by utilizing three straightforward solid phase reactions. First, aminolysis was executed to introduce amino groups onto the surface, followed by a reaction with 2-bromoisobutyryl bromide introducing a bromine leaving group at the surface which was finally reacted with DC-H leading to an iniferter-modified PP-surface from which a copolymer of AAm and ethylene glycol dimethacrylate were polymerized.<sup>141</sup>

In the early 2000s, De Boer et al. synthesized an organosilane containing a DC group (Figure 10 A, SDBC). In this fundamental work, they modified silicon-wafers by graft-photopolymerization of MMA and St.<sup>142</sup> SDBC was then used in several publications. Rahane et al. used SDBC to modify silicon surfaces and studied the kinetics of SI-PIMP of MMA by measuring the layer thickness as a function of reaction time, monomer concentration and light intensity via variable angle ellipsometry. The results indicated a pseudo living nature of the photopolymerization due to irreversible bimolecular termination reactions, which decreased the amount of surface free radicals with increasing exposure time.<sup>143</sup> In later publications, Rahane et al. proposed a kinetic model for SI-PIMP,<sup>144</sup> and suggested using tetraethylthiuram

disulfide to reduce irreversible termination reactions and to provide controlled radical polymerization behavior.<sup>145</sup> Schönherr and colleagues used SDBC to grow thin films of PAAM and covalently crosslinked, swellable hydrogel brushes from iniferter-functionalized silicon substrates, and reported thick films (up to 1  $\mu\text{m}$ ) within 1 h of reaction time in aqueous environment and in absence of side reactions.<sup>146</sup> In a more recent publication SBDC functionalized silicon wafers were used to prepare zwitterionic poly (3-(dimethyl (4-vinylbenzyl) ammonium) propyl sulfonate) brushes with an anti-polyelectrolyte effect via SI-PIMP.<sup>147</sup>

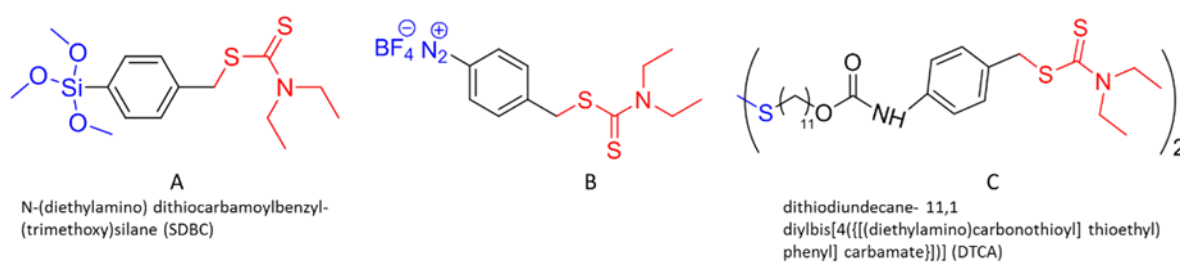


Figure 10: Iniferter compounds (red) bearing different anchor moieties (blue).

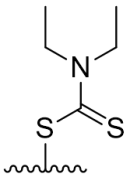
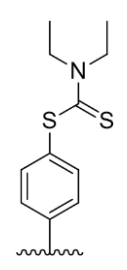
Gold surfaces were firstly modified with iniferter groups by Vansco and co-workers who synthesized a disulphide containing photoiniferter (Figure 10C, DTCA). Surface-initiated polymerization from gold is desirable because it is compatible with a broad variety of surface analytical techniques. Furthermore, the Au-S bond can be easily cleaved by treatment in a dilute solution of iodine leading into the release of formerly tethered macromolecules which can then be further characterized.<sup>148</sup> DTCA built a self-assembled monolayer on gold surfaces and was subsequently used to initiate controlled radical photopolymerization from aqueous NIPAM solutions to provide a temperature responsive surface. Although it is well known that the Au-SH bond is not stable upon UV irradiation (exposure with 254 nm UV light of self-assembled monolayers of alkanethiols on gold and silver leads to photochemical oxidation, generating sulphur trioxide anions and therefore lead to Au-S bond breaking<sup>149</sup>), the group reported successfully controlled photopolymerization using a UV lamp with a 280 nm cut-off filter.<sup>150</sup> The same group later investigated how the composition of the self-assembled monolayer of DTCA on Au influences the morphology and property of the photografted PMMA layer, and also modified PMAA layers with cell-adhesive arginine-glycine-aspartic acid for biochemical applications.<sup>151,152</sup> By growing zwitterionic monomers from a DTCA-functionalized gold surface, Krause et al. developed a coating, which was ultra-low fouling to undiluted human blood plasma, and also showed specific protein detection properties.<sup>153</sup>

Another strategy for coupling photoiniferter groups to different surfaces was shown by Griffete et al., who attached iniferter groups to the surface of iron oxide nanoparticles using aryl diazonium salt chemistry.<sup>154</sup> The coupling mechanism relies on the reduction of the diazonium salt by the metal surface or reducing agents in solution, generating aryl radicals

that are able to covalently couple to metal or oxide surfaces.<sup>155</sup> This coupling method does not require dry or oxygen free conditions.<sup>156</sup> Diazonium salts provide an excellent alternative to thiols and silanes. While the latter mostly bind to oxidized surfaces, it was proven that Au-aryl bonds have an enhanced stability compared to Au-SH bonds (bond strengths 132.9 and 118.7 kJ/mol, respectively).<sup>86</sup> Based on this, Griffete et al. designed two different molecules bearing diazonium salt coupling units. One directly carried the coupling agent (a diazonium salt) and the iniferter group (Figure 10B), and the other one contained the coupling agent and a chloromethyl unit ( $\text{BF}_4$ ,  $\text{N}_2$ ,  $\text{C}_6\text{H}_4\text{-CH}_2\text{-Cl}$ ), which was reacted with DC-H in a two-step method. Magnetic nanoparticles (iron oxide) with a pH-sensitive PMAA coating were then produced with both coupling reagents.<sup>154</sup> Extending the scope of this technology, the same group successfully functionalized aluminum nanoparticles with photografted PMAA,<sup>155</sup> and improved the colloidal stability of PMAA-coated ultra-small superparamagnetic iron oxide nanoparticles in water. Therefore, oligo(ethylene oxide) spacers of various sizes were introduced between the diazonium salt moiety and the iniferter group of the coupling reagent, which improved the colloidal stability of the nanoparticles in water and ethanol due to the hydrophilic chains.<sup>157</sup> Furthermore, they also modified Au nanorods with a crosslinked MAA and N,N-methylenebisacrylamide copolymer by combining diazonium salt chemistry and SI-PIMP.<sup>158</sup>

Table 2 summarizes surface coupled photoiniferters presented in this chapter. The wavy lines in the first column indicate the surface to which the photosensitive group is coupled. The substrate materials as well as the related references are included in columns 2 and 3.

Table 2: Summary of surface coupled photoiniferters.

Photoiniferter	Substrate	Reference	
	PSt	133,134	
	Glass substrate	135	
	Poly(urethane)	136	
	Cellulose membrane	138	
	Cycloolefine substrate	139	
	Silica microparticles	137	
	Magnetic microspheres (Fe <sub>3</sub> O <sub>4</sub> )	140	
	Hydrophilized PP	141	
		Silicon substrate	142–147
		Gold	150–153,158
Iron oxide nanoparticles		154,157	
Aluminum nanoparticles		155	

### 2.2.2 Surface-initiated atom transfer radical polymerization (SI-ATRP)

ATRP is the most frequently used controlled radical polymerization for the synthesis of polymers with adjustable molecular weight, dispersity and architecture. Compared to other controlled radical polymerization techniques, ATRP is chemically versatile and robust.<sup>126</sup> Since its discovery by Matyjaszewski, Sawamoto and Percec in 1995, there has been huge progress in polymer synthesis, metal catalytic systems, scope of polymerizable monomers, industrial applications, etc. The development and mechanisms of ATRP is well described in the literature, especially with respect to the metal catalyst systems (see ref.<sup>159</sup>). This chapter focuses on light triggered ATRP with surface coupled initiators. In traditional ATRP the initiating species is an alkylhalide (labelled in orange), which is activated by a low oxidation state transition-metal (photo)-catalyst (labelled in red), generating an alkyl radical and an oxidized form of the transition-metal complex through halogen atom transfer. The latter one is also referred to act as the deactivator. Numerous monomers are added to the alkyl radical or propagating chain before it becomes deactivated by the high oxidation state metal complex.<sup>130</sup> The general mechanism of the ATRP process and a polymerization example with MMA is given in Figure 11. In this figure,  $Mt^n/L$ , labelled in red, represents the photo-redox catalyst  $Ir(ppy)_3$  (tris[2-phenylpyridinato-C<sub>2</sub>,N]iridium (III)).

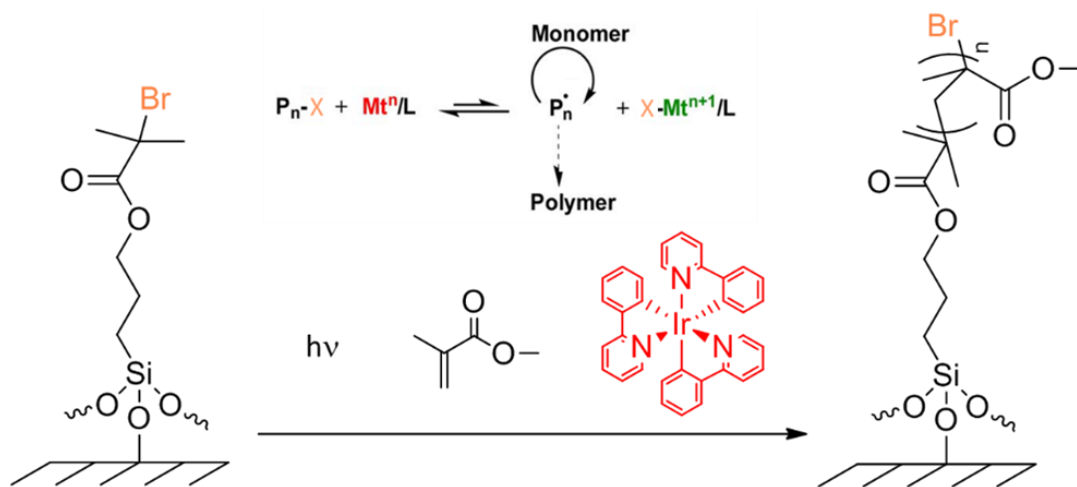
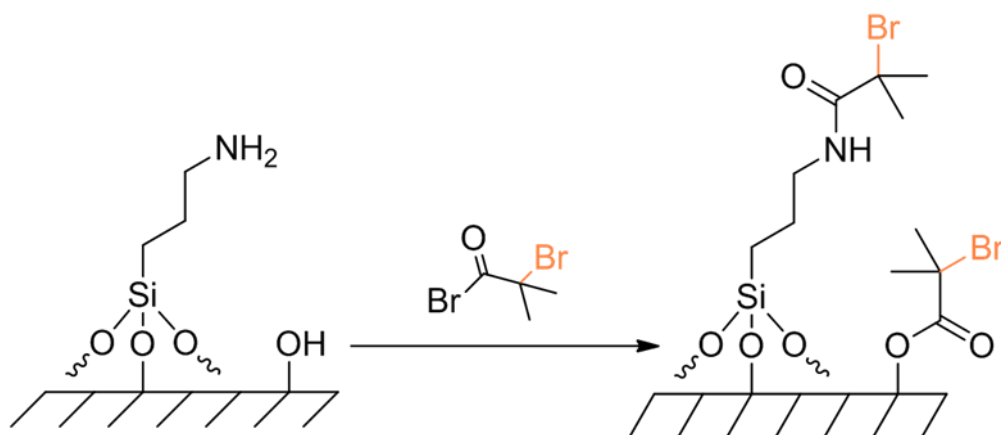


Figure 11: ATRP mechanism and “grafting from” photopolymerization of MMA on a silane-functionalized surface. The ATRP initiator is labelled in orange, and the photoredox catalyst ( $Mt^n/L = Ir(ppy)_3$ ) is labelled in red.

To give one recent example of an application, Zholdassov et al. used a photochemical printer, equipped with a digital micromirror, capable of rapidly elucidating the kinetics of light induced SI-ATRP of different monomers in order to develop patterned “5D and 6D hypersurfaces” with tailored polymer brush heights, chemical compositions and changes upon an external stimulus. They impressively demonstrated how to encrypt data within those hypersurfaces using stimuli responsive polymer brushes surrounded by nonresponsive brushes. In doing so,

they firstly introduced amino groups to silicon substrates by silanization with APTES, followed by the treatment with  $\alpha$ -bromoisobutyryl bromide, leading to alkyl halide species that served as the ATRP initiator (see Scheme 16). Photopolymerization of NIPAM and DMAAm was carried out in the presence of tris[2-phenylpyridinato- C<sub>2</sub>,N]iridium (III) (Ir(ppy)<sub>3</sub>) as the photocatalyst.<sup>19</sup>



Scheme 16: Coupling of an ATRP initiator (orange) to an amino-functionalized surface.

Many other examples of SI-ATRP derivatized polymer brushes on different surfaces are given in the reviews of Chen and co-workers<sup>125</sup> and Barbey et al.<sup>126</sup> However, novel metal-free catalytic systems are sparsely, or even not, described in those contributions and will be outlined herein. The use of organic photoredox catalysts (PC) such as 10-phenylphenoxanine or 10-phenylphenothiazine extended the use of light-induced SI-ATRP for biomedical and electronic applications.<sup>160</sup> A proposed mechanism involves the photoexcitation of PC to an excited state, which is employed to reduce alkyl bromides via an oxidative quenching pathway, generating a carbon centered radical for the polymerization and the radical-ion pair PC<sup>\*</sup>+Br<sup>-</sup>. The latter one deactivates the propagating chain, leading to recovered alkyl bromide and PC, which can be reinitiated upon UV irradiation.<sup>161</sup>

Ma et al. used the same initiator-coupling strategy (silanization with APTES and subsequent treatment with  $\alpha$ -bromoisobutyryl bromide, Scheme 16) to modify mesoporous silica materials with polymer layers derived from SI-ATRP of MMA, NIPAM and DMAEMA using 10-phenylphenothiazine as a photoredox catalyst. The obtained hybrid material (PMMA modification) showed enhanced adsorption ability for toluene as a representative example.<sup>162</sup> Another photoassisted SI-ATRP approach was demonstrated by Zeng et al.,<sup>163</sup> who immobilized an ATRP initiator onto the surface of nanodiamonds via direct esterification between superficial hydroxyl groups and  $\alpha$ -bromoisobutyryl bromide (Scheme 16). Surface initiated photopolymerization with 10-phenylphenothiazine of 2-methacryloyloxyethyl phosphorylcholine resulted in a biocompatible surface and enhanced the nanodiamonds' dispersibility in various solvents. Conventional esterification reactions employing carboxylic

halides and anhydrides<sup>164</sup> have also been used for the surface functionalization of wood<sup>165</sup> and cellulosic materials.<sup>166</sup>

Zeng and colleagues also developed an ATRP initiator for the surface functionalization of Eu<sup>3+</sup>-doped luminescent hydroxyapatite (HAp) nanorods. First, NH<sub>2</sub>-containing HAp was prepared via ligand exchange reaction using adenosine monophosphate as ligand. The amino groups were subsequently reacted with  $\alpha$ -bromoisobutyryl bromide yielding a photoreactive surface from which (ethyleneglycol) methylether methacrylate was grafted, generating hydrophilic luminescent HAp nanorods.<sup>167</sup>

Diszeciki et al. used the same inexpensive organic phenothiazine-based photo-catalyst to grow patterned (co)-polymer brushes of MMA, 2,2,2-trifluoroethyl methacrylate and 2-(methylthio)ethyl methacrylate from Si-wafer surfaces and silica nanoparticles using visible light (405 nm). Therefore, they synthesized a compound which comprised a trichloro-silane and an initiator moiety (Figure 12 A), which was coupled to the corresponding surface via silanization.<sup>168</sup> In a continuative and comparative study, Yan. Et al. pointed out that surface-tethered ATRP initiators derived from ethyl 2-bromo-2-phenylacetate are much more reactive than previously used ethyl 2-bromoisobutyrate-derived structures, thus leading to a higher grafting density. In this context they synthesized four ATRP-initiators by combining the two mentioned structures with chloro- and alkoxy silane anchors (Figure 12 B–E) and coupled them to silica nanoparticles of different sizes. Surface photopolymerization of MMA was carried out using 10-phenylphenothiazine as photocatalyst.<sup>160</sup>

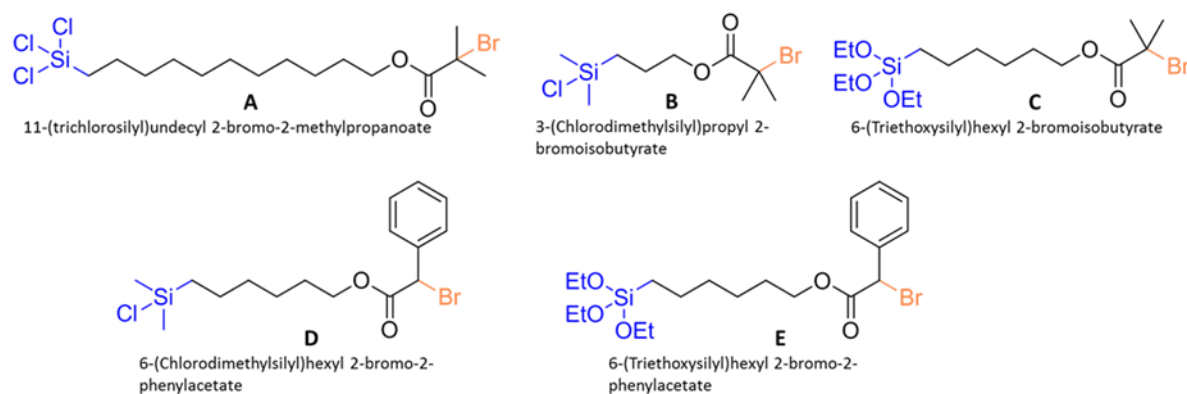


Figure 12: Different compounds containing both an ATRP initiator (orange) and a coupling moiety (blue).

To conclude this subchapter, clickable initiators can also be used for the combination with different types of controlled radical polymerizations for preparing highly functional tailor-made macromolecules. Just to name a few, alkyne and ene-functionalized initiators, azide-functionalized initiators and maleimide-functionalized initiators for pre or post modifications are included. More detailed information can be found elsewhere.<sup>169</sup>



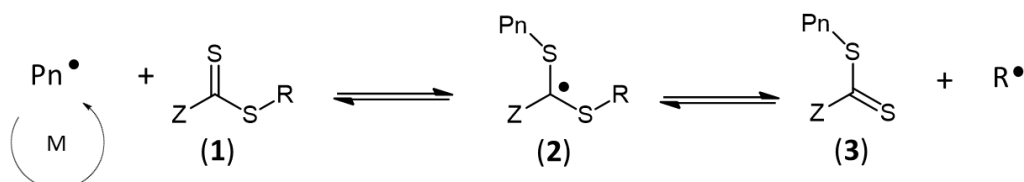
### 2.2.3 Surface-initiated photoinduced electron/energy transfer reversible addition-fragmentation chain transfer polymerization (SI-PET-RAFT)

The RAFT polymerization technique was introduced in 1998 by Chiefary et al., and is a versatile method for the controlled synthesis of functional polymers in different reaction conditions (aqueous or organic solutions, bulk, emulsion and dispersion).<sup>170</sup> The living character relies on a simple and accessible class of organic materials containing a thiocarbonylthio moiety, which is capable of reversibly reacting with propagating chains via a chain transfer mechanism leading into the dormant (end-capped) species. Switching between the propagating and the dormant state suppresses terminating reactions and therefore provides control over the molecular weight and dispersity of the polymer. The general mechanism is shown in Figure 13. The first step includes an initiating step (i), typically done by an initiator, followed by chain propagation. The propagating radical ( $\bullet\text{Pn}$ ) reacts (ii) with the so-called RAFT agent (**1**) and forms radical **2**, which then decomposes to compound **3** and the radical  $\text{R}\bullet$  (for subsequent re-initiation (iii)). Compound **3** can react with another propagating radical ( $\bullet\text{Pm}$ ), giving radical **4**, which then releases the radical  $\bullet\text{Pn}$  (iv). The most important aspect of the RAFT process is the rapid equilibrium (iv) between the two propagating radicals,  $\bullet\text{Pn}$  and  $\bullet\text{Pm}$ , and dormant species, **5** and **3**, via intermediate **4**. This provides equal opportunities for all chains to grow, thus leading to low polydispersity. The rapid interchange within this equilibrium also limits termination reactions by recombination of  $\bullet\text{Pn}$  and  $\bullet\text{Pm}$  (v). The chemical structure of the substituents R and Z and the monomer choice is crucial for successful RAFT processes.<sup>170,171</sup> More detailed information on the chemical structure of RAFT agents and the resulting properties can be found, e.g., in the contribution of Keddie et al.<sup>172</sup>

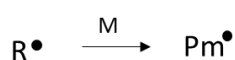
## i) Initiation



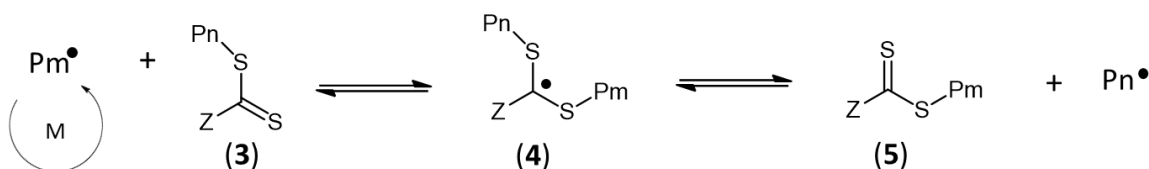
## ii) Reversible chain transfer and propagation



## iii) Reinitiation



## iv) Chain equilibrium and propagation



## v) Termination



Figure 13: General mechanism of RAFT polymerization (adopted from reference [172]).

Recently, light induced RAFT processes have attracted much attention because of the well-known advantages of light, including the spatial and temporal control of the polymerization and the possibility to act at low temperatures.<sup>173</sup> In comparison to conventional RAFT polymerizations, in which the processes are initiated by a thermal initiator such as AIBN or benzoyl peroxide, light-triggered RAFT polymerizations require a photoredox catalyst (PC) and provide several advantages. First, a very low amount of PC is needed (ppm range) and the polymerization can be carried out in the presence of molecular oxygen, which provides the possibility to translate polymerization processes from controlled environments such as gloveboxes to the benchtop. Commonly used PCs which have been reported in the literature are transition-metal complex photocatalysts (for example, fac-Ir(ppy)<sub>3</sub>, Ru(bpy)<sub>3</sub>Cl<sub>2</sub>, ZnTPP), eosin Y, porphyrines and metal oxides.<sup>170,173,174</sup> Since the pioneering work referred to PET-RAFT in 2014, the interaction between an excited state PC and the RAFT agent remains uncertain and challenging. A comprehensive article by Allegranza et al. focuses on this topic. In general, possible mechanisms involve electron or charge transfer processes from the excited PC to the RAFT agent, both yielding a radical ( $\bullet R$  or  $\bullet Pn$ ) which initiates the RAFT process.<sup>175</sup>

In this sub-chapter some examples of surface tethered RAFT agents for subsequent surface initiated photopolymerizations are given. However, it can be concluded from above that a surface coupled RAFT agent does not constitute a surface coupled photoinitiator. Therefore, only some recent examples are shown in this manuscript.

Ng et al. used oxygen tolerant SI-PET-RAFT for the synthesis of homo-, block- and gradient polymer brushes on glass slides, employing a broad range of monomers (acrylamides, methacrylates, acrylates) to develop antifouling surfaces. The RAFT agent was immobilized using silanization chemistry. Thus, they synthesized two different RAFT agents, which carried a silane anchor moiety (see Figure 14 A, B). Visible light mediated photopolymerization was carried out using a zinc-porphyrin PC (5,10,15,20-tetraphenyl-21H,23H-porphine zinc). Because of the lower experimental effort, which results from the oxygen tolerance of SI-PET-RAFT (absence of inert gas, vacuum, etc.), the authors pointed out that this benchtop methodology provides a high throughput approach for the identification and evaluation of polymer brush structure-property-performance relationships.<sup>174</sup> One year later the same group prepared a polymer brush with antifouling and visible light triggered bactericidal properties, on circular glass substrate using the same bifunctional RAFT agent (Figure 14 A).<sup>21</sup>

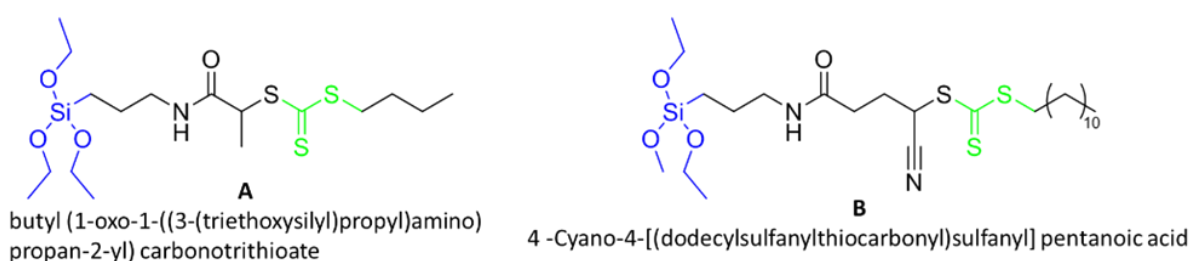
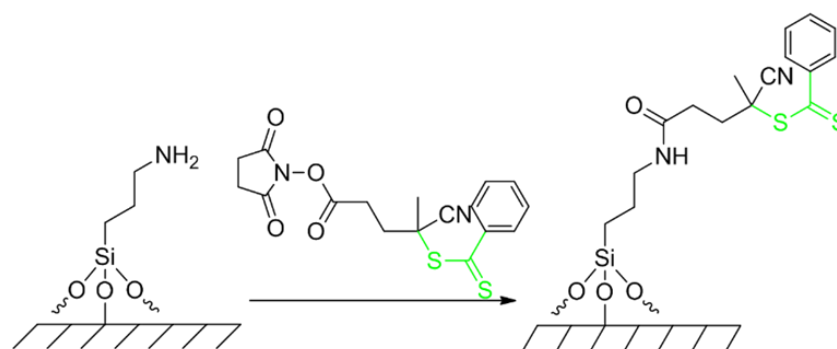


Figure 14: RAFT agents (green) with organosilane anchor moieties (blue).

Staying with anti-fouling surfaces, Kuzmyn et al. used SI-PET-RAFT and eosin Y and triethanolamine as catalysts to polymerize three different monomers (oligo (ethylene glycol) methacrylate, N-(2- hydroxypropyl) methacrylamide and carboxybetaine methacrylamide) from silicon surfaces that were functionalized with a RAFT agent. A mechanism of that photopolymerization, triggered with visible light, was proposed by Xu et al. in 2015.<sup>176</sup> The reaction may proceed via a reductive quenching cycle of eosin Y in which the amine acts as a sacrificial electron donor to reduce oxygen, allowing for the polymerization system to proceed under atmospheric conditions. To immobilize the RAFT agent, silicon substrates were firstly modified with APTES, yielding surface coupled amino groups. In the next step, the amino groups were exposed to 4-cyano-4-(phenylcarbonothioylthio) pentanoic acid N-succinimidyl ester in the presence of triethylamin as a catalyst, leading to surface tethered RAFT agents (see Scheme 17).<sup>177</sup> A similar coupling strategy was then used by the same group in a later publication, modifying gold surfaces with cysteamine, followed by the reaction, which was previously mentioned (see Scheme 17). The group pointed out that SI-PET-RAFT with eosin Y

and triethanolamine as catalyst is a scalable, robust, mild, oxygen-tolerant and heavy-metal-free method for the synthesis of antifouling (co)-polymer brushes on gold surfaces.<sup>22</sup>

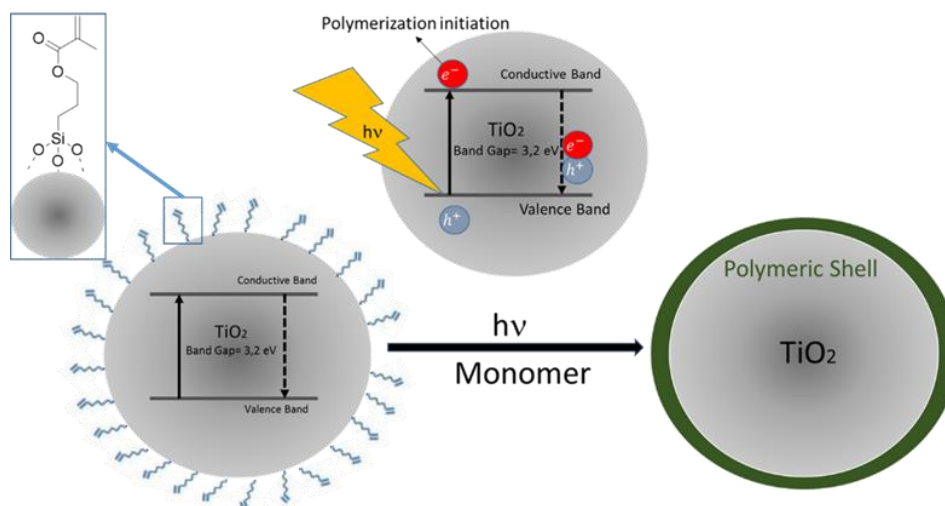


Scheme 17: Coupling strategy for the introduction of the RAFT agent (green) to surfaces.

A different coupling strategy to immobilize a RAFT agent onto the surface of cadmium selenide (CdSe) quantum dots was recently presented by Egap et al. CdSe is a novel class of PC because of the unique electrical and optical properties based on quantum confinement effects. Two RAFT agents were immobilized via ligand exchange between the oleic acid capped quantum dot surface and the bithiol group of the RAFT agent. Organic-inorganic polymer-coated quantum dot nanocomposites were obtained in a grafting-from approach, where the quantum dots act as the PC and as the building block at the same time. These reactions were carried out with different methacrylates under blue light exposure (460–480 nm) in the presence of diisopropylethylamine as an electron donor. The advantages of this method are (i) oxygen tolerance, (ii) low catalyst loading, (iii) one pot synthesis and (iv) the simplicity in tuning the quantum dot properties.<sup>178</sup> A similar process for RAFT agent immobilization, through ligand exchange, with subsequent growth of polymer brushes onto lanthanide-doped up-conversion nanoparticles was conducted by Hu et al. PMMA layers were obtained after near infrared mediated RAFT polymerization. The authors pointed out that this efficient one-pot “grafting from” process could be also conducted in a vessel, which is shielded by a bio tissue barrier due to the good penetration performance of the near infrared laser.<sup>179</sup>

Finally, one example of photocatalytic surface-initiated polymerization is presented, which does not rely on SI-ATRP, SI-PIMP or SI-PET-RAFT mechanisms, but on self-initiation. Titanium dioxide (TiO<sub>2</sub>) is a photocatalyst, which has been widely applied for photovoltaics, nanoscience, biomedical fields and for the oxidative degradation of harmful organics upon light irradiation.<sup>180,181</sup> Excitation of TiO<sub>2</sub> with light in the range between 388 and 414 nm transfers electrons (labelled in red in Scheme 18) from the valence band to the conductive band, generating electron hole pairs as illustrated in Scheme 18. The free electrons as well the positive charge carriers migrate towards the surface and react with chemicals in the vicinity of the surface.<sup>182</sup> This was exploited by Wang et al. to produce core/shell composite nanospheres. To ensure covalent linkage between the TiO<sub>2</sub> core and the polymeric shell, the

particle surface was pretreated with 3-(trimethoxysilyl)propyl methacrylate, yielding surface coupled methacrylic functionalities (Ti-O-Si bond). These C=C bonds are expected to capture electrons generated by TiO<sub>2</sub> upon UV excitation, thus starting the polymerization reaction. With this method a PSt and PMMA shell was grown from the TiO<sub>2</sub> particle surface as shown in Scheme 18.<sup>183</sup>

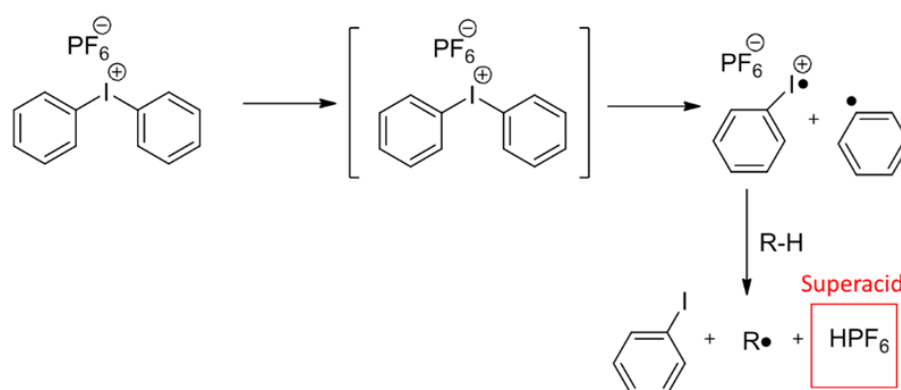


Scheme 18: Generation of inorganic/polymer nanocomposites via self-catalytic photopolymerization of pre-modified TiO<sub>2</sub> particles.

### 2.2.4 Coupled photoacids and photoacid generators

Radical photopolymerization, which has been covered in the previous chapters, exhibits some drawbacks. Firstly, oxygen inhibition by atmospheric oxygen can inactivate the propagation reaction. Secondly, radical photopolymerization suffers from volume shrinkage due to irradiation, which can have a severe influence on the structural material properties and, last but not least, the choice of monomers is generous but limited. Polymerizations, based on nucleophilic substitutions, including most ring opening mechanisms, as well as step growth polymerizations, cannot be initiated by radicals. Therefore, the photogeneration of a base or acid as catalyst is desirable.<sup>184</sup>

The phenomenon of photoacidity has been extensively studied since the pioneering work of Förster and Weller in the middle of the last century. Generally, there are two types of photoacids: photoacid generators (PAGs) and photoacids (PAHs). Photoacid generators, such as the prominent Crivello salts (first introduced in 1970) typically undergo irreversible cleavage reactions generating a strong Brönsted acid under UV irradiation (< 300 nm). The mechanism is shown in Scheme 19.<sup>184</sup>



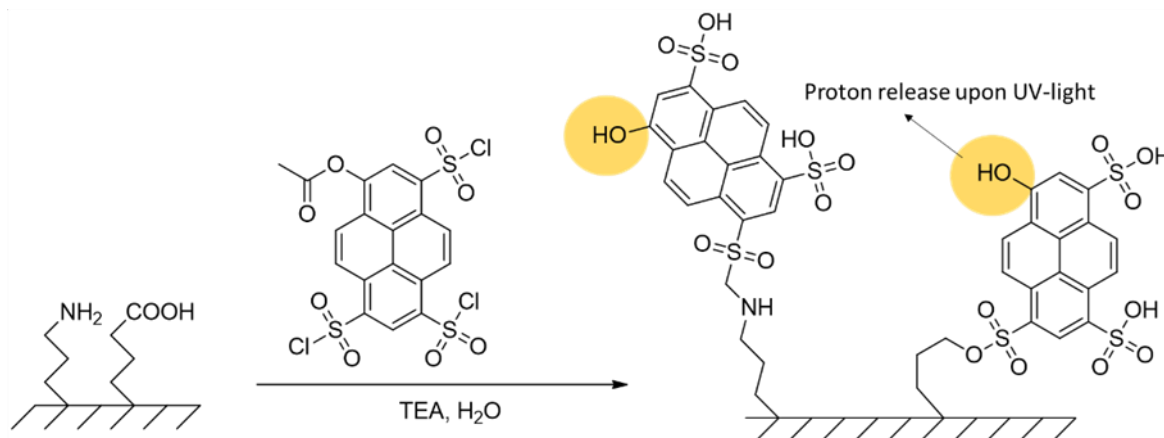
Scheme 19: Photolysis mechanism of a photoacid generator as described by Crivello.<sup>184</sup>

In contrast to PAGs, typical photoacids (PAHs) including aromatic alcohols, such as phenols, naphthols and pyrenols, do not decompose upon UV irradiation, but increase their acidity in the excited state. Upon UV irradiation of aromatic alcohols, an electron is removed from the non-bonding orbital located at the oxygen atom, and transferred into the lowest unoccupied molecular orbital, which is generally not located at the oxygen atom. Therefore, the electron density and — as a consequence — the basicity of the oxygen atom is reduced significantly. To give an example, the acidity of 2-naphthol becomes 107 times higher as a result of UV excitation.<sup>185</sup> In a similar way, a photobase undergoes an increase of the pKa value upon excitation, and excited state proton capture upon UV radiation is observed. A fundamental difference between PAG and PAH is that in the case of PAG the acidic moiety (i.e., a Brönsted acid such as HPF<sub>6</sub>) remains after termination of UV irradiation, which gives rise to so-called dark reactions. In contrast to this, the increased acidity of a PAH (e.g. pyrenol) vanishes when

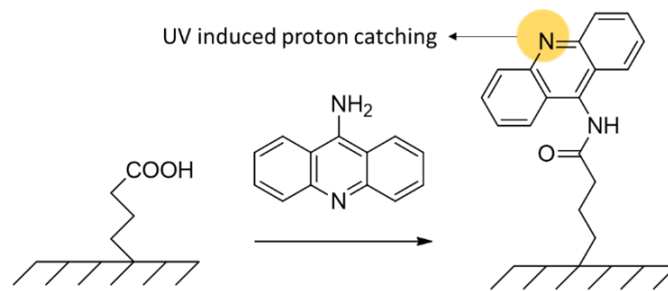
the light is cut off, because it recombines with the proton reaching its former state.<sup>186,187</sup>

This chapter is dedicated to surface coupled photoacids and photobases as well as photoacid generators. Surface tethered photobase generators have not been described in the literature as yet.

Quite recently (2021) and for the first time, Amdursky et al. explored the capability of biopolymer-tethered photoacids and photobases to conduct excited state proton transfer and capture, respectively. The authors used pyranine (8-hydroxypyrene-1,3,6-trisulfonic acid) as a Brønsted photoacid with a pKa-value of approximately 7.4 in the ground state and 0.3–1.3 in the excited state. To attach this molecule to the surface of electrospun mats, made of bovine serum albumin (BSA) proteins, the molecule was firstly reacted with thionyl chloride generating a triple electrophilic sulfonyl chloride derivative, which was attacked by amines and hydroxy groups from the surface, leading to sulfonamides and sulfonate esters, respectively (see Scheme 20). In a second part of the study, 9-aminoacridine as a photobase (pKa of 10.7 in the excited state) was employed to be coupled to the same surface. This molecule was coupled utilizing the reaction between amino groups of the photobase and carboxylic groups of the surface in the presence of a carbodiimide as a coupling agent, forming amide bonds (see Scheme 21). The results showed a change in the measured ionic conductivity upon UV irradiation, due to excited state proton transfer/capture of the surface tethered photoactive species.<sup>188</sup>



Scheme 20: Coupling strategy for a photoacid onto a surface.



Scheme 21: Coupling strategy for a photobase onto a surface.

Surface immobilized PAGs were described by Dai et al. in a recent US patent.<sup>186</sup> This strategy is based on PAGs which contain a polymerizable unit in the anion. Characteristic examples are (triphenylsulfonium) 3-sulfopropyl methacrylate and (triphenylsulfonium) 2,3,5,6-tetrafluoro-4-(methacryloyloxy)benzene, with both anions being derivatives of methacrylic acid. Those monomers were copolymerized with methacrylates bearing anchor units, such as glycidyl methacrylate or 3-(trimethoxysilyl)propyl methacrylate. The resulting copolymers, which comprised the PAG and the anchor unit were introduced to the surface of a semiconductor. The immobilized PAGs can then be used to pattern materials coated on top of the immobilized PAGs, allowing for direct patterning without the use of a photoresist, thereby reducing process steps and cost.



## 2.3 Immobilization of light-sensitive molecules for coupling reactions

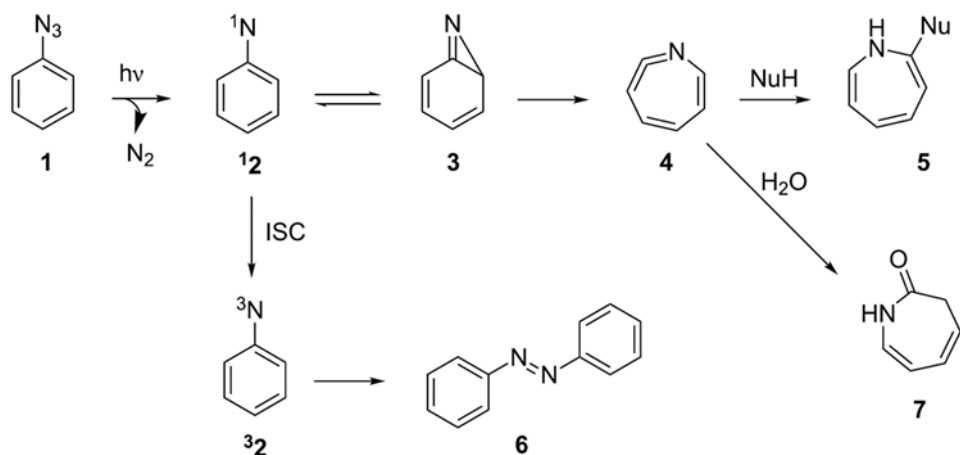
Since the beginning of modern chemistry, reactions which are accompanied by few or no side-reactions, high yield and well-defined linking reactions, are desired. For this, Sharpless et al. established the concept of so called “click reactions” in 2001. These reactions include: (i) cycloadditions (1,3- dipolar Huisgen-cycloadditions, Diels–Alder reactions), (ii) nucleophilic ring-opening of stressed electrophiles such as epoxides, (iii) reactions of non-aldol carbonyl compounds and (iv) the addition to carbon-carbon multiple bonds (in particular thiol-ene chemistry and Michael additions). Light induced click reactions combine the advantages of above mentioned click reactions with the benefit of photoinduced “grafting to” processes. The most important benefits are the temporal and spatial control of light-induced stimulation.<sup>189</sup> In this chapter, some prominent light induced click reactions between (polymer-) surface coupled initiating groups and different (polymer-) compounds in terms of the “grafting to” approach will be reviewed. It has to be mentioned that some reactions presented in the following do not always meet the strict conditions of click reactions. However, this does not mitigate their importance.

### 2.3.1 Coupled azides

Copper(I)-catalyzed azide-alkyne cycloaddition (CuAAC) between azides and terminal alkynes (developed by the Sharpless and Meldal groups) is an efficient, versatile and regiospecific click reaction which proceeds under mild conditions. There is more than one possibility to start the reaction, including direct and indirect photolysis. With respect to direct photolysis, a ligand coordinating Cu(II) center absorbs UV light, resulting in intramolecular electron transfer and the conversion of Cu(II) into Cu(I).<sup>189</sup> However, contributions found in the literature mainly include the indirect approach to catalyze azide-alkene click reactions including a free photoinitiator. Since the photoinitiator was not coupled to surfaces in those studies, these examples will not be presented in detail here.<sup>190–192</sup>

Phenyl azides are popular photosensitive compounds because of their high efficiency, fast reaction kinetics, high storage stability and their simplicity in synthesis [5]. Upon UV irradiation, phenyl azides (**1**) are converted into singlet nitrene (<sup>1</sup>**2**), a highly reactive intermediate, by splitting off molecular nitrogen. This singlet nitrene can either reach its triplet state (<sup>3</sup>**2**) via intersystem crossing (followed by further reaction pathways such as dimerization to diazo compounds (**6**)), undergo insertion or addition reactions with nucleophiles and rearrange (ring expansion) to form benzazirine (**3**), which in turn rearranges to didehydroazepine (**4**). The didehydroazepine itself readily reacts with secondary amines and other nucleophiles yielding the corresponding azepine (**5**). If the reaction is performed in water, 3H-azepinone (**7**) is typically generated. These reactions are summarized in Scheme 22. Generally, the product distribution of particular aryl azides is dependent on the experimental conditions and the substituents which are attached to the aromatic ring (electron-

withdrawing groups in para position to the nitrene lead to insertion and less rearrangement reactions).<sup>193,194</sup>



Scheme 22: Phenyl azide photochemistry.<sup>194</sup>

Photosensitive self-assembled monolayers of phenyl azides were covalently coupled to gold surfaces by Wollmann et al. in 1994, who synthesized a compound bearing a phenyl azide and a disulfide functionality (Figure 15 A). The reaction of excited phenyl azides with different secondary amines was exploited to form Au-confined derivatives of 3-H azepine and hydrazine. Furthermore, they demonstrated photopatterning by using azido functionalized Au surfaces and a liquid amine between the mask and the substrate.<sup>195</sup> About twenty years later, phenyl azide modified gold nanoparticles were produced by Snell et al., who synthesized a compound bearing both a phenyl azide and a thiol moiety (Figure 15 B). The high reactivity of the nitrenes, generated from the azide, was employed to tether the AuNP to the native surface of carbon nanotubes, reduced graphene oxide and micro-diamond powder to yield hybrid materials.<sup>196</sup>

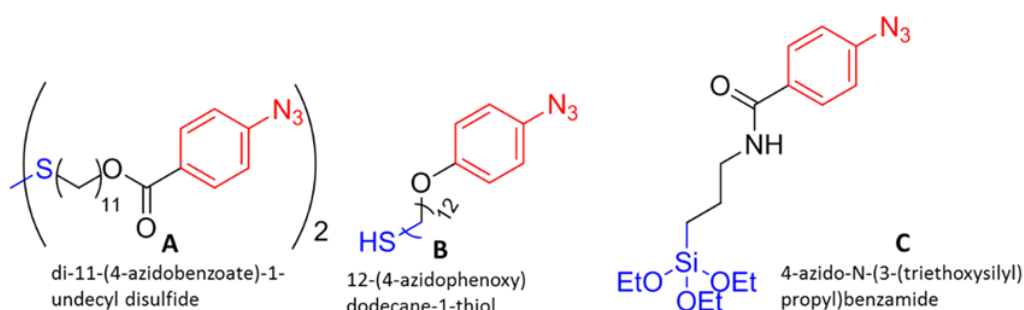
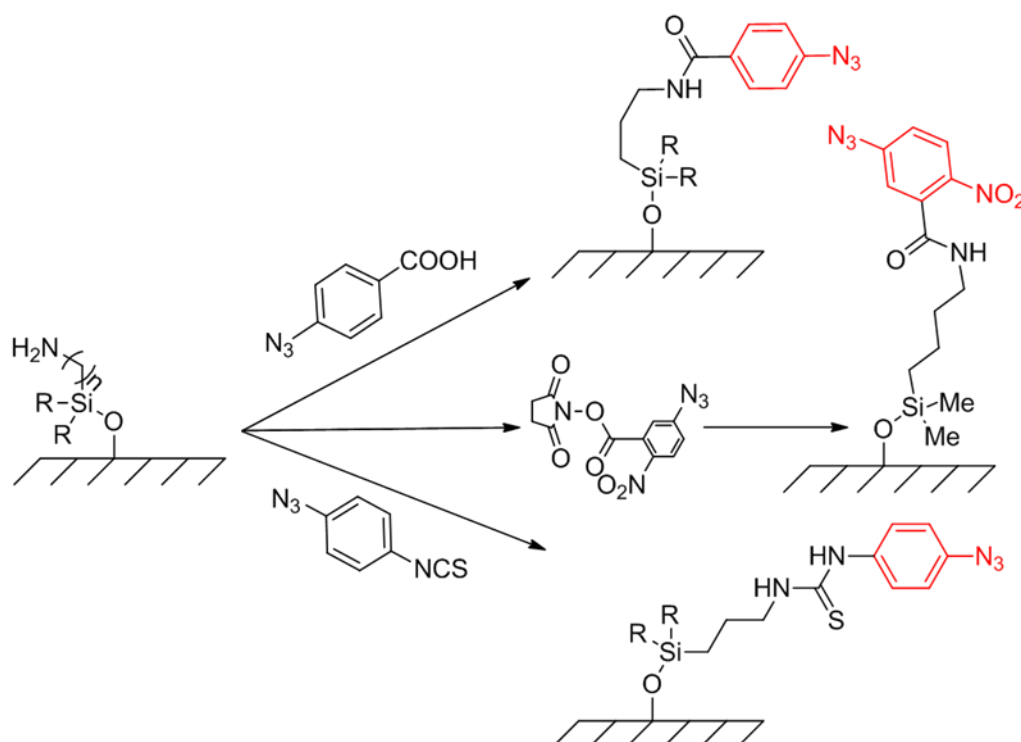


Figure 15: Phenyl azides (red) with anchor moieties (blue).

The preparation of ultrathin and hydrophilic polymeric cushions on glass slides and Si-wafer surfaces was done by Elender et al. Firstly, the corresponding surface was modified with amino groups by silanization with 4-aminobutyl-dimethyl-mono-methoxysilane, followed by the coupling of the phenyl azide moiety on the surface using N-5-azido-2-nitrobenzoyloxysuccinimide (see Scheme 23). Upon UV radiation, azide groups were converted into nitrenes which performed insertion reactions with hydroxyl groups from dextran achieving the covalent linkage of a reversibly swelling dextran film, which was found useful for biosensors.<sup>197</sup>



Scheme 23: Coupling strategies for phenyl azide (red) immobilization.

Azido terminated silica nanoparticles were prepared by Zhao and co-workers through upstream surface-modification of virgin silica nanoparticles with amino groups via silanization with APTES, followed by reaction with 4-azidobenzoic acid forming an amide bond (Scheme 23). To overcome the problem of small contact between spherical nanoparticles and the solid substrate during the immobilization, poly (allylamine hydrochloride) was also functionalized with phenyl azido groups via the reaction between sidechain amino groups and 4-azidobenzoic acid in the presence of a carbodiimide as coupling agent. After a layer-by-layer assembly, a tailored and crosslinked network was established among the silica nanoparticles, the surrounding polymer chains, and the substrate ( $O_2$ -plasma treated cotton fabrics) under UV irradiation, utilizing azide photochemistry. The authors pointed out that this strategy may be suitable to form stable nanoparticle coatings on almost any organic substrate.<sup>198</sup> Staying

with silica nanoparticles, Kern and colleagues prepared phenyl azide modified SiO<sub>2</sub> nanoparticles via the reaction between surface tethered amino groups and 4-azidophenyl isothiocyanate (Scheme 23). Photo-crosslinking experiments with poly (norbornene dicarboxylic acid, dimethyl ester) and polyisoprene revealed that these particles act as non-migrating photoinitiators. Moreover, the successful immobilization of the nanoparticles on virgin PET, polyethylene and polyamide surfaces upon UV radiation has been demonstrated.<sup>199</sup>

Recently, Picu et al. developed epoxy nanocomposites, which are reinforced with silica nanoparticles, also bearing phenyl azide groups at the surface.<sup>200</sup> In this context the mechanical properties of the filler-matrix-interface was controlled upon light exposure. For this, an azidophenyl-silane was synthesized (Figure 15 C) and grafted onto the surface through silanization. The received particles were mixed into epoxy resin systems followed by thermal curing. Cured samples containing the photosensitive filler displayed a strong decrease in toughness upon UV illumination. This photo-embrittlement results from the covalent coupling between the silica nanoparticles and the epoxy resin matrix, generating a strong interface. This is one of the few examples where the (photo)triggered change from a weak to a strong interface in a composite was evidenced by mechanical analysis.

Significant work was done by Yan and co-workers, who performed intense research on perfluorophenyl azides (PFPA) which were applied as photosensitive coupling agents in surface functionalization and nanomaterial synthesis. An important finding in the photochemistry of PFPA was that halogen atoms such as F or Cl on the aromatic ring significantly increased the lifetime, and suppressed ring expansion reactions of the singlet nitrene species. Therefore, the extent of insertion reactions was increased which was decisive to graft organic materials. Nitrenes generated from PFPA reacted with CH, NH and C=C bonds, so that the coupling chemistry is suitable for a broad range of molecules regardless of their structures, architecture and properties.<sup>201</sup> In some proof-of-concept experiments, SiO<sub>2</sub> surfaces were modified with a synthesized PFPA-trimethoxysilane (Figure 16 A). The UV grafting of PSt and PEOX to the surface was carried out after spin casting and followed by solvent extraction.<sup>202–205</sup> The UV-induced immobilization of highly crystalline materials such as isotactic PP and low molecular weight PEG did not work well with this method, since efficient insertion reactions require a close contact between the solid polymer and the surface azido groups. In this case, thermal activation was applied, melting the polymer film to increase surface-polymer interaction and simultaneously trigger the cleavage of the azido group.<sup>201,206</sup>

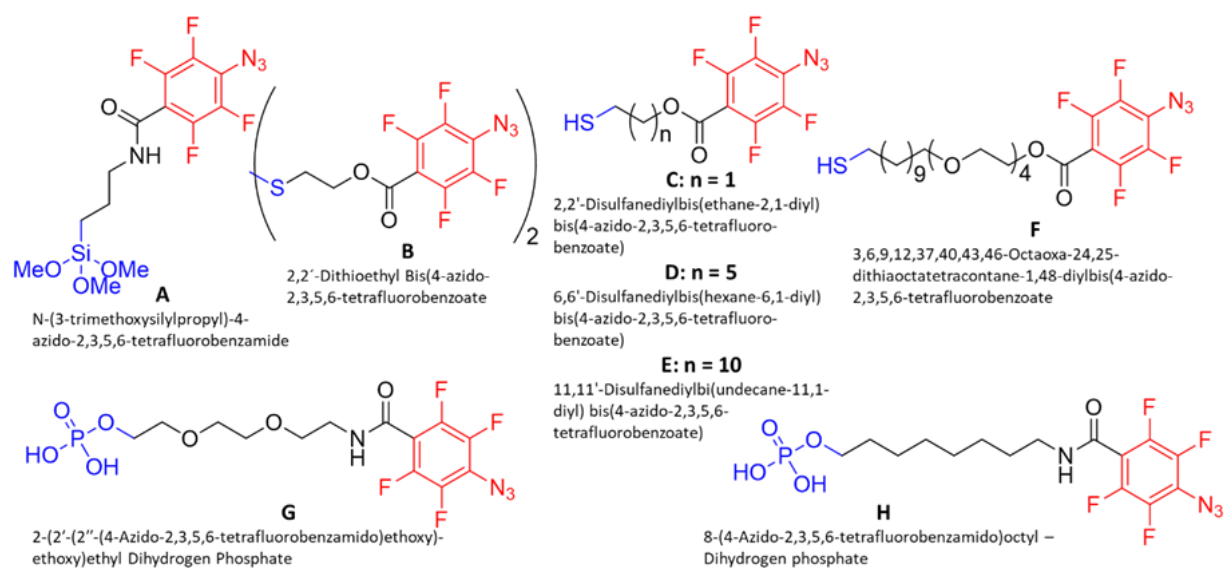


Figure 16: Perfluorophenyl azides (red) with anchor moieties (blue).

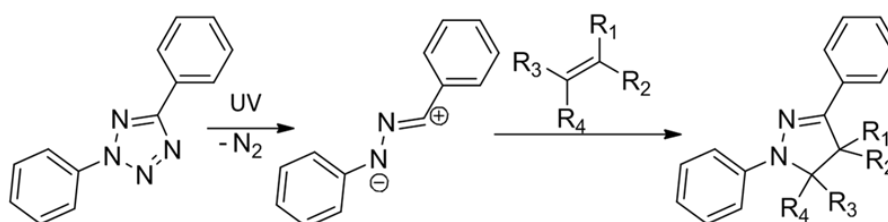
Aryl azide chemistry has also been used to generate biocompatible surfaces based on carbohydrates. Carbohydrates received high attention because of their interactions with proteins and other biological entities. Therefore, Pei et al. synthesized a novel compound, carrying a PFPA as well as a disulfide moiety (Figure 16 B), which was able to build a self-assembled monolayer on Au. This PFPA-derivatized surface was subsequently used to tether a thin layer of PEG upon thermal activation, because of the above-mentioned reasons. Carbohydrate-derivatized surfaces for selective protein binding were achieved, using different PFPA-derivatized carbohydrates, which coupled onto the surface upon UV irradiation via insertion reactions.<sup>207</sup> The scope of PFPA derivatized surfaces in biomedical applications was extended by the synthesis of four thiols (Figure 16C–F) with different chain lengths (spacer) containing hydrocarbon and ethylene oxide units between the thiol and the PFPA functionality. Gold nanoparticles were modified with these compounds followed by UV-coupling of different carbohydrates to study their interaction with proteins (binding affinity) depending on the size of the nanoparticle, spacer length, PFPA-density, etc.<sup>208</sup> The photochemical properties of PFPA were also employed to produce thin PEOX films on amino-functionalized glass slides by Pei et al. A monolayer of PFPA moieties was achieved by treating the aminosilylated glass slides with N-hydroxylsuccinimide-derivatized PFPA which was then irradiated with UV light after the PEOX film had been deposited. In the end, spatially addressable carbohydrate microarrays were produced through insertion reactions of PFPA derivatives in carbohydrates upon UV irradiation.<sup>209</sup> To modify (magnetic) iron oxide nanoparticles with carbohydrates for sensor applications, Yan and colleagues also synthesized two phosphate-functionalized PFPAs (Figure 16 G, H), which can both react with superficial hydroxyl groups to form a stable Fe-O-P bond.<sup>210</sup>

An efficient photocoupling agent, based on PFPA conjugated polyallylamine, was developed by Kuba et al. for the photo-induced immobilization of polymers (PSt, PEOX, poly(vinyl

pyrrolidone)), nanoparticles (PSt fluorescent silica nanoparticles), graphene and small molecules (carbohydrates) on Si-wafers, which were pre-modified with epoxy groups at the surface via silanization with 3-glycidyloxypropyltrimethoxysilane. The photocoupling agent was received through the reaction between amino groups of polyallylamine hydrochloride and N-hydroxysuccinimide-derivatized PFPA. The remaining amino groups were then used to covalently couple the reagent to the Si-wafer surface via the reaction with epoxides. The authors claimed a higher immobilization efficiency compared to PFPA-silane functionalized surfaces.<sup>211</sup>

### 2.3.2 Surface-attached tetrazoles

The concept of light-induced 1,3-dipolar cycloaddition of a tetrazole and an alkene was firstly shown in 1967 by Huisgen and Sustmann. Upon UV irradiation (302 nm) the tetrazole moiety decomposes by splitting off molecular nitrogen, leading into a highly reactive nitrilimine-intermediate. This intermediate, as can be seen in Scheme 24, readily reacts with electron-poor terminal alkenes such as (meth)acrylics, fumarates and alkynes through a 1,3-dipolar-cycloaddition forming stable, fluorescent pyrazoline products. The advantages of this chemistry include high quantum yield and reaction rate, the benefit that no metal catalysts are required and that this reaction is biorthogonal.<sup>189,212</sup>



Scheme 24: Schematic illustration of the photo-induced formation of the nitrile imine from tetrazole and following 1,3-dipolar cycloaddition with dipolarophiles.<sup>213</sup>

The nitrile imine-mediated tetrazole-ene cycloaddition reaction (NITEC) was exploited to graft polymers onto inorganic (silicon) and bioorganic (cellulose) surfaces, forming a highly fluorescent linkage under ambient conditions by Dietrich et al. Covalently coupled tetrazole moieties at the surface of cleaned and activated silicon wafers were obtained via silanization with a tetrazole silane (Figure 17 A). Subsequently maleimide-functionalized polymers were utilized to perform the NITEC reaction, leading to a surface tethered polymer film. Furthermore, within the same contribution, the authors synthesized a carboxy-containing tetrazole (Figure 17 B), which was coupled to the surface of cellulose materials via esterification. After grafting of the same maleimide containing polymers (maleimide served as the dipolarophile), highly fluorescent and patterned cellulose sheets were obtained.<sup>213</sup>

More recently, interfaces with precise control of cell adhesion were produced utilizing the NITEC reaction. Thus, a novel diaryltetrazole-initiator with an acid-chloride moiety (Figure 17 C) was synthesized, including an electron donating methoxy group in para position to the N<sub>2</sub>-phenyl ring increasing the reactivity of the nitrile-imine dipole within the NITEC mechanism. Furthermore, the methoxy group shifted the absorption spectrum from the UVC to UVA region (approx. 320 nm) allowing for the functionalization of more sensitive bio-systems. The photoinitiator was coupled to amino groups at polydopamine surfaces, followed by photo triggered NITEC of a maleimide-functional ATRP-initiator. Surface initiated photopolymerization of oligoethylene glycol methyl ether methacrylate leads to patterned cell-repellent surfaces.<sup>214</sup>

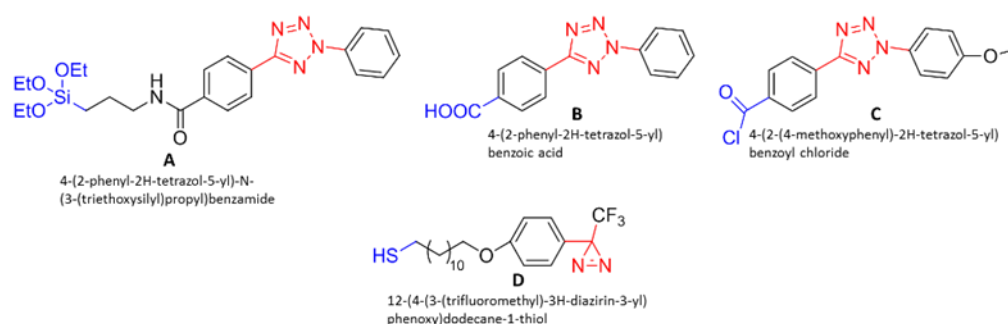


Figure 17: Tetrazole and diazirine compounds (red) which can be covalently coupled to surfaces using anchor moieties (blue).

### 2.3.3 Immobilized diazirines

Aryldiazirine compounds are well-known photocoupling agents, which were first described as photoaffinity probes in 1973 by Smith and Knowles. Among them, 3-aryl-3-(trifluoromethyl)diazirine received attention because of its high thermal and chemical stability and, in addition, its advantageous photochemical properties. Upon exposure to UV light the diazirine species generates a highly reactive carbene intermediate (by splitting of molecular nitrogen) which can undergo insertion reactions with X-H groups (X = C, O, N) or addition reactions with alkenes. Furthermore, an isomerization leading to azo-compounds is also observed.<sup>215,216</sup>

Ismaili and co-workers extensively used diazirine photochemistry to couple diazirine modified Au nanoparticles onto hydroxylated diamond powder via insertion of hydroxyl groups. In a similar way, carbon nanotubes were functionalized via an addition reaction to the  $\pi$ -conjugated carbon skeleton. Furthermore, reduced graphene and glass were functionalized via addition and insertion reactions. As an example, Au nanoparticles were modified using a thiol bearing diazirine derivative (Figure 17 D).<sup>216–219</sup>

Kanoh et al. employed diazirine modified glass slides to immobilize structurally distinct and small molecules with specific protein-binding abilities by UV irradiation. For this concept, the authors prepared a linker bearing both an amino group (as anchor) and the photosensitive diazirine moiety. For preparing photosensitive surfaces, amino functionalized glass slides were treated with N,N-disuccinimidyl carbonate to yield succinimidyl groups at the surface. These groups were then reacted with the diazirine compound, thus providing diazirine units covalently coupled to glass.<sup>220</sup>



## 2.4 Summary

In section 2 it has been shown that the attachment of photoinitiators and other photolabile units to surfaces is a versatile tool, in most cases aiming at the functionalization of surfaces. The large variety of initiators available nowadays provides different possibilities, taking into account the wavelength of excitation, the avoidance of unwanted side reactions and the strength of the generated bonds. Generally, the employed substrate governs the coupling reaction for immobilization of the initiator. Consequently, silane chemistry is found most frequently with respect to oxidic surfaces of metals and ceramics, and for surfaces of gold, silver and copper thiol chemistry has been utilized exhaustively.

In most cases, light-initiated surface reactions are employed to cover surfaces with polymeric layers by grafting-from approaches, to attach functional surface layers onto (nano)particles, to confer hydrophilicity and antifouling properties onto plastic surface, and to achieve the covalent coupling of different phases. Nanoparticle immobilized initiators enable the initiation of photopolymerization by non-migrating photoinitiators, and it has been shown that they can outperform their parent compounds.

The utilization of UV and visible light is of general advantage when mild reaction conditions are required, when thermally sensitive materials such as biomaterials have to be processed and when the reaction has to be performed in a very short interval.

Whilst most of the surface coupled initiators belong to the group of free radical initiators, comparably little research has been performed with surface immobilized photoacid and photobase generators. This is remarkable as it would provide the possibility to generate acidic (or basic) surfaces under UV irradiation, and to initiate cationic or anionic polymerizations at surfaces. This is certainly a field which has to be unlocked in the future.

## 3 Experimental Part

### *Disclaimer*

Chapter 4.1 as well as the respective description of the applied methods reproduces for the most part the original article “Nanoparticles bearing germanium based photoinitiators at their surface: Preparation and use in grafting-from photopolymerization reactions”. DOI: <https://doi.org/10.1016/j.apsusc.2024.160035>

Chapter 4.2 as well as the respective description of the applied methods reproduces for the most part the original article “Surface-Initiated Polymerizations Mediated by Novel Germanium-Based Photoinitiators”. DOI: <https://doi.org/10.1021/acsami.3c05528>

Both research articles are open-access, distributed under the terms and conditions of the Creative Commons Attribution (CC BY) license. I affirm, under penalty of perjury, that I retain the rights to reuse these publications in their entirety for this dissertation and hereby explicitly declare this intention.

### 3.1 Materials

N,N-diisopropylethylamine (99%, DIPEA), anhydrous toluene (99.8 %), anhydrous tetrahydrofuran (99.9 %, THF) fluorescein-o-acrylate (97 %, FIACr), 1-pyrenemethyl methacrylate (99 %, PyrMAcr), acrylamide (99 %, AAm), hydrofluoric acid (48 %), tetraoctylammonium bromide (98 %, TBAB), diphenyliodonium hexafluorophosphate (99 %, DPIHFP), bisphenol A diglycidylether (97 %, DGEBA) and 1H,1H,2H,2H-perfluorodecyl acrylate (97 %, PFAcr), 1,6-hexanedithiol (97%, HDT), 1,3,5-triallyl-1,3,5-triazin-2,4,6(1H,3H,5H)-trion (98 %, TTT), cyclohexane oxide (98 %, CHO), n-propylvinyl ether (99 %, nPVE) were all purchased from Sigma Aldrich. Hexafluoroisopropanol (99 %, HFIP) was purchased from ABCR. Tetrahydrofurfuryl acrylate (98 %, THFA) was obtained from TCI chemicals (Shanghai, China). Anhydrous dichloromethane (99 %, DCM) was obtained from VWR chemicals.

Optically polished quartz plates were obtained from Korth Kristalle GmbH (Altenholz, Germany), and silicon wafers with one polished side were kindly provided by Infineon Technologies Austria AG (Villach, Austria). Silica nanoparticles (spherical, 184 nm in diameter) were purchased from General Engineering and Research (San Diego, USA). Smaller silica nanoparticles (spherical, 30 nm in diameter (measured by SEM)) were purchased from Sigma Aldrich.

Germanium-based photoinitiators including bromo-tris(2,4,6-trimethylbenzoyl)germane (compound **1**), ethoxy-tris(2,4,6-trimethylbenzoyl)germane (compound **2**), hydroxy-tris(2,4,6-trimethylbenzoyl)germane (GeOH), ethyl-tris(2,4,6-trimethylbenzoyl)germane (GeEt) and tetrakis(2,4,6-trimethylbenzoyl)germane (Tetra) were provided within a cooperation by the group of M.Haas (institut of inorganic chemistry, TU-Graz). Ivocerin was purchased from Ivoclar Vivadent GmbH (Austria) und used without any further purification.

## 3.2 Methods

### 3.2.1 Surface functionalization of silica nanoparticles with bromo-tris(2,4,6-trimethylbenzoyl)germane (compound 1)

Herein, silica nanoparticles with two different particle diameters (30 and of 184 nm, measured by SEM), were modified. In a first step, the particles were pre-activated by etching with an alkaline solution, according to the method given by Zhang et al.<sup>221</sup> In a typical procedure, 700 mg of silica particles were immersed in 60 mL of water and ultrasonicated for at least 30 min until a homogeneous dispersion was observed. Subsequently, 4 mL of an aqueous solution of potassium hydroxide (50 mg mL<sup>-1</sup>) was added, and the mixture was vigorously stirred for 24 hours at 20°C. After that, the mixture was centrifuged, washed with deionized water for multiple times until the pH was constant, and finally washed with ethanol to remove excess water. Ethanol was then allowed to evaporate at 100 °C before the particles were weighed and dried under vacuum at 120 °C overnight. In our previous experiments this procedure proved to be the most efficient activation method to generate a large number of surface-hydroxyl units when compared to other methods such as corona-discharge. This was evidenced by the immobilization of aminopropyltriethoxy silane at the surface of the activated particles. More information on that topic can be found in the Bachelor's Thesis of **Leonie Wenk** (*"Funktionalisierung von Silica-Nanopartikeln mit neuartigen Germanium-basierten Photoinitiatoren zur Polymerisation von Acrylaten"*, University of Leoben, 2023).

For surface-functionalization with the germanium-based compound **1**, the activated particles were transferred into a glove box, and dispersed in THF (8 mg particles per mL THF) by grinding with a glass rod and stirring. The same amount of compound **1** (13.5 mM) in respect to the particle weight and DIPEA (0.66 µl per mg of compound **1**) were added, and the mixture was stirred under exclusion of light at 60 °C for 24 h. The modified particles were centrifuged for 1 h at 4000 rpm, and re-dispersed in anhydrous THF via ultrasonication for 5 min. This cycle was repeated two times with anhydrous THF and one time with anhydrous toluene. Finally, the functionalized particles were dried under vacuum at 20°C, and stored under the exclusion of light.

### 3.2.2 Surface-initiated photopolymerization of 1H,1H,2H,2H-perfluorodecylacrylate (PFACr) and styrene from silica nanoparticles

Photopolymerizations were carried out with styrene and PFACr, respectively. For "grafting from" reactions with PFACr, the monomer was diluted with freshly distilled and degassed THF (50 /50 vol.-%). Functionalized particles were added so that the particle concentration was 15 mg mL<sup>-1</sup>. The mixture was stirred until a homogenous dispersion was achieved, followed by illumination under constant stirring and nitrogen flow for three minutes. Here, a LED light source (Opsytec Dr. Gröbel, Germany) emitting light between 370 and 450 nm (peak maximum at 405 nm) was employed. The applied light intensity was 137 mW cm<sup>-2</sup> (41 J cm<sup>-2</sup> as measured

with a spectrometer from Ocean Inside, Germany). After photopolymerization the grafted particles were carefully washed with HFIP conducting three redispersion (ultrasonication for 15 min) and centrifugation cycles. Using a similar technique, distilled and degassed styrene was diluted with anhydrous and oxygen-free toluene in various quantities to investigate the effect of the monomer concentration on the average molar mass of the grafted polystyrene chains as well as on the grafting density. Three different solutions of styrene in toluene (100 vol.-%, 50 vol.-%, and 25 vol.-%) were prepared, and nanoparticles functionalized with compound **1** were added (2.5 mg mL<sup>-1</sup>). The mixtures were homogenized and illuminated as described above. After that, the nanoparticles were separated by centrifugation, washed with toluene, and finally dried.

#### **3.2.3 Surface-initiated radical promoted cationic polymerization (SI-RPCP) of n-propyl vinyl ether (nPVE) and cyclohexane oxide (CHO)**

For SI-RPCP experiments anhydrous conditions are mandatory. Therefore, **1**-modified nanoparticles (30 nm in diameter) were carefully dried, and the used solvents as well as the monomers were distilled over CaH<sub>2</sub> and transferred into the glove box. The solvents were additionally stored over molecular sieves and filtered with a syringe filter before usage. The used glassware was heated well above 100 °C using a heat gun, evacuated and also stored in the glove box. For particle drying, the samples were heated to 100 °C in the glove box after which they were transferred into the vacuum lock and evacuated until a temperature of 23 °C was reached. This cycle was then repeated for two more times. This was done to prevent the particles from coming into contact with ambient air. The iodonium salt (DPIHFP) was also dried under vacuum and stored in the glove box.

##### SI-RPCP with nPVE

In a typical standard procedure for SI-RPCP with nPVE at 23 °C, 100 mg of **1**-modified nanoparticles were dispersed in 8 mL of anhydrous DCM/toluene (6/2 mL) containing 200 mg of dissolved DPIHFP. The mixture was stirred for 1 h until a homogeneous mixture was obtained. Next, an illumination with 450 nm (LED light source, Opsytec Dr. Gröbel, Germany) for 8 minutes (35 mW cm<sup>-2</sup>, 17 J cm<sup>-2</sup>) was performed in the glove box under constant stirring. Thereafter, 200 µL of nPVE was added dropwise (*caution: The cationic polymerization of vinyl ethers is highly exothermic and can be explosive*). In that way a reaction between germyl radicals and the monomer can be excluded. A similar procedure was carried out at lower temperatures, so that the mixture was cooled to -30 °C after the illumination step, and prior to monomer addition, using a liquid nitrogen cooled acetone bath. The polymerizations were allowed to proceed for one hour under inert gas atmosphere. Subsequently, the samples were centrifuged (1 h at 3000 rpm) and washed with fresh DCM (ultrasonication for 5 minutes) before repeated centrifugation. In total, this washing cycle was conducted for 3 times.

Regarding monomer addition experiments with nPVE in order to elucidate if some living character can be achieved, the procedure was similar for both polymerization temperatures as described above. The only exception was that after 1 hour in each case 25 vol.-% of the

mixture was removed followed by the addition of further 200  $\mu\text{L}$  of monomer. In total two times 200  $\mu\text{L}$  of monomer was added (batches 2 and 3). Last but not least, 400  $\mu\text{L}$  nPVE was added for the third and last monomer addition step and the mixture was continuously stirred for another 60 minutes. Finally, all batches (4 in total) were then washed with DCM (sonication and centrifugation cycles) as mentioned above.

Moreover, two control experiments were elaborated with nPVE, aiming to confirm the SI-RPCP (proof of principle). For the first one, the standard SI-RPCP procedure at 23  $^{\circ}\text{C}$  was repeated with the exception that no iodonium salt (DPIHFP) was used. Hence, it was expected that no p(nPVE) can be grafted-from the surface, since no cationic germanium-based species can be formed in that case. For the second one, pristine nanoparticles (30 nm in diameter) along with Ivocerin (20 mg) and 200 mg of DPIHFP as a free initiating system were employed instead of **1**-modified nanoparticles, again for the standard SI-RPCP procedure (23  $^{\circ}\text{C}$ ). This was done in order to test if any polymer can be surface-attached via the reaction between free cationic propagating chains and surface silanol groups. The non-coupled polymer in the DCM-toluene solution was separated from the nanoparticles by centrifugation. The supernatant was collected and the solvent was removed under reduced pressure. The polymer was re-dissolved in diethyl ether and non-dissolved DPIHFP was then removed via filtration. Diethyl ether was removed and the obtained polymer was dried at 60  $^{\circ}\text{C}$  overnight and appeared as highly viscous and slightly yellow coloured material.

#### SI-RPCP with CHO

Epoxides cannot be polymerized by means of radical mechanisms. Therefore, the monomer was used as a solvent when SI-RPCP with CHO was carried out. In doing so, 100 mg of dried 30 nm sized nanoparticles bearing trisacylgermanium units at their surface were carefully dispersed in 8 mL of CHO, containing 200 mg of DPIHFP. SI-RPCP was triggered with visible light (450 nm), again for 8 minutes using the same light source. Subsequently the mixture was stirred for 4 hours before washing. The washing procedure was also similar to those applied in the experiments using nPVE. Furthermore, this procedure was repeated without DPIHFP as a reference.

For reasons of comparison, p(CHO) was homopolymerized using GeEt and DPIHFP as initiating species. 2 mL of monomer were diluted with 2 mL of anhydrous DCM, and 80 mg of GeEt and 126 mg of DPIHFP (1 eq. to GeEt) were added. After exposing to visible light (LED light source, 450 nm, 8 min, 5 cm distance) the reaction was quenched with ammonia after one hour. The polymer was re-precipitated twice from methanol and dried at 60  $^{\circ}\text{C}$ . The solid product appeared in slightly yellow colour.

#### **3.2.4 De-grafting of polystyrene with hydrofluoric acid**

72 mg of polystyrene-grafted particles were ultrasonicated in 10 mL of toluene in a PTFE tube before 6 mL of deionized water and 1230  $\mu\text{L}$  of HF (48 %) were added (*caution: HF is extremely*

*corrosive and etching*). Ultimately, 8.6 mg of tetraoctylammonium bromide, acting as a phase transfer catalyst, was added as suggested in the literature.<sup>222</sup> After 24 h of vigorous stirring at room temperature, ammonium hydroxide (25 % in water) was used to neutralize HF until a pH value of 7 was measured. The mixture was then transferred into a separation funnel. The organic phase was separated, and centrifuged for 1 h at 4000 rpm in order to remove solid residuals. After that, the organic phase was washed with deionized water for three times. Toluene was removed using rotary evaporation, and the solid material was refluxed in methanol for the sake of purification (30 min). After cooling to room temperature, methanol was removed and the pure polystyrene was characterized by FT-IR spectroscopy, TGA and SEC.

### 3.2.5 Calculation of the polymer content as well as initiator and polymer grafting density

The amount of coupled polymer, per unit area ( $\sigma_{mg}$ , mg m<sup>-2</sup>) on the particles was determined by TGA and SEC data, and calculated according to equation 1. In TGA, only the weight losses between 200 and 900 °C were considered to eliminate the contribution of physically adsorbed water or other volatile components.

$$\sigma_{mg} = \frac{\Delta m_{mod,200-900^{\circ}C} - \Delta m_{pristine,200-900^{\circ}C} * \frac{m_{mod,900^{\circ}C}}{m_{pristine,900^{\circ}C}}}{3 * \frac{m_{mod,900^{\circ}C}}{\rho * r_{etched}}} \dots \dots \dots (1)$$

In this equation,  $\Delta m_{mod,200-900^{\circ}C}$  and  $\Delta m_{pristine,200-900^{\circ}C}$  are the weight losses of polymer grafted and pristine particles between 200 and 900 °C, respectively. Furthermore,  $m_{mod,900^{\circ}C}$  and  $m_{pristine,900^{\circ}C}$  are the final weights of polymer coated and neat particles after heating up to 900 °C,  $\rho$  represents the density of silica nanoparticles, which is 2 g cm<sup>-3</sup><sup>223</sup>, and  $r_{etched}$  is the particle radius of alkaline etched particles. Note that the size of alkaline treated particles (30 nm in the pristine state, measured by SEM) could not be reliably determined by SEM. In this case  $r_{etched}$  was mathematically approximated based on SEM data, which was obtained for the 180 nm sized nanoparticles before (184 nm) and after etching (133 nm). In this manner a diameter decrease of 27 % was observed for the bigger particles, which was then taken into account to approximate the particles size of the etched nanoparticles with 30 nm in the pristine state ( $r_{etched} = 10.87$  nm). Moreover, the grafting density ( $\sigma_{chains}$ , chains per nm<sup>2</sup>) was calculated by taking the molar mass Mn (number average), which was obtained from SEC measurements, and the Avogadro constant  $N_a$  into account (see equation 2).

$$\sigma_{chains} = \frac{\sigma_{mg} * N_a}{Mn} \dots \dots \dots (2)$$

The number of photoinitiating moieties at the particle surfaces ( $\sigma_{PI}$ ) was estimated using data from UV-Vis spectroscopy, according to equation 3. Here,  $E_{390}$  and  $E_{450}$  are the values for the extinction at 390 and 450 nm (maximum of the  $n/\sigma - \pi^*$  transition), observed for particles functionalized with compound **1**,  $\varepsilon_2$  is the molar decadic absorption coefficient of compound **2** at 390 nm ( $1150 \text{ L mol}^{-1} \text{ cm}^{-1}$ , see Figure 54), and  $c_{\text{Particles}}$  is the concentration of the particles in the solution.

$$\sigma_{PI} = \frac{\frac{E_{390} - E_{450} * Na}{\varepsilon_2}}{3 * \frac{c_{\text{Particles}}}{\rho * r_{\text{etched}}}} \dots \dots \dots (3)$$

Furthermore, the theoretical initiator density ( $\sigma_{PI,theo}$ ) was approximated based on the space requirements for a single coupled trisacylgermanium moiety on the condition of almost equal molecular conformations, as observed through X-ray crystallography analysis of compound **1**.<sup>224</sup> For each of the three acyl groups, the maximum right-angled distance to the respective hydrogen atom of the corresponding mesityl group was determined graphically, starting from the germanium center (Ge-Br bond, in y-direction). This is depicted in Figure 18, and the mean distance was found to be  $6.5 \pm 0.5 \text{ \AA}$ . For measuring those distances, the software “Mercury 3.7” was employed.

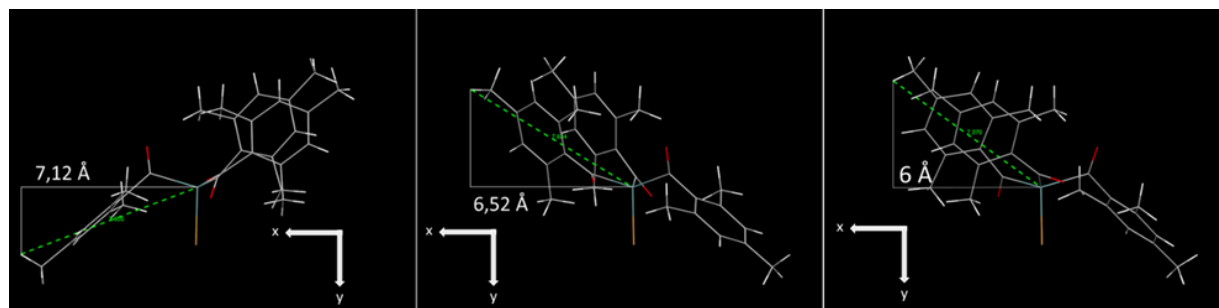


Figure 18: Molecular expansion in x-direction based OTREP of compound **1** (CCDC 2233933). OTREP data was downloaded from the “Cambridge Crystallographic Data Centre”.

Assuming an intermolecular non-bonded contact distance of two neighboring hydrogen atoms of about  $2.4 \text{ \AA}$  (hydrogen van der Waals radius of  $1.2 \text{ \AA}$ ),<sup>225,226</sup> each coupled molecule claims a distance radius of  $7.75 \text{ \AA}$ , from which a circular area of  $1.89 \text{ nm}^2$  can be concluded. A circular area can be assumed since each of the three acyl groups is oriented in a different direction as shown in Figure 19. Therefore, the theoretical maximum photoinitiator density  $\sigma_{PI,theo}$  is found with  $0.53$  molecules per  $\text{nm}^2$ .

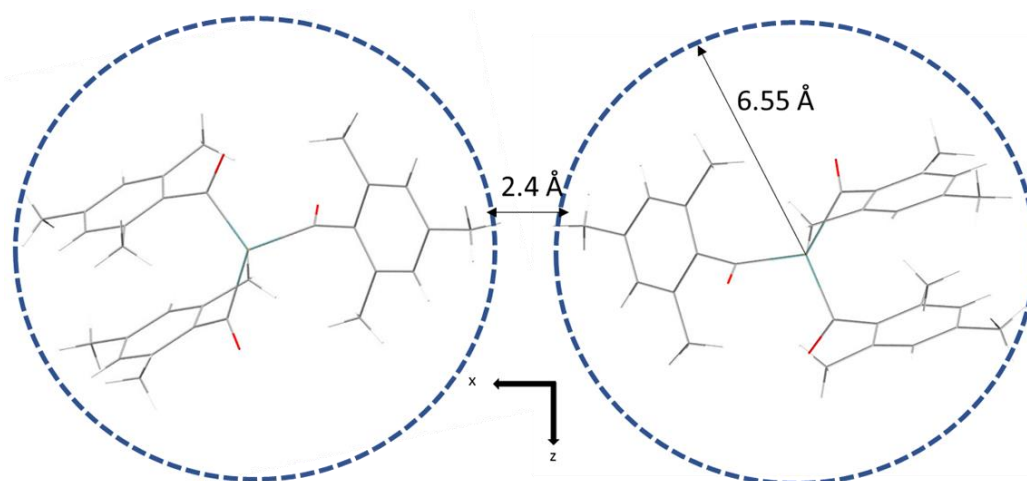


Figure 19: Model for the calculation of  $\sigma_{PI,theo}$  for the trisacyl germanium photoinitiator (compound **1**).

### 3.2.6 Surface functionalization of silicon substrates and quartz plates with bromo-tris(2,4,6-trimethylbenzoyl)germane (compound **1**)

Silicon wafers and quartz plates were immersed in acetone and isopropanol, respectively, and ultra-sonicated in each solvent for 10 min. After washing, both types of substrates were pre-treated by exposure to oxygen plasma using a plasma etching system from Oxford Instruments (Abingdon, United Kingdom). The treatment was carried out for 2 min with 100 W, 0.05 mbar oxygen pressure and an oxygen flow of  $50 \text{ cm}^3 \text{ min}^{-1}$ . For the quartz plates, this treatment was repeated to activate both the top and bottom side of the plates. Silicon wafers were treated on the polished, reflecting side only.

The activated substrates were then immediately immersed in a filtered THF solution of compound **1** ( $45.45 \text{ mmol L}^{-1}$ ). Additionally, an excess of Hünig's base (diisopropylethylamine, 2.4 equiv.) was added to scavenge hydrogen bromide in order to avoid unwanted side reactions. The reaction was carried out under exclusion of light and under inert gas atmosphere at  $60 \text{ }^\circ\text{C}$  for 24 h. After the coupling process, the samples were washed with anhydrous THF and toluene for multiple times.

### 3.2.7 Surface-initiated photopolymerization of fluorescent monomers from 1-functionalized quartz plates

The functionalized quartz plates were placed in a 50 mL round flask (made from borosilicate glass) containing a solution of 1-pyrenylmethyl methacrylate or fluorescein-o-acrylate (PyrMAcr or FlAcr, both  $353 \text{ mmol L}^{-1}$ ) in distilled and degassed THF. Subsequently, the samples were illuminated with  $\lambda = 405 \text{ nm}$  through the flask under inert gas atmosphere for 10 min. Here, the same LED light source (Opsytec Dr. Gröbel, Germany) was used, and the distance between light source and sample was 5.5 cm (light intensity of approximately 420



mW cm<sup>-2</sup> at the sample surface). After illumination, the samples were washed thoroughly for three times (2 min each) with THF under ultra-sonication.

Those experiments as well as respective UV-Vis and fluorescence measurements were carried out by **Lisa Reisinger** as part of her diploma thesis (*“Oberflächen-initiierte Polymerisation von Monomeren mit Fluoreszenzeigenschaften”*, Chemie Akademie – Kolleg für Chemie, 8055 Graz, 2022).

#### **3.2.8 Surface-initiated photopolymerization of non-polar and polar monomers from 1-functionalized silicon wafers**

Films of poly(1H,1H,2H,2H-perfluordecyl-acrylate) (p(PFAcr)) and poly(acrylamide) (p(AAm)) were grafted from silicon wafers bearing the initiating group at the surface. Therefore, the functionalized silicon wafers were placed in an illumination chamber equipped with a gas in- and outlet, and a quartz window for illumination from top. Then, the respective monomer was drop coated onto the functionalized wafer. While PFAcr was used without dilution, AAm was diluted with EtOH (50 mg of AAm in 200 µl of EtOH). After drop coating, the chamber was closed and flushed with nitrogen for several minutes. Surface initiated photopolymerization was then carried out upon irradiation with  $\lambda = 405$  nm at a distance of 5 cm for 1 min (PFAcr, 650 mW cm<sup>-2</sup>) or 1,5 min (AAm), respectively. Finally, the samples were ultra-sonicated (a) for 2 min in HFIP, DCM and acetone for p(PFAcr), or (b) for 10 min in EtOH for p(AAm), respectively, to remove non-attached homopolymer.

#### **3.2.9 Spatially resolved photopolymerization of 1H,1H,2H,2H-perfluordecyl-acrylate and acrylamide from 1-modified silicon wafers**

Spatially resolved polymer films of p(PFAcr) were generated on 1-modified silicon wafers. In a first step, the immobilized germanium-based photoinitiator on the surface was locally deactivated by UV exposure. Therefore, the silicon wafers were covered by a photomask and irradiated under ambient conditions with  $\lambda = 405$  nm at a distance of 5 cm for 20 s, employing the same lamp as described before. After 10 min the sample with the photomask on top was irradiated again for 20 s with the same parameters. This cycle was then repeated for one more time so that the final illumination time was 60 s (light intensity at the sample surface 650 mW cm<sup>-2</sup>, light dose of about 39 J cm<sup>-2</sup>). This procedure (procedure A) proved to be the most efficient one in order to locally deactivate the photo-initiating species and to deliver the best resolution. Since no monomers or other species were placed between the sample and the mask during the deactivation step, it is assumed that oxygen from the air is needed to react with the surface-radicals produced by the photoinitiator upon illumination. By interrupting the illumination for 10 min, oxygen is allowed to diffuse between the sample surface and the photomask. In order to investigate the resolution depending on the experimental setup, two more procedures for the spatial deactivation of the photoinitiator were elaborated. For procedure B the intensity was decreased to 39 mW cm<sup>-2</sup> along with an increase of the

continuous illumination time up to 30 minutes (final light dose of approximately  $70 \text{ J cm}^{-2}$ ). Procedure C comprised a continuous illumination with 405 nm at a distance of 5 cm for 60 s ( $650 \text{ W cm}^{-2}$ ,  $39 \text{ J cm}^{-2}$ ).

After one of these spatially resolved deactivation steps, surface-initiated photopolymerization was carried out in the illumination chamber as described above. It has to be mentioned here, that the monomer was drop coated all over the wafer. However, photopolymerization was only possible at the regions, which were shielded during the deactivation step, and thus still contained active photoinitiator groups. Finally, the samples were ultra-sonicated for two minutes in HFIP (three times), and one time in DCM and acetone, respectively.

In addition, also polymer films with combined structures of p(PFAcr) and p(AAm) were prepared on silicon wafers. For this purpose, functionalized wafers were placed in the illumination chamber, drop coated with AAm (dissolved in EtOH; 50 mg in 200  $\mu\text{L}$ ) and covered by a photomask. The surface-initiated photopolymerization was carried out under inert gas atmosphere as described above. Subsequently, the partially surface-modified wafers were ultra-sonicated in EtOH for 10 minutes, and dried at 60 °C. In a second step, the structured wafers were again placed in the chamber and drop coated with PFAcr. Another surface initiated photopolymerization step was carried out under the same conditions as described for the polymerization of PFAcr. Finally, the samples were ultra-sonicated in HFIP, DCM and acetone (2 min each), and subsequently dried.

**Benjamin Sydor** and **Amelie Krug**, who both succeeded in completing their Bachelor's Theses, contributed a lot due to their experimental work, which is described in the chapters 3.2.8 and 3.2.9 (**Benjamin Sydor**: Bachelor's Thesis "Oberflächeninitiierte Photopolymerisation mit Germanium-Photoinitiatoren", University of Leoben, 2022; **Amelie Krug**: Bachelor's Thesis "Surface initiated Photopolymerization of Acrylamide by immobilized Germanium-based Photoinitiators", University of Leoben, 2022).

### 3.3 Characterization methods

#### 3.3.1 FT-IR Spectroscopy

Infrared spectroscopy was conducted using an FT-IR spectrometer Vertex 70 from Bruker Optics (Germany). The FTIR spectra of silica-nanoparticles bearing a grafted polymer were recorded from solid samples, using either ATR or transmission mode. Prior to measuring in transmission, the material was placed on clean silicon wafers, from which the background measurements were taken. The herein synthesized homopolymers, including polystyrene, p(PFAcr), p(CHO) etc., as well as other synthesis products were all measured in ATR mode. Each measurement was conducted with a total number of 32 scans at a resolution of  $1\text{ cm}^{-1}$ .

#### 3.3.2 XPS Spectroscopy

The chemical composition of the sample surfaces (flat samples as well as nanoparticles) was analysed by XPS at room temperature using a Nexsa G2 Surface Analysis System from ThermoFisher Scientific with monochromatic Al K $\alpha$  radiation. Survey scans were carried out at a pass energy of 200 eV and an energy resolution of 1.0 eV, whilst high-resolution spectra were recorded at a pass energy of 50 eV and a resolution of 0.1 eV. The C 1s line was used to calibrate the binding energy scale for the measurements, assuming a binding energy of 284.8 eV for C-C bonds. Hydrogen is omitted in the calculation of the surface composition. For each sample, at least two measurements with a spot size of 100 to 200  $\mu\text{m}$  were conducted. For mapping laterally structured polymer layers on silicon wafers, two elements were mapped: fluorine (centre energy 689.5 eV) and silicon (centre energy 103 eV). The map size was 2 x 2 mm, and the spot size was 200 x 200  $\mu\text{m}$ .

All the herein provided XPS measurements including data processing were kindly performed by **Dr. Christine Bandl** (University of Leoben, Chair of Chemistry of Polymeric Materials, 8700 Leoben).

#### 3.3.3 UV-Vis Spectroscopy

UV-Vis absorption spectra were recorded with a Cary 50 UV-Vis spectrometer from Varian (Australia), which was equipped with a xenon-flashlight lamp.

For characterizing the fluorescent polymer films, which were grafted from the quartz surfaces, the samples were placed on a proper sample holder for transmission measurements. Since the polymerization process is expected not to significantly change the absorption properties of the chromophore moiety, the absorption spectra of the grafted polymer films were compared to those of the corresponding monomers in solution, which were measured in THF using a 1 cm quartz cuvette. From these data, the molar absorbance of the respective monomers was calculated. The same was done for the herein presented germanium-based compounds.

For characterization of initiator-modified nanoparticles, the samples were dispersed in THF using ultrasonication for at least 20 min, and measured in a 1 cm quartz cuvette. Notably, when measuring these colloidal solutions, significant extinction due to light scattering occurred over the entire wavelength range,<sup>227</sup> which superimposed the absorbance of the initiating species in the range between 350 and 460 nm. To overcome this, the photo-bleaching properties of the immobilized acyl germanium units were exploited. Illumination with 405 nm light caused a complete depletion of absorbance in the wavelength region 350 – 460 nm as a result of the photo-decomposition of the germanium-based initiator. Therefore, a second UV-Vis measurement, acting as a blank, was recorded after irradiation of the colloidal dispersion with 405 nm light ( $650 \text{ mW cm}^{-2}$ ,  $390 \text{ J cm}^{-2}$ ) for 10 min. The scattering contribution was then eliminated by subtraction of the blank, and the optical absorbance caused by the presence of the acyl germanium moieties was obtained.

Polymer-covered nanoparticles, derived from cationic grafting-from polymerization of nPVE, were dispersed in DCM for 5 minutes under sonication, and subsequently measured using the same instrument and cuvette as described above.

Photo-bleaching experiments (steady state photolysis) were carried out on a TIDAS UV-Vis spectrometer (J&M, Germany). For measuring, DCM-solutions of GeEt (0.54 mM) with and without DPIHFP (1 eq.) were prepared and put into a quartz cuvette (1 x 1 cm). The samples were continuously stirred and irradiated with 405 nm using a low-power LED light source (30 mW, Roithner Lasertechnik, Austria), while the absorption spectra were recorded every 10 seconds.

#### 3.3.4 Fluorescence Spectroscopy

Fluorescence emission spectra of the polymer coated quartz plates were investigated using a Cary Eclipse spectrometer (Varian; Australia). The samples were excited by UV irradiation with a scan rate of 600 nm per minute. For this purpose, the quartz plate covered with poly(fluorescein-*o*-acrylate) was excited at 405 nm, and the plate covered with poly(pyrenylmethylmethacrylate) was excited at 347 nm. In general, the intensity of the fluorescent signals of the coated quartz plates are strongly dependent on the geometric position of the plates in the sample holder. Therefore, these measurements only provided qualitative information. The recorded fluorescence spectra were compared to the fluorescence spectra of the corresponding monomers in THF solution.

#### 3.3.5 Contact angle measurements

The contact angles of water (WCA) on the flat sample surfaces were recorded at room temperature with a drop shape analyzer (DSA 100, Krüss GmbH, Germany). Ultrapure water droplets with a volume of 2  $\mu\text{l}$  were deposited on the sample surfaces, and evaluated using the software “Drop Shape Analysis” from Krüss GmbH. The WCA was averaged over two or three measurements on each sample.

### 3.3.6 Spectroscopic ellipsometry

Ellipsometric measurements were performed, employing polymer grafted silicon wafers, in order to determine the thickness of the deposited polymeric layers. An ex-situ variable angle spectroscopy ellipsometer (model M-2000 from J.A. Woollam Corp., Lincoln, USA) was used for these measurements.

### 3.3.7 Thermogravimetric analysis (TGA)

The modified nanoparticles, in any stage of modification, were also investigated by means of TGA. The measurements were conducted with a TGA/DSC 3+ from Mettler Toledo (USA). Measuring both particle sizes (30 and 180 nm), the procedure comprised three steps. In the first step, the samples were heated from room temperature to 190 °C at a heating rate of 10 K min<sup>-1</sup> under nitrogen flow (10 mL min<sup>-1</sup>). After this, the samples were kept at 190 °C for 60 min under a constant nitrogen flow of 10 mL min<sup>-1</sup> in order to remove physically adsorbed water and other volatile components. The last step comprised heating from 190 to 900 °C at a heating rate of 10 K min<sup>-1</sup> under nitrogen flow (10 mL min<sup>-1</sup>). The obtained data was processed using Microsoft Excel.

### 3.3.8 Photo differential scanning calorimetry (photo-DSC)

In order to prove the capability of particles functionalized with compound **1** to act as initiating species in polymerization reactions, photo-DSC measurements were conducted, employing a Photo-DSC 204 F1 Phoenix (Netzsch, Germany) equipped with an S1500 A Hg lamp (Omniculture, United Kingdom) as the UV radiation source (320-500 nm). For these measurements, a filter was employed to ensure radical generation with light in the spectral range 400-500 nm. In this respect, selected amounts of compound **1** (0.1 wt.-%) or photoactive nanoparticles with 30 nm in diameter (3.1 wt.-%), were mixed with either THFA or a thiol-ene resin system, which consisted of 1,6-hexanedithiol (HDT, 1 eq.) and 1,3,5-triallyl-1,3,5-triazin-2,4,6(1H,3H,5H)-trion (TTT, 0.66 eq.).

To compare the efficiency of the photoactive particles to those of the parent (uncoupled) photoinitiator (compound **1**), UV-Vis data was considered in order to calculate which mass of photoactive particles results in the same absorbance at 390 and 450 nm as 1 mg of compound **1** (uncoupled PI). This conversion factor ( $\chi=31$ ) was approximated according to equation 4. In this equation  $c[\text{Particles}]$  is the concentration of photoactive particles in THF during the UV-Vis measurements,  $E_{\text{Particles},390}$  and  $E_{\text{Particles},450}$  are the corresponding absorbance values at 390 nm and 450 nm,  $\varepsilon_1$  and  $M_1$  are the molar decadic absorption coefficient (1985 L mol<sup>-1</sup> cm<sup>-1</sup>) and molar mass (594 g mol<sup>-1</sup>) of compound **1**, respectively.

$$\chi = \frac{c[\text{Particles}]}{\frac{E_{\text{Particles},390} - E_{\text{Particles},450}}{\varepsilon_1} * M_1} \dots \dots \dots (4)$$

In photo DSC experiments, the prepared samples (10-15 mg) were illuminated twice at 25°C for 5 min with a light intensity of about 230 mW cm<sup>-2</sup> at the sample surface. A one-minute idle phase was performed between those two illumination steps. In order to obtain the reaction enthalpy curve, the second run was subtracted from the first one. The double bond conversion (DBC) was calculated for THFA by dividing the measured polymerization heat  $\Delta H$  by the theoretical heat ( $\Delta H_{\text{theo}}$ ) of acrylates, which is 86 kJ/mol.<sup>228</sup> Moreover, the maximum of reaction rate  $R_{p,\text{max}}$  was calculated according to equation 5. In this equation  $h$  and  $\rho$  are the maximum height of the exothermic signal and the density of THFA at room temperature, respectively.

$$R_{p,\text{max}} = \frac{h}{\rho * \Delta H_{\text{theo}}} \dots \dots \dots (5)$$

In order to evaluate the capability of different germanium-based compounds to induce cationic polymerization of DGEBA along with the iodonium salt (diphenyliodonium hexafluoro phosphate, DPIHFP), photo-DSC measurements were carried out. For that Ivocerin, compound **1**, ethyl and hydroxy substituted trisacylgermanes (GeEt, GeOH) and the tetracylgermane (Tetra) were taken into account. Prior to the measurements, the respective germanium-based molecule (1 mol.-% with respect to the monomer) and 1 eq. of DPIHFP (1 mol.-%) together with DGEBA (98 mol.-%) were dissolved in anhydrous DCM (0.8  $\mu\text{L}$  per mg monomer). After constant stirring for at least one hour, the solvent was removed under reduced pressure at 50 °C. Next, the samples (10-15 mg) were transferred into the photo-DSC device and measured. The programme comprised seven steps: I) Sample heating from 23 – 50 °C at a rate of 10 K min<sup>-1</sup>, II) keeping this temperature for 4 minutes, III) illumination with light in the wavelength range between 380 and 480 nm for 2 minutes, IV) idle phase of 10 minutes keeping the sample at 50°C, V) repetition of the illumination step, VI) again keeping at 50 °C for 10 minutes, and finally VII) cooling down to 20 °C. To extract the reaction enthalpy curve, steps V and VI were subtracted from III and IV.

Photo-DSC measurements for the cationic polymerization of DGEBA were undertaken by **Yijing Wang** and **Yansen Tang** as part of their Bachelor's Theses (Yijing Wang: Bachelor's Thesis "*Radical Promoted Cationic Photopolymerization Mediated by Surface-coupled Germanium-based Photoinitiators*", University of Leoben, 2023; Yansen Tang: Bachelor's Thesis in progress at University of Leoben, 2024).

Another important contribution was made by **Benjamin Holter** for his diploma thesis, who also performed multiple photo-DSC measurements for the described radical polymerization techniques ("*Photohärtung von Acrylharzen mit neuartigen Photoinitiatoren*", Chemie Akademie – Kolleg für Chemie, 8055 Graz, 2023).

### 3.4 Scanning electron microscopy (SEM)

Pristine, NaOH etched and polymer coated nanoparticles were imaged by employing a Crossbeam 340 SEM supplied by Carl Zeiss, Germany. Prior to measurement, the samples were dispersed either in toluene (pristine, etched and polystyrene modified nanoparticles) or in HFIP (p(PFAcr)-grafted nanoparticles), and drop cast onto freshly cleaned silicon wafers. After the solvent was evaporated, the samples were transferred into the SEM and investigated with regard to morphology and particle size (aperture 20  $\mu\text{m}$ , in-lens SE detection)

### 3.5 Size exclusion chromatography (SEC)

For quantification of the grafting density, SEC measurements were performed for all de-grafted polystyrene samples. In doing so, SEC was conducted employing a system provided by Shimadzu, which was equipped with two separating columns from MZ-Gel SDplus (500 and 100 A, linear 5  $\mu\text{m}$ ) as well as an UV (SPD-20A) and RI detector (RID-20A). THF was chosen as the eluent. The polystyrene standards were purchased from Polymer Standards Service (PSS; Mainz, Germany). Before measuring, each solution was filtered through a syringe filter (PTFE, 0.45  $\mu\text{m}$ ). Additionally, reference measurements of the eluent (THF) were carried out, because *di-tert.*-butylhydroxytoluene was added to the solvent as internal standard.

### 3.6 Time-of-flight secondary ion mass spectrometry (TOF-SIMS)

Additional chemical information on the nanoparticles' surface composition was obtained from time-of-flight secondary ion mass spectrometry (ToF-SIMS). For this purpose, nanoparticles (30 nm in diameter) bearing p(St) as well as p(PFAcr) graft layers were measured, and compared to freshly prepared p(St) and p(PFAcr). For the synthesis of the homopolymers p(St) and p(PFAcr), 2 mL of styrene or PFAcr, respectively, were mixed with 2 mL of distilled and degassed THF and 50 mg of AIBN. The polymerization was carried out at 80°C under inert gas atmosphere for 12 hours. The homopolymers were precipitated from methanol, and washed with methanol for multiple times.

ToF-SIMS measurements were carried out at Tascon GmbH (Münster, Germany). The samples were mounted on a polysiloxane-free adhesive substrate and transferred into the instrument (TOF.SIMS5 supplied by IONTOF GmbH, Münster, Germany). The spectra, utilizing a 30 keV  $\text{Bi}^{3+}$  primary beam, were captured for both secondary positive and negative ions, with masses ranging from  $m/z = 0$  to  $m/z = 800$ . Prior to analysis, the obtained spectra were processed in Origin (OriginPro 2022b), and normalized relative to the maximum detected signal.

## 4 Results and Discussion

This section comprises three parts. Regarding the surface modification of silica nanoparticles (chapter 4.1), the focus was set on i) the immobilization of a difunctional germanium based (type I) photoinitiator (compound **1**), equipped with a bromine unit, and ii) subsequent visible light induced surface-initiated photopolymerization (SIPP) reactions leading to organic/inorganic hybrid nanomaterials. Furthermore, the achieved grafting density, which is a crucial parameter for applications, will be discussed in detail and compared to theoretical values.

In chapter 4.2, modification of flat substrates, e.g. optically polished quartz plates and silicon wafers, with functional surfaces (e.g., high and low hydrophilicity as well as fluorescence) are reported, also in a spatially resolved manner.

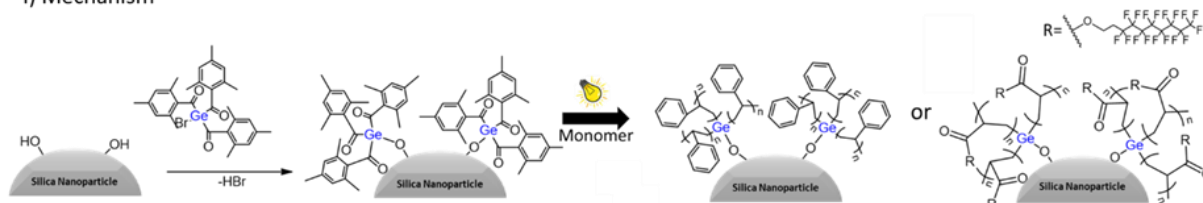
The third chapter (4.3) describes a so called surface-initiated radical promoted cationic photopolymerization (SI-RPCP), which is a unique and novel method, reported for the very first time. This is again based on nanoparticles bearing covalently coupled photosensitive germanium-based units at their surface. Emphasis is placed on the overall proof of principle. Please note that the syntheses of the employed acylgermanes were not elaborated by the author of this thesis, and will therefore be not presented herein. A discussion on the synthesis of bromo-tris(2,4,6-trimethylbenzoyl)germane (compound **1**) can be found elsewhere.<sup>224</sup>

### 4.1 Surface-initiated radical photopolymerization, mediated by photoinitiator-functionalized silica nanoparticles

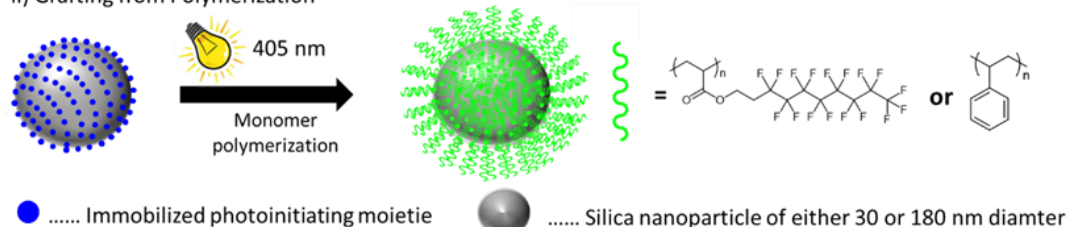
In this section a straightforward and convenient technique to modify silica nanoparticles with a polymer-brush shell via a visible light induced “grafting-from” polymerization, which is illustrated in Scheme 25, is reported. In doing so, a novel and highly efficient, germanium-based photoinitiator (bromo-tris(2,4,6-trimethylbenzoyl)germane, compound **1**) was covalently coupled to the surface of spherically shaped silica nanoparticles with either 30 or 180 nm in diameter, and employed to induce radical polymerization reactions of styrene (St), 1H,1H,2H,2H-perfluorodecyl acrylate (PFACr), tetrahydrofurfuryl acrylate (THFA) and a thiol-ene resin system upon illumination with visible light (405 nm). Styrene was grafted from the silica nanoparticles under different conditions, varying the monomer concentration during photopolymerization (see experimental section). This allowed to investigate the impact of monomer concentration on the final polymer content, the average molar mass of the grafted polymer, and the polymer grafting density. In order to determine the grafting density, the SiO<sub>2</sub> cores were removed by etching with hydrofluoric acid, leaving the de-grafted p(St) homopolymer behind, which was then characterized by size exclusion chromatography (SEC), also see Scheme 25.



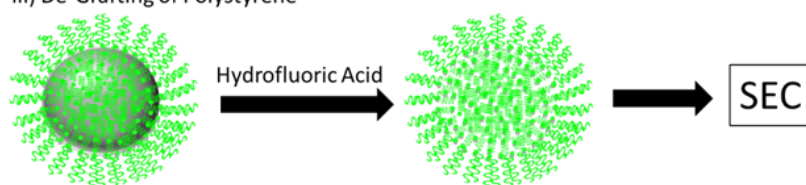
## i) Mechanism



## ii) Grafting from Polymerization



## iii) De-Grafting of Polystyrene



Scheme 25: Schematic illustration of the immobilization of compound **1** onto spherically shaped silica nanoparticles (top row), subsequent surface-mediated photopolymerizations of styrene and PFACr respectively (middle row) and de-grafting of the polymer shell (bottom row).

#### 4.1.1 Surface-functionalization of silica nanoparticles with light sensitive units

For the functionalization of the silica nanoparticles with acyl germanium units, the first step comprised etching with an aqueous NaOH solution, leaving the particle surfaces with an increased number of geminal and isolated silanol moieties. This was proven via  $^{29}\text{Si}$ -NMR and Sears titration studies in the literature.<sup>229,230</sup> After this activation step, the immobilization of compound **1** was achieved by dispersing and stirring the particles in a THF solution containing compound **1** and DIPEA. The reaction followed the proposed nucleophilic substitution pathway according to Scheme 25. This proposed mechanism was concluded from literature reports on the reactions of alcohols with bromo-substituted germanes, yielding the respective alkoxy and hydroxy derivatives in the presence of bases.<sup>231</sup> Additionally, this pathway was supported by the formation of a tertiary ammonium salt (N-ethyl-N-isopropylpropan-2-ammonium bromide) from DIPEA and hydrogen bromide, which in turn is a side product of the reaction between surface hydroxyl groups and compound **1**. The tertiary ammonium salt was characterized with FTIR spectroscopy, showing a set of sharp and strong absorption bands at 2684, 2664, and 2618  $\text{cm}^{-1}$ , which were assigned to hydrohalide  $\text{N-H}^+$  stretching vibrations.<sup>232</sup> The respective FTIR spectrum is depicted in Figure 20.

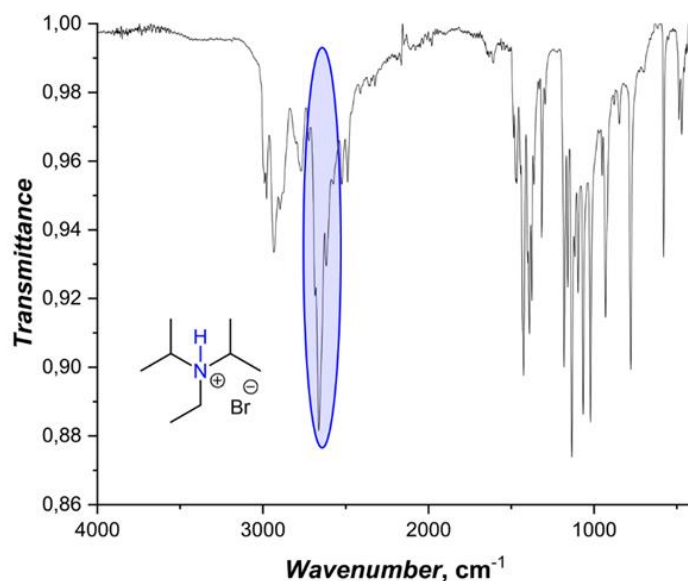


Figure 20: FTIR spectrum of the side-product (tertiary ammonium salt) during immobilization of compound **1** onto nanoparticle surfaces.

The successful functionalization of nanoparticles with compound **1** was proven by XPS analysis, that confirmed the presence of germanium (Figure 21, Ge 2p<sup>1/2</sup> and Ge 2p<sup>3/2</sup> detected at 1220 and 1250 eV, respectively) and the absence of bromine (Figure 21, 69 eV) at the corresponding surfaces, again supporting the reaction pathway mentioned above.<sup>233</sup> Furthermore, the elemental surface composition of the particles prior to and after modification are also compared in this Figure. Germanium was found to contribute 0.4 at.-% to the overall elemental surface composition, whereas the carbon content of approximately 20 at.-% exceeded the theoretical value of 12 at.-%. The theoretical value is based on the fact that every coupled light-sensitive moiety consists of 30 carbon atoms per germanium atom (Ge/C = 1/30). However, as can be seen in Figure 21, 8.8 at.-% of carbon species are detected at the surface of pristine SiO<sub>2</sub> nanoparticles, which indicates an incomplete hydrolysis of the alkoxide precursor during the particles synthesis.<sup>234</sup> When subtracting this amount (8.8 at.-%) from 20 at.-%, the surface composition of the functionalized particles perfectly meets the theoretical Ge / C ratio. In addition, characteristic signals of silicon (Si 2p at 103 eV and Si 2s at 155 eV) and oxygen (533 eV) as well as some trace impurities (Na 1s at 1071 eV) were also detected.

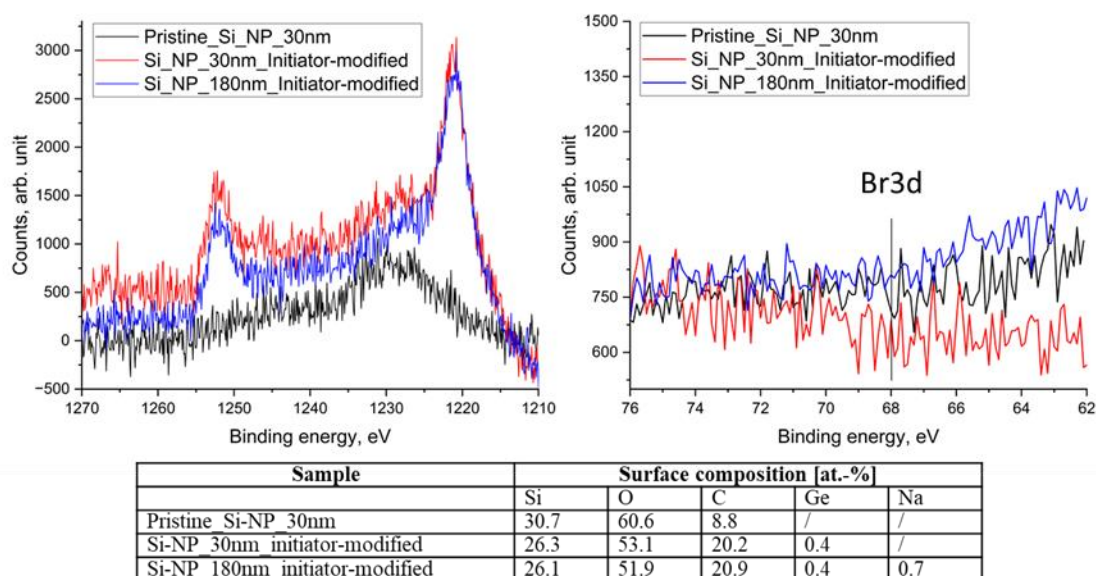


Figure 21: High resolution XPS spectra of germanium (Ge 3p), left) and bromine (Br 3d, right) for pristine and modified silica nanoparticles including the percentage atomic surface composition.

In addition to XPS investigations, the light absorption of photoactive nanoparticles was analysed by UV-Vis measurements. Figure 22 depicts the original and processed spectra, where the light absorption of trisaclygermanium moieties was filtered out via the subtraction of the photo-bleached blue curve from the original black one. When measuring, a change in the curve shape was observed over the whole spectrum, which suggests the presence of agglomerated particles. The size of the agglomerates coincided with the wavelength of light, resulting in scattering effects, and consequently reducing the detected light intensity.<sup>235</sup> Agglomeration is a well-known problem when using nanoparticles in multiple applications, as it reduces the surface area to volume ratio. This effect is not limited to silica-based materials, and is usually the more pronounced the smaller the particles are.<sup>236,237</sup> The higher agglomeration tendency for smaller nanoparticles was also found in this work, based on the fact that a steeper rise of the absorption curve was seen for 30 nm sized nanoparticles, when compared to that of 180 nm nanoparticles at the same concentration (compare black and blue curves in Figure 22).

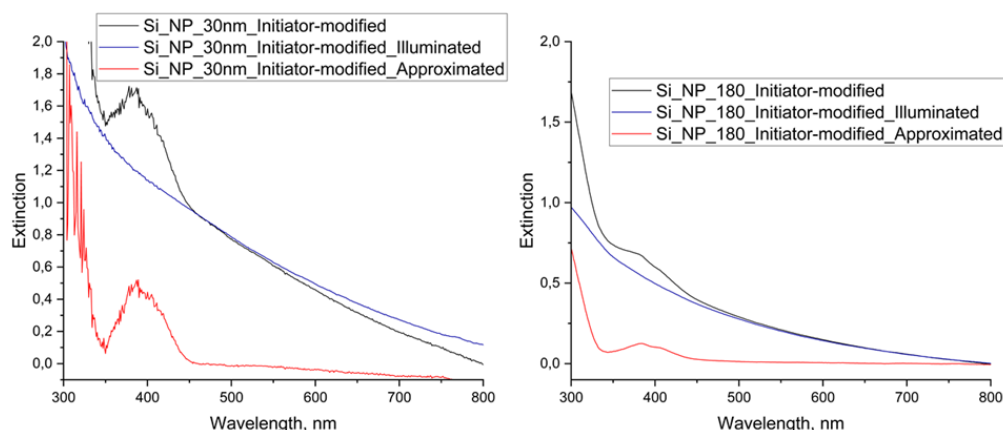


Figure 22: UV-Vis absorption measurements of photoinitiator-modified nanoparticles (Left: 30 nm particles; right: 180 nm particles,  $c = 4.7 \text{ mg mL}^{-1}$ ). The red trace was obtained by subtraction of the blue curve from the black curve.

However, Figure 23 clearly reveals significant visible light absorption of the **1**-modified nanoparticles between 460 and 350 nm, which was assigned to the immobilized triacyl germanium moieties, due to the shape and position. For comparison, the absorption spectrum of the parent initiator is also included in Figure 23 (compound **1**, black dash-dotted curve). Notably, the signal of the modified 180 nm sized particles (blue curve in Figure 23), which is shown on the secondary y-axis, is approximately 5 times weaker. This is due to the lower specific surface area when compared to the 30 nm sized particles. Furthermore, differences in the curve shape (noisy shape of the red curve) can also be seen, which may be a consequence of unequal agglomeration tendencies.

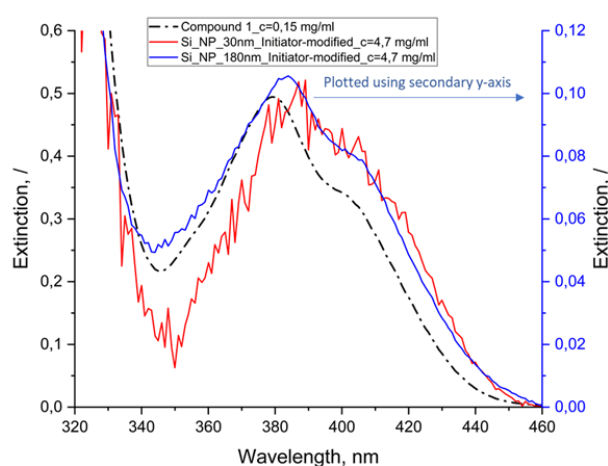


Figure 23: UV-Vis spectra of functionalized nanoparticles (red and blue curve) and the parent initiator (compound **1**, black dash-dotted line). Please note that the blue curve refers to the secondary y-axis.

#### 4.1.2 Surface-initiated photopolymerization (SIPP) from silica nanoparticles and characterization of the polymeric shell

In order to prove the capability of the tethered photoinitiator to start free radical polymerization reactions, photo-DSC measurements were performed initially. Therefore, functionalized particles (30 nm in diameter) were dispersed in either tetrahydrofurfurylacrylate (THFA) or a thiol-ene resin system (TTT+HDT) (3.1 wt.-%), followed by an illumination step with visible light (400 - 500 nm). As described in the experimental section, formulations with calculated quantities of compound **1** (0.1 wt.-% to achieve equal light absorbance according to UV-Vis) were also prepared as reference samples to compare the curing kinetics of free and immobilized initiating species. In this context, kinetic parameters including the maximum polymerization rate ( $R_{p,max}$ ) and the time at which 95% of the final conversion was reached ( $t_{95\%}$ ), were determined. Moreover, the monomer conversion was calculated for THFA from the overall reaction enthalpy  $\Delta H$  (peak area) and the theoretical polymerization heat of acrylates  $\Delta H_{theo}$ , which is 86.2 kJ mol<sup>-1</sup> according to literature.<sup>29,228</sup> As can be concluded from Figure 24 and Table 3, the polymerization kinetics differ significantly when functionalized nanoparticles were used as initiating species, resulting in a remarkably lower reaction rate with a decrease of  $R_{p,max}$  by nearly 45 % and an increase of  $t_{95\%}$  by a factor of two. It is proposed that those deviations are again caused by the optical properties of agglomerated silica nanoparticles. Similar to our observations regarding UV-Vis measurements, scattering effects may interfere during photopolymerization, leading to a decreased light intensity and curing depth.<sup>235,238</sup> Besides, the monomer conversion seemed to be rather low in both cases (free and immobilized photoinitiator). However, considering the low amount of initiating species (0.1 wt.-% of parent initiator compound **1** correspond to 0.026 mol.-%), the conversion is in good accordance with comparable photo-active systems described in the literature.<sup>29</sup>

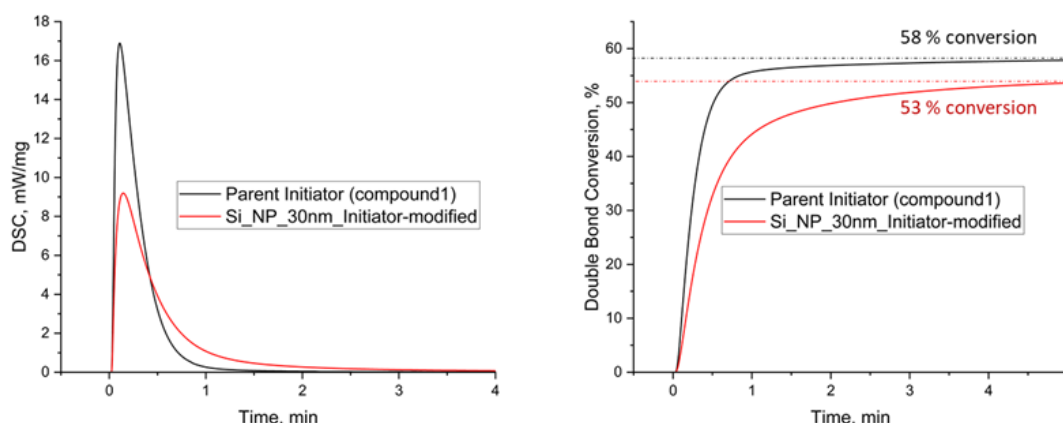


Figure 24: Photo-DSC curves (left) and double-bond conversion plot (right) for photopolymerization of THFA with 0.1 wt.-% of parent initiator (compound **1**, black curve) and 3.1 wt.-% of nanoparticles (30 nm diameter) functionalized with compound **1** (red curve).

Table 3: Results of DSC measurements with THFA and comparison of kinetic parameters including maximum reaction rate ( $R_{p,max}$ ) and time to reach 95% of the final conversion ( $t_{95\%}$ ).

	$\Delta H$ [J g <sup>-1</sup> ]	h [mW mg <sup>-1</sup> ]	$t_{95\%}$ [min]	$R_{p,max}$ [mol L <sup>-1</sup> s <sup>-1</sup> ]
Parent Initiator	320.3 ± 13.5	17.6 ± 0,6	0.96 ± 0.23	0.218 ± 0
Si-NP_30nm_Initiator-modified	296.7 ± 19.5	9.9 ± 1	2.26 ± 0.43	0.123 ± 0.012

Notably, photo-DSC measurements additionally proved that **1**-modified nanoparticles can also be employed in thiol-ene systems. The results are given in Figure 25 and Table 4. Due to the above discussed reasons, the polymerization kinetics differ, revealing a slower polymerization (approx. 2.6 times larger value for  $t_{95\%}$ , compare Table 4) when **1**-functionalized nanoparticles were used. However, the final heat release  $\Delta H$  was found to be nearly the same value, indicating the same degree of polymerization. This is in contrast to DSC results obtained for THFA as monomer. However, this might be assigned to the characteristics of thiol-ene click-chemistry, which generally proceeds in high yield and, furthermore, is known to be insensitive to water and/or oxygen.<sup>239</sup>

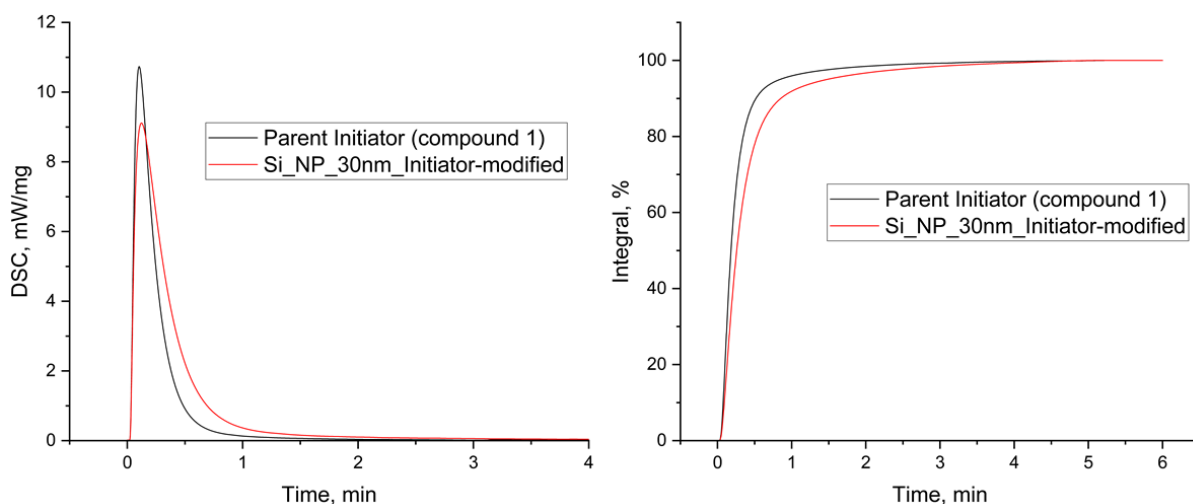


Figure 25: Photo-DSC curves (left) and integral plot (right) for photopolymerization of TTT+HDT with 0.1 wt.-% of parent initiator (compound **1**, black curve) and 3.1 wt.-% of nanoparticles (30 nm diameter), bearing coupled light-sensitive moieties (red curve).

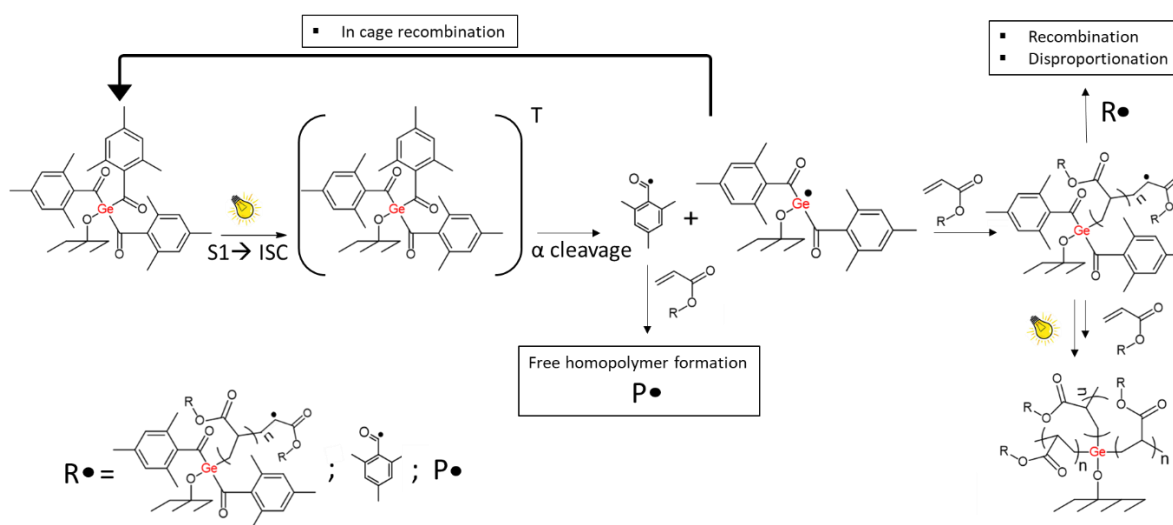
Table 4: Results of photo-DSC measurements with TTT+HDT and comparison of the time to reach 95% of the final conversion ( $t_{95\%}$ ).

	$\Delta H$ [J g <sup>-1</sup> ]	$t_{95\%}$ [min]
Parent Initiator	200 ± 23.9	0.56 ± 0.14
Si-NP_30nm_Initiator-modified	205 ± 17.6	1.49 ± 0.61

Staying with the pronounced photo-reactivity of the functionalized nanoparticles, it was also aimed to develop spherically shaped organic-inorganic hybrid materials, comprising an SiO<sub>2</sub> core, which is covered by a polymeric shell. This was achieved by visible light induced (405 nm) surface-initiated photopolymerizations of styrene and PFAcr ("grafting from" technique). Therefore, nanoparticles bearing photo-initiating units were carefully dispersed in the respective monomer solution and subsequently illuminated for 5 min with 405 nm under constant nitrogen flow. Upon visible light illumination, covalently coupled acyl germanium moieties undergo an  $\alpha$ -cleavage pathway once the molecule has reached an excited triplet state  $T_1$ , due to intersystem crossing from the excited  $S_1$  state (refer to Scheme 26). Consequently, highly reactive germanium centred (germyl) radicals and comparatively less reactive carbon centred (acyl) radicals are formed in each cleavage step. If the radicals are not diffusing away from each other, "in-cage recombination" might occur, which was observed in literature reports by using <sup>1</sup>H-CIDNP spectroscopy of mono-, bis-, and triacylgermanes in deoxygenated acetonitrile.<sup>240</sup> This effect, however, can be seen as negligible, since the resulting (initial) bond can easily be cleaved again upon light absorption. In fact, the synthesis of the polymer brush systems originated from the immobilized germyl radical (red coloured in Scheme 26) and its pronounced ability to add to acrylic or vinyl double bonds. In previous studies, measurements of the addition rate constants of different germyl radicals towards acrylates were found to significantly exceed those of acyl-based radicals (and also phosphorus analogues. Depending on the structure, the addition rate constant of germyl radicals towards butyl acrylate (as an example) ranges between  $0.2 \times 10^8$  and  $3.6 \times 10^8$  M<sup>-1</sup> sec<sup>-1</sup>.<sup>240</sup> For the addition reaction of phosphinoyl radicals to the same monomer a value of  $0.22 \times 10^8$  M<sup>-1</sup> sec<sup>-1</sup> was reported by Weber et al.<sup>241</sup> Significantly lower values were reported for benzoyl type radicals, having addition rate constants between  $1.3 \times 10^5$  and  $5.5 \times 10^5$  M<sup>-1</sup> sec<sup>-1</sup>.<sup>242</sup> Since the latter values are about three magnitudes lower than those for germyl radicals, it can be concluded that the initiation step is predominantly caused by the surface immobilized germyl radical, followed by multiple chain growth reactions according to Scheme 26. Nevertheless, the non-coupled acyl radicals might also start radical polymerization, albeit on a rather small scale, which in turn leads to the formation of non-coupled homopolymers (P in Scheme 26). However, those polymers can easily be removed afterwards by careful washing of the particles with appropriate solvents.<sup>16</sup>

In typical instances of "non-controlled" radical polymerization, termination reactions occur by

recombination and disproportionation, involving surface-tethered and free propagating chains as well as acyl and other radical species (see Scheme 26). Importantly, termination reactions of surface tethered propagating chains will have an impact on the resulting macromolecular architecture of the grafted polymers. In this context, the molecular architecture is governed by termination between two propagating chains anchored on either the same or two adjacent germanium atoms, and furthermore between attached polymer chains and free radical species. In addition, chain transfer reactions will also contribute to this multitude of possible side and termination reactions.



Scheme 26: Radical generation pathway and mechanism of surface-initiated photopolymerization using the example of acrylic monomers.

Differently sized nanoparticles, comprising a polymer shell of either p(St) and p(PfAc) were investigated by XPS, FTIR, ToF-SIMS, TGA as well as electron microscopy (SEM). Results from XPS measurements (Figure 26) proved successful surface-initiated polymerizations, revealing a pronounced signal of carbon at 284.8 eV (C1s) in all measured samples. Additionally, for nanoparticles bearing surface-grafted p(PfAc), a strong fluorine contribution (up to 48.8 at. %) to the surface composition was obtained (strong signal at 690 eV (F1s)). Moreover, after deconvolution of the C1s spectra, peaks at 292.2 eV and 294 eV were identified, which proved the presence of  $-CF_2-$  and  $-CF_3$  units (refer to Figure 28). Besides, silicon and oxygen signals at 103.4 (Si2p) and 533 eV (O1s), respectively, originating from the  $SiO_2$  core, as well as a weak Ge signal (1220 and 1250 eV), were also observed.<sup>243</sup> In a plausible manner, a rather low or even neglectable Ge contribution to the atomic surface composition was expected since the germanium atoms are supposed to be covered by the grafted polymeric layer.



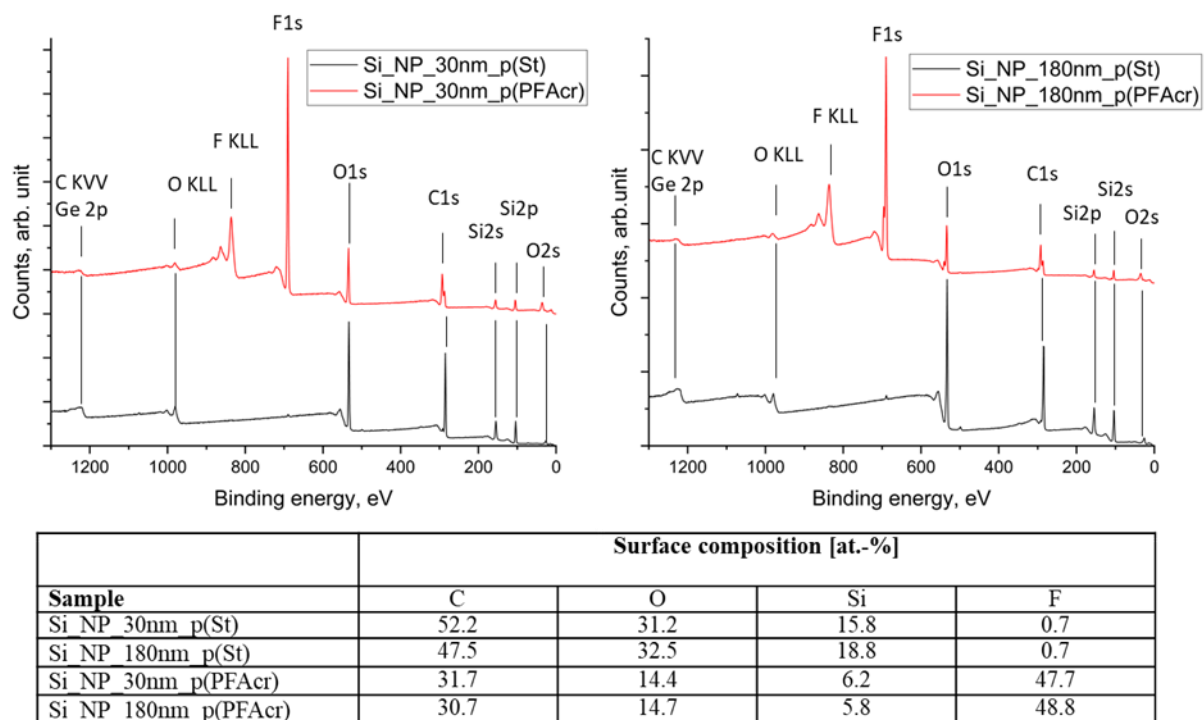


Figure 26: XPS survey spectra of p(St) and p(PFAcr) grafted SiO<sub>2</sub> nanoparticles including the atomic surface composition (in at.-%).

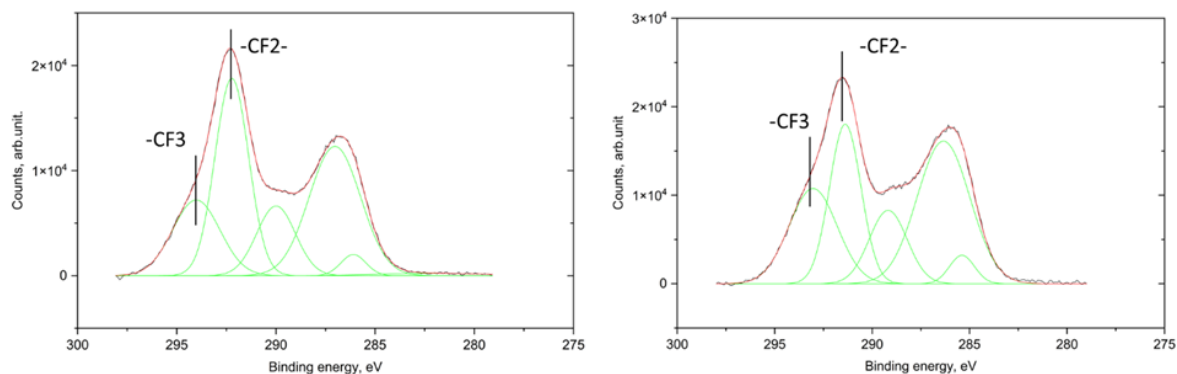


Figure 27: XPS C1s-deconvolution spectra of p(PFAcr) grafted nanoparticles (left: 30 nm particles; right: 180 nm particles).

With respect to the atomic surface composition, grafted nanoparticles (obtained from polymerization of styrene) exhibited a carbon content of about 50 %, whereas a similar contribution of fluorine atoms to the overall surface composition was found for p(PFAcr) covered nanoparticles. As already mentioned, silicon contents ranging from 5.8 to 18.8 % were assigned to the underlying base material (SiO<sub>2</sub>). Besides, negligible traces of fluorine were found for polystyrene covered nanoparticles.

FTIR measurements additionally proved the successful synthesis of polymer covered

nanoparticles, as peaks attributable to p(St) and p(PFAcr) were recorded. Measuring nanoparticles with a p(PFAcr) shell (Figure 28), peaks at  $1738\text{ cm}^{-1}$  ( $-\text{C}=\text{O}$  stretching vibration) as well as multiple signals between  $1201$  and  $1145\text{ cm}^{-1}$  ( $-\text{CF}$  stretching vibration) were observed. Figure 29 depicts infrared spectra of p(St) modified nanoparticles, highlighting peaks at  $1494$  and  $1451\text{ cm}^{-1}$  due to aromatic  $-\text{C}=\text{C}$  stretching, and a characteristic signal at  $698\text{ cm}^{-1}$  (out-of-plane  $-\text{C}-\text{H}$  deformation for monosubstituted aromatic rings). Furthermore, aromatic and aliphatic  $-\text{CH}$  stretching vibrations occurred in the regions  $3080 - 3030\text{ cm}^{-1}$  and  $3000 - 2800\text{ cm}^{-1}$ . In a plausible manner, those peaks (normalized to the  $-\text{Si}-\text{O}-\text{Si}-$  signal at  $1063\text{ cm}^{-1}$ ) decreased in dependence of the styrene concentration in the monomer solution (100, 50 and 25 vol.-%), as a lower yield of grafted polymer is expected. This is also illustrated in Figure 29, showing a decrease of the peak height at  $698\text{ cm}^{-1}$ .<sup>232</sup> Comparing the normalized FTIR signal intensities relevant for the grafted polymers on differently sized particles, it can be concluded that a lower organic content is present on 180 nm sized nanoparticles, which is again a consequence of the lower specific surface area.

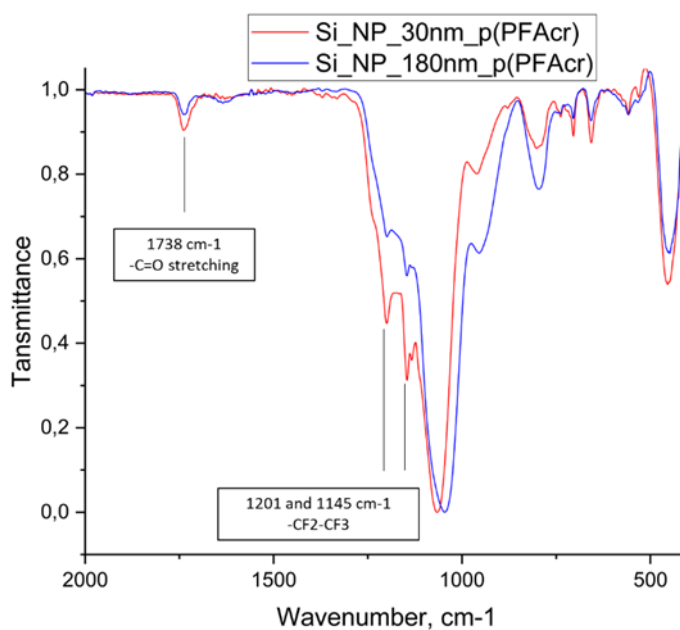


Figure 28: FTIR spectra (ATR) of differently sized nanoparticles grafted with p(PFAcr). The spectra are normalized to the  $-\text{Si}-\text{O}-\text{Si}-$  stretching vibration at  $1060\text{ cm}^{-1}$ .

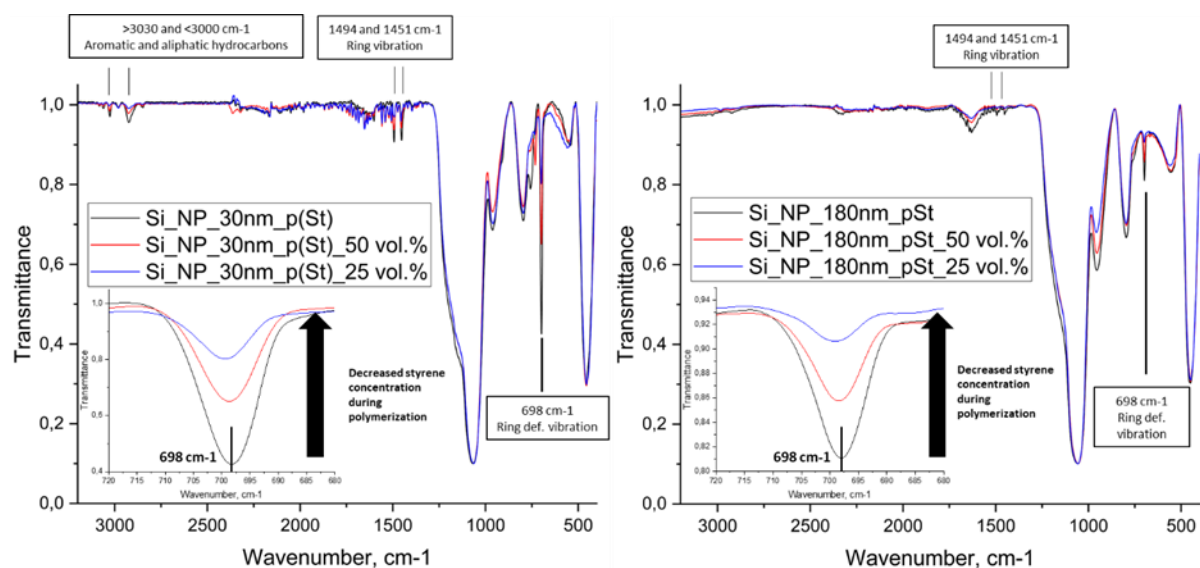


Figure 29: Infrared spectra of nanoparticles bearing a p(St) shell, prepared via photopolymerization of styrene using solutions of different concentrations (left: nanoparticles with a diameter of 30 nm; right: nanoparticles with a diameter of 180 nm). The polymer content is compared by relating the peak intensity at  $698\text{ cm}^{-1}$  to the -Si-O-Si- signal at  $1060\text{ cm}^{-1}$ .

To ensure that a polymeric structure is present at the particles' surface after SIPP without any doubt, time-of-flight secondary ion mass spectrometry (ToF-SIMS) measurements were undertaken. This is an analytical technique used to unveil the surface composition of materials at molecular levels, and offers high sensitivity and spatial resolution. In ToF-SIMS measurements, ions such as  $\text{Ar}^+$ ,  $\text{Ga}^+$ ,  $\text{Bi}^+$  or  $\text{Bi}_3^+$  are employed for surface bombardment detaching secondary species including molecular fragments or atomic ions from the surface. Those secondary species are then analyzed by a mass spectrometer.<sup>244</sup>

Prior to ToF-SIMS, p(St) as well as p(PfAc) homopolymers were synthesized radically by using AIBN as the initiator for reasons of comparability. The obtained solid white products were characterized by FTIR, and the spectra are shown in Figure 30 below. In accordance with FTIR-results for polymer grafted nanoparticles, the same signals were found for the corresponding homopolymers, including most characteristic  $\text{-C=O}$  ( $1738\text{ cm}^{-1}$ ) and  $\text{C-F}$  ( $1201, 1145\text{ cm}^{-1}$ ) signals of p(PfAc) as well as the  $\text{-CH}$  out of plane deformation ( $698\text{ cm}^{-1}$ ) signal for p(St).

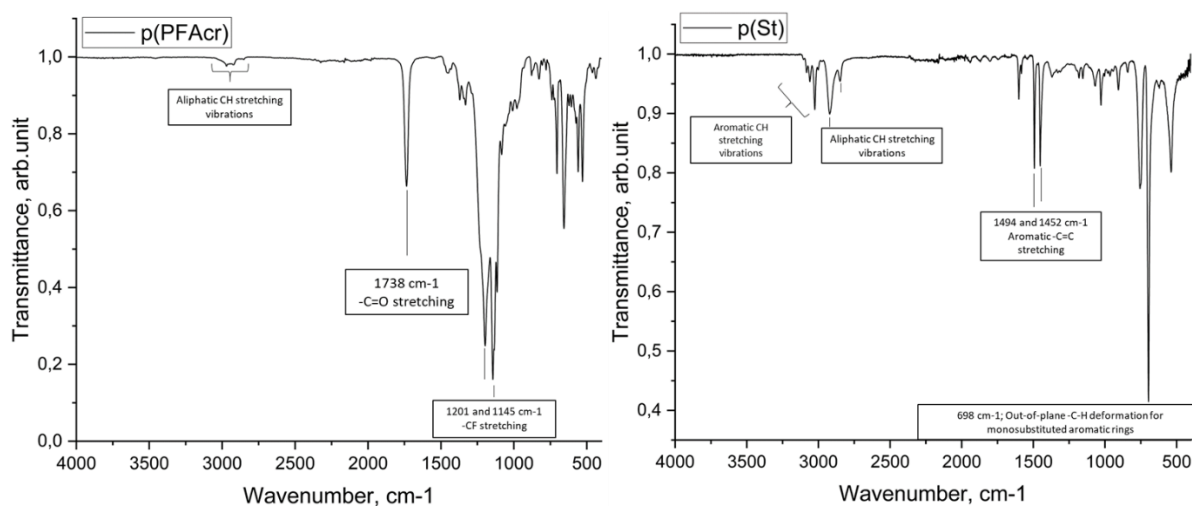


Figure 30: FTIR-spectra of homopolymerized p(St) and p(PFAcr).

The presence of a polymeric shell on the nanoparticles was confirmed by ToF-SIMS investigations. Figure 31 shows the positive secondary ion SIMS spectrum of p(St)-grafted nanoparticles (30 nm in diameter) in comparison to the p(St) homopolymer. The spectra resemble each other, displaying characteristic peaks at  $m/z = 41.04$  ( $C_3H_5^+$ ),  $77$  ( $C_6H_5^+$ ),  $91.05$  ( $C_7H_7^+$ ),  $105.01$  ( $C_8H_9^+$ ),  $117.07$  ( $C_9H_9^+$ ),  $128.03$  ( $C_{10}H_8^+$ ) and  $193.07$  ( $C_{15}H_{13}^+$ ).<sup>245</sup> Furthermore, a very weak signal of  $Si^+$  ( $m/z = 28$ ) was obtained when measuring the p(St) grafted nanoparticles (Figure 31, top spectrum). This indicates that the surface might not be perfectly covered by the grafted polymer.

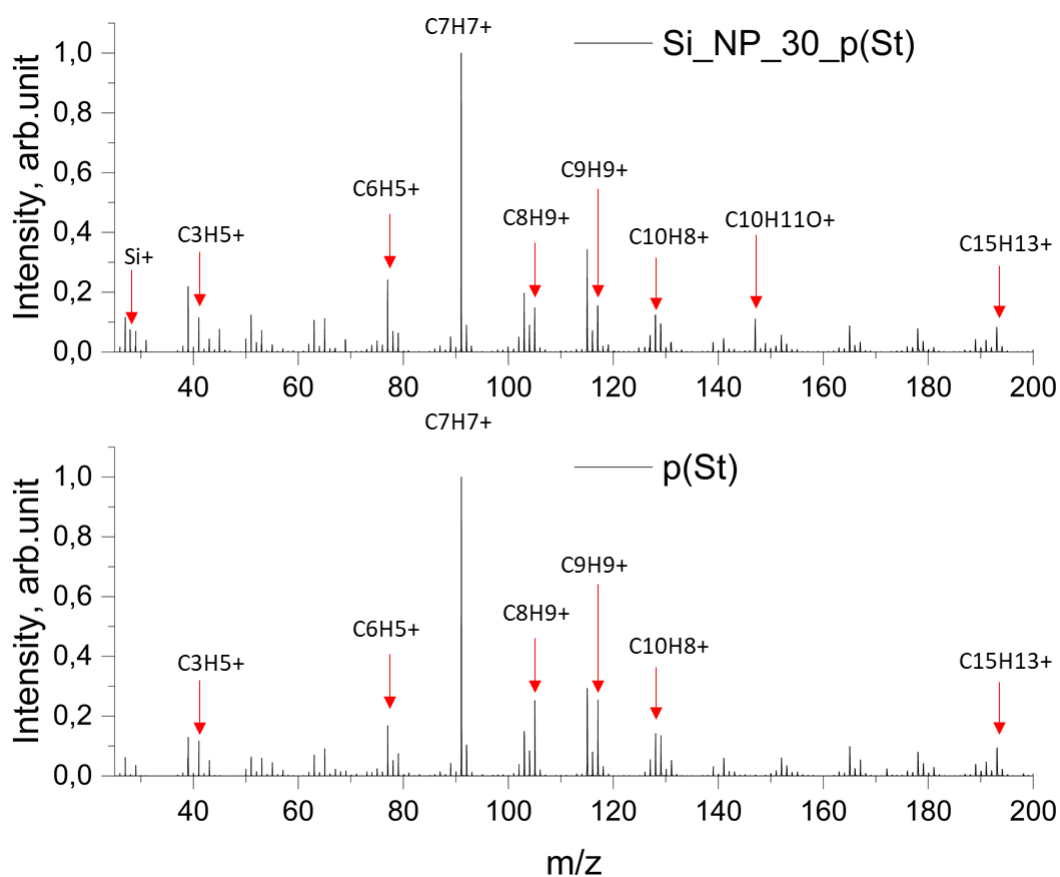


Figure 31: Positive secondary ToF-SIMS spectrum of p(St)-grafted nanoparticles (top) in comparison to neat polystyrene (bottom).

A similar conclusion can be drawn from the negative ion ToF-SIMS spectra of the same samples, showing in both cases characteristic hydrocarbon as well as siloxane peaks at  $m/z = 12.01$  ( $C^-$ ),  $13.02$  ( $CH^-$ ),  $25.01$  ( $C_2H^-$ ),  $49.04$  ( $C_4H^-$ ),  $73.02$  ( $C_6H^-$ ) and  $77$  ( $SiO_3H^-$ ).<sup>245</sup> In addition, pronounced oxygen ( $m/z = 16$ ), hydroxide ( $m/z = 17$ ) and weak fluorine ( $m/z = 19$ ) signals were observed from the nanoparticle surfaces (see Figure 32, top side). While the low fluorine content is attributed to a contamination, the comparatively higher amount of oxygen species could be assigned to the  $SiO_2$  core.

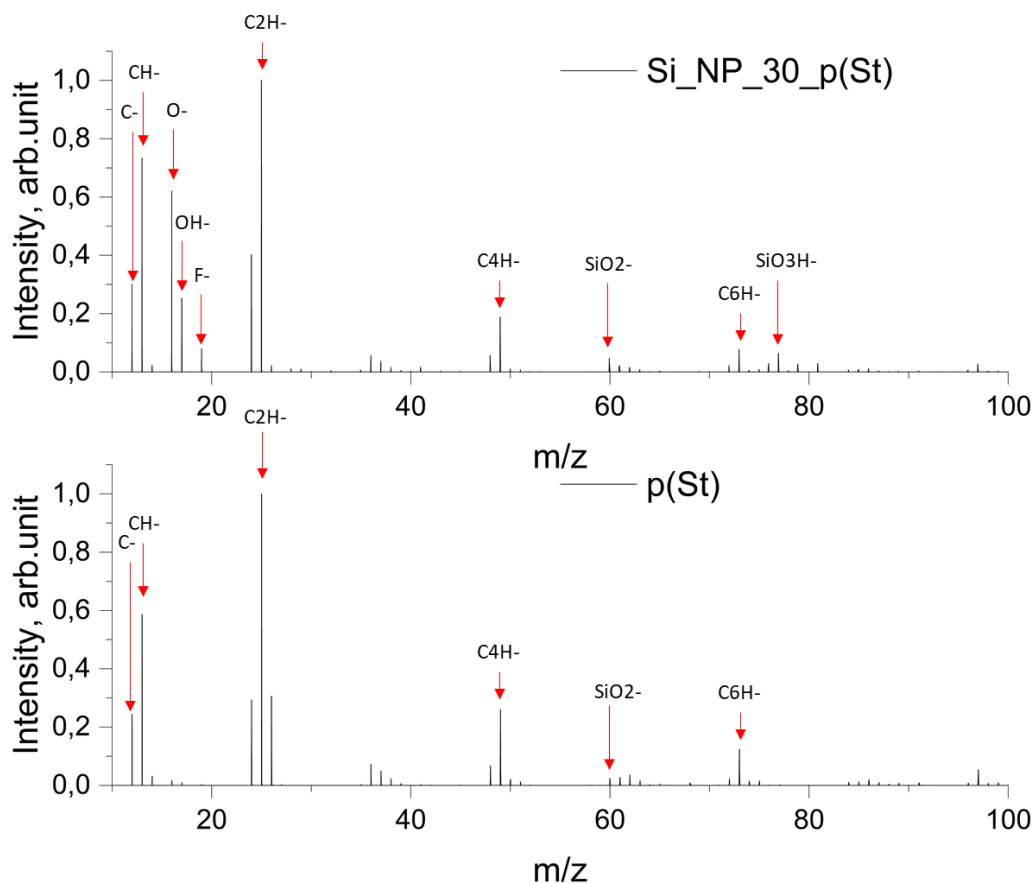


Figure 32: Negative secondary ion ToF-SIMS spectrum of p(St)-grafted nanoparticles (top) in comparison to neat polystyrene (bottom).

TOF-SIMS measurements were also conducted for the p(PFAcr) counterparts, and the corresponding spectra are presented in Figure 33 and Figure 34. Except for traces of sodium contaminations ( $m/z = 23$ , Figure 33, top spectrum), the obtained negative and positive secondary ion spectra of the polymer modified nanoparticles are in perfect agreement with those of the homopolymer. This is a further proof of the presence of a p(PFAcr) shell on the nanoparticles' surface.

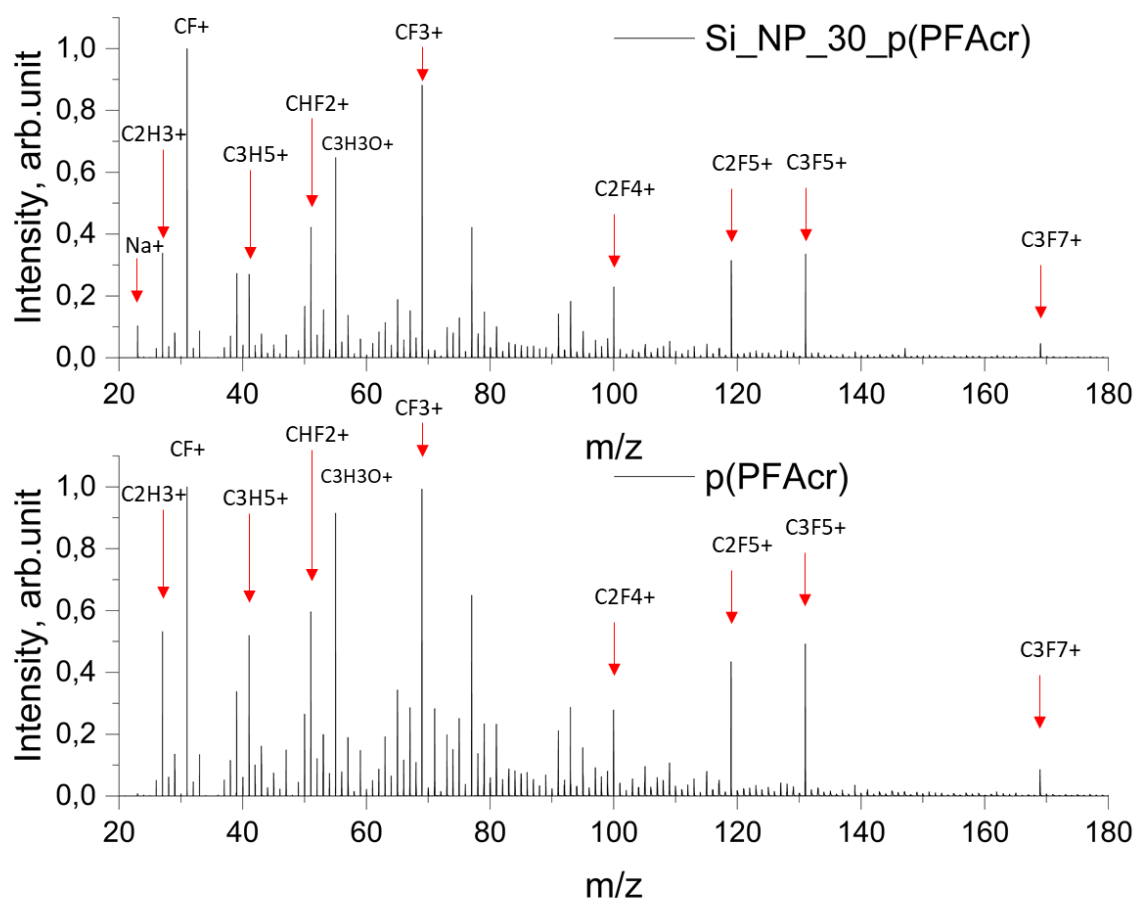


Figure 33: Positive secondary ion ToF-SIMS spectrum of p(PFAcr) grafted nanoparticles (top) in comparison to neat p(PFAcr) (bottom). Positively charged fragments were assigned as followed:  $\text{Na}^+$  (23),  $\text{C}_2\text{H}_3^+$  (27.02),  $\text{CF}^+$  (31),  $\text{C}_3\text{H}_5^+$  (41.04),  $\text{CHF}_2^+$  (51),  $\text{C}_3\text{H}_3\text{O}^+$  (55.02),  $\text{CF}_3^+$  (69),  $\text{C}_2\text{F}_4^+$  (100.07),  $\text{C}_2\text{F}_5^+$  (119),  $\text{C}_3\text{F}_5^+$  (130.99),  $\text{C}_3\text{F}_7^+$  (169).<sup>246</sup>

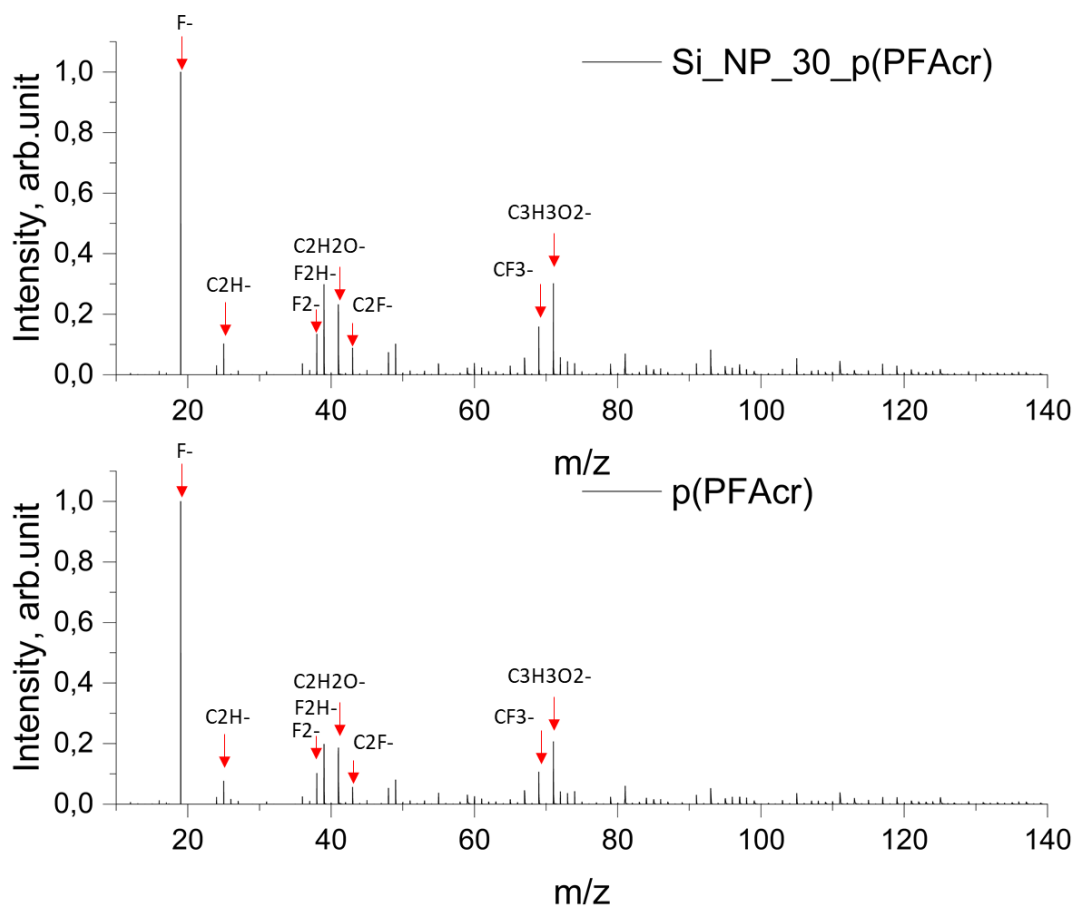


Figure 34: Comparison of the negative secondary ion ToF-SIMS spectrum of p(PFAcr) grafted nanoparticles (top) with that of neat p(PFAcr) (bottom). Negatively charged fragments were assigned as followed: F<sup>-</sup> (19), C<sub>2</sub>H<sup>-</sup> (13.01), F<sub>2</sub><sup>-</sup> (38), F<sub>2</sub>H<sup>-</sup> (39.01), C<sub>2</sub>H<sub>2</sub>O<sup>-</sup> (42), C<sub>2</sub>F<sup>-</sup> (43), CF<sub>3</sub><sup>-</sup> (69), C<sub>3</sub>H<sub>3</sub>O<sub>2</sub><sup>-</sup> (71.01).<sup>246</sup>



### 4.1.3 Visualization of polymer covered silica nanoparticles

In order to directly visualize the morphology of polymer-covered nanoparticles on a nanometer scale, SEM measurements were carried out. For SEM investigations, pristine, etched, p(PFAcr) and p(St)-grafted nanoparticles were dispersed either in toluene or in HFIP, and drop cast onto freshly cleaned silicon wafers. After solvent evaporation, the samples were transferred into the vacuum chamber of the SEM device, and surface characteristics were obtained from the secondary electrons. Figure 35 and Figure 36 both display pristine and surface treated nanoparticles that underwent the etching procedure with alkaline solution. The measured particle diameter of the neat (larger) nanoparticles was found to be  $184 \pm 7.4$  nm ( $30.01 \pm 8.8$  for the smaller counterparts). The diameter decreased to  $133 \pm 10$  nm once the particles were surface-etched with NaOH.<sup>230</sup> This diameter served then as a reference value to evaluate the layer thickness of polymer covered nanoparticles, and to calculate the grafting density, because further changes in diameter owing to the immobilization of compound **1** were not expected. Both figures below reveal a porous surface structure after etching, which is in good accordance with reports in the literature.<sup>221</sup> The same applies to the smaller nanoparticles, placing even more emphasis on the obtained porous surface (see Figure 35). However, as far as the 30 nm particles are concerned, the corresponding diameter (also for the polymer-grafted samples) could not be determined with certainty as the resolution limit of the SEM instrument was exceeded.

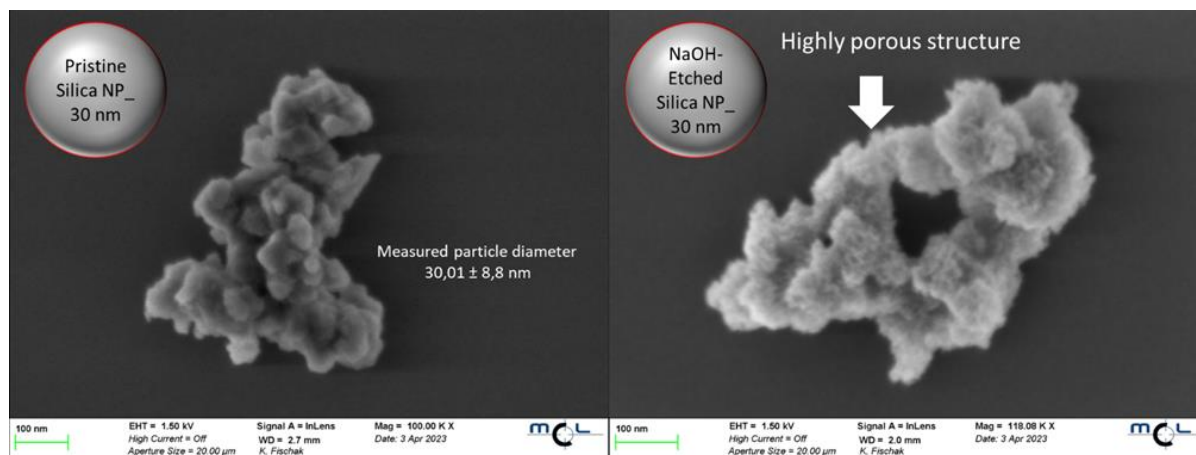


Figure 35: SEM images of pristine and neat nanoparticles (30 nm initial diameter size). The green scale bar is 100 nm.

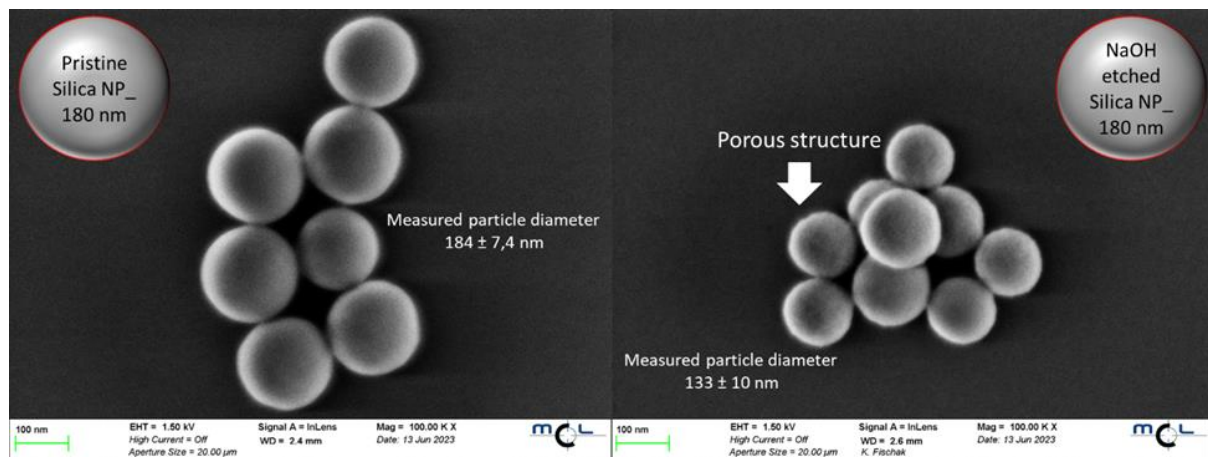


Figure 36: SEM images of neat (left) and NaOH etched nanoparticles (right). The green scale bar is 100 nm.

After surface-initiated photopolymerization of styrene the appearance of the larger nanoparticles changed significantly. The spherical shape was still maintained after the grafting-from reaction, but the nanoparticles exhibited no clear spatial separation any more. This is attributed to the polymeric shell, which seemed to connect the individual particles, see Figure 37. Also, the particle diameter increased from  $133 \pm 7$  nm (etched samples) to approximately  $157 \pm 16$  nm after the grafting-from reaction, suggesting that the thickness of the polystyrene shell is approx. 12 nm.

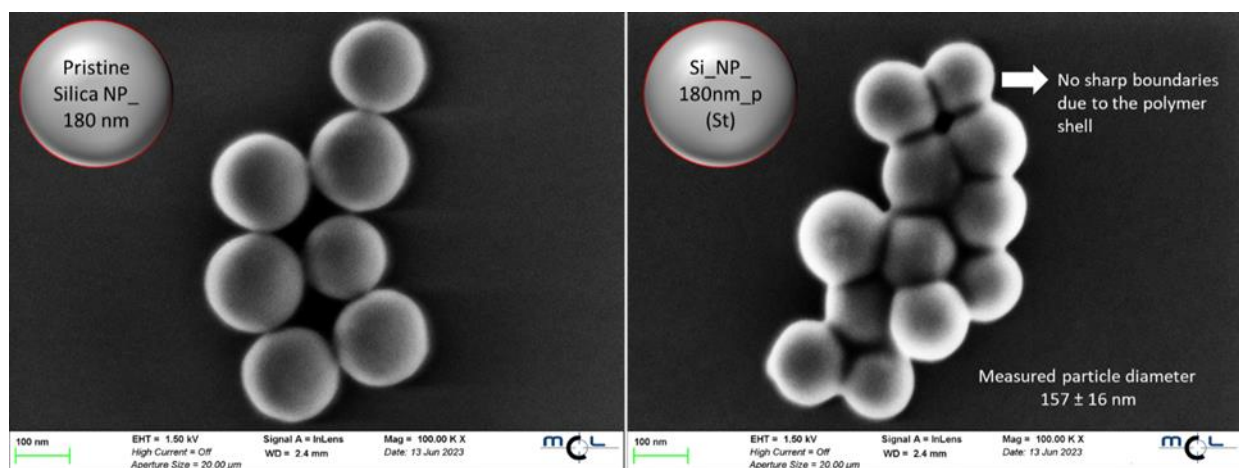


Figure 37: SEM images of neat (left) and p(St)-covered nanoparticles (right).

Moreover, the grafted p(St) shell significantly changed the surface properties of the particles regarding their dispersibility behaviour in toluene. By using a simple flashlight, the differences between neat and p(St) grafted nanoparticles (30 nm initial diameter) with an organic content of about 40 wt.-% (according to TGA) are illustrated in Figure 38. Note that 40 % more p(St)-

modified nanoparticles (12.3 mg) than pristine nanoparticles (8.8 mg) were dispersed in toluene to ensure the same SiO<sub>2</sub> content. Pristine nanoparticles (Figure 38, left side) agglomerated to a large extent whereas p(St)-covered particles showed enhanced dispersibility in toluene. Strong light scattering was visible with the naked eye.

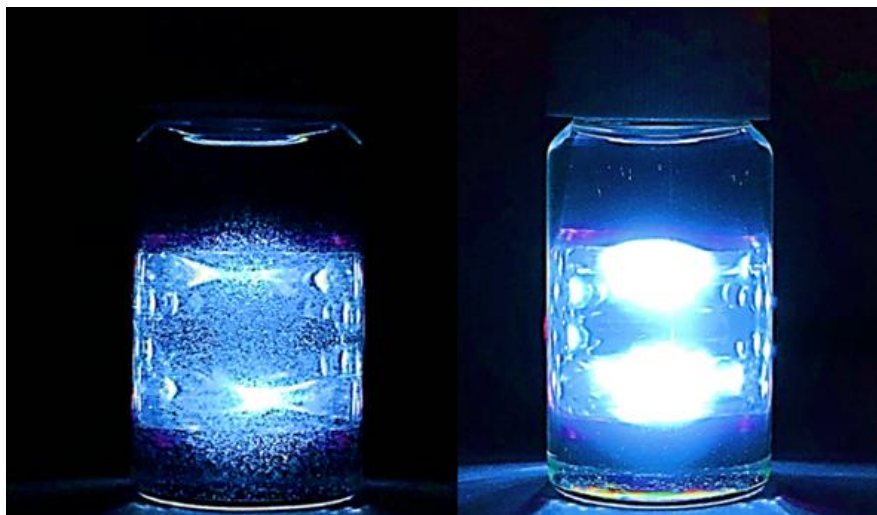


Figure 38: Pristine and p(St)- modified nanoparticles (30 nm in diameter) dispersed in toluene. Left: 8.8 mg of neat nanoparticles in 20 mL of toluene; right: 12.3 mg of p(St)-modified nanoparticles in 20 mL of toluene.

Nanoparticles bearing a p(PFAcr) shell exhibited a pronounced tendency to agglomerate, since no isolated single particles could be identified in SEM measurements. SEM images of those highly aggregated nanoparticles are presented in Figure 39. Similar to Figure 37, brush layers consisting of p(PFAcr) seemed to interpenetrate into each other, which is especially visible in regions where the particle agglomerates were broken apart (Figure 39, 50K of magnification). The observed diameter ( $145 \pm 21$  nm) suggested a thickness of the graft layer of 6 nm. This thickness is smaller than that one determined for the p(St) grafted counterparts, although TGA measurements indicated a noteworthy higher polymer content (compare Figure 40). We propose that the perfluorinated macromolecules are more densely packed at the surface, which is also suggested by a relatively higher bulk density of perfluorinated polymers (e.g.,  $2.23 \text{ g cm}^{-3}$  for poly(tetrafluoroethylene); compared to polystyrene ( $1.05 \text{ g cm}^{-3}$ ).<sup>247</sup>

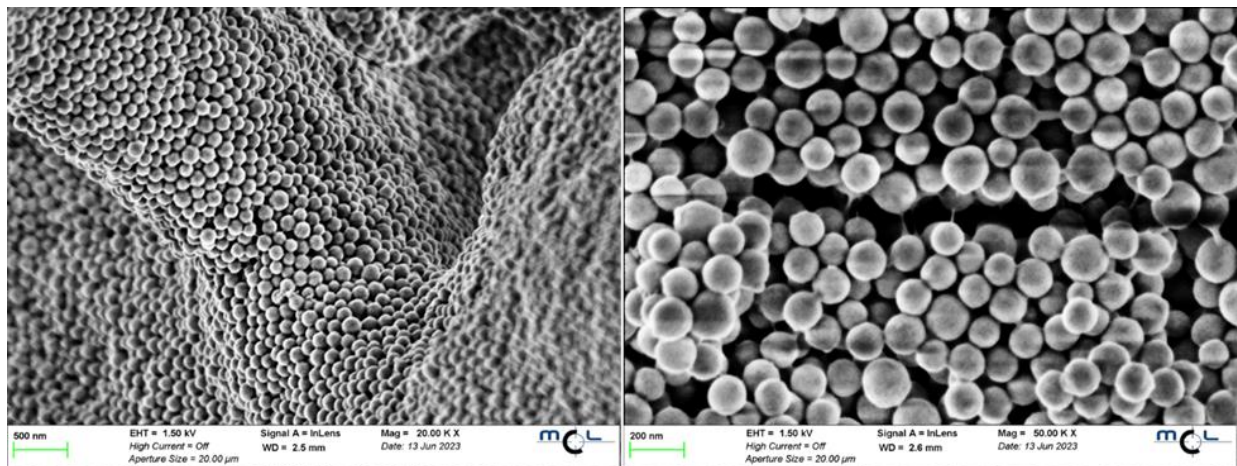


Figure 39: SEM images of highly agglomerated nanoparticles bearing a p(PFAcr) shell. Left: 20 K magnification; right: 50 K magnification.

Summing up, SEM results clearly prove the presence of spherically-shaped polymer shells all over the particle surfaces. As a consequence of SIPP, the appearance of the surface was changed, and a plausible increase of the particles' sizes was observed. After all, it can be confirmed that the presented "grafting-from" technique, relying on the covalent attachment of trisacyl germanium units, is well-suited for surface modification and functionalization.

#### 4.1.4 Evaluation of the grafting yield and calculation of the grafting density

After confirming the presence of the organic shell, the respective polymer content of the organic-inorganic hybrid materials was investigated by TGA. Therefore, the samples were heated from room temperature to 190 °C at which they were kept for one hour in order to remove physisorbed water or other volatile residuals.<sup>248</sup> Subsequently, heating up to 900 °C under constant nitrogen flow allowed to evaluate the organic polymer content based on the weight loss between 200 and 900 °C. Figure 40 depicts the TGA traces of polymer-grafted nanoparticles, which were derived from SIPP of styrene at different concentrations, and PFAcr (left: modified 30 nm SiO<sub>2</sub> particles, right: modified 180 nm SiO<sub>2</sub> particles). In accordance with the FTIR results, the p(St) content varies in dependence of the monomer concentration, revealing lower contents when the grafting polymerization was carried out at lower monomer concentrations. Overall, SIPP with 30 nm sized nanoparticles yielded a notably higher polymer content when compared to SIPP with 180 nm particles, which is a direct consequence of the higher specific surface area.

Based on TGA and SEM data, the grafting yield related to the surface area ( $\sigma_{mg}$ ) was calculated, and is summarized in Table 5. Interestingly, the  $\sigma_{mg}$  values of grafted 180 nm particles are higher when compared to those of 30 nm particles, which is even more pronounced when PFAcr was used as the monomer. On the one hand, this may result from the fact that the radius for etched 30 nm sized particles, which was considered for the calculation of  $\sigma_{mg}$ , was not directly measured via SEM but mathematically approximated as described in the experimental section. On the other hand, we propose differences related to dispersibility in the monomer solution based on our observation from UV-Vis studies. Due to the fact that inter-particle forces increase with decreasing particle sizes, it can be assumed that modified 30 nm sized particles remained at high agglomerated states during photopolymerization, which may result in limited accessibility of the initiating Ge-species at the surface.<sup>237</sup>

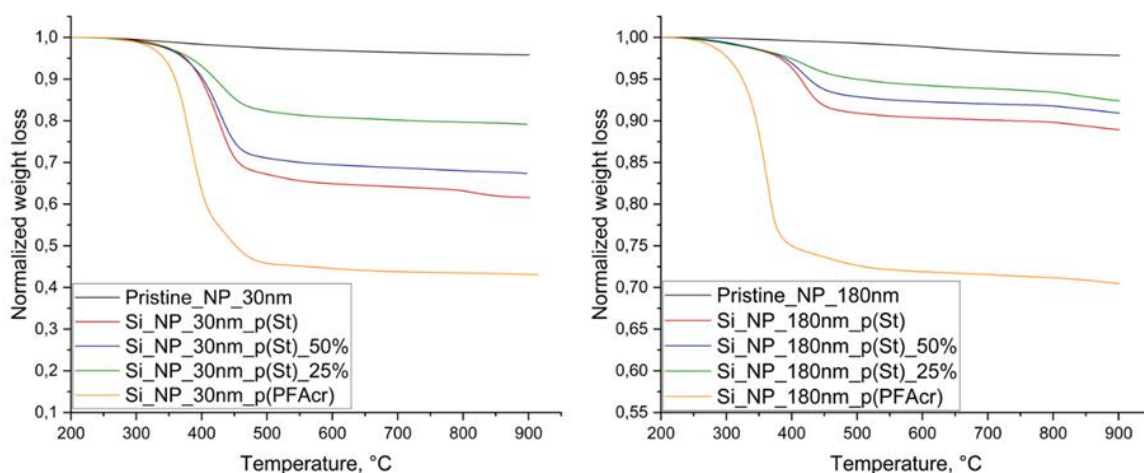


Figure 40: Results of TGA measurements for polymer-covered and neat SiO<sub>2</sub> nanoparticles (left: 30 nm particles; right: 180 nm particles).

When comparing the grafting yield of samples derived from polymerization of styrene and PFAcr, respectively, a significantly higher p(PFAcr) content (9.26 mg m<sup>-2</sup> vs. 4.21 mg m<sup>-2</sup>, and 18.0 mg m<sup>-2</sup> vs. 4.61 mg m<sup>-2</sup>) was observed. This can be explained by the high molar mass of the perfluorinated side chains, considering the molar mass of the monomers PFAcr (518.17 g mol<sup>-1</sup>) and styrene (104.15 g mol<sup>-1</sup>).

Table 5: Calculated polymer content and  $\sigma_{mg}$  for the organic-inorganic hybrid materials.

Sample (30 nm diameter)	Polymer content %	$\sigma_{mg}$ * mg m <sup>-2</sup>	Sample (180 nm diameter)	Polymer content %	$\sigma_{mg}$ mg m <sup>-2</sup>
Si_NP_30nm_p(St)	38.5	<b>4.21*</b>	Si_NP_180nm_p(St)	11.3	<b>4.61</b>
Si_NP_30nm_p(St)_50%	32.7	<b>3.19*</b>	Si_NP_180nm_p(St)_50%	9.4	<b>3.53</b>
Si_NP_30nm_p(St)_25%	21.3	<b>1.64*</b>	Si_NP_180nm_p(St)_25%	7.9	<b>2.76</b>
Si_NP_30nm_p(PFAcr)	57	<b>9.26*</b>	Si_NP_180nm_p(PFAcr)	30.1	<b>18</b>

\* Values were calculated based on the mathematically approximated value for the radius of etched nanoparticles.

The grafting density is an important parameter in terms of surface modification with a high impact on the surface properties, thus having a crucial relevance related to different applications, such as protein adsorption,<sup>249</sup> redox flow batteries,<sup>250</sup> or in-vivo imaging of subcutaneous tumors.<sup>251</sup> To determine the graft density of our organic-inorganic hybrid nanomaterials, p(St) modified nanoparticles of both sizes were chosen for de-grafting experiments, followed by SEC measurements. The following discussion on grafting density relations exclusively considers nanoparticles modified with p(St), as the utilization of polystyrene calibration standards in SEC ensures a high degree of accuracy, which cannot be provided for p(PFAcr).

To de-graft p(St) from SiO<sub>2</sub> surfaces, the particles were dispersed in a mixture of hydrofluoric acid and toluene, and vigorously stirred for 24 h. Thereafter the organic phase was recovered, and washed with water for several times. After evaporation of toluene, the obtained material was refluxed in methanol for purification, and a solid white powder was gained, which was subsequently characterized via by TGA, FTIR, and SEC. The corresponding FTIR spectra (one of them is shown in Figure 41) indicated successful de-grafting of p(St) as this FTIR spectrum is identical with the FTIR spectrum of homopolymerized p(St) as well as with reference spectra of p(St).<sup>252</sup> Moreover, TGA revealed the complete decomposition at temperatures < 900°C (Figure 41) proving that no inorganic SiO<sub>2</sub> species remained after the de-grafting process.

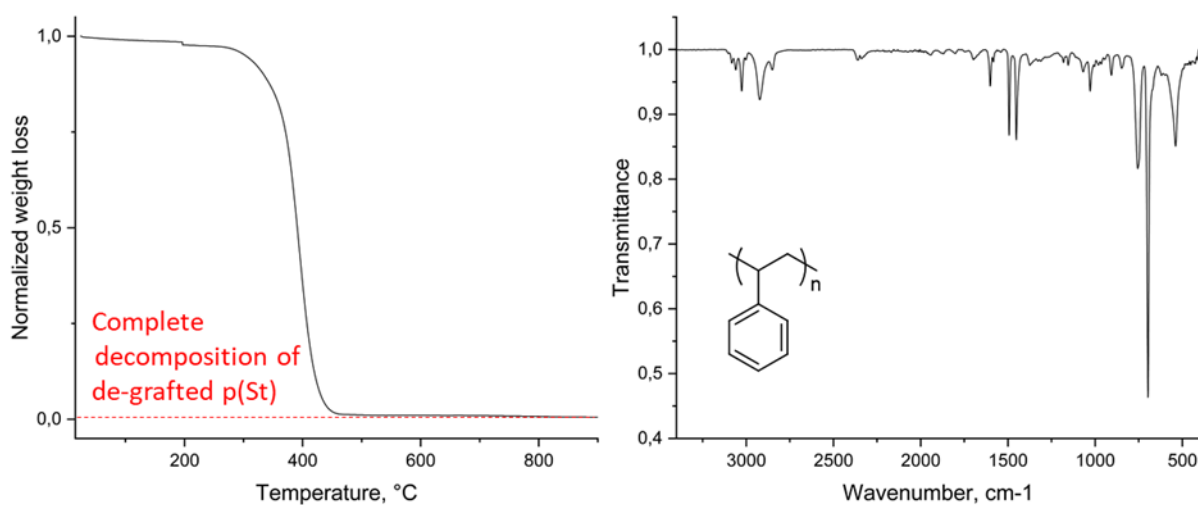
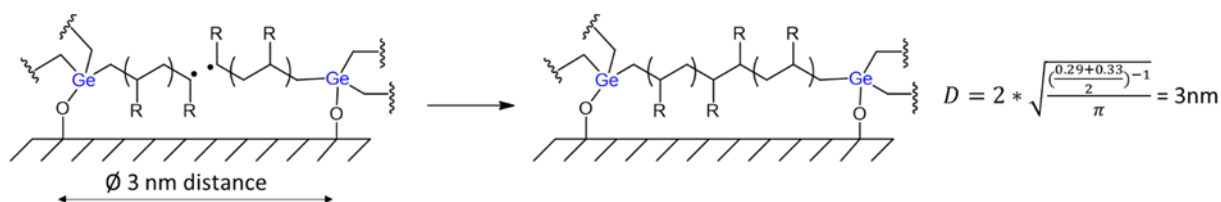


Figure 41: Characterization of de-grafted polystyrene by TGA (left) and FTIR spectroscopy (right).

Finally, the grafting density  $\sigma_{\text{chains}}$  was calculated from SEC data according to equation 2. The results are summarized in Table 6. As expected, the grafting density  $\sigma_{\text{chains}}$  was independent of the styrene concentration during SIPP, and the obtained values are in the range between 0.17 and 0.23 chains per  $\text{nm}^2$ . Hence, it can be concluded, that the polymer grafting density is mainly limited by the surface density of the photoinitiator. For the calculation of the number of initiating species per square nanometer ( $\sigma_{\text{PI}}$ , see experimental section), UV absorption properties of nanoparticles modified with compound **1** were used, along with those of compound **2** (ethoxy-derivative) as a similar molar decadic absorption coefficient can be assumed. Regarding nanoparticles modified with compound **1**, grafting density values for the photoinitiator of  $\sigma_{\text{PI}} = 0.29$  and  $\sigma_{\text{PI}} = 0.33$  were revealed for 30 and 180 nm silica particles, respectively. These results are lower than the theoretical initiator density, which was found to be 0.53 molecules per square nm. It is important to note that the latter value has been derived for idealized reaction conditions. The lower experimental values for  $\sigma_{\text{PI}}$  may be caused by insufficient particle dispersion during functionalization with compound **1**, and also by limitations of its reactivity due to sterical hindrance.

Interestingly, the final polymer grafting density (0.17 - 0.23 chains per  $\text{nm}^2$ ) is below  $\sigma_{\text{PI}}$ , which might be either caused by radical recombination of propagating chains, which were attached to different germanium centers, or particle agglomeration. The latter would result in a limited availability of the initiating species during illumination and polymerization. To clarify the probability of “neighbouring” recombination according to Scheme 27 the following consideration is presented. Based on the experimental initiator density, an average distance of 3 nm (calculation included in Scheme 27) between initiating radicals, i.e., germanium centers, can be assumed in that case. Taking into account a C-C bond length of 0.154 nm and a C-C-C bond angle of  $111^\circ$ , a minimum of only 11 repetition units of styrene, which means 5

to 6 from each side, are necessary to overcome this gap, thus enhancing the probability for recombination reactions according to Scheme 27. Taking into account this recombination, more than one surface-attached initiating unit contributes to the final macromolecule. Consequently, the number of polymer chains per square nm would be lower than the density of the Ge initiator. Besides, disproportionation might also occur in this scenario but would, on the other hand, not decrease the macromolecular grafting density.



Scheme 27: Possible recombination reaction of highly crowded and surface-tethered propagating chains.

The group of Fukuda investigated the mechanism and kinetics of RAFT-mediated graft polymerization of styrene initiated on silica particles, which in fact is a representative of controlled radical polymerization. Nevertheless, these authors proved that graft radicals can undergo bimolecular termination to a large extent, especially at high grafting densities, which also resulted in a severe broadening of the molar mass of de-grafted products.<sup>253</sup> In terms of surface-initiated atom-transfer radical polymerization, significant termination reactions of highly crowded radicals, which are anchored on solid substrates, were discussed by Gao et al.<sup>254</sup> In accordance with that, a very broad molar mass distribution was also observed in the herein presented system, especially when bulk polymerizations were conducted (see Table 6). Although the obtained molar mass of de-grafted polystyrene was expected to follow the simple mass-monomer concentration dependency, it cannot be explained with certainty why the polydispersity narrowed when the styrene concentration was reduced. To the best of our knowledge, no kinetic model was developed so far, which meets the circumstances of highly crowded surface-radicals, non-controlled conditions, surface-mediated initiation and simultaneous formation of non-immobilized radical species.

It should be pointed out that, from a theoretical point of view, each immobilized triacyl germanium moiety could potentially generate up to three germyl radicals at the same germanium centre in a sequential manner. This suggests another complex cascade of reactions, including initiation, chain transfer and termination. However, given that the grafting density and grafting yield (amount of immobilized species) primarily dictate the practicality of surface modifications, we infer that the molecular architecture of polymer grafts plays a minor role with regard to applications.



Table 6: Results for average molar masses ( $M_n$ ,  $M_w$ ,  $M_w/M_n$ ,  $M_z/M_w$ ) of de-grafted polystyrene, and calculated grafting density  $\sigma_{chains}$ .

Sample	$M_n \times 10^3$ g mol <sup>-1</sup>	$M_w \times 10^3$ g mol <sup>-1</sup>	$M_w/M_n$ [/]	$M_z/M_w$ [/]	$\sigma_{chains}$ $\frac{chains}{nm^2}$
Si_NP_30nm_p(St)	14.500	59.100	4.06	3.43	<b>0.17*</b>
Si_NP_30nm_p(St)_50%	10.800	31.900	2.96	2.35	<b>0.18*</b>
Si_NP_30nm_p(St)_25%	5.800	12.600	2.15	1.90	<b>0.17*</b>
Si_NP_180nm_p(St)	14.300	40.700	2.83	2.12	<b>0.19</b>
Si_NP_180nm_p(St)_50%	10.800	24.900	2.30	1.83	<b>0.20</b>
Si_NP_180nm_p(St)_25%	7.100	10.900	1.54	1.51	<b>0.23</b>
* Values were calculated based on the mathematically approximated value for the radius of etched nanoparticles					

To sum up, the polymer grafting density (0.17 – 0.23 chains per nm<sup>2</sup>) is lower than that of the immobilized initiating species due to above discussed reasons, but is, nevertheless, well comparable to literature values for similar free and even controlled radical “grafting-from” systems. A survey of the grafting densities of several systems by Michalek et al. demonstrates that they range from very low values (0.021) up to 31.1 molecules per nm<sup>2</sup>. However, some reported grafting densities can be called into question as they significantly exceed the physically possible maximum. For grafted polystyrene, as an example, this maximum is 1.28 chains per nm<sup>2</sup>.<sup>255</sup>

#### 4.1.5 Conclusion on surface-initiated photopolymerization mediated by photoinitiator-functionalized silica nanoparticles

This chapter presents a convenient and novel pathway to produce spherically shaped organic/inorganic hybrid materials based on visible light induced surface-initiated photopolymerization techniques. This was achieved via covalent coupling of a novel and highly efficient group 14 based photoinitiator (bromo-tris(2,4,6-trimethylbenzoyl) germane, compound **1**) onto silica nanoparticles with different sizes (diameters of 30 and 180 nm, respectively). Successful immobilization was proven via XPS and UV-Vis measurements, and the initiator grafting density was found between 0.29 and 0.33 molecules per nm<sup>2</sup>, which is beneath the theoretical value of 0.53 units per nm<sup>2</sup>. Surface-initiated photopolymerizations were carried out upon visible light (405 nm) irradiation, using styrene and 1H,1H,2H,2H-perfluorodecyl acrylate as monomers, leading to hybrid materials bearing a polymeric shell and a SiO<sub>2</sub> core. The produced material was carefully studied by means of XPS, FTIR, TOF-SIMS, TGA and SEM. While XPS unveiled the presence of surface atoms that can be assigned to

grafted polymers, FTIR and ToF-SIMS clearly proved the existence of the respective macromolecular structures at the surface. Especially TGA and SEM strongly suggested the presence of the polymeric shell as TGA showed a high mass fraction of organic material (up to 57 %), and SEM revealed spherically shaped particles, which are larger in diameter after grafting-from reactions, and also exhibited a significantly different appearance in SEM images when compared to pristine nanoparticles. Furthermore, by simply varying the monomer concentration during SIPP, the derived polymer content can be tailored.

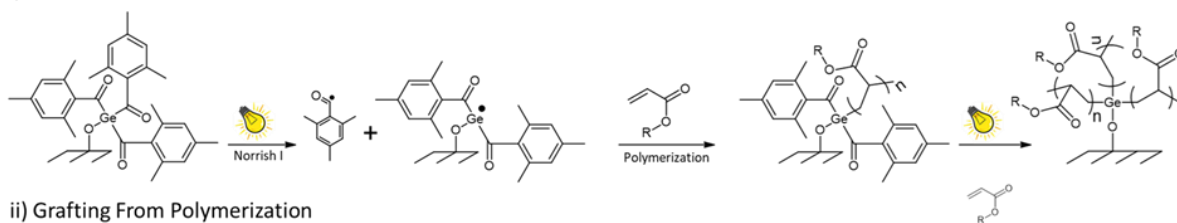
Moreover, the grafting density of polymer brushes, which were grafted from compound **1**-functionalized nanoparticles, was studied. From SEC data of the de-grafted polymer, and TGA measurements of the core-shell particles, the grafting density was found in the range from 0.17 and 0.23 chains per square nm, which is well comparable to literature values.

Also, it should be emphasized that the herein presented method is not limited to silica surfaces. According to the synthesis protocol of compound **2** (see experimental section), which was obtained via the reaction between ethanol and the germanium bromide center in high yield (99%), it can be concluded that the organogermanium halide (compound **1**) is also suitable to undergo coupling reactions to materials bearing surface hydroxyl groups, such as cellulose (nano)-materials. Those materials are for example frequently applied in the field of biomedicine in terms of tissue engineering, wound healing, regeneration, drug delivery, anti-fouling and antibacterial agents.<sup>256</sup> For the future, due to the low cytotoxicity and visible light sensitivity of germanium-based photoinitiators, we propose that the herein reported method opens up new perspectives in a very broad field of high-end applications, especially in nanomedicine.<sup>257</sup> More precisely, these applications include dental nanocomposite resins,<sup>258</sup> controlled drug release systems,<sup>259</sup> dye-doping,<sup>260</sup> cancer therapy,<sup>261</sup> silica coated quantum dots,<sup>262</sup> and many more. Apart from that, the herein reported nanoparticles functionalized with compound **1** are now being studied for cationic SIPP of vinyl ethers and epoxides in our laboratory (see chapter 4.3). This paves the way towards further possibilities in the general field of surface modification, and will be the subject of a subsequent publication.

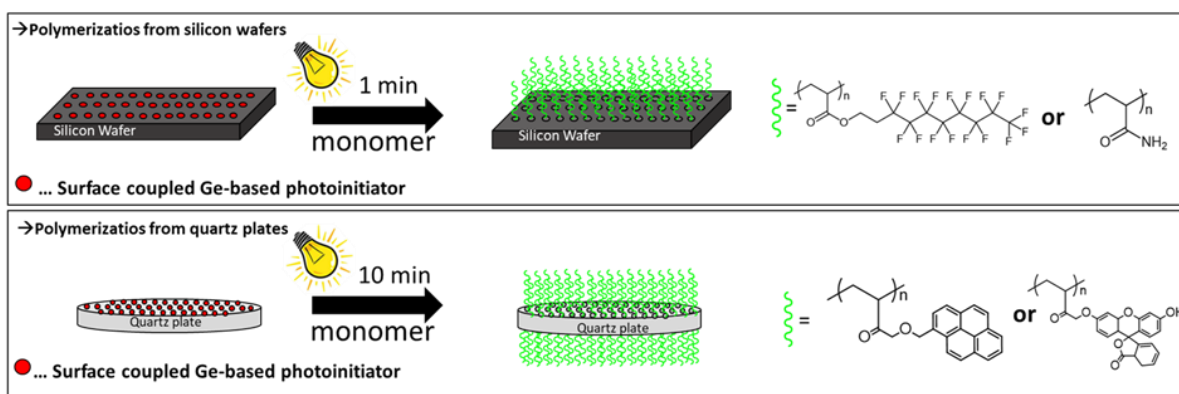
## 4.2 Surface modification of silicon substrates and quartz plates with light sensitive moieties and subsequent grafting-from photopolymerization

In this section the immobilization procedure described in the previous chapter was also applied for flat surfaces such as silicon wafers and optically polished quartz plates. Again, the surface modification was achieved via the immobilization of compound **1**. Those surface tethered species were exploited to initiate a radical polymerization reaction of different functional monomers upon irradiation with visible light (405 nm). The certain functionalities included hydrophilic/hydrophobic as well as fluorescent behaviour. In addition, spatially resolved polymer layers were also produced. An overall representation is given in Scheme 28.

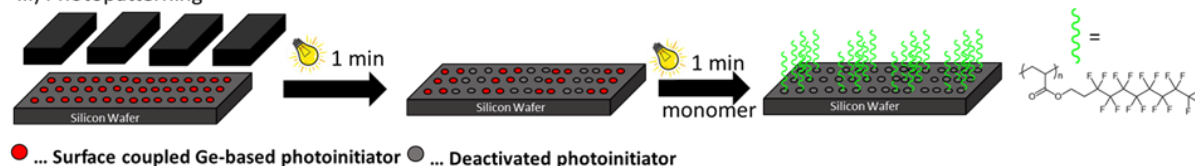
### i) Mechanism



### ii) Grafting From Polymerization



### iii) Photopatterning



Scheme 28: Schematic representation of the applied “grafting from” method (i, ii) and the prepared polymer layers, including spatially resolved structures (iii).

#### 4.2.1 Immobilization of the photo-initiating species derived from compound **1**

The immobilization of compound **1** onto silicon substrates was accomplished in two steps and slightly adapted from the procedure, which was reported for modifying nanoparticles in the preceding chapters. Here, the first step comprised surface activation with oxygen plasma, resulting in hydroxy terminated silicon and quartz surfaces, respectively.<sup>263–265</sup> Whilst the silicon wafers were only activated and modified on the polished surface (top), the quartz plates were activated on top and bottom sides to couple the photoinitiator to both sides. Immobilization of initiating species was carried out by immersing the activated substrates in a THF solution of compound **1** and DIPEA at 60 °C for 24 h. As already described previously, it is proposed that this reaction follows a nucleophilic substitution pathway, which is illustrated in Scheme 25. Similar to observations in nanoparticle modification with compound **1**, the formation of a tertiary ammonium salt (N-ethyl-N-isopropylpropan-2-ammonium bromide) was also observed and characterized with FTIR spectroscopy, revealing a group of sharp and strong absorption bands at 2684, 2664, and 2618 cm<sup>-1</sup> due to hydrohalide N-H<sup>+</sup> stretching vibrations.

The immobilization of the photoinitiator **1** was again proven by XPS analyses of the functionalized silicon wafers, and the signal peaks were identified with reference data.<sup>243</sup> As it can be seen from the survey spectra in Figure 42, the presence of Ge (1220 and 1251 eV) and the absence of Br (69 eV) was evidenced, strongly suggesting successful covalent linkage of the initiating species following the pathway described above. Moreover, the elemental composition of silicon wafers before and after surface functionalization is compared in Table 7. Besides, some traces of impurities were also observed at the surface, including Na, F and Ca atoms. However, these elements were also detected on neat silicon wafers after activation with oxygen plasma without further surface functionalization (see Figure 42, green curve). It is also worth mentioning that a significant amount of carbon was found on neat silicon wafers too. This was assigned to absorbed carbonaceous species including carbon dioxide etc., as already documented in previous work.<sup>2</sup>

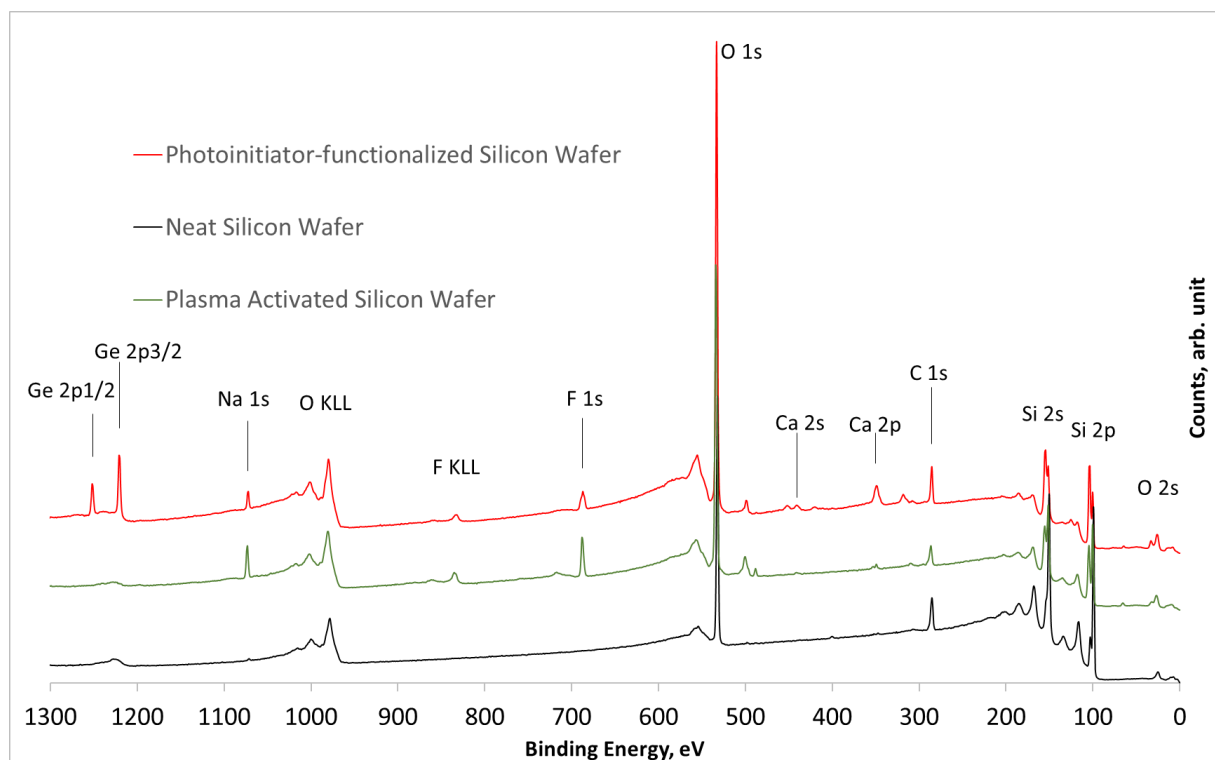


Figure 42: XPS survey spectra including peak assignments of a neat Si wafer (bottom, black curve), oxygen plasma activated Si wafer (green curve), and Si wafer functionalized with photoinitiator **1** (red curve).

Table 7: Relative atomic surface composition of a neat and a functionalized Si wafer (data obtained from high resolution XPS spectra).

Sample	Surface composition [at%]						
	C	Ge	F	O	Si	N	Na
Neat Si wafer	14.7 ± 0.6	/	/	32.3 ± 0.34	51.6 ± 0.0	0.9 ± 0.1	/
Si wafer functionalized with photoinitiator <b>1</b> moieties	10.4 ± 0.5	2.5 ± 0.1	2.9 ± 0.1	49.8 ± 0.3	33.4 ± 0.2	/	0.9 ± 0.0

#### 4.2.2 Surface-initiated photopolymerization from **1**-functionalized silicon wafer and quartz plate surfaces

From **1**-modified flat substrates, surface initiated photopolymerization reactions with four different monomers were carried out upon visible light illumination. In doing so, the quartz plates functionalized with the initiator on both sides were immersed in solutions of FIACr or PyrMAcr in THF, and exposed to light (405 nm) for 10 minutes. p(PFIACr) and p(AAm), respectively, were grafted from photoactive silicon wafers by drop coating of those substrates with liquid monomers (or monomer solutions) and subsequent illumination with light (405 nm) for 1.0 and 1.5 minutes, respectively. Finally, all wafers were intensely rinsed and ultrasonicated with appropriate solvents for multiple times, dried, and then characterized with regard to their surface composition and individual surface properties.

Similar to SIPP-reactions from **1**-functionalized nanoparticles, the initiating species at the surface undergo an  $\alpha$ -cleavage process (Norrish type I reaction) once the molecule has reached its triplet state T1 (after intersystem crossing from the S1 state), upon visible light illumination. As a consequence of each cleavage step, highly reactive germanium centred (germyl) radicals and - far less reactive - acyl radicals are formed. The surface coupled germanium centred radical readily adds to (meth)acrylic double bonds and therefore starts the radical chain growth mechanism from the surface.<sup>27,28</sup>

The grafted polymer layers p(FIACr) and p(PyrAc) on the quartz plates were characterized by XPS, proving successful surface-initiated polymerization on both sides (top and bottom). As can be seen from Table 8, a comparison of the surface composition before and after modification of the quartz plates revealed significantly increased carbon contents, which were assigned to the coupled polymer layers of p(FIACr) and p(PyrAc), respectively. Furthermore, a decrease of O and Si was observed after polymerization, indicating the formation of a polymer layer on top of the quartz substrate. Also, the polymer-modified quartz plates showed a significantly increased amount of Ge in relation to Si when compared to silicon wafers functionalized with compound **1** (Ge/Si ratio of about 0.28 and 0.07, respectively; see Table 8). This can be explained as a result of the grafted polymer layer because of which less material of the quartz plate, consisting of Si and O, was measured, therefore enhancing the contribution of the Ge-rich interface to the overall atomic surface composition. However, since Si and Ge, which originate from the substrate functionalized with compound **1**, were still detected after polymerization, the polymer layers were expected to be thinner than the XPS penetration depth, which is within the top 10 nm of the investigated surface.<sup>243,266</sup> In addition, also small amounts of Na, F and Zn were detected, but are considered to be negligible contaminations.

Table 8: Relative atomic surface composition of a neat quartz plate, and of quartz plates after surface modification via photoinduced “grafting from” of poly(fluorescein-o-acrylate) (p(FIAcr)) and poly(pyrene methacrylate) (p(PyrMAcr)).

Sample	Surface composition [at.-%]						
	C	O	Si	Ge	Na	F	Zn
Neat quartz plate	15.4 ± 3.0	60.6 ± 2.1	22.7 ± 1.3	/	1.3 ± 0.2		1.7*
Quartz plate_ p(FIAcr)	32.2 ± 1.1	46.3 ± 0.9	15.6 ± 1.2	4.4 ± 1.1	1.0 ± 0.3	1.2*	
Quartz plate_ p(PyrMAcr)	30.6 ± 1.8	47.0 ± 1.0	16.6 ± 0.8	5.5 ± 0.4	0.9*		

\*... single value, detected on only one of 4 measurement spots on the sample.

Besides XPS analyses the presence of fluorescent polymer layers p(FIAcr) and p(PyrMAcr) was proven by their specific UV-Vis absorbance and fluorescence spectra. As can be seen from Figure 43, the UV-Vis absorbance of the grafted polymer layers (see secondary y-axis) shows a similar curve shape compared to the corresponding monomer in solution. As the quartz plates were thoroughly washed before the measurements, this result evidenced the presence of immobilized polymers grafted from the quartz surfaces.

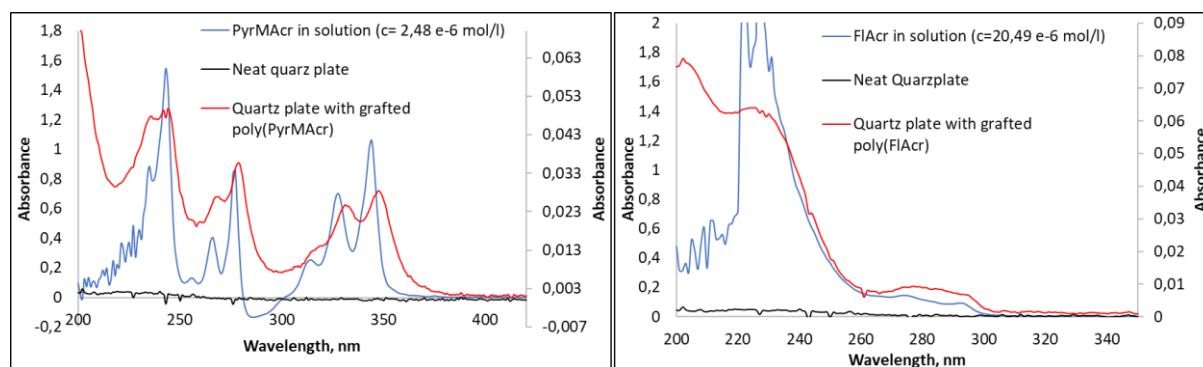


Figure 43: UV-Vis absorption of neat and modified quartz plates compared with the corresponding monomers in solution (absorption of the modified quartz plates is plotted using the secondary y-axis).

These results were supported by the fluorescence spectra which are depicted in Figure 45. Notably, the quartz plate with grafted p(PyrMAcr) showed a strong and visible fluorescence upon excitation with UV-light ( $\lambda = 366$  nm), which is also shown in this figure. On the other hand, visible fluorescence was not observed when exciting the quartz plate grafted with p(FIAcr) at the same wavelength. This is assigned to the fact that PyrMAcr displays a significantly higher molar decadic absorption coefficient in this region of about  $4500 \text{ L mol}^{-1} \text{ cm}^{-1}$  (at 366 nm) when compared to that of FIAcr ( $21 \text{ L mol}^{-1} \text{ cm}^{-1}$  at 366 nm (data from UV-Vis measurements, see Figure 44)).

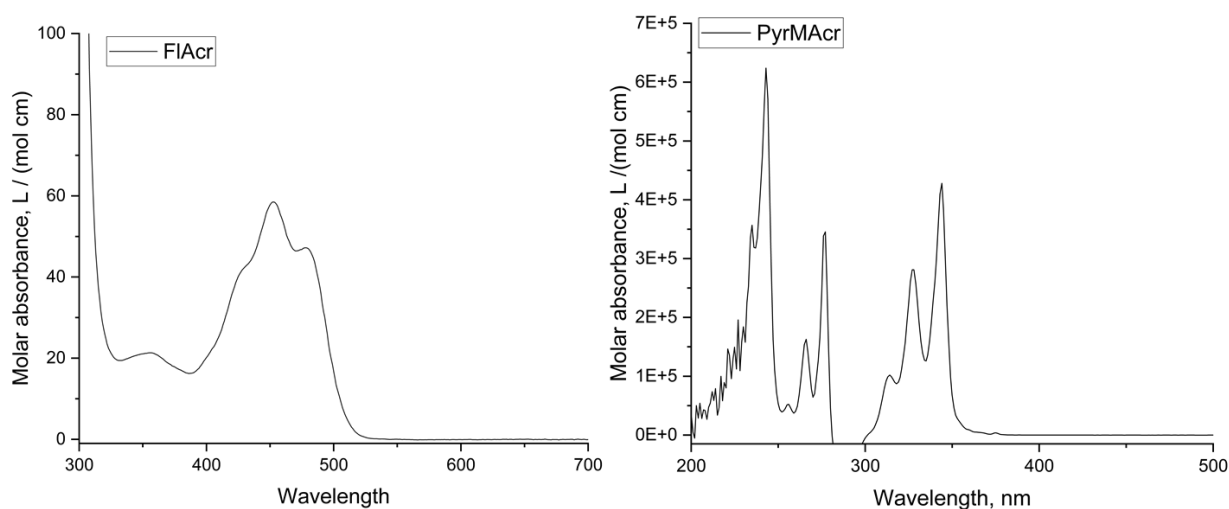


Figure 44: UV absorption properties of the used fluorescent monomers. Left: FIAcr; Right: PyrMAcr.

Nevertheless, when measuring the p(FIAcr)-grafted plate employing a fluorescence spectrometer, a signal, albeit rather weak, was observed which was in accordance with the signals of FIAcr in solution, thus also suggesting a successful grafting via photopolymerization. In contrast, fluorescence spectra of the quartz plate coated with p(PyrMAcr) revealed significant differences in respect to the spectra of the monomer in solution and the polymer layers (Figure 45). Especially the two sharp emission peaks in the region around 372 and 391 nm were only detected for the monomer solution but not observed for the polymer coated plate. In solution these peaks decreased with increasing monomer concentration (see Figure 45, blue and green curves). This phenomenon was also observed by Förster et al. who performed fluorescence measurements of dissolved pyrene at different concentrations. With increasing concentrations, they observed a change in the fluorescence properties, quenching violet fluorescence (peaks at 372 and 391 nm), which is accompanied by an appearance or increase of a broad blue fluorescence signal. This effect is attributed to singlet state excimer formation between an excited and unexcited pyrene molecule.<sup>267</sup> This explains those results as the grafted polymer layers contain a high concentration of pyrene moieties, resulting in the red-shifted fluorescence signal (see Figure 45).



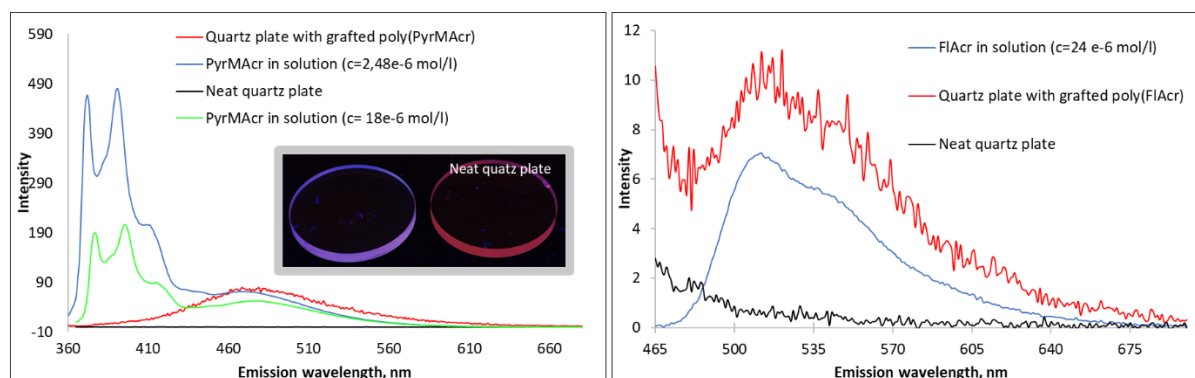


Figure 45: Fluorescence emission spectra of quartz plates bearing grafted p(PyrMAcr) (right, 347 nm excitation wavelength) and p(FIACr) (left, 450 nm excitation wavelength). The visible fluorescence upon excitation of grafted p(PyrMAcr) with 366 nm light is also shown (insert).

The successful grafting of PFACr and AAm onto modified silicon wafer surfaces was proven by quantitative evaluation of the respective XPS survey spectra. As shown in Table 9, coupling of p(PFACr) layers introduced a high amount of F (56.2 at.-%), whilst the deposition of p(AAm) resulted in a significant amount of N (16.7 at.-%). Additionally, the C content increased from 10.4 at.-% (functionalized wafer) to 38.2 at.-% after polymerization of PFACr, and to 65.8 at.-% after polymerization of AAm. In contrast, the elements Si, O and Ge could not be detected as the substrates were covered by the polymer layers, whose thickness exceeded the XPS penetration depth of about 5 nm. The thicknesses of the p(PFACr) and p(AAm) layers were measured with spectroscopic ellipsometry. The measurements revealed a thickness of 38 nm and 126 nm for p(AAm) and p(PFACr), respectively. The significantly higher thickness of p(PFACr) compared to that of p(AAm) is related to the fact that AAm was polymerized in diluted phase (see experimental part), thus limiting the degree of polymerization and, in further consequence, the layer thickness. However, the obtained thicknesses correspond well with already reported layer thicknesses (range from 8 to 190 nm), which were obtained from non-living surface-initiated polymerization reactions.<sup>40,62,64</sup> Interestingly, p(FACr) layers were visible with the naked eye as intensively coloured films (see Figure 47). The colouring results from Fabry-Perot interference, which is determined by the thickness and the refractive index of a thin layer meeting Bragg's condition. Interference colouring appears when a layer with a thickness of around 100 nm is deposited on a highly reflective surface. This phenomenon was, for example, used by Kado et al., who produced three dimensional polymeric nanostructures, which displayed interference colouring in dependence of their film thickness.<sup>79</sup>

Table 9: Overview of atomic surface compositions obtained from XPS survey spectra, and water contact angles (WCA) of a neat Si wafer, a Si wafer functionalized with photoinitiator **1**, and Si wafers bearing photo-grafted layers of p(PFAcr) and p(AAm).

sample	Surface composition [at.-%]							WCA [°]
	C	Ge	F	O	Si	N	Na	
Neat Si wafer	14.7 ± 0.6	/	/	32.3 ± 0.3	51.6 ± 0.0	0.9 ± 0.1	/	45.1 ± 1.4
Si wafer functionalized with photoinitiator <b>1</b>	10.4 ± 0.5	2.5 ± 0.1	2.9 ± 0.1	49.8 ± 0.3	33.4 ± 0.2	/	0.9 ± 0.0	58.6 ± 3.1
Si wafer with photo- grafted p(PFAcr)	38.2 ± 1.3	/	56.2 ± 1.6	5.55 ± 0.4	/	/	/	124.5 ± 0,8
Si wafer with photo- grafted _p(AAm)	65.8 ± 0.6	/	/	17.5 ± 0.2	/	16.7 ± 0.7	/	11.8 ± 0.8

Supporting the results of XPS analysis, high and low water contact angles (WCA, depicted in Figure 46) were obtained for p(PFAcr) and p(AAm) layers, respectively. The value of 124 ° significantly exceeds the initial WCA of the wafer functionalized with compound **1** (58 °), and is typical for fluorinated polymer surfaces.<sup>268,269</sup> In contrast to this, p(AAm) gave a low WCA (11 °) which results from the polar amide moieties on the polymer surface interacting well with the polar test liquid (water).

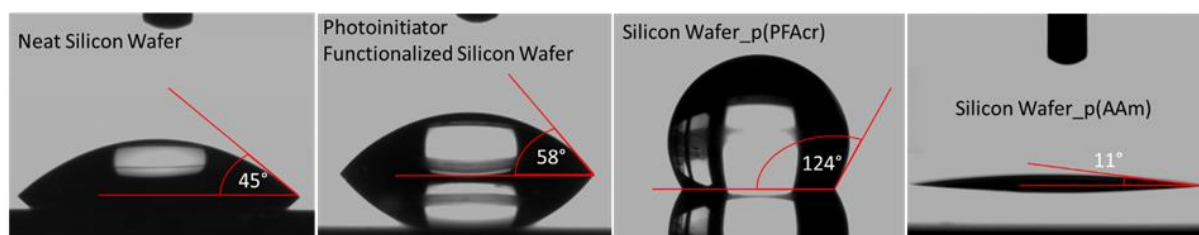


Figure 46: Water contact angles (WCA) on different Si wafers. From left to right: Neat silicon wafer, Si wafer functionalized with photoinitiator **1**, Si wafer with photo-grafted p(PFAcr), Si wafer with photo-grafted p(AAm).

### 4.2.3 Spatially resolved surface-initiated photopolymerization

Besides polymerization all over the wafer surface, spatially resolved photopolymerization reactions were carried out with PFAcr on functionalized silicon wafers. In a first step, the initiating species **1** was locally deactivated by illumination through a photomask. Subsequently, the photomask was removed, the substrates were completely covered with PFAcr, and a flood illumination (1 min) was carried out. This allowed for surface-initiated photopolymerization only at previously shielded and thus still photoactive areas. After multiple ultrasonication in HFIP, the patterned polymer layer of p(PFAcr) was investigated by optical microscopy as depicted in Figure 47, which shows a well reproduced logo with clear boundaries.

Both the zones bearing a photo-grafted polymer layer and the zones lacking a graft layer were characterized with XPS measurements. The resulting survey spectra are displayed in Figure 47. In accordance with the molecular structure of p(PFAcr) the polymer layer only consists of C, O and above all F (Figure 47, red curve). Notably, very small amounts of F (690 eV) were also found on the surface of the non-polymerized areas (compare black curve Figure 47), which can be assigned to a few grafted chains of p(PFAcr). This is supported by the corresponding high-resolution XPS-spectra of C1s and F1s (see Figure 48). From the deconvolution procedure applied to C1s, five contributions can be identified, two of which clearly proving the presence of CF<sub>2</sub> (291.4 eV) and CF<sub>3</sub> (293.8 eV) units.<sup>243</sup> Moreover, the F1s spectrum shows only one peak at 688-689 eV, which is attributed to organic fluorine compounds. It is anticipated that, after the deactivation step (illumination without monomer being present), still some few photosensitive moieties remained on the surface, which in turn were capable to initiate photopolymerization of PFAcr during the second (flood) illumination step. Those moieties could be either (a) Ge-COMes formed via in-cage recombination (see Scheme 26), or (b) a germy-peroxyl species derived from the reaction between a germyl radical and oxygen (from air), followed by hydroperoxide formation.<sup>270</sup>

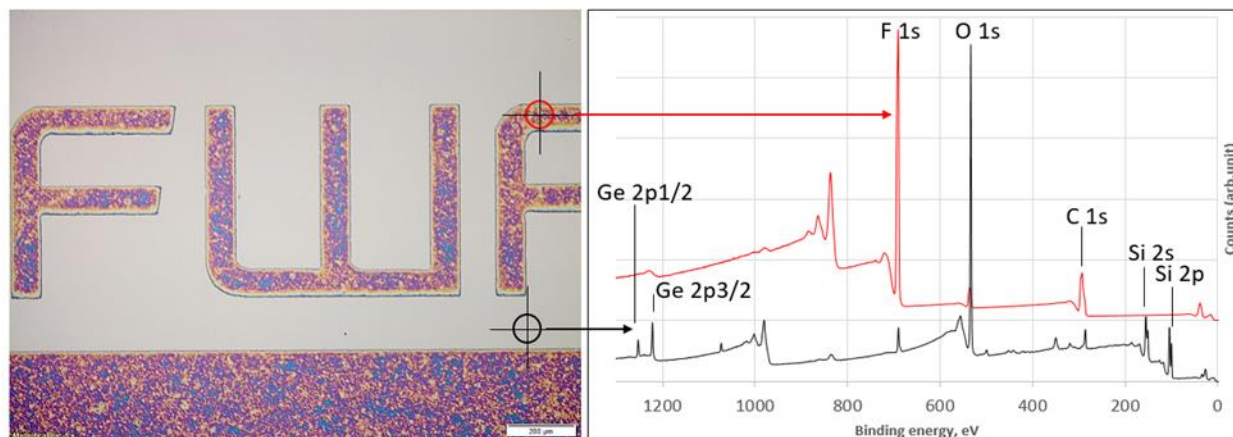


Figure 47: Microscope image of a patterned p(FACr) film (coloured areas) grafted on a Si wafer (grey areas are lacking a graft-layer), and corresponding XPS survey spectra. The red curve is assigned to the area bearing a photo-grafted polymer layer, and the black curve is assigned to areas lacking a graft-layer.

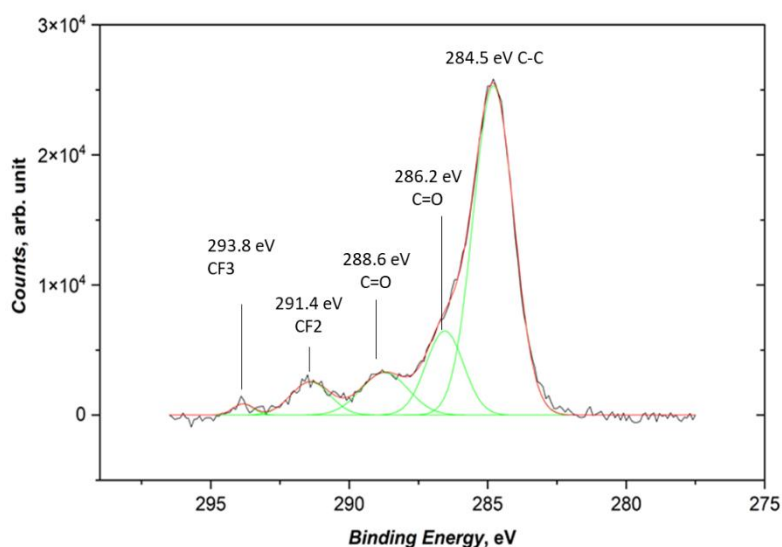


Figure 48: XPS C1s-deconvolution spectra of patterned samples (non-polymerized area).

The optical resolution in dependence on the experimental illumination conditions was also investigated. In doing so, different procedures - varying the illumination time and intensity - for the first illumination step (spatially resolved deactivation step, without drop cast PFAcr) were applied. The resolution of the patterned structure was followed with XPS-mapping (F, Si mapping) and optical microscopy (refer to experimental section) after subsequent SIPP of PFAcr. When comparing the images below, it can be inferred that the resolution shows a strong dependence on the different experimental procedures. Although optical microscopy in all cases evidenced patterns with sufficiently sharp borders, XPS mapping results, on the other hand, demonstrated a rather poor resolution, most significant for illumination procedure C

(Figure 51), which consisted of a continuous light exposure time of only 60 seconds ( $39.0 \text{ J cm}^{-2}$ ). In that case, by mapping F1s and Si2p, no spatially resolved atomic distribution can be seen. The best results were found for procedure A (Figure 49), where the same light dose of  $39.0 \text{ J cm}^{-2}$  was used as for procedure C. The difference was that after 20 s of illumination a 10 min idle phase (without illumination) was performed, followed by another 20 s illumination step and another idle phase (10 min). This cycle was repeated for one last time so that the total illumination time was 60 s. After final SIPP with PFACr, the areas comprising a high fluorine content, due to the grafted p(PFACr), appeared in red colour and are in accordance with the multicoloured layer, obtained via optical microscopy. Vice versa, the largest amount of Si (highlighted in blue) was found at “polymer-free” surfaces. From these results, it can be concluded that time is required to allow oxygen to diffuse between the mask and the sample. Procedure B (Figure 50), which also proved to enhance the spatial resolution when compared to C, comprised continuous illumination for 30 minutes ( $70 \text{ J cm}^{-2}$ ). Since no better resolution was obtained when compared to procedure A, the increased light dose does not seem to have a significant impact.

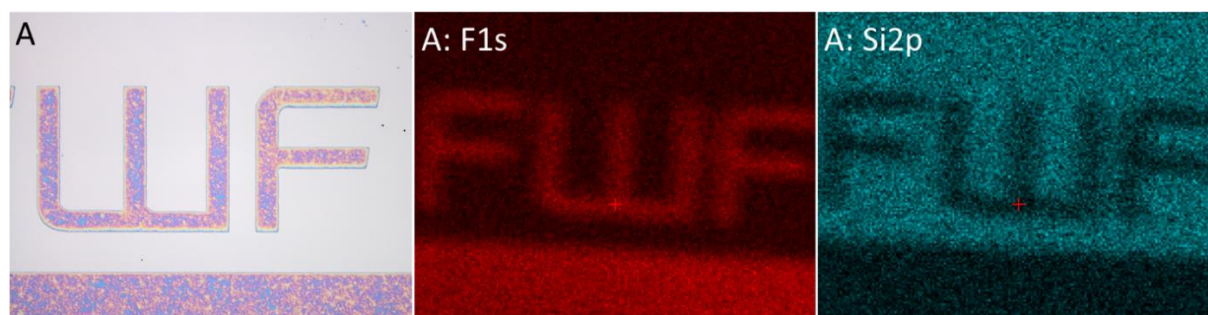


Figure 49: Achieved resolution derived by procedure A; Left: Imaging via optical microscopy with 10 times magnification; Red: XPS F1s mapping (fluorine atoms are highlighted red); right: Si2p mapping (silicon atoms appear in blue colour).

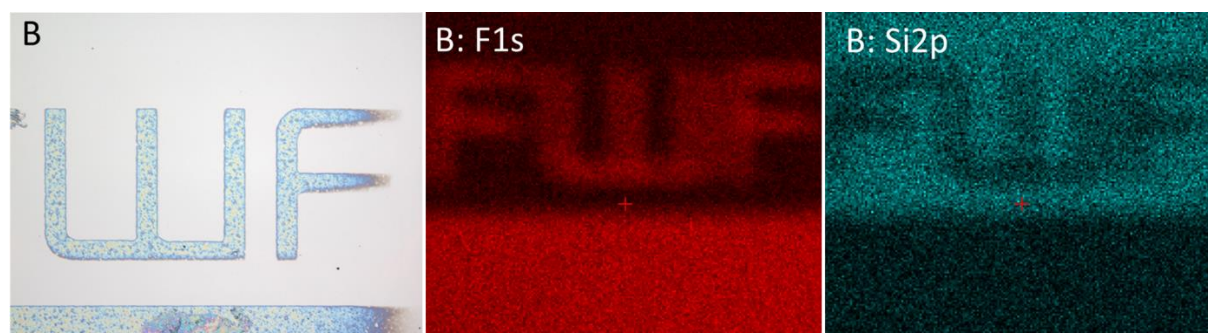


Figure 50: Achieved resolution derived by procedure B; Left: Imaging via optical microscopy with 10 times magnification; Red: XPS F1s mapping; right (fluorine atoms are highlighted red): Si2p mapping (silicon atoms appear in blue colour).

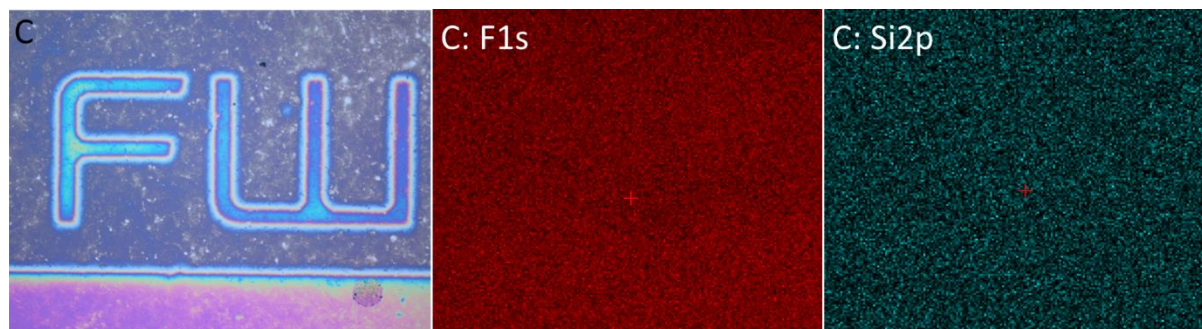
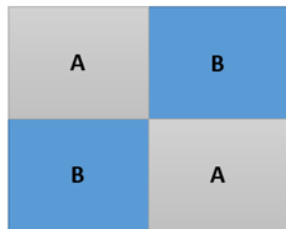


Figure 51: Achieved resolution derived by procedure C; Left: Imaging via optical microscopy with 10 times magnification; Red: XPS F1s mapping (fluorine atoms are highlighted red); right: Si2p mapping (silicon atoms appear in blue colour).

In addition, combined polymer layers with both p(PFAcr) and p(AAm) regions were prepared by the use of a simpler designed photomask. Therefore, a solution of AAm in EtOH was drop coated onto a Si wafer functionalized with compound **1**, and illuminated through a photomask that covers two quarters of the wafer diagonal to each other (see Figure 52a). After light exposure through the respective photomask, the wafers were washed with EtOH, drop coated with PFAcr, and again illuminated without a mask in order to initiate graft-polymerization in those regions which were covered in the first step. After thorough rinsing and drying, contact angle measurements (WCA) were performed.

As shown in Figure 52b, WCA measurements of the quarter-structured polymer layer indeed proved hydrophilic areas of p(AAm) ( $\text{WCA} < 15^\circ$ ) in those areas, where the photo-grafting was performed in the first step, while hydrophobic areas of p(PFAcr) ( $\text{WCA} > 120^\circ$ ) were found in those areas which were initially shielded by the mask, and covered with a photo-grafted polymer layer in the second illumination step.

a) Mask covering two diagonal quarters of the substrate



A...non-covered side of the substrate  
B...covered side of the substrate

b) quarter structured polymer layers comprising a combination of hydrophobic and hydrophilic areas

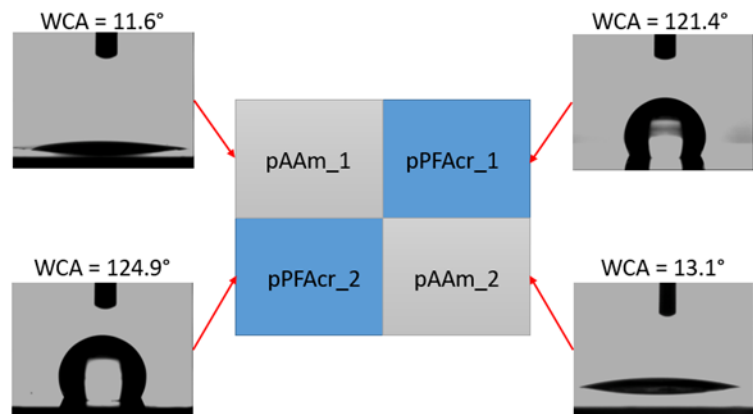


Figure 52: (a) Schematic representation of the applied photomask to prepare quarter-structured polymer layers on a silicon wafer, and (b) WCA measurements on the structured polymer surface with hydrophobic and hydrophilic areas.

#### **4.2.4 Conclusion with respect to grafting-from techniques using planar surfaces functionalized with initiator 1**

Using the halogen substituted trisacylgermane (bromo-tris(2,4,6-trimethylbenzoyl)germane, compound **1**) for surface modification of silicon wafers and quartz plates lead to photo-sensitive surfaces, as evidenced by XPS studies. Similar to the findings for silica nanoparticles (section 4.1.1), the presence of germanium and the absence of bromine atoms at the surface suggested the covalent immobilization of the initiating species. Furthermore, it is shown that the attached Ge based photoinitiator is capable of efficiently initiating a visible light-induced and surface-mediated polymerization of various monomers. The resulting layers were characterized with regard to their chemical composition employing XPS, UV-Vis and fluorescence spectroscopy as well as water contact angle (WCA) measurements to investigate their specific surface functionality. Using neat 1H,1H,2H,2H-perfluorodecyl acrylate as the monomer for the grafting from reaction, thick hydrophobic layers (thickness up to 126 nm) with water contact angles  $> 120^\circ$  were obtained. Also, those layers were visible with the naked eye due to the strong colouring of the surface, based on an interference effect. When performing a spatially resolved depletion of the immobilized photoinitiator, patterned photo-grafted polymer layers were obtained after flood illumination in the presence of monomers. The ability of the patterned layers to withstand multiple rinsing cycles once more proved their covalent attachment to the surface. In addition, acrylamide was used for surface-initiated polymerization reactions, leading to hydrophilic surfaces as demonstrated by a water contact angle lower than  $15^\circ$ . With a similar approach structured surfaces bearing both hydrophobic and hydrophilic areas were prepared. Hence, it can be inferred that this technology is also suitable to produce smart surfaces.

Last but not least, poly(fluorescein-o-acrylate) and poly(1-pyrenemethyl methacrylate) were successfully grafted from **1**-modified quartz plates. For the grafted poly(fluorescein-o-acrylate) strong fluorescence upon excitation with 366 nm was observed. This fluorescence was also visible with the naked eye.



### 4.3 Free radical promoted cationic photopolymerization with acylgermanes

As already mentioned in the introductory section, acylgermanes can also be employed for starting cationic polymerization reactions. In earlier works benzoyltrimethylgermane (BTG) and dibenzoyldiethylgermane (Ivocerin), which are representatives of mono-, -and difunctional acylgermanes, proved to efficiently drive free radical promoted cationic polymerization reactions of epoxides and vinyl ethers.<sup>35,271</sup> So far, tris- and tetraacylgermanes, whether they are surface-attached or not, have not been used in that context. Therefore, this chapter focuses on the usability of free as well as surface-attached trisacylgermanes in starting so called (surface-initiated) “free radical promoted cationic polymerizations” (SI-RPCP) of epoxides and vinyl ethers.

Notably, the outcomes, presented in this chapter, were developed in close cooperation with **Zizheng Zhang** (PhD candidate, Chair of Chemistry of Polymeric Materials, University of Leoben, AUT).

#### 4.3.1 Capability of acylgermanes for curing epoxide resins

In the first step of this investigation, different non-coupled germanium based photoinitiators including bis-, tris- and tetraacylgermanes as well as  $\text{Ph}_2\text{I}^+\text{PF}_6^-$  (DPIHFP) were characterized by means of UV-Vis measurements in order to choose the correct light source for subsequent photo-DSC and surface-initiated photopolymerization experiments. Notably,  $\text{Ph}_2\text{I}^+\text{PF}_6^-$  and other onium salts are commonly used as photo acid generators (PAGs), which form  $\text{HPF}_6$  upon UV-illumination (up to 325 nm).  $\text{HPF}_6$  is an exceptionally strong acid for inducing cationic polymerization reactions. However, when acylgermanes are present and visible light ( $\lambda$  well above 325 nm) is used,  $\text{Ph}_2\text{I}^+\text{PF}_6^-$  is observed to be ineffective as PAG, but is readily reduced by germyl radicals. Vice versa, the germyl radical is oxidized, hence forming a germanium centred cation, which is capable of inducing cationic polymerization (refer to the mechanism in Scheme 29).<sup>35</sup> Therefore, light sources emitting wavelengths above the absorption of DPIHFP (325 nm) must be chosen in order to ensure the exclusive formation of the germanium-based cationic species. The optical absorption properties of DPIHFP as well as the emission spectra of the employed light sources are depicted in Figure 53. As can be seen, the iodonium salt does not absorb at wavelengths emitted by the filtered Hg lamp (dashed red) and the LED (dashed black curve), respectively. Consequently, the formation of  $\text{HPF}_6$  by direct excitation of the photoacid generator  $\text{Ph}_2\text{I}^+\text{PF}_6^-$  can be excluded.

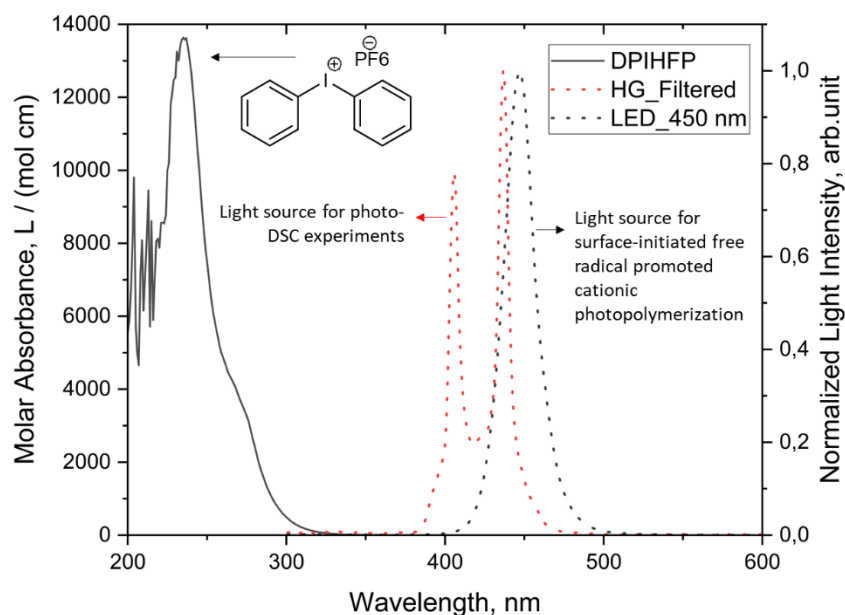


Figure 53: UV absorption properties of  $\text{Ph}_2\text{I}^+\text{PF}_6^-$  (DPIHFP) and emission spectra of the employed light sources.

The optical absorption spectra of the acylgermanium derivatives are shown in Figure 54. Additionally, the molecular structures of the presented compounds are included, except for compound **1**, the structure of which has already been presented in previous sections. By comparison it has been found that the measured germanium-based compounds differ in respect to their molar absorbance. The highest visible light absorbance was observed for hydroxy-tris(2,4,6-trimethylbenzoyl)germane (GeOH), followed by compound **1**. It is assumed that electron withdrawing groups such as halides, hydroxyl and alkoxy units cause this increase in absorbance due to an enhanced oscillation strength of the  $n/\sigma - \pi^*$  transition. This is supported when comparing the higher molar absorbance of compound **2** (ethoxy-derivative) to that of the respective ethyl substituted trisacylgermane (GeEt, black curve in Figure 54). Given that the only difference between these molecules is the oxygen atom coupled to the germanium center, the increased molar absorbance has to be related to this factor. However, an intensive investigation of this effect was beyond the scope of this research, and is therefore not included herein. Nevertheless, it is shown that the light absorption of each germanium-based compound lies within the emission of the used light sources. Hence, those light sources are suitable for RPCP.

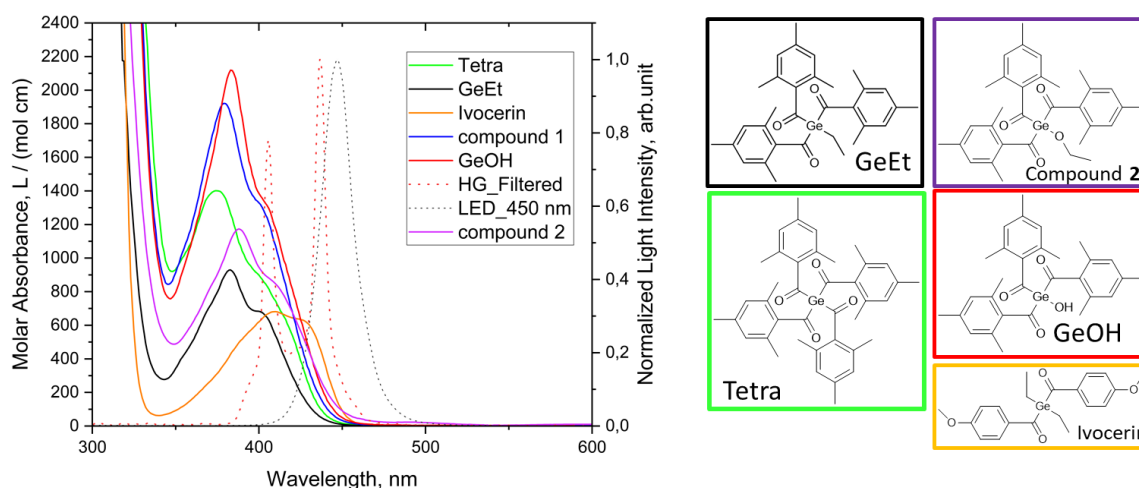


Figure 54: Light absorption properties of bis-, tris-, and tetraacylgermanes.

In order to test whether bis-, tris- and tetraacylgermanes are suitable for radical promoted cationic photopolymerization (RPCP), photo-DSC measurements were conducted. For this purpose, different acylgermanes (1 mol.-%) were dissolved in anhydrous DCM and mixed with bisphenol-A -diglycidylether (DGEBA) and DPIHFP (1 mol.-%). After the solvent was removed under reduced pressure and elevated temperature, the samples were transferred into the DSC device and illuminated with wavelengths between 380 and 480 nm, using a Hg- lamp in combination with a light filter. Moreover, a control experiment, without the addition of any Ge-based moiety was performed. The results are presented in Figure 55, and the polymerization parameters (polymerization heat release  $\Delta H$ , maximum peak height  $h$ , time when 95% of the final conversion was reached [  $t_{95\%}$  ]) are summarized in Table 10.

As expected, no polymerization took place when the germanium based photoinitiator was absent as no heat flow was detected (refer to the grey curve in Figure 55). This result clearly highlights the dominant role of those species in RPCP. The situation changed when either Ivocerin, Tetra, GeEt, GeOH or compound 1 was added to the mixture, showing a significant heat release due to the cationic polymerization of DGEBA in each case. Surprisingly, the polymerization parameters such as the maximum peak height ( $h$ ,  $W g^{-1}$ ), polymerization heat ( $\Delta H$ ,  $J g^{-1}$ ) as well as the time until 95% of the final conversion was reached ( $t_{95\%}$ , min) differed among the used photoinitiators (see Table 10). The most efficient polymerization was observed when difunctional Ivocerin was used, followed by the fourfold functional tetraacylgermane. This is even more surprising when the low molar absorption of Ivocerin is compared to that of the other investigated molecules in Figure 54. However, the light absorption spectrum of Ivocerin is slightly red shifted, therefore matching the light emission of the Hg light source in a better way. Nevertheless, this effect seems to be negligibly small so that this fast and extensive polymerization cannot be explained herewith. Obviously, the amount of light absorption does not have a clear influence on the polymerization kinetics at

all. When using compound **1** or GeOH for RPCP, which both exhibit high molar decadic absorption coefficients, comparatively low values for the polymerization heat ( $\Delta H = 161.4$  and  $174.4 \text{ J g}^{-1}$ , respectively) were observed. This indicates that the electron withdrawing bromine atom and the hydroxyl unit both might have an inhibition effect on the formation of the germanium centred cationic species. Besides, the hydroxyl group might act as Lewis-base during the cationic curing. When comparing with GeEt and Tetra, which are representatives of tris- and tetraacylgermanes, no significant difference related to the polymerization parameters was found.

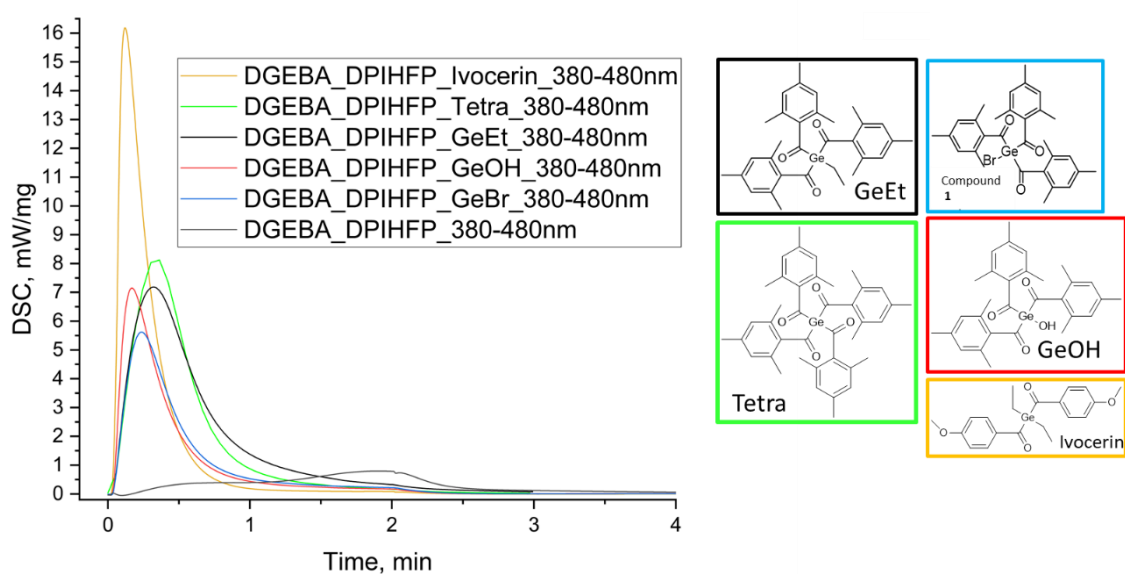


Figure 55: Photo-DSC traces for different germanium based photoinitiators in combination with DPIHFP.

Table 10: Comparison of the polymerization kinetic parameters including the maximum peak height ( $h$ ,  $W g^{-1}$ ), polymerization heat ( $\Delta H$ ,  $J g^{-1}$ ) and the time until 95% of the final conversion was reached ( $t_{95\%}$ ).

	$\Delta H$ [ $J g^{-1}$ ]	$h$ [ $W g^{-1}$ ]	$t_{95\%}$ [min]
DGEBA_DPIHFP_Ivocerin_380-480nm	$308 \pm 4.3$	$13.1 \pm 0.6$	$1.26 \pm 0.09$
DGEBA_DPIHFP_Tetra_380-480nm	$265 \pm 2.2$	$7.4 \pm 0.5$	$1.45 \pm 0.07$
DGEBA_DPIHFP_GeEt_380-480nm	$284.7 \pm 4.7$	$7.3 \pm 0.1$	$1.58 \pm 0.02$
DGEBA_DPIHFP_GeOH_380-480nm	$174.4 \pm 7.0$	$7.1 \pm 0.5$	$1.5 \pm 0.04$
DGEBA_DPIHFP_1_380-480nm	$161.4 \pm 5.9$	$5.7 \pm 0.6$	$1.61 \pm 0.02$
DGEBA_DPIHFP_380-480nm	/	/	/

All in all, it can be concluded that all tested photoinitiators, which are depicted in Figure 55 are capable to initiate RPCP of DGEBA. The kinetics of the RPCP process is first and foremost dependent on the molecular structure of the used germanium-based compound. It has to be emphasized that a detailed mechanism for the oxidation of germyl radicals, derived by visible light illumination of bis-, tris- and tetraacylgermanes, has not been studied so far. Hence, it cannot be predicted how the sequential photoinduced  $\alpha$ -scission from two (Ivocerin), three (trisacylgermane) or four reactive sites (Tetra) leads to the formation of the cationic species in the presence of DPIHFP. Also, a set of side reactions such as hydrogen abstraction or molecular rearrangements, cannot be ruled out.

### 4.3.2 Results on surface-initiated, free radical promoted cationic photopolymerization (SI-RPCP)

After photo-DSC investigations had proven that trisacylgermanes are capable to start a visible-light induced cationic polymerization process in the presence of DPIHFP, efforts have been made in order to test whether this can also be done by means of grafting-from techniques, using nanoparticles bearing trisacylgermanium moieties at their surface. An overview of the applied methodology is provided in Scheme 29. The general mechanism (first row) is presented with the example of monofunctional benzoyltrimethylgermane (BTG) as had originally been described by Yagci et al.<sup>35</sup> Upon light illumination, BTG undergoes an  $\alpha$ -cleavage pathway from the excited triplet state resulting in the formation of two radicals, namely trimethylgermyl and benzoyl. The latter one is not considered to undergo significant redox reactions due to the low reactivity towards even stronger oxidants than DPIHFP. Germyl radicals, on the other hand, are electron donating, making them suitable to undergo redox reactions with iodonium salts, having a high reduction potential. The so formed germanium centred cation proved its capability to initiate cationic polymerization of various vinyl ethers and epoxides. Besides, Lalevee et al. additionally confirmed the oxidation of triphenylgermyl and tris(trimethyl-silyl)germyl radicals by iodonium salts.<sup>272</sup> As previously mentioned, a mechanism for the formation of germanium centred cations derived from trisacylgermanes and DPIHFP is not clear. In order to test if all (three) cleavable groups ( $\text{Ge}-(\text{COMe})_3$ ) can be consumed when DPIHFP is present, photo-bleaching experiments were conducted. For this, GeEt and 1 eq. of DPIHFP were dissolved in DCM and illuminated with 405 nm (30 mW) for 5 minutes. UV-Vis spectra were recorded every 10 seconds. A control experiment in the absence of DPIHFP was also carried out. The results, which are shown in Figure 56, indicate that all the cleavable Ge-COMe groups were consumed, since no absorption at 415 nm was observed after 5 minutes of irradiation. Combining this with the principally possible oxidation of germyl radicals by  $\text{Ph}_2\text{I}^+\text{PF}_6^-$ , the mechanism is assumed to be as shown in Scheme 29 (second row), where R stands for an organic or inorganic group.

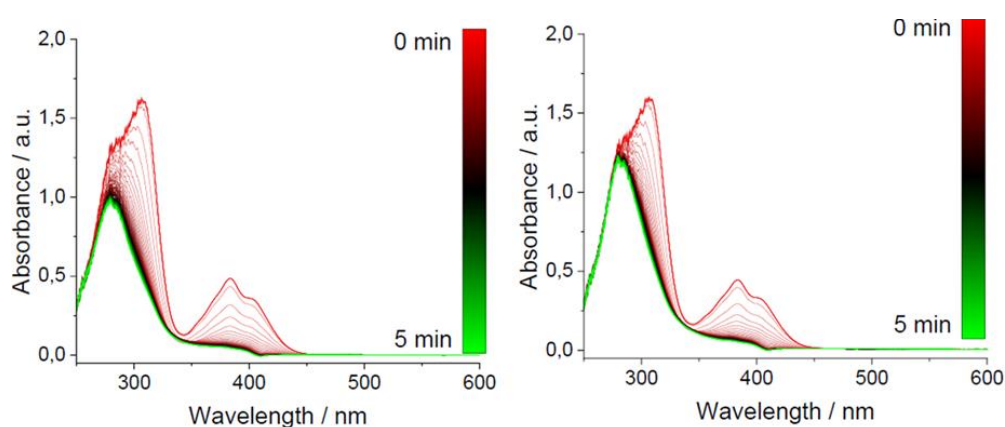
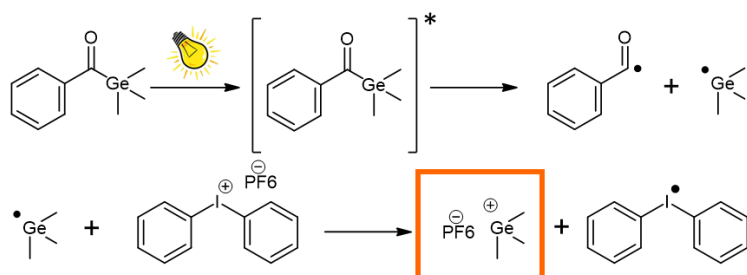
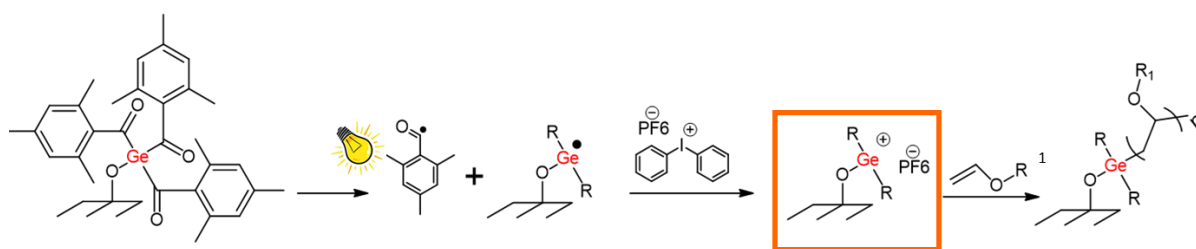
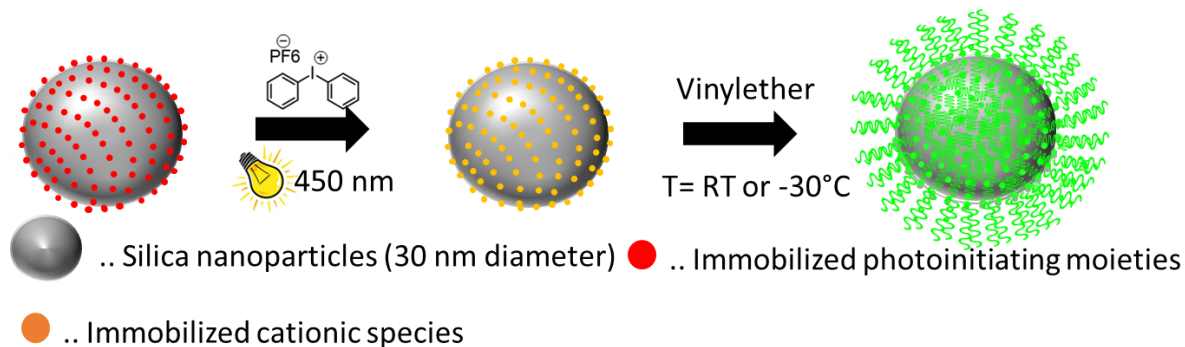
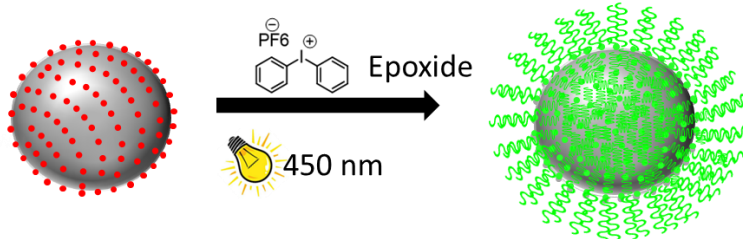


Figure 56: Photo-bleaching test using GeEt in DCM with (left) and without (right) the addition of DPIHFP; monochromatic illumination with 405 nm.

## I) General mechanism on the oxidation of germyl radicals



## II) Proposed mechanism for coupled trisacylgermanes

III) Grafting-from **cationic** polymerization of vinyl ethersIV) Grafting-from **cationic** polymerization of Ge of epoxides

Scheme 29: Schematic illustration of the surface-initiated radical promoted cationic polymerization process including the assumed mechanism for surface-attached photo-sensitive moieties (second row); the first row was reproduced from ref. 35.

For surface-mediated polymerization experiments, 30 nm sized silica particles and one representative of cationic polymerizable epoxides and vinyl ethers (cyclohexene oxide CHO, and n-propyl vinyl ether nPVE, respectively) were chosen.

For grafting p(nPVE), the **1**-modified nanoparticles (III in Scheme 29) as well as  $\text{Ph}_2\text{I}^+\text{PF}_6^-$  were dried carefully, after which they were dispersed/ dissolved in a mixture of anhydrous DCM

and toluene. This was followed by an illumination step with visible light (450 nm) for 8 min. Thereafter the mixture was cooled to -30 °C or kept at room temperature. After that, 200  $\mu\text{L}$  of the distilled and dried monomer per 100 mg of nanoparticles was added slowly. This was done to avoid any interaction of germyl radicals with the monomer, especially for nPVE. Finally, the functionalized nanoparticles were washed with DCM for multiple times, dried, and characterized by FTIR and TGA.

In fact, the presence of grafted p(nPVE) was confirmed by FTIR-investigations (Figure 57), revealing a set of aliphatic C-H stretching vibrations at 2967, 2939 and 2880  $\text{cm}^{-1}$  along with C-H deformation vibrations at 1465 and 1383  $\text{cm}^{-1}$  for the p(nPVE) grafted nanoparticles. Those peaks were compared to homopolymerized p(nPVE) using Ivocerin and DPIHFP as initiating system, the spectrum of which is also included in that figure and highlighted as blue dashed line. As can be seen from the enlarged illustration, the previously mentioned signals agree with those of the corresponding homopolymer, albeit a little bit shifted. Unfortunately, the strong characteristic -C-O-C asymmetric stretching vibration at 1082  $\text{cm}^{-1}$  cannot be seen measuring the particles, because it is overlapped by the very broad and intense -Si-O-Si stretching signal in this region.<sup>232</sup>

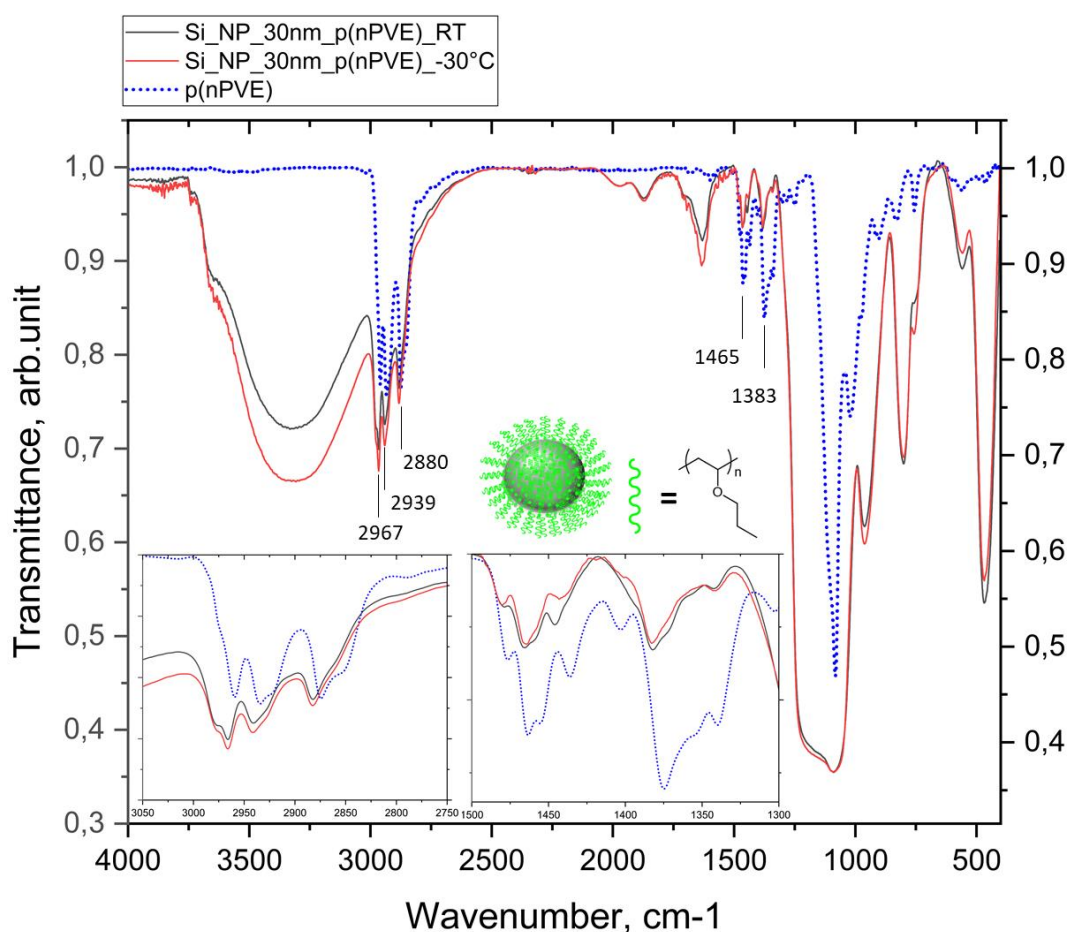


Figure 57: Results from FTIR spectroscopy (transmission mode) for p(nPVE) grafted nanoparticles, and comparison with the homopolymer p(nPVE).



Moreover, TGA data suggested a polymer content of approximately 20 %, as shown in Figure 58. Similar to radically derived polymer grafts, the corresponding grafting yields ( $\sigma_{mg}$ ,  $\text{mg m}^{-2}$ ) were calculated from equation 1. For p(nPVE) grafted products the grafting yield was  $1.63 \text{ mg m}^{-2}$ . From that perspective, the efficiency of the applied method can be compared to the radical polymerization of styrene in diluted phase (25 vol.-% of styrene in toluene) yielding  $1.64 \text{ mg m}^{-2}$  of immobilized polymer with a molar mass  $M_n = 5.800 \text{ g mol}^{-1}$  (number average).

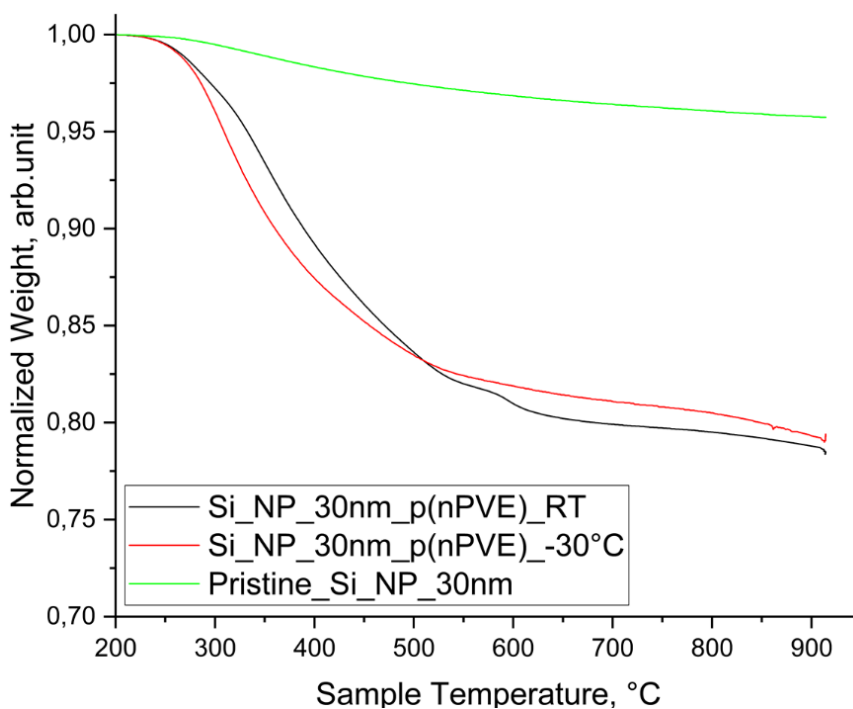
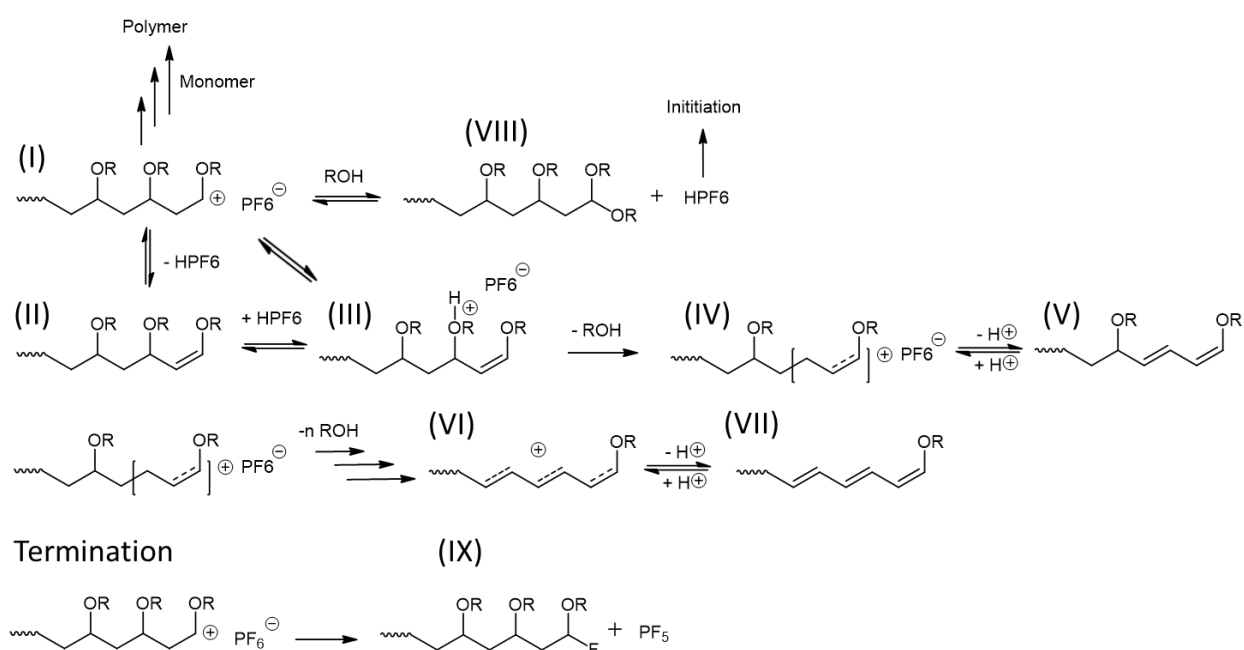


Figure 58: TGA investigations of  $\text{SiO}_2$  nanoparticles with surface grafted p(nPVE).

Interestingly, the different polymerization temperatures did not have a significant impact on the grafting yield. However, when polymerizing nPVE at room temperature, it was observed that the colour of the reaction mixture changed from colourless to deep black after the monomer was added. Furthermore, the finally obtained nanoparticles appeared in a yellow colour, which was not the case for the products that were derived via SI-RPCP at  $-30^\circ\text{C}$ . The discoloration phenomena were originally discussed by Aoshima and Higashimura more than four decades ago.<sup>273</sup> In their work the authors gave proof that discoloration is related to several chain transfer and termination processes during cationic chain growth, leading to unsaturated polyene structures via splitting off alcohol molecules. These mechanisms are described according to Scheme 30. The propagating chains (I) undergo rearrangements yielding an oxonium ion (III) either via direct  $\beta$ -proton migration or due to  $\beta$ -proton abstraction by the counter ion across olefin (II). Owing to the well-known decomposition of protonated ethers into alcohols and carbocations under acidic conditions, the intermediate species (III) is transformed into a conjugated species (IV), which is in equilibrium with structure

(V). From structure (III) multiple dealcoholation steps can occur, which finally leads to the formation of a widely or even fully conjugated and black coloured polyene cation (VI). The neutralized polymer (VII) usually appears in yellow colour,<sup>274</sup> which is in agreement with the observed colour of the produced p(nPVE)-grafted nanoparticles. Besides, the released alcohol molecules (Lewis base) are well known transfer agents in cationic polymerization processes, so that terminated acetal end-capped polymers (VIII) are formed upon the reaction of ROH with (I). Furthermore, the yielded HPF<sub>6</sub> super acid can again induce polymerisation of remaining monomers in the solution. Supporting this, the formation of non-coupled homopolymers was indeed observed when nanoparticles were modified with SI-RPCP. Homopolymers were obtained as yellow to red coloured and highly viscous materials.



Scheme 30: Side reactions during non-controlled cationic polymerization of vinyl ethers.

Although the strong fluorine-phosphorus bond, present in the PF<sub>6</sub><sup>-</sup> counterion, is difficult to cleave, an irreversible termination according to the reaction in Scheme 30 (last row) can also be considered for the applied SI-RPCP.<sup>274</sup>

As mentioned above, lowering the temperature during SI-RPCP did surprisingly not increase the amount of grafted polymer, although carrying out cationic polymerizations at deep temperatures usually suppresses termination and other side reactions, and therefore yields higher molar masses.<sup>275</sup> Nevertheless, no black colouring of the reaction mixture and no yellowish discoloration of the core-shell nanoparticles was observed in that case. In order to demonstrate this, UV-Vis spectra of the respective p(nPVE)-grafted nanoparticles were taken, see Figure 59. It is demonstrated that p(nPVE)-grafted nanoparticles, which were synthesized at room temperature, exhibit a notably higher light absorption, tailing widely in the visible

light range (compare to black curve in Figure 59). Since that was not observed for the products obtained at  $-30\text{ }^{\circ}\text{C}$ , it can be concluded that polyene formation can be suppressed at low temperatures.

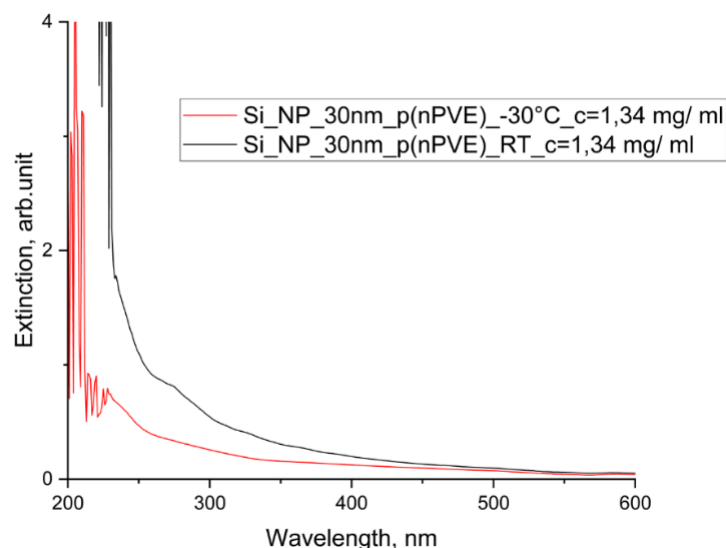


Figure 59: Light absorption of p(nPVE) grafted nanoparticles, produced at different temperatures (red:  $-30\text{ }^{\circ}\text{C}$ , black: room temperature).

Finally, and to ensure that the grafted polymer was synthesized as a consequence of SI-RPCP without any doubt, two control experiments were performed. For the first one, the SI-RPCP procedure for grafting nPVE was repeated but without the addition of the oxidizing iodonium salt (DPIHFP) in order to emphasize the dominant role of the formed germanium centred cationic species. Furthermore, and aiming to explore if amphoteric surface silanol groups generally react with free cationic propagating chains (possibly resulting in free  $\text{HPF}_6$ , see first row in Scheme 30), pristine silica nanoparticles were dispersed into a DCM/toluene solution of Ivocerin and DPIHFP. After illumination, nPVE was added slowly, and the polymerization was allowed to proceed for one hour. The nanoparticles from those experiments were washed thoroughly and characterized via TGA and FTIR.

Surprisingly, TGA and FTIR results indeed indicated the presence of some immobilized organic species in the first control experiment (SI-RPCP procedure without DPIHFP), although to a much lesser extent when compared to nPVE grafting in the presence of DPIHFP. The organic content was found to be approximately 13 % (refer to blue curve in Figure 60). When comparing the FTIR spectra in Figure 61 through normalization to the Si-O-Si stretching vibration at  $1076\text{ cm}^{-1}$ , aliphatic C-H signals occurred also for this sample, but both the peak shapes and their position differed when compared to p(nPVE)-grafted nanoparticles. This was also true for the corresponding signals in the region between  $1500$  and  $1350\text{ cm}^{-1}$ . Hence, it is

concluded that this immobilized organic species is not p(nPVE) but rather a side product. It cannot be said with certainty which organic moieties are present, but it is assumed that this attachment is a consequence of reactions of coupled germyl radicals. It can be inferred that highly reactive and usually short-lived radicals react in some way, especially when no suitable reaction partners such as DPIHFP or unsaturated monomers are present.

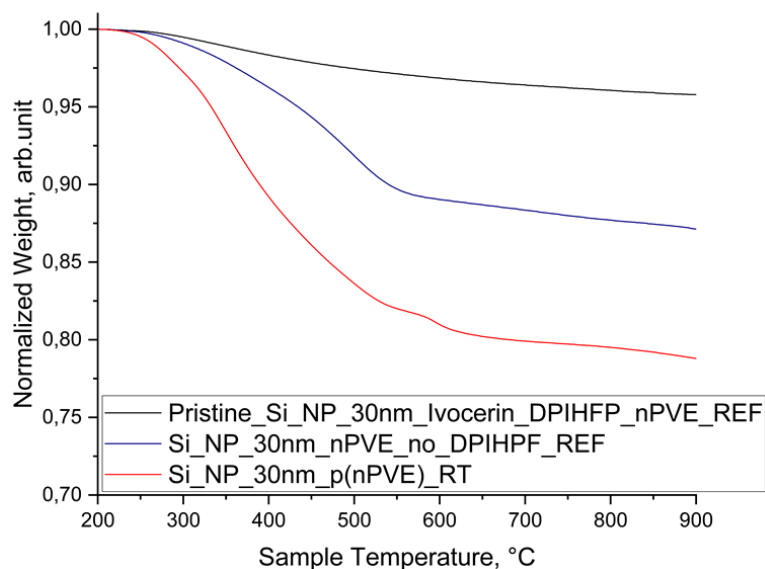


Figure 60: TGA results for 30 nm sized nanoparticles with surface-tethered p(nPVE) including weight loss curves of products obtained from control experiments.

On the other hand, no significant mass loss (TGA) was observed in the second control experiment. Here, nPVE was polymerized (using Ivocerin and DPIHFP as initiators) in the presence of neat SiO<sub>2</sub> nanoparticles. Therefore, a significant contribution of silanol groups to surface-attached polymers, according to first row in Scheme 30, can be ruled out.

Summing up, it has been shown that using a typical vinyl ether as monomer and 1-functionalized nanoparticles in combination with an iodonium salt, surface-attached polymers with a grafting yield of 1.63 mg m<sup>-2</sup> were obtained by means of SI-RPCP. Although undesired, the black colour of the reaction mixture and the yellow colour of the SiO<sub>2</sub> core-shell nanoparticles confirm the cationic polymerization mechanism. This is also evidenced by control experiments, which proved that without the iodonium salt for oxidizing the covalently coupled germyl radical, no attached p(nPVE) can be identified at the nanoparticles' surfaces. Also, the p(nPVE)-grafts did certainly not result from free propagating chains, and subsequent coupling reactions with surface silanols.

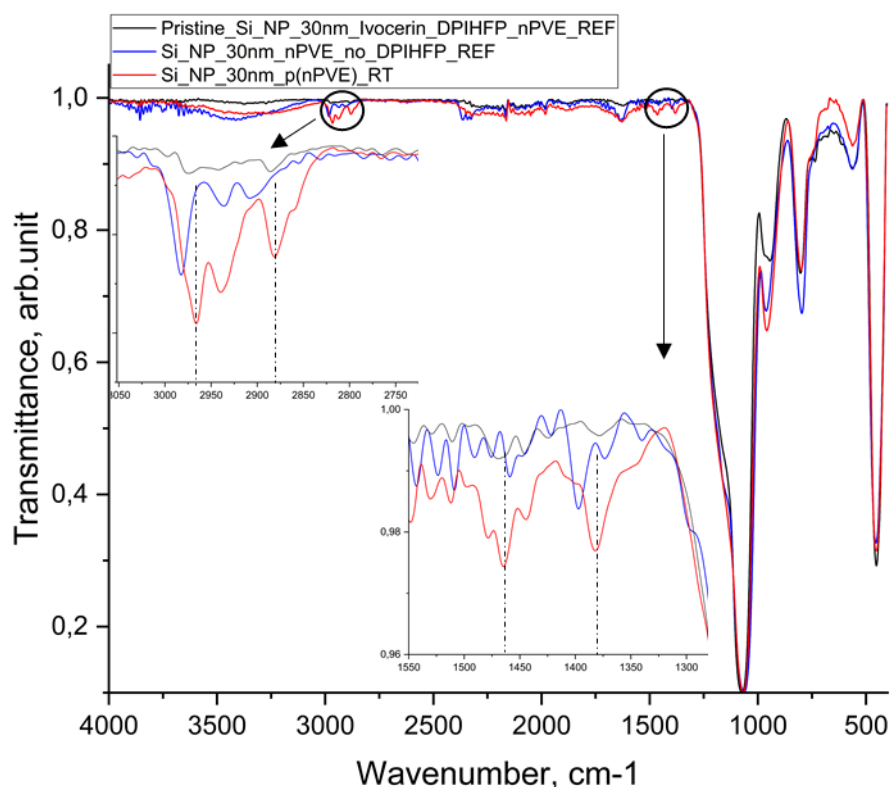


Figure 61: ATR-FTIR spectra of nanoparticles bearing p(nPVE) at their surface and products from control experiments.

Last but not least, it has to be pointed out that, for experiments using nPVE, the monomer was added after illuminating the **1**-functionalized nanoparticles for 8 minutes when the iodonium salt  $\text{Ph}_2\text{I}^+\text{PF}_6^-$  was present. Based on the fact that the immobilized polymer was evidenced afterwards, it can be concluded that the light-generated cationic species (highlighted in orange in Scheme 28) was long-lived enough to induce the polymerization.

Apart from grafting vinyl ether polymers from **1**-modified nanoparticles surfaces, cyclohexene oxide (CHO) was also employed for SI-RPCP. Since epoxides cannot be polymerized radically, the illumination step was carried using the monomer as the solvent, which is in contrast to the procedure for vinyl ethers (IV in Scheme 29). In doing so, the photosensitive nanoparticles (bearing trisacylgermanium moieties at their surface) were dispersed in a solution of DPIHFP in CHO. Subsequent illumination with 450 nm led to p(CHO) grafted to the nanoparticles' surface, which was evidenced by FT-IR as well as by TGA. Additionally, the same procedure was conducted without DPIHFP in order to again emphasize the dominant role of germyl radicals in SI-RPCP. For comparison, p(CHO) homopolymer was synthesized using GeEt and DPIHFP as the initiating system (refer to the experimental section). The results are shown in the figures below.

In FTIR spectra of surface grafted nanoparticles, several peaks, that can be assigned to p(CHO) were found. Especially, the characteristic signals at  $2932\text{ cm}^{-1}$  ( $\nu_{\text{as}}\text{CH}_2$ ),  $2861\text{ cm}^{-1}$  ( $\nu_{\text{s}}\text{CH}_2$ , CH) and  $1449$  and  $1366\text{ cm}^{-1}$  ( $\delta\text{CH}_2$ ) prove the successful grafting of p(CHO), as can be seen by comparison of the FTIR spectra of grafted p(CHO) and p(CHO) homopolymer in Figure 62.<sup>276</sup> In contrast, the absorption peak at  $2981\text{ cm}^{-1}$ , can obviously not be assigned to the surface attached polymer.<sup>232</sup> Notably, similar  $\text{CH}_3$ ,  $\text{CH}_2$  and CH stretching vibrations were also observed for the material derived by the control experiment (SI-RPCP procedure without DPIHFP), which is illustrated as the dashed black curve in the same figure. Although to a much lesser extent, which is most significant for the signals located at  $1449$  and  $1366\text{ cm}^{-1}$ , this indicated the presence of an organic material at the  $\text{SiO}_2$  particles' surface as well. Similar to the conclusion drawn for the control experiments with nPVE, it cannot be said with certainty which organic species remained surface attached when no DPIHFP was present during polymerization.

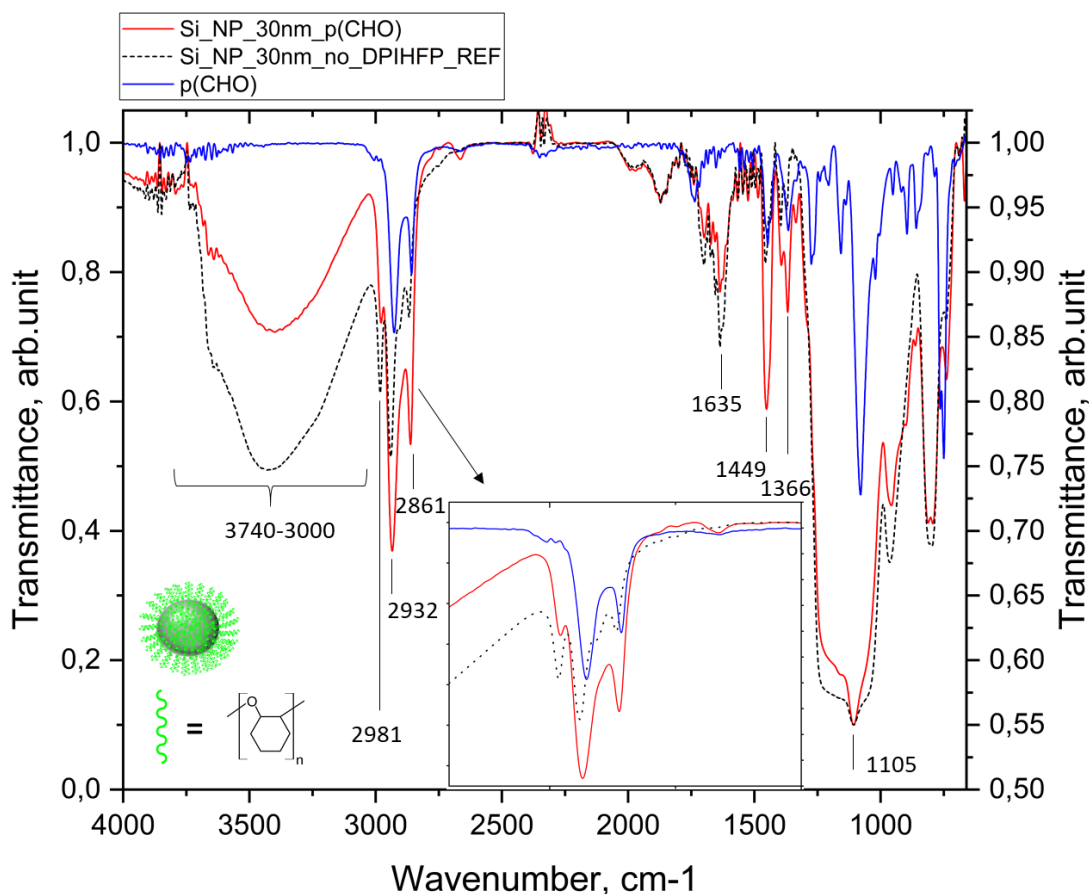


Figure 62: FTIR-spectra of p(CHO) homopolymer (blue, secondary y-axis), p(CHO)-grafted nanoparticles (red, primary y-axis) and nanoparticles derived from the SI-RPCP procedure without DPIHFP (black dashed curve, primary y-axis).

More significant, TGA result clearly prove that a high grafted p(CHO) content can only be achieved when DPIHFP is present, thus outlining the dominant role of DPIHFP for generating germanium centred cations as initiating species. The red curve in Figure 63 reveals a polymer content of approximately 33.6 %, which is well comparable to p(St)-grafted nanoparticles (38.5 %, refer to Table 5 in section 4.1.4) and significantly higher than that of p(nPVE)-grafted nanoparticles. This is also reflected when calculating the grafting yield  $\sigma_{mg}$ , which was found to be  $3.48 \text{ mg m}^{-2}$  ( $\sigma_{mg} = 4.21 \text{ mg m}^{-2}$  and  $1.63 \text{ mg m}^{-2}$  for p(St) and p(nPVE) grafted analogues, respectively).

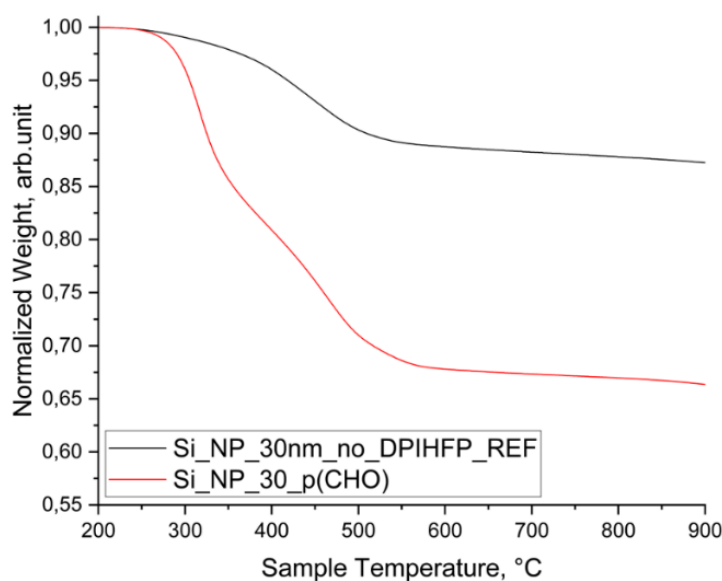
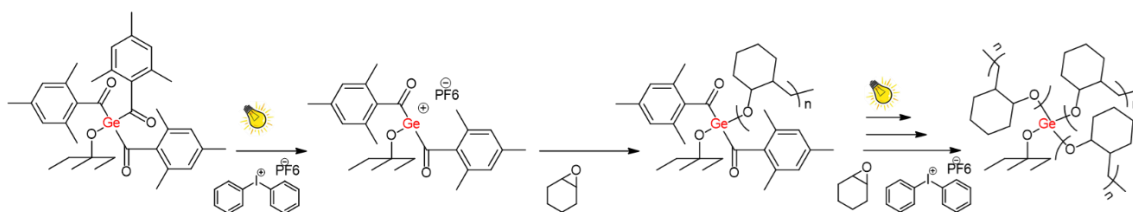


Figure 63: TGA measurements of silica nanoparticles bearing immobilized p(CHO). During the photografting experiments, DPIHFP was present (red curve) or absent (black curve).

A higher grafting yield using the SI-RPCP procedure with CHO instead of nPVE was expected, since the monomer-particle ratio (8 mL CHO per 100 mg 1-modified nanoparticles) was much higher during polymerization in that case. More important, the monomer was present during the illumination step, therefore providing a chance that another cationic species might be formed at the same germanium atom, according to the mechanism depicted in Scheme 31. This proposed mechanism was concluded from the higher grafting yield, and from the complete visible light induced photo-bleaching of trisaclygermanes in the presence of DPIHFP (see Figure 56 in chapter 4.3.2).



Scheme 31: Proposed mechanism for the SI-RPCP procedure using CHO as monomer.

### 4.3.3 Investigation on the potential living character of SI-RPCP

In principle, cationic polymerizations can be carried in a controlled living way under certain conditions. However, the existence of a living nature was called into question, especially in the early stages of research. The high reactivity of the carbocation frequently leads to multiple side reactions, leading to a severe broadening of the molar mass distribution of the synthesized polymers. As a result, this instability has restricted the progress of living cationic polymerization (LCP) for a long period.<sup>277</sup> The picture then changed after the major breakthrough made by Higashimura and Sawamoto in 1984. In their work, a HI/I<sub>2</sub> initiating system was employed, to synthesize living poly vinyl ethers with a very narrow polydispersity.<sup>278,279</sup> The key element for the elimination of side reactions was to create an equilibrium of reactive and dormant species by adding nucleophilic counteranions.<sup>274</sup> The resulting dormant carbon-halide or oxygen-ester bonds (C-X; X=I, Cl, OC(O)R) can be reactivated via C-X cleavage, again forming the carbon centred cationic species. This is usually catalysed by metal-based Lewis acids.<sup>280</sup> Since then, the following decades witnessed a rapid expansion of the field dealing with living cationic polymerization techniques. A comprehensive summary on this topic can be found in the literature.<sup>277,281</sup>

Aiming to see if a living character of the polymerization can be achieved with the presented SI-RPCP method, simple monomer addition experiments were carried out. In doing so, the experimental procedure was similar to that of the SI-RPCP process with nPVE, described in the previous section, with the exception that additional monomer was added four times, each after one hour. Prior to each monomer addition step, approximately 25% of modified nanoparticles were removed from the reaction mixture. The final products were ultrasonicated in DCM and centrifuged for multiple times, followed by FTIR and TGA investigations.

Apparently, p(nPVE)-grafted nanoparticles, derived from SI-RPCP at room temperature, did not show any increase in weight, which would have been the result of monomer addition, as can be seen from the TGA curves (Figure 64). In contrast to that, a slight increase (3 wt.-%) can be seen in experiments at -30 °C at least after the second monomer addition (refer to the black curve in Figure 64). This indicated that some propagating chains were still active after 60 min. However, from a theoretical point of view, a doubling of the polymer content can be considered after the second monomer addition step, related to the amount of added monomer. Therefore, the low percentage of weight increase (3 %) does not meet the requirements to label this polymerization as “living”, suggesting that a living character is not



possible with that method. According to Matyjaszewski et al., living conditions presume i) rate constants for transfer and termination equal to zero, ii) a very narrow molar mass distribution, and iii) a linear relationship between the molar mass and the monomer conversion.<sup>274</sup>

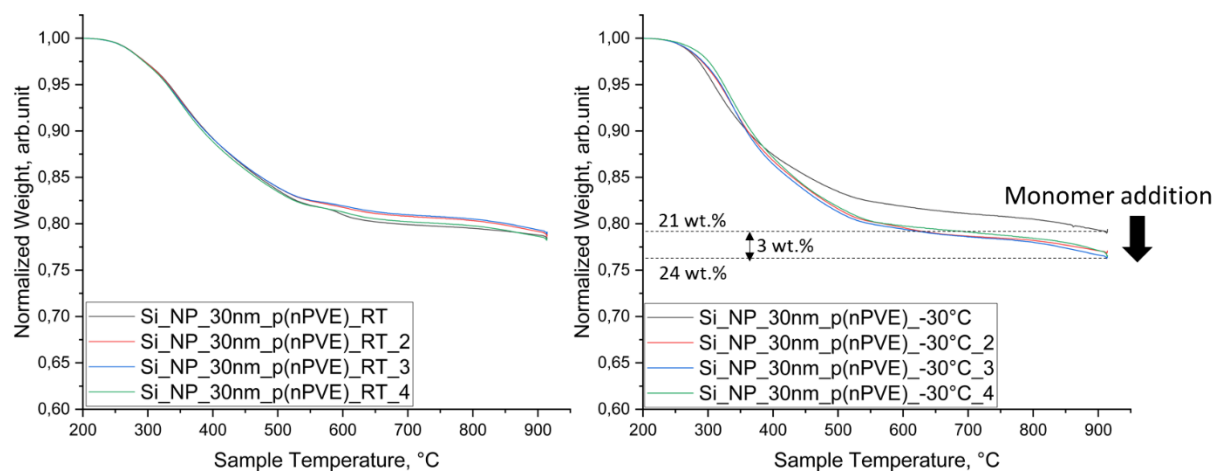


Figure 64: TGA investigation of the living character via monomer-addition experiments. The abbreviations “2”, “3” and “4” are representative for the respective monomer-addition steps.

As mentioned above, the livingness or controllability of cationic polymerizations are first and foremost dependent on the nature of the counterion. For  $\text{PF}_6^-$ , no living controlled cationic polymerization can be found in the literature. In order to achieve a controlled and living character anyway, a convenient solution was provided by Satoh and Kamigaito in 2014.<sup>280</sup> The authors presented the first example of a so-called cationic RAFT polymerization, which mechanism is quite similar to conventional radical RAFT techniques. Based on the pronounced affinity of carbocations for sulphur atoms, a series of thiocarbonyl compounds, acting as reversible chain transfer agents, were synthesized and successfully used for LCP of isobutyl vinyl ether. The number average of the molar mass followed a linear dependency on the monomer conversion, and even after monomer addition experiments, a very narrow molar mass distribution ( $M_w/M_n < 1.1$ ) was achieved. Using this technique for the herein presented SI-RPCP will give excess to living (co)-polymer grafts with tailorable thicknesses, structures and functionalities, and is therefore a promising future aspect.

#### 4.3.4 Conclusion on surface-initiated radical-promoted cationic photopolymerization with functionalized nanoparticles

Chapter 4.3 focuses on the grafting-from technique, which is based on a unique cationic photopolymerization mechanism. This mechanism relies on covalently coupled trisacylgermanes, acting as scaffolds for the formation of surface-tethered germyl radicals upon light irradiation. These highly reactive radicals are oxidized by iodonium salts such as  $\text{Ph}_2\text{I}^+\text{PF}_6^-$  (DPIHFP), leading to germanium centred cations for polymerization initiation. Overall, the emphasis was placed to prove the basic functionality.

Initially, photo-DSC measurements evidenced that differently substituted acylgermanes can be used to cationically polymerize a difunctional bisphenol-A-diglycidylether when the iodonium salt is present, furthermore revealing that Ivocerin is the most efficient compound in doing so. When nanoparticles bearing photosensitive trisacylgermanium moieties at their surface were employed in SI-RPCP, grafted polymer brushes derived from a vinyl ether (n-propyl vinyl ether) or an epoxide (cyclohexene oxide) were evidenced by FTIR and TGA. These results were accompanied by the outcomes of control experiments, which gave an indication that the cationic-germanium species was present at the surface. A grafting yield of up to  $3.48 \text{ mg m}^{-2}$  was obtained with this method. However, a detailed oxidation mechanism of trisacylgermanes and a living/controlled character of this type of polymerization cannot be provided as the moment. This technique is indeed highly novel, and might open up new perspectives in the field of surface modification with polymers.

Up to now, surface-mediated cationic polymerizations have scarcely been investigated. One example was given by Ulman et al., who performed cationic polymerization of 2-oxazolines from planar gold substrates using surface-coupled methyl tosylate as the initiator.<sup>282</sup> However, this technique can only be elaborated for 2-oxazoline monomers. More than two decades ago Ingall and co-workers provided an example of surface-immobilized phenyl silanes, which can be de-arylated employing trifluoromethanesulfonic acid, resulting in the formation of reactive silyl cations for initiation.<sup>283</sup> Some more examples can be found in the contribution by Advincula et al.<sup>284</sup> All in all, no surface-mediated cationic polymerization processes, which can be triggered by light, are available in the literature. Consequently, the herein presented radical-promoted cationic photopolymerization is the very first example of a visible-light induced process generating surface-attached cationic species, that can be employed for starting a cationic chain growth reaction of different monomers.

## 5 Summary and Outlook

This thesis provides a novel and fundamental pathway to produce light sensitive surfaces which can be easily employed for the development of a covalently coupled polymer brush system. For this, a novel and unique germanium-based photoinitiator, which was equipped with a halogen unit for attaching it to hydroxyl rich surfaces, was taken into account. The functionalized surfaces comprised silicon wafers, optically polished quartz plates, and spherically shaped silica nanoparticles with 30 and 180 nm in diameter, respectively.

In a first step the target materials were pre-activated either with oxygen plasma or alkaline solutions, leaving the respective surface with a maximum of hydroxyl moieties. Subsequently, the covalent attachment of the photoinitiator was carried out following a proposed nucleophilic substitution pathway by splitting off hydrogen bromide, which in turn was evidenced via the formation of a tertiary ammonium salt with Hünig's base (DIPEA). After the functionalized materials had undergone a thorough washing procedure, the derived surfaces were studied with XPS. The density of tethered photoinitiator was calculated based on UV-Vis absorption data, giving 0.29 to 0.33 molecules per  $\text{nm}^{-2}$  (result for  $\text{SiO}_2$  nanoparticles).

Most important, it has been shown that those species are capable of inducing surface-initiated radical photopolymerization reactions of acrylic, methacrylic and vinyl monomers by means of a grafting-from approach. In that way, the formed polymers were surface-attached through a covalent bond, and the thickness of the polymer brushes ranged between 6 and 126 nm. By selecting proper monomers, functional polymer brushes were attached to the surface of silicon wafers and quartz plates, also in a spatially resolved manner. These functionalities comprised both hydrophobic, hydrophilic and fluorescent properties, which was studied by contact angle measurements, XPS as well as UV-Vis and fluorescence spectroscopy. The fluorescent behaviour was even visible with the naked eye when pyrene-containing polymers were grafted from.

When nanoparticles were used in that context, the obtained polymer structure was confirmed by ToF-SIMS investigations via comparison to the respective non-coupled homopolymers. The polymeric shell of the synthesized organic/inorganic hybrid materials was successfully visualized with electron microscopy (SEM). Moreover, the polymer yield ( $\text{mg m}^{-2}$ ) as well as grafting density (chains per square nanometre), which both are important parameters to evaluate the overall efficiency of the applied grafting-from method, is also discussed in detail. It was found out that the calculated values ranged between 4.21 and 18  $\text{mg m}^{-2}$  for the grafting yield, and between 0.17 and 0.23 chains per  $\text{nm}^{-2}$  for the grafting density, respectively. Especially the latter one is well comparable to literature reported values.

As a fundamentally new approach, a so-called surface-initiated radical promoted cationic photopolymerization (SI-RPCP) is presented for the very first time. With photo-sensitive nanoparticles (30 nm in diameter) bearing trisacylgermanium groups at their surface, in combination with an iodonium salt it has been shown that polymers, derived from vinyl ethers

and epoxides, can be grafted from the surface in a cationic fashion. Up to now a detailed mechanism for the oxidation of one (or more) of the three possible germyl radicals, formed upon illumination of trisacylgermanium moieties, by the iodonium salt is not clear. Therefore, a follow-up study on this topic is highly desirable. Besides, the grafting density needs to be calculated for the cationic approach by applying the herein presented procedure (i.e., de-grafting the polymers with hydrofluoric acid and subsequent SEC-measurements). For the future, the two-fold functionality of the Ge-based photoinitiators as well as the fact that each moiety can theoretically form three radicals can be exploited to produce radical and cationic polymer grafts, coupled to the Ge-centre and/or surface. This can be achieved with precise illumination experiments, by choosing the correct light dose in order to partially trigger light sensitive moieties for radical surface-initiated polymerization. After that, the cationic procedure can be elaborated in a second illumination step, making use of the remaining photo-labile groups.

Other future aspects comprise controlled and living surface-mediated polymerizations, by, for example, simply adding RAFT agents, applicable for cationic and radical polymerization techniques. When combined with each other, those perspectives have the potential to lift the field of surface-modification science up to a higher level. Last but not least, it has to be emphasized that, considering the advantages of Ge-based photoinitiators in terms of low toxicity and strong visible light absorbance, the herein reported methods are suitable for biomedical applications. Especially for nanoparticles, the use in drug/gene delivery systems or as platforms for up-conversion nanoparticles can be considered.

## 6 Bibliography

- (1) Pasparakis, G.; Vamvakaki, M. Multiresponsive Polymers: Nano-Sized Assemblies, Stimuli-Sensitive Gels and Smart Surfaces. *Polym Chem* **2011**, *2* (6), 1234–1248. <https://doi.org/10.1039/c0py00424c>.
- (2) Bandl, C.; Kern, W.; Krempf, N.; Friesenbichler, W. Simple and Rapid Method for Restoring Anti-Adhesive Organosilane Coatings on Metal Substrates. *Prog Org Coat* **2020**, *140*. <https://doi.org/10.1016/j.porgcoat.2019.105490>.
- (3) Iqbal, M.; Dinh, D. K.; Abbas, Q.; Imran, M.; Sattar, H.; Ul Ahmad, A. Controlled Surface Wettability by Plasma Polymer Surface Modification. *Surfaces* **2019**, *2* (2), 349–371. <https://doi.org/10.3390/surfaces2020026>.
- (4) Xiao, M.; Xu, A.; Zhang, T.; Hong, L. Tailoring the Wettability of Colloidal Particles for Pickering Emulsions via Surface Modification and Roughness. *Front Chem* **2018**, *6* (JUN). <https://doi.org/10.3389/fchem.2018.00225>.
- (5) Manyangadze, M.; Chikuruwo, N. H. M.; Narsaiah, T. B.; Chakra, C. S.; Radhakumari, M.; Danha, G. Enhancing Adsorption Capacity of Nano-Adsorbents via Surface Modification: A Review. *S Afr J Chem Eng* **2020**, *31*, 25–32. <https://doi.org/10.1016/j.sajce.2019.11.003>.
- (6) Padmanabhan, N. T.; John, H. Titanium Dioxide Based Self-Cleaning Smart Surfaces: A Short Review. *J Environ Chem Eng* **2020**, *8* (5). <https://doi.org/10.1016/j.jece.2020.104211>.
- (7) Lee, C. C.; El-Zahlanieh, S.; Wang, Y. H.; Chen, C. C.; Chen, S. H.; Chang, Y. W. 6061 Aluminum Surface Treatment by High Quality Coloring Anodic Film. *Materials Science Forum* **2020**, *975 MSF*, 31–36. <https://doi.org/10.4028/www.scientific.net/MSF.975.31>.
- (8) Ayyavoo, J.; Nguyen, T. P. N.; Jun, B. M.; Kim, I. C.; Kwon, Y. N. Protection of Polymeric Membranes with Antifouling Surfacing via Surface Modifications. *Colloids Surf A Physicochem Eng Asp* **2016**, *506*, 190–201. <https://doi.org/10.1016/j.colsurfa.2016.06.026>.
- (9) Osman, N.; Devnarain, N.; Omolo, C. A.; Fasiku, V.; Jaglal, Y.; Govender, T. Surface Modification of Nano-Drug Delivery Systems for Enhancing Antibiotic Delivery and Activity. *Wiley Interdiscip Rev Nanomed Nanobiotechnol* **2022**, *14* (1). <https://doi.org/10.1002/wnan.1758>.
- (10) Stich, T.; Alagboso, F.; Křenek, T.; Kovářik, T.; Alt, V.; Docheva, D. Implant-Bone-Interface: Reviewing the Impact of Titanium Surface Modifications on Osteogenic Processes in Vitro and in Vivo. *Bioeng Transl Med* **2022**, *7* (1). <https://doi.org/10.1002/btm2.10239>.
- (11) Mueller, M.; Bandl, C.; Kern, W. Surface-Immobilized Photoinitiators for Light Induced Polymerization and Coupling Reactions. *Polymers (Basel)* **2022**, *14* (3). <https://doi.org/10.3390/polym14030608>.
- (12) Nemani, S. K.; Annavarapu, R. K.; Mohammadian, B.; Raiyan, A.; Heil, J.; Haque, M. A.; Abdelaal, A.; Sojoudi, H. Surface Modification of Polymers: Methods and Applications. *Adv Mater Interfaces* **2018**, *5* (24). <https://doi.org/10.1002/admi.201801247>.
- (13) Cruz, J.; Figueiro, R. Surface Modification of Natural Fibers: A Review. *Procedia Eng* **2016**, *155*, 285–288. <https://doi.org/10.1016/j.proeng.2016.08.030>.
- (14) Missoum, K.; Belgacem, M. N.; Bras, J. Nanofibrillated Cellulose Surface Modification: A Review. *Materials* **2013**, *6* (5), 1745–1766. <https://doi.org/10.3390/ma6051745>.
- (15) Smith, J. R.; Lamprou, D. A. Polymer Coatings for Biomedical Applications: A Review. *Transactions of the Institute of Metal Finishing* **2014**, *92* (1), 9–19. <https://doi.org/10.1179/0020296713Z.000000000157>.

- (16) Sangermano, M.; Periolatto, M.; Castellino, M.; Wang, J.; Dietliker, K.; Grützmacher, J. L.; Grützmacher, H. A Simple Preparation of Photoactive Glass Surfaces Allowing Coatings via the "Grafting-from" Method. *ACS Appl Mater Interfaces* **2016**, *8* (30), 19764–19771. <https://doi.org/10.1021/acsami.6b05822>.
- (17) Wang, Z.; Chen, K.; Hua, C.; Guo, X. Conformation Variation and Tunable Protein Adsorption through Combination of Poly(Acrylic Acid) and Antifouling Poly(N-(2-Hydroxyethyl) Acrylamide) Diblock on a Particle Surface. *Polymers (Basel)* **2020**, *12* (3). <https://doi.org/10.3390/polym12030566>.
- (18) Wang, X.; Yan, S.; Song, L.; Shi, H.; Yang, H.; Luan, S.; Huang, Y.; Yin, J.; Khan, A. F.; Zhao, J. Temperature-Responsive Hierarchical Polymer Brushes Switching from Bactericidal to Cell Repellency. *ACS Appl Mater Interfaces* **2017**, *9* (46), 40930–40939. <https://doi.org/10.1021/acsami.7b09968>.
- (19) Zholdassov, Y. S.; Valles, D. J.; Uddin, S.; Korpanty, J.; Gianneschi, N. C.; Braunschweig, A. B. Orthogonal Images Concealed Within a Responsive 6-Dimensional Hypersurface. *Advanced Materials* **2021**, *33* (21). <https://doi.org/10.1002/adma.202100803>.
- (20) Poisson, J.; Polgar, A. M.; Fromel, M.; Pester, C. W.; Hudson, Z. M. Preparation of Patterned and Multilayer Thin Films for Organic Electronics via Oxygen-Tolerant SI-PET-RAFT. *Angewandte Chemie - International Edition* **2021**, *60* (36), 19988–19996. <https://doi.org/10.1002/anie.202107830>.
- (21) Ng, G.; Judzewitsch, P.; Li, M.; Pester, C. W.; Jung, K.; Boyer, C. Synthesis of Polymer Brushes Via SI-PET-RAFT for Photodynamic Inactivation of Bacteria. *Macromol Rapid Commun* **2021**, *42* (18). <https://doi.org/10.1002/marc.202100106>.
- (22) Kuzmyn, A. R.; Teunissen, L. W.; Fritz, P.; van Lagen, B.; Smulders, M. M. J.; Zuilhof, H. Diblock and Random Antifouling Bioactive Polymer Brushes on Gold Surfaces by Visible-Light-Induced Polymerization (SI-PET-RAFT) in Water. *Adv Mater Interfaces* **2021**, 2101784. <https://doi.org/10.1002/admi.202101784>.
- (23) Sangermano, M.; Razza, N. Light Induced Grafting-from Strategies as Powerful Tool for Surface Modification. *Express Polym Lett* **2019**, *13* (2), 135–145. <https://doi.org/10.3144/expresspolymlett.2019.13>.
- (24) Mochida, K.; Ichikawa, K.; Okui, S.; Sakaguchi, Y.; Hayashi, H. Direct Observation of Germyl Radicals by a Laser-Photolysis of Germyl Ketones. *Chem Lett* **1985**, 1433–1436. <https://doi.org/https://doi.org/10.1246/cl.1985.1433>.
- (25) Ganster, B.; Fischer, U. K.; Moszner, N.; Liska, R. New Photocleavable Structures. Diacylgermane-Based Photoinitiators for Visible Light Curing. *Macromolecules* **2008**, *41* (7), 2394–2400. <https://doi.org/10.1021/ma702418q>.
- (26) Radebner, J.; Eibel, A.; Leybold, M.; Gorsche, C.; Schuh, L.; Fischer, R.; Torvisco, A.; Neshchadin, D.; Geier, R.; Moszner, N.; Liska, R.; Gescheidt, G.; Haas, M.; Stueger, H. Tetraacylgermanes: Highly Efficient Photoinitiators for Visible-Light-Induced Free-Radical Polymerization. *Angewandte Chemie - International Edition* **2017**, *56* (11), 3103–3107. <https://doi.org/10.1002/anie.201611686>.
- (27) Neshchadin, D.; Rosspeintner, A.; Griesser, M.; Lang, B.; Mosquera-Vazquez, S.; Vauthey, E.; Gorelik, V.; Liska, R.; Hametner, C.; Ganster, B.; Saf, R.; Moszner, N.; Gescheidt, G. Acylgermanes: Photoinitiators and Sources for Ge-Centered Radicals. Insights into Their Reactivity. *J Am Chem Soc* **2013**, *135* (46), 17314–17321. <https://doi.org/10.1021/ja404433u>.
- (28) Radebner, J.; Leybold, M.; Eibel, A.; Maier, J.; Schuh, L.; Torvisco, A.; Fischer, R.; Moszner, N.; Gescheidt, G.; Stueger, H.; Haas, M. Synthesis, Spectroscopic Behavior, and Photoinduced

- Reactivity of Tetraacylgermanes. *Organometallics* **2017**, *36* (18), 3624–3632. <https://doi.org/10.1021/acs.organomet.7b00539>.
- (29) Frühwirt, P.; Knoechl, A.; Pillinger, M.; Müller, S. M.; Wasdin, P. T.; Fischer, R. C.; Radebner, J.; Torvisco, A.; Moszner, N.; Kelterer, A. M.; Griesser, T.; Gescheidt, G.; Haas, M. The Chemistry of Acylgermanes: Triacylgermenolates Represent Valuable Building Blocks for the Synthesis of a Variety of Germanium-Based Photoinitiators. *Inorg Chem* **2020**, *59* (20), 15204–15217. <https://doi.org/10.1021/acs.inorgchem.0c02181>.
- (30) Catel, Y.; Angermann, J.; Fässler, P.; Fischer, U.; Schnur, T.; Moszner, N. High Refractive Index Monofunctional Monomers as Promising Diluents for Dental Composites. *Dental Materials* **2021**, *37* (2), 351–358. <https://doi.org/10.1016/j.dental.2020.11.029>.
- (31) Catel, Y.; Fässler, P.; Fischer, U.; Pesch, C.; Pruvost, C.; Tauscher, S.; Moszner, N. Synthesis of Acidic Vinylcyclopropanes for Dental Applications. *Polym Int* **2017**, *66* (10), 1410–1417. <https://doi.org/10.1002/pi.5403>.
- (32) Catel, Y.; Fischer, U.; Fässler, P.; Moszner, N. Bis(4-Methoxybenzoyl)Diethylgermane: A Highly Efficient Photoinitiator for the Polymerization of Vinylcyclopropanes. *Macromol Chem Phys* **2016**, *217* (24), 2686–2691. <https://doi.org/10.1002/macp.201600463>.
- (33) Catel, Y.; Fässler, P.; Fischer, U.; Gorsche, C.; Liska, R.; Schörpf, S.; Tauscher, S.; Moszner, N. Synthesis and Polymerization of Vinylcyclopropanes Bearing Urethane Groups for the Development of Low-Shrinkage Composites. *Eur Polym J* **2018**, *98*, 439–447. <https://doi.org/10.1016/j.eurpolymj.2017.11.042>.
- (34) Moszner, N.; Fischer, U. K.; Ganster, B.; Liska, R.; Rheinberger, V. Benzoyl Germanium Derivatives as Novel Visible Light Photoinitiators for Dental Materials. *Dental Materials* **2008**, *24* (7), 901–907. <https://doi.org/10.1016/j.dental.2007.11.004>.
- (35) Durmaz, Y. Y.; Moszner, N.; Yagci, Y. Visible Light Initiated Free Radical Promoted Cationic Polymerization Using Acylgermane Based Photoinitiator in the Presence of Onium Salts. *Macromolecules* **2008**, *41* (18), 6714–6718. <https://doi.org/10.1021/ma801208n>.
- (36) Lago, M. A.; Rodríguez-Bernaldo de Quirós, A.; Sendón, R.; Bustos, J.; Nieto, M. T.; Paseiro, P. Photoinitiators: A Food Safety Review. *Food Addit Contam Part A Chem Anal Control Expo Risk Assess* **2015**, *32* (5), 779–798. <https://doi.org/10.1080/19440049.2015.1014866>.
- (37) Qin, X. H.; Ovsianikov, A.; Stampfl, J.; Liska, R. Additive Manufacturing of Photosensitive Hydrogels for Tissue Engineering Applications. *BioNanoMaterials* **2014**, *15* (3–4), 49–70. <https://doi.org/10.1515/bnm-2014-0008>.
- (38) Cheng, L.; Zhang, Y.; Shi, W. Photoinitiating Behavior of Benzophenone Derivatives Covalently Bonded Tertiary Amine Group for UV-Curing Acrylate Systems. *Polym Adv Technol* **2012**, *23* (3), 669–676. <https://doi.org/10.1002/pat.1944>.
- (39) Koehler, M.; Ohngemach, J. Coreactive Photoinitiators for Surface Polymerization. **1990**, 106–124. <https://doi.org/10.1021/bk-1990-0417.ch009>.
- (40) Schuh, C.; Santer, S.; Prucker, O.; Rühle, J. Polymer Brushes with Nanometer-Scale Gradients. *Advanced Materials* **2009**, *21* (46), 4706–4710. <https://doi.org/10.1002/adma.200901515>.
- (41) Hensarling, R. M.; Doughty, V. A.; Chan, J. W.; Patton, D. L. “Clicking” Polymer Brushes with Thiol-Yne Chemistry: Indoors and Out. *J Am Chem Soc* **2009**, *131* (41), 14673–14675. <https://doi.org/10.1021/ja9071157>.
- (42) Rahane, S. B.; Hensarling, R. M.; Sparks, B. J.; Stafford, C. M.; Patton, D. L. Synthesis of Multifunctional Polymer Brush Surfaces via Sequential and Orthogonal Thiol-Click Reactions. *J Mater Chem* **2012**, *22* (3), 932–943. <https://doi.org/10.1039/c1jm14762e>.

- (43) Roszkowski, P.; Sahin, M.; Ayalur-Karunakaran, S.; Gammer, C.; Schlögl, S.; Kern, W.; Krawczyk, K. K. Synthesis and Evaluation of New Radical Photoinitiators Bearing Trialkoxysilyl Groups for Surface Immobilization. *Polymer (Guildf)* **2017**, *129*, 207–220. <https://doi.org/10.1016/j.polymer.2017.09.054>.
- (44) Sahin, M.; Krawczyk, K. K.; Roszkowski, P.; Wang, J.; Kaynak, B.; Kern, W.; Schlögl, S.; Grützmacher, H. Photoactive Silica Nanoparticles: Influence of Surface Functionalization on Migration and Kinetics of Radical-Induced Photopolymerization Reactions. *Eur Polym J* **2018**, *98*, 430–438. <https://doi.org/10.1016/j.eurpolymj.2017.11.046>.
- (45) Tan, H.; Yang, D.; Xiao, M.; Han, J.; Nie, J. Preparation of Silica/Polyurethane Nanocomposites by UV-Induced Polymerization from Surfaces of Silica. *J Appl Polym Sci* **2009**, *111* (4), 1936–1941. <https://doi.org/10.1002/app.28700>.
- (46) Huber, A.; Kuschel, A.; Ott, T.; Santiso-Quinones, G.; Stein, D.; Bräuer, J.; Kissner, R.; Krumeich, F.; Schönberg, H.; Levalois-Grützmacher, J.; Grützmacher, H. Phosphorous-Functionalized Bis(Acyl)Phosphane Oxides for Surface Modification. *Angewandte Chemie* **2012**, *124* (19), 4726–4730. <https://doi.org/10.1002/ange.201201026>.
- (47) Sahin, M.; Schlögl, S.; Kaiser, S.; Kern, W.; Wang, J.; Grützmacher, H. Efficient Initiation of Radical-Mediated Thiol-Ene Chemistry with Photoactive Silica Particles. *J Polym Sci A Polym Chem* **2017**, *55* (5), 894–902. <https://doi.org/10.1002/pola.28442>.
- (48) Romano, A.; Polymer Chemistry. Hybrid Silica Micro-Particles with Light-Responsive Surface Properties and Janus-like Character. *Polym Chem* **2021**. <https://doi.org/10.1039/D1PY00459J>.
- (49) Razza, N.; Rizza, G.; Coulon, P. E.; Didier, L.; Fadda, G. C.; Voit, B.; Synytska, A.; Grützmacher, H.; Sangermano, M. Enabling the Synthesis of Homogeneous or Janus Hairy Nanoparticles through Surface Photoactivation. *Nanoscale* **2018**, *10* (30), 14492–14498. <https://doi.org/10.1039/c8nr04239j>.
- (50) Moehrke, J.; Vana, P. Termination Kinetics of Surface-Initiated Radical Polymerization Measured by Time-Resolved ESR Spectroscopy after Laser-Pulse Initiation. *Macromolecules* **2015**, *48* (10), 3190–3196. <https://doi.org/10.1021/acs.macromol.5b00662>.
- (51) Ohar, H.; Dolynska, L.; Tokarev, V. Synthesis and Application of Macrophotoinitiators Obtained via Benzoin Tethering with Copolymers of Maleic Anhydride. *Chemistry & Chemical Technology* **2013**, *7* (2). <https://doi.org/10.23939/chcht07.02.125>.
- (52) Wang, J.; Siqueira, G.; Müller, G.; Rentsch, D.; Huch, A.; Tingaut, P.; Levalois-Grützmacher, J.; Grützmacher, H. Synthesis of New Bis(Acyl)Phosphane Oxide Photoinitiators for the Surface Functionalization of Cellulose Nanocrystals. *Chemical Communications* **2016**, *52* (13), 2823–2826. <https://doi.org/10.1039/c5cc09760f>.
- (53) Tsubokawa, N.; Kogure, A.; Maruyama, K.; Sone, Y.; Shimomura, M. Graft Polymerization of Vinyl Monomers from Inorganic Ultrafine Particles Initiated by Azo Groups Introduced onto the Surface. *Polym J* **1990**, *22* (9), 827–833. <https://doi.org/10.1295/polymj.22.827>.
- (54) Tsubokawa, N.; Shirai, Y.; Tsuchida, H.; Handa, S. Photografting of Vinyl Polymers onto Ultrafine Inorganic Particles: Photopolymerization of Vinyl Monomers Initiated by Azo Groups Introduced onto These Surfaces. *J Polym Sci A Polym Chem* **1994**, *32*, 2327–2332. <https://doi.org/10.1002/pola.1994.080321214>.
- (55) Prucker, O.; Rühle, J. Synthesis of Poly(Styrene) Monolayers Attached to High Surface Area Silica Gels through Self-Assembled Monolayers of Azo Initiators. *Macromolecules* **1998**. <https://doi.org/10.1021/ma970660x>.



- (56) Rhe, J. Mageschneiderte Oberflchen. *Nachrichten aus Chemie, Technik und Laboratorium* **1994**, *42* (12), 1237–1246. <https://doi.org/10.1002/nadc.19940421207>.
- (57) Prucker, O.; Rhe, J. Grafting of Polymers to Solid Surfaces by Using Immobilized Azoinitiators. *Materials Research Society* **1993**. <https://doi.org/10.1557/PROC-304-167>.
- (58) Prucker, O.; Rhe, J. Mechanism of Radical Chain Polymerizations Initiated by Azo Compounds Covalently Bound to the Surface of Spherical Particles. **1998**. <https://doi.org/10.1021/ma970661p>.
- (59) Prucker, O.; Habicht, J.; Park, I.-J.; Ruhe, J. Photolithographic Structuring of Surface-Attached Polymer Monolayers. **1999**. [https://doi.org/10.1016/S0928-4931\(99\)00080-6](https://doi.org/10.1016/S0928-4931(99)00080-6).
- (60) Konradi, R.; Rhe, J. Fabrication of Chemically Microstructured Polymer Brushes. *Langmuir* **2006**, *22* (20), 8571–8575. <https://doi.org/10.1021/la061379r>.
- (61) Huang, W.; Skanth, G.; Baker, G. L.; Bruening, M. L. Surface-Initiated Thermal Radical Polymerization on Gold. *Langmuir* **2001**, *17* (5), 1731–1736. <https://doi.org/10.1021/la001325w>.
- (62) Schmidt, R.; Zhao, T.; Green, J. B.; Dyer, D. J. Photoinitiated Polymerization of Styrene from Self-Assembled Monolayers on Gold. *Langmuir* **2002**, *18* (4), 1281–1287. <https://doi.org/10.1021/la011445j>.
- (63) Paul, R.; Schmidt, R.; Feng, J.; Dyer, D. J. Photoinitiated Polymerization of Styrene from Self-Assembled Monolayers on Gold. II. Grafting Rates and Extraction. *J Polym Sci A Polym Chem* **2002**, *40* (19), 3284–3291. <https://doi.org/10.1002/pola.10418>.
- (64) Feng, J.; Haasch, R. T.; Dyer, D. J. Photoinitiated Synthesis of Mixed Polymer Brushes of Polystyrene and Poly(Methyl Methacrylate). *Macromolecules* **2004**, *37* (25), 9525–9537. <https://doi.org/10.1021/ma048681w>.
- (65) Kaholek, M.; Lee, W. K.; Feng, J.; Lamattina, B.; Dyer, D. J.; Zauscher, S. Weak Polyelectrolyte Brush Arrays Fabricated by Combining Electron-Beam Lithography with Surface-Initiated Photopolymerization. *Chemistry of Materials* **2006**, *18* (16), 3660–3664. <https://doi.org/10.1021/cm060276r>.
- (66) Schmelmer, U.; Paul, A.; Kller, A.; Steenackers, M.; Ulman, A.; Grunze, M.; Glzhuser, A.; Jordan, R. Nanostructured Polymer Brushes. *Small* **2007**, *3* (3), 459–465. <https://doi.org/10.1002/smll.200600528>.
- (67) Yang, W.; Rnby, B. Radical Living Graft Polymerization on the Surface of Polymeric Materials. **1996**. <https://doi.org/10.1021/ma9515543>.
- (68) Ma, H.; Davis, R. H.; Bowman, C. N. Novel Sequential Photoinduced Living Graft Polymerization. *Macromolecules* **2000**, *33* (2), 331–335. <https://doi.org/10.1021/ma990821s>.
- (69) Ma, H.; Davis, R. H.; Bowman, C. N. Principal Factors Affecting Sequential Photoinduced Graft Polymerization. **2001**. [https://doi.org/10.1016/S0032-3861\(01\)00328-7](https://doi.org/10.1016/S0032-3861(01)00328-7).
- (70) Yu, H. Y.; Li, W.; Zhou, J.; Gu, J. S.; Huang, L.; Tang, Z. Q.; Wei, X. W. Thermo- and PH-Responsive Polypropylene Microporous Membrane Prepared by the Photoinduced RAFT-Mediated Graft Copolymerization. *J Memb Sci* **2009**, *343* (1–2), 82–89. <https://doi.org/10.1016/j.memsci.2009.07.012>.
- (71) Lee, J. S.; Shin, B. H.; Yoo, B. Y.; Nam, S. Y.; Lee, M.; Choi, J.; Park, H.; Choy, Y. Bin; Heo, C. Y.; Koh, W. G. Modulation of Foreign Body Reaction against PDMS Implant by Grafting Topographically Different Poly(Acrylic Acid) Micropatterns. *Macromol Biosci* **2019**, *19* (12). <https://doi.org/10.1002/mabi.201900206>.

- (72) Janorkar, A. V.; Metters, A. T.; Hirt, D. E. Modification of Poly(Lactic Acid) Films: Enhanced Wettability from Surface-Confined Photografting and Increased Degradation Rate Due to an Artifact of the Photografting Process. *Macromolecules* **2004**, *37* (24), 9151–9159. <https://doi.org/10.1021/ma049056u>.
- (73) Stachowiak, T. B.; Svec, F.; Fréchet, J. M. J. Patternable Protein Resistant Surfaces for Multifunctional Microfluidic Devices via Surface Hydrophilization of Porous Polymer Monoliths Using Photografting. *Chemistry of Materials* **2006**, *18* (25), 5950–5957. <https://doi.org/10.1021/cm0617034>.
- (74) Kuşçuoğlu, C. K.; Güner, H.; Söylemez, M. A.; Güven, O.; Barsbay, M. A Smartphone-Based Colorimetric PET Sensor Platform with Molecular Recognition via Thermally Initiated RAFT-Mediated Graft Copolymerization. *Sens Actuators B Chem* **2019**, *296*. <https://doi.org/10.1016/j.snb.2019.126653>.
- (75) Castell, P.; Wouters, M.; De With, G.; Fischer, H.; Huijs, F. Surface Modification of Poly(Propylene) by Photoinitiators: Improvement of Adhesion and Wettability. **2004**. <https://doi.org/10.1002/app.20276>.
- (76) Castell, P.; Wouters, M.; Fischer, H.; De With, G. Study of Wettability and Improvement of Adhesion of UV Curable Powder Coatings on Polypropylene Substrates. *J Appl Polym Sci* **2007**, *106* (5), 3348–3358. <https://doi.org/10.1002/app.27032>.
- (77) Gao, Z.; Henthorn, D. B.; Kim, C. S. Enhanced Wettability of an SU-8 Photoresist through a Photografting Procedure for Bioanalytical Device Applications. *Journal of Micromechanics and Microengineering* **2008**, *18* (4). <https://doi.org/10.1088/0960-1317/18/4/045013>.
- (78) Prucker, O.; Naumann, C. A.; Ru, rgen; Knoll, W.; Frank, C. W. Photochemical Attachment of Polymer Films to Solid Surfaces via Monolayers of Benzophenone Derivatives. **1999**. <https://doi.org/10.1021/ja990962>.
- (79) Kado, Y.; Mitsuishi, M.; Miyashita, T. Fabrication of Three-Dimensional Nanostructures Using Reactive Polymer Nanosheets. *Advanced Materials* **2005**, *17* (15), 1857–1861. <https://doi.org/10.1002/adma.200500884>.
- (80) Braun, L.; Schafforz, S. L.; Lorenz, A. Surface Grafted Crosslinker in Polymer Network Liquid Crystals. *J Mol Liq* **2018**, *267*, 109–114. <https://doi.org/10.1016/j.molliq.2018.01.173>.
- (81) Leshem, B.; Sarfati, G.; Novoa, A.; Breslav, I.; Marks, R. S. Photochemical Attachment of Biomolecules onto Fibre-Optics for Construction of a Chemiluminescent Immunosensor. *Luminescence* **2004**, *19* (2), 69–77. <https://doi.org/10.1002/bio.760>.
- (82) Naumann, C. A.; Prucker, O.; Lehmann, T.; Rühle, J.; Knoll, W.; Frank, C. W. The Polymer-Supported Phospholipid Bilayer: Tethering as a New Approach to Substrate-Membrane Stabilization. *Biomacromolecules* **2002**, *3* (1), 27–35. <https://doi.org/10.1021/bm0100211>.
- (83) Murata, H.; Chang, B. J.; Prucker, O.; Dahm, M.; Ruhe, J. Polymeric Coatings for Biomedical Devices. *Surf Sci* **2004**, *570* (1–2), 111–118. <https://doi.org/10.1016/j.susc.2004.06.185>.
- (84) Griep-Raming, N.; Karger, M.; Menzel, H. Using Benzophenone-Functionalized Phosphonic Acid to Attach Thin Polymer Films to Titanium Surfaces. *Langmuir* **2004**, *20* (26), 11811–11814. <https://doi.org/10.1021/la0485327>.
- (85) Raghuraman, G. K.; Dhamodharan, R.; Prucker, O.; Rühle, J. A Robust Method for the Immobilization of Polymer Molecules on SiO<sub>2</sub> Surfaces. *Macromolecules* **2008**, *41* (3), 873–878. <https://doi.org/10.1021/ma0708489>.
- (86) Gam-Derouich, S.; Carbonnier, B.; Turmine, M.; Lang, P.; Jouini, M.; Hassen-Chehimi, D. Ben; Chehimi, M. M. Electrografted Aryl Diazonium Initiators for Surface-Confined

- Photopolymerization: A New Approach to Designing Functional Polymer Coatings. *Langmuir* **2010**, *26* (14), 11830–11840. <https://doi.org/10.1021/la100880j>.
- (87) Gam-Derouich, S.; Gosecka, M.; Lepinay, S.; Turmine, M.; Carbonnier, B.; Basinska, T.; Slomkowski, S.; Millot, M. C.; Othmane, A.; Ben Hassen-Chehimi, D.; Chehimi, M. M. Highly Hydrophilic Surfaces from Polyglycidol Grafts with Dual Antifouling and Specific Protein Recognition Properties. *Langmuir* **2011**, *27* (15), 9285–9294. <https://doi.org/10.1021/la200290k>.
- (88) Gam-Derouich, S.; Mahouche-Chergui, S.; Turmine, M.; Piquemal, J. Y.; Hassen-Chehimi, D. Ben; Omastová, M.; Chehimi, M. M. A Versatile Route for Surface Modification of Carbon, Metals and Semi-Conductors by Diazonium Salt-Initiated Photopolymerization. *Surf Sci* **2011**, *605* (21–22), 1889–1899. <https://doi.org/10.1016/j.susc.2011.06.029>.
- (89) Gam-Derouich, S.; Mahouche-Chergui, S.; Truong, S.; Ben Hassen-Chehimi, D.; Chehimi, M. M. Design of Molecularly Imprinted Polymer Grafts with Embedded Gold Nanoparticles through the Interfacial Chemistry of Aryl Diazonium Salts. *Polymer (Guildf)* **2011**, *52* (20), 4463–4470. <https://doi.org/10.1016/j.polymer.2011.08.007>.
- (90) Khelifi, A.; Gam-Derouich, S.; Jouini, M.; Kalfat, R.; Chehimi, M. M. Melamine-Imprinted Polymer Grafts through Surface Photopolymerization Initiated by Aryl Layers from Diazonium Salts. *Food Control* **2013**, *31* (2), 379–386. <https://doi.org/10.1016/j.foodcont.2012.10.013>.
- (91) Hong, K. H.; Liu, N.; Sun, G. UV-Induced Graft Polymerization of Acrylamide on Cellulose by Using Immobilized Benzophenone as a Photo-Initiator. *Eur Polym J* **2009**, *45* (8), 2443–2449. <https://doi.org/10.1016/j.eurpolymj.2009.04.026>.
- (92) Biyani, M. V.; Jorfi, M.; Weder, C.; Foster, E. J. Light-Stimulated Mechanically Switchable, Photopatternable Cellulose Nanocomposites. *Polym Chem* **2014**, *5* (19), 5716–5724. <https://doi.org/10.1039/c4py00487f>.
- (93) Melinte, V.; Chibac, A.; Buruiana, T.; Buruiana, E. C. Hybrid Nanocomposites Prepared by in Situ Photopolymerization Using Photoinitiator-Modified Montmorillonite. *Prog Org Coat* **2017**, *104*, 125–134. <https://doi.org/10.1016/j.porgcoat.2016.12.019>.
- (94) Srivastava, V.; Singh, P. P. Eosin y Catalysed Photoredox Synthesis: A Review. *RSC Adv* **2017**, *7* (50), 31377–31392. <https://doi.org/10.1039/c7ra05444k>.
- (95) Avens, H. J.; Randle, T. J.; Bowman, C. N. Polymerization Behavior and Polymer Properties of Eosin-Mediated Surface Modification Reactions. *Polymer (Guildf)* **2008**, *49* (22), 4762–4768. <https://doi.org/10.1016/j.polymer.2008.08.054>.
- (96) Kizilel, S.; Pérez-Luna, V. H.; Teymour, F. Photopolymerization of Poly(Ethylene Glycol) Diacrylate on Eosin-Functionalized Surfaces. *Langmuir* **2004**, *20* (20), 8652–8658. <https://doi.org/10.1021/la0496744>.
- (97) Hansen, R. R.; Sikes, H. D.; Bowman, C. N. Visual Detection of Labeled Oligonucleotides Using Visible-Light-Polymerization-Based Amplification. *Biomacromolecules* **2008**, *9* (1), 355–362. <https://doi.org/10.1021/bm700672z>.
- (98) Satoh, M.; Shirai, K.; Saitoh, H.; Yamauchi, T.; Tsubokawa, N. Photografting of Polymers onto Nanosized Silica Surface Initiated by Eosin Moieties Immobilized onto the Surface. *J Polym Sci A Polym Chem* **2005**, *43* (3), 600–606. <https://doi.org/10.1002/pola.20539>.
- (99) Lilly, J. L.; Romero, G.; Xu, W.; Shin, H. Y.; Berron, B. J. Characterization of Molecular Transport in Ultrathin Hydrogel Coatings for Cellular Immunoprotection. *Biomacromolecules* **2015**, *16* (2), 541–549. <https://doi.org/10.1021/bm501594x>.

- (100) Lilly, J. L.; Berron, B. J. The Role of Surface Receptor Density in Surface-Initiated Polymerizations for Cancer Cell Isolation. *Langmuir* **2016**, *32* (22), 5681–5689. <https://doi.org/10.1021/acs.langmuir.6b01146>.
- (101) Cho, S. K.; Kwon, Y. J. Polyamine/DNA Polyplexes with Acid-Degradable Polymeric Shell as Structurally and Functionally Virus-Mimicking Nonviral Vectors. *Journal of Controlled Release* **2011**, *150* (3), 287–297. <https://doi.org/10.1016/j.jconrel.2010.12.004>.
- (102) Staneva, D.; Grabchev, I.; Bosch, P. Fluorescent Hydrogel-Textile Composite Material Synthesized by Photopolymerization. *International Journal of Polymeric Materials and Polymeric Biomaterials* **2015**, *64* (16), 838–847. <https://doi.org/10.1080/00914037.2015.1030654>.
- (103) Kizilel, S.; Sawardecker, E.; Teymour, F.; Pérez-Luna, V. H. Sequential Formation of Covalently Bonded Hydrogel Multilayers through Surface Initiated Photopolymerization. *Biomaterials* **2006**, *27* (8), 1209–1215. <https://doi.org/10.1016/j.biomaterials.2005.08.025>.
- (104) Nikitas, N. F.; Gkizis, P. L.; Kokotos, C. G. Thioxanthone: A Powerful Photocatalyst for Organic Reactions. *Org Biomol Chem* **2021**, *19* (24), 5237–5253. <https://doi.org/10.1039/d1ob00221j>.
- (105) Jiang, X.; Yin, J. Dendritic Macrophotoinitiator Containing Thioxanthone and Coinitiator Amine. *Macromolecules* **2004**, *37* (21), 7850–7853. <https://doi.org/10.1021/ma0488360>.
- (106) Jiang, X.; Wang, W.; Xu, H.; Yin, J. Water-Compatible Dendritic Macrophotoinitiator Containing Thioxanthone. *J Photochem Photobiol A Chem* **2006**, *181* (2–3), 233–237. <https://doi.org/10.1016/j.jphotochem.2005.12.002>.
- (107) Jia, X.; Jiang, X.; Liu, R.; Yin, J. Poly(N-Isopropylacrylamide) Brush Fabricated by Surface-Initiated Photopolymerization and Its Response to Temperature. *Macromol Chem Phys* **2009**, *210* (21), 1876–1882. <https://doi.org/10.1002/macp.200900291>.
- (108) Jia, X.; Jiang, X.; Liu, R.; Yin, J. Facile Approach to Patterned Binary Polymer Brush through Photolithography and Surface-Initiated Photopolymerization. *ACS Appl Mater Interfaces* **2010**, *2* (4), 1200–1205. <https://doi.org/10.1021/am100035d>.
- (109) Chen, F.; Jiang, X.; Liu, R.; Yin, J. Well-Defined PMMA Brush on Silica Particles Fabricated by Surface-Initiated Photopolymerization (SIPP). *ACS Appl Mater Interfaces* **2010**, *2* (4), 1031–1037. <https://doi.org/10.1021/am900758j>.
- (110) Li, X.; Liu, Z.; Hong, P.; Chen, L.; Liu, X. Synthesis of Organic and Inorganic Hybrid Nanoparticles as Multifunctional Photoinitiator and Its Application in UV-Curable Epoxy Acrylate-Based Coating Systems. *Prog Org Coat* **2020**, *141*. <https://doi.org/10.1016/j.porgcoat.2020.105565>.
- (111) Bai, H.; Huang, Z.; Yang, W. Visible Light-Induced Living Surface Grafting Polymerization for the Potential Biological Applications. *J Polym Sci A Polym Chem* **2009**, *47* (24), 6852–6862. <https://doi.org/10.1002/pola.23724>.
- (112) Lin, Z.; Ma, Y.; Zhao, C.; Chen, R.; Zhu, X.; Zhang, L.; Yan, X.; Yang, W. An Extremely Simple Method for Fabricating 3D Protein Microarrays with an Anti-Fouling Background and High Protein Capacity. *Lab Chip* **2014**, *14* (14), 2505–2514. <https://doi.org/10.1039/c4lc00223g>.
- (113) Zhao, C.; He, B.; Wang, G.; Ma, Y.; Yang, W. Hierarchical PEG-Based 3D Patterns Grafting from Polymer Substrate by Surface Initiated Visible Light Photolithography. *Macromol Rapid Commun* **2016**, *37* (19), 1611–1617. <https://doi.org/10.1002/marc.201600307>.
- (114) Fukumori, K.; Akiyama, Y.; Yamato, M.; Okano, T. A Facile Method for Preparing Temperature-Responsive Cell Culture Surfaces by Using a Thioxanthone Photoinitiator Immobilized on a Polystyrene Surface. *ChemNanoMat* **2016**, *2* (5), 454–460. <https://doi.org/10.1002/cnma.201600056>.

- (115) Liu, N.; Sun, G.; Gaan, S.; Rupper, P. Controllable Surface Modifications of Polyamide by Photo-Induced Graft Polymerization Using Immobilized Photo-Initiators. *J Appl Polym Sci* **2010**, *116* (6), 3629–3637. <https://doi.org/10.1002/app.31909>.
- (116) Liu, N.; Sun, G.; Zhu, J. Photo-Induced Self-Cleaning Functions on 2-Anthraquinone Carboxylic Acid Treated Cotton Fabrics. *J Mater Chem* **2011**, *21* (39), 15383–15390. <https://doi.org/10.1039/c1jm12805a>.
- (117) He, D.; Ulbricht, M. Surface-Selective Photo-Grafting on Porous Polymer Membranes via a Synergist Immobilization Method. *J Mater Chem* **2006**, *16* (19), 1860–1868. <https://doi.org/10.1039/b601546h>.
- (118) He, D.; Ulbricht, M. Synergist Immobilization Method for Photo-Grafting: Factors Affecting Surface Selectivity. *Macromol Chem Phys* **2007**, *208* (14), 1582–1591. <https://doi.org/10.1002/macp.200700039>.
- (119) He, D.; Ulbricht, M. Preparation and Characterization of Porous Anion-Exchange Membrane Adsorbers with High Protein-Binding Capacity. *J Memb Sci* **2008**, *315* (1–2), 155–163. <https://doi.org/10.1016/j.memsci.2008.02.014>.
- (120) He, D.; Sun, W.; Schrader, T.; Ulbricht, M. Protein Adsorbers from Surface-Grafted Copolymers with Selective Binding Sites. *J Mater Chem* **2009**, *19* (2), 253–260. <https://doi.org/10.1039/b810752a>.
- (121) Dyer, D. J.; Feng, J.; Schmidt, R.; Wong, V. N.; Zhao, T.; Yagci, Y. Photoinduced Polymerization from Dimethylamino-Terminated Self-Assembled Monolayers on Gold. *Macromolecules* **2004**, *37* (19), 7072–7074. <https://doi.org/10.1021/ma048950i>.
- (122) Gam-Derouich, S.; Lamouri, A.; Redeuilh, C.; Decorse, P.; Maurel, F.; Carbonnier, B.; Beyaz, S.; Yilmaz, G.; Yagci, Y.; Chehimi Langmuir, M. M.; Beyazit, S.; Chehimi, M. M. Diazonium Salt-Derived 4-(Dimethylamino)Phenyl Groups as Hydrogen Donors in Surface-Confined Radical Photopolymerization for Bioactive PHEMA Grafts. **2012**. <https://doi.org/10.1021/la300690d>.
- (123) Kim, S.; Kim, E.; Kim, S.; Kim, W. Surface Modification of Silica Nanoparticles by UV-Induced Graft Polymerization of Methyl Methacrylate. *J Colloid Interface Sci* **2005**, *292* (1), 93–98. <https://doi.org/10.1016/j.jcis.2005.09.046>.
- (124) Chen, F.; Jiang, X.; Liu, R.; Yin, J. Polymeric Vesicles with Well-Defined Poly(Methyl Methacrylate) (PMMA) Brushes via Surface-Initiated Photopolymerization (SIPP). *Polym Chem* **2011**, *2* (3), 614–618. <https://doi.org/10.1039/c0py00288g>.
- (125) Chen, W. L.; Cordero, R.; Tran, H.; Ober, C. K. 50th Anniversary Perspective: Polymer Brushes: Novel Surfaces for Future Materials. *Macromolecules* **2017**, *50* (11), 4089–4113. <https://doi.org/10.1021/acs.macromol.7b00450>.
- (126) Barbey, R.; Lavanant, L.; Paripovic, D.; Schüwer, N.; Sugnaux, C.; Tugulu, S.; Klok, H. A. Polymer Brushes via Surface-Initiated Controlled Radical Polymerization: Synthesis, Characterization, Properties, and Applications. *Chem Rev* **2009**, *109* (11), 5437–5527. <https://doi.org/10.1021/cr900045a>.
- (127) Zoppe, J. O.; Ataman, N. C.; Mocny, P.; Wang, J.; Moraes, J.; Klok, H. A. Surface-Initiated Controlled Radical Polymerization: State-of-the-Art, Opportunities, and Challenges in Surface and Interface Engineering with Polymer Brushes. *Chem Rev* **2017**, *117* (3), 1105–1318. <https://doi.org/10.1021/acs.chemrev.6b00314>.
- (128) Otsu, T.; Yoshida, M.; Tazaki, T. A Model for Living Radical Polymerization. *Makromol. Chem., Rapid Commun* **1982**, *3*, 133–140. <https://doi.org/10.1002/marc.1982.030030209>.

- (129) Otsu, T. Iniferter Concept and Living Radical Polymerization. *J Polym Sci A Polym Chem* **2000**, *38*. [https://doi.org/10.1002/\(SICI\)1099-0518\(20000615\)38:12<2121::AID-POLA10>3.0.CO;2-X](https://doi.org/10.1002/(SICI)1099-0518(20000615)38:12<2121::AID-POLA10>3.0.CO;2-X).
- (130) Chen, M.; Zhong, M.; Johnson, J. A. Light-Controlled Radical Polymerization: Mechanisms, Methods, and Applications. *Chem Rev* **2016**, *116* (17), 10167–10211. <https://doi.org/10.1021/acs.chemrev.5b00671>.
- (131) Yan, S.; Luan, S.; Shi, H.; Xu, X.; Zhang, J.; Yuan, S.; Yang, Y.; Yin, J. Hierarchical Polymer Brushes with Dominant Antibacterial Mechanisms Switching from Bactericidal to Bacteria Repellent. *Biomacromolecules* **2016**, *17* (5), 1696–1704. <https://doi.org/10.1021/acs.biomac.6b00115>.
- (132) Silies, L.; Didzoleit, H.; Hess, C.; Stühn, B.; Andrieu-Brunsen, A. Mesoporous Thin Films, Zwitterionic Monomers, and Iniferter-Initiated Polymerization: Polymerization in a Confined Space. *Chemistry of Materials* **2015**, *27* (6), 1971–1981. <https://doi.org/10.1021/cm503748d>.
- (133) Otsu, T.; Ogawa, T.; Yamamoto, T. Solid-Phase Block Copolymer Synthesis by the Iniferter Technique. *Macromolecules*, Vol. 19, No. 7 **1986**. <https://doi.org/10.1021/ma00161a056>.
- (134) Nakayama, Y.; Matsuda, T. Surface Macromolecular Architectural Designs Using Photo-Graft Copolymerization Based on Photochemistry of Benzyl N,N-Diethyldithiocarbamate. **1996**. <https://doi.org/10.1021/ma9606014>.
- (135) Lee, H. J.; Nakayama, Y.; Matsuda, T. Spatio-Resolved, Macromolecular Architectural Surface: Highly Branched Graft Polymer via Photochemically Driven Quasi-living Polymerization Technique. *Macromolecules* **1999**, *32* (21), 6989–6995. <https://doi.org/10.1021/ma990566b>.
- (136) Lee, H. J.; Matsuda, T. Surface Photograft Polymerization on Segmented Polyurethane Using the Iniferter Technique. **1999**. [https://doi.org/10.1002/\(sici\)1097-4636\(19991215\)47:4<564::aid-jbm13>3.0.co;2-3](https://doi.org/10.1002/(sici)1097-4636(19991215)47:4<564::aid-jbm13>3.0.co;2-3).
- (137) Derouet, D.; Chi, N. H. T. Synthesis and Characterization of Poly(Methyl Methacrylate)-Grafted Silica Microparticles. *J Appl Polym Sci* **2008**, *109* (4), 2113–2127. <https://doi.org/10.1002/app.28290>.
- (138) Hattori, K.; Hiwatari, M.; Iiyama, C.; Yoshimi, Y.; Kohori, F.; Sakai, K.; Piletsky, S. A. Gate Effect of Theophylline-Imprinted Polymers Grafted to the Cellulose by Living Radical Polymerization. *J Memb Sci* **2004**, *233* (1–2), 169–173. <https://doi.org/10.1016/j.memsci.2003.12.013>.
- (139) Ma, J.; Luan, S.; Song, L.; Jin, J.; Yuan, S.; Yan, S.; Yang, H.; Shi, H.; Yin, J. Fabricating a Cycloolefin Polymer Immunoassay Platform with a Dual-Function Polymer Brush via a Surface-Initiated Photoiniferter-Mediated Polymerization Strategy. *ACS Appl Mater Interfaces* **2014**, *6* (3), 1971–1978. <https://doi.org/10.1021/am405017h>.
- (140) Ma, J.; Song, L.; Shi, H.; Yang, H.; Ye, W.; Guo, X.; Luan, S.; Yin, J. Development of Hierarchical Fe<sub>3</sub>O<sub>4</sub> Magnetic Microspheres as Solid Substrates for High Sensitive Immunoassays. *J Mater Chem B* **2018**, *6* (22), 3762–3769. <https://doi.org/10.1039/c8tb00846a>.
- (141) He, D.; Ulbricht, M. Tailored “Grafting-From” Functionalization of Microfiltration Membrane Surface Photo-Initiated by Immobilized Iniferter. *Macromol Chem Phys* **2009**, *210* (13–14), 1149–1158. <https://doi.org/10.1002/macp.200900069>.
- (142) De Boer, B.; Simon, H. K.; Werts, M. P. L.; Van Der Vegte, E. W.; Hadziioannou, G. ‘Living’ Free Radical Photopolymerization Initiated from Surface-Grafted Iniferter Monolayers. *Macromolecules* **2000**, *33* (2), 349–356. <https://doi.org/10.1021/ma9910944>.
- (143) Rahane, S. B.; Kilbey, S. M.; Metters, A. T. Kinetics of Surface-Initiated Photoiniferter-Mediated Photopolymerization. *Macromolecules* **2005**, *38* (20), 8202–8210. <https://doi.org/10.1021/ma0509661>.

- (144) Rahane, S. B.; Michael Kilbey, S.; Metters, A. T. Kinetic Modeling of Surface-Initiated Photoiniferter-Mediated Photopolymerization in Presence of Tetraethylthiuram Disulfide. *Macromolecules* **2008**, *41* (24), 9612–9618. <https://doi.org/10.1021/ma702516w>.
- (145) Rahane, S. B.; Metters, A. T.; Kilbey, S. M. Impact of Added Tetraethylthiuram Disulfide Deactivator on the Kinetics of Growth and Reinitiation of Poly(Methyl Methacrylate) Brushes Made by Surface-Initiated Photoiniferter-Mediated Photopolymerization. *Macromolecules* **2006**, *39* (26), 8987–8991. <https://doi.org/10.1021/ma0617217>.
- (146) Li, A.; Benetti, E. M.; Tranchida, D.; Clasohm, J. N.; Schönherr, H.; Spencer, N. D. Surface-Grafted, Covalently Cross-Linked Hydrogel Brushes with Tunable Interfacial and Bulk Properties. *Macromolecules* **2011**, *44* (13), 5344–5351. <https://doi.org/10.1021/ma2006443>.
- (147) Fu, Y.; Zhang, L.; Huang, L.; Xiao, S.; Chen, F.; Fan, P.; Zhong, M.; Yang, J. Salt- and Thermo-Responsive Polyzwitterionic Brush Prepared via Surface-Initiated Photoiniferter-Mediated Polymerization. *Appl Surf Sci* **2018**, *450*, 130–137. <https://doi.org/10.1016/j.apsusc.2018.04.112>.
- (148) Dyer, D. J. Photoinitiated Synthesis of Grafted Polymers. *Advances in Polymer Science* **2006**, *197* (1), 47–65. [https://doi.org/10.1007/12\\_064](https://doi.org/10.1007/12_064).
- (149) Brewer, N. J.; Janusz, S.; Critchley, K.; Evans, S. D.; Leggett, G. J. Photooxidation of Self-Assembled Monolayers by Exposure to Light of Wavelength 254 Nm: A Static SIMS Study. *Journal of Physical Chemistry B* **2005**, *109* (22), 11247–11256. <https://doi.org/10.1021/jp0443299>.
- (150) Benetti, E. M.; Zapotoczny, S.; Vancso, G. J. Tunable Thermoresponsive Polymeric Platforms on Gold by “Photoiniferter”-Based Surface Grafting. *Advanced Materials* **2007**, *19* (2), 268–271. <https://doi.org/10.1002/adma.200601554>.
- (151) Benetti, E. M.; Reimhult, E.; De Bruin, J.; Zapotoczny, S.; Textor, M.; Vancso, G. J. Poly(Methacrylic Acid) Grafts Grown from Designer Surfaces: The Effect of Initiator Coverage on Polymerization Kinetics, Morphology, and Properties. *Macromolecules* **2009**, *42* (5), 1640–1647. <https://doi.org/10.1021/ma8014678>.
- (152) Navarro, M.; Benetti, E. M.; Zapotoczny, S.; Planell, J. A.; Vancso, G. J. Buried, Covalently Attached RGD Peptide Motifs in Poly(Methacrylic Acid) Brush Layers: The Effect of Brush Structure on Cell Adhesion. *Langmuir* **2008**, *24* (19), 10996–11002. <https://doi.org/10.1021/la800999y>.
- (153) Krause, J. E.; Brault, N. D.; Li, Y.; Xue, H.; Zhou, Y.; Jiang, S. Photoiniferter-Mediated Polymerization of Zwitterionic Carboxybetaine Monomers for Low-Fouling and Functionalizable Surface Coatings. *Macromolecules* **2011**, *44* (23), 9213–9220. <https://doi.org/10.1021/ma202007h>.
- (154) Griffete, N.; Lamouri, A.; Herbst, F.; Felidj, N.; Ammar, S.; Mangeney, C. Synthesis of Highly Soluble Polymer-Coated Magnetic Nanoparticles Using a Combination of Diazonium Salt Chemistry and the Iniferter Method. *RSC Adv* **2012**, *2* (3), 826–830. <https://doi.org/10.1039/c1ra00577d>.
- (155) Atmane, Y. A.; Sicard, L.; Lamouri, A.; Pinson, J.; Sicard, M.; Masson, C.; Nowak, S.; Decorse, P.; Piquemal, J. Y.; Galtayries, A.; Mangeney, C. Functionalization of Aluminum Nanoparticles Using a Combination of Aryl Diazonium Salt Chemistry and Iniferter Method. *Journal of Physical Chemistry C* **2013**, *117* (49), 26000–26006. <https://doi.org/10.1021/jp406356s>.
- (156) Adenier, A.; Cabet-Deliry, E.; Lalot, T.; Pinson, J.; Podvorica, F. Attachment of Polymers to Organic Moieties Covalently Bonded to Iron Surfaces. *Chemistry of Materials* **2002**, *14* (11), 4576–4585. <https://doi.org/10.1021/cm0211397>.

- (157) Ahmad, R.; Griffete, N.; Lamouri, A.; Mangeney, C. Functionalization of Magnetic Nanocrystals by Oligo (Ethylene Oxide) Chains Carrying Diazonium and Iniferter End Groups. *J Colloid Interface Sci* **2013**, *407*, 210–214. <https://doi.org/10.1016/j.jcis.2013.06.002>.
- (158) Ahmad, R.; Félidj, N.; Boubekour-Lecaque, L.; Lau-Truong, S.; Gam-Derouich, S.; Decorse, P.; Lamouri, A.; Mangeney, C. Water-Soluble Plasmonic Nanosensors with Synthetic Receptors for Label-Free Detection of Folic Acid. *Chemical Communications* **2015**, *51* (47), 9678–9681. <https://doi.org/10.1039/c5cc01489a>.
- (159) Dadashi-Silab, S.; Atilla Tasdelen, M.; Yagci, Y. Photoinitiated Atom Transfer Radical Polymerization: Current Status and Future Perspectives. *J Polym Sci A Polym Chem* **2014**, *52* (20), 2878–2888. <https://doi.org/10.1002/pola.27327>.
- (160) Yan, J.; Pan, X.; Schmitt, M.; Wang, Z.; Bockstaller, M. R.; Matyjaszewski, K. Enhancing Initiation Efficiency in Metal-Free Surface-Initiated Atom Transfer Radical Polymerization (SI-ATRP). *ACS Macro Lett* **2016**, *5* (6), 661–665. <https://doi.org/10.1021/acsmacrolett.6b00295>.
- (161) Pearson, R. M.; Lim, C. H.; McCarthy, B. G.; Musgrave, C. B.; Miyake, G. M. Organocatalyzed Atom Transfer Radical Polymerization Using N-Aryl Phenoxazines as Photoredox Catalysts. *J Am Chem Soc* **2016**, *138* (35), 11399–11407. <https://doi.org/10.1021/jacs.6b08068>.
- (162) Ma, L.; Li, N.; Zhu, J.; Chen, X. Visible Light-Induced Metal Free Surface Initiated Atom Transfer Radical Polymerization of Methyl Methacrylate on SBA-15. *Polymers (Basel)* **2017**, *9* (2). <https://doi.org/10.3390/polym9020058>.
- (163) Zeng, G.; Liu, M.; Shi, K.; Heng, C.; Mao, L.; Wan, Q.; Huang, H.; Deng, F.; Zhang, X.; Wei, Y. Surface Modification of Nanodiamond through Metal Free Atom Transfer Radical Polymerization. *Appl Surf Sci* **2016**, *390*, 710–717. <https://doi.org/10.1016/j.apsusc.2016.08.154>.
- (164) Tang, S.; Yuan, J.; Liu, C.; Lei, A. Direct Oxidative Esterification of Alcohols. *Dalton Transactions* **2014**, *43* (36), 13460–13470. <https://doi.org/10.1039/c4dt01133c>.
- (165) Teacă, C. A.; Tanasa, F. Wood Surface Modification-Classic and Modern Approaches in Wood Chemical Treatment by Esterification Reactions. *Coatings* **2020**, *10* (7). <https://doi.org/10.3390/coatings10070629>.
- (166) Belgacem, M. N.; Gandini, A. The Surface Modification of Cellulose Fibres for Use as Reinforcing Elements in Composite Materials. *Compos Interfaces* **2005**, *12* (1–2), 41–75. <https://doi.org/10.1163/1568554053542188>.
- (167) Zeng, G.; Liu, M.; Heng, C.; Huang, Q.; Mao, L.; Huang, H.; Hui, J.; Deng, F.; Zhang, X.; Wei, Y. Surface PolyPEGylation of Eu<sup>3+</sup> Doped Luminescent Hydroxyapatite Nanorods through the Combination of Ligand Exchange and Metal Free Surface Initiated Atom Transfer Radical Polymerization. *Appl Surf Sci* **2017**, *399*, 499–505. <https://doi.org/10.1016/j.apsusc.2016.12.107>.
- (168) Discekici, E. H.; Pester, C. W.; Treat, N. J.; Lawrence, J.; Mattson, K. M.; Narupai, B.; Toumayan, E. P.; Luo, Y.; McGrath, A. J.; Clark, P. G.; Read De Alaniz, J.; Hawker, C. J. Simple Benchtop Approach to Polymer Brush Nanostructures Using Visible-Light-Mediated Metal-Free Atom Transfer Radical Polymerization. *ACS Macro Lett* **2016**, *5* (2), 258–262. <https://doi.org/10.1021/acsmacrolett.6b00004>.
- (169) Mansfeld, U.; Pietsch, C.; Hoogenboom, R.; Becer, C. R.; Schubert, U. S. Clickable Initiators, Monomers and Polymers in Controlled Radical Polymerizations - A Prospective Combination in Polymer Science. *Polym Chem* **2010**, *1* (10), 1560–1598. <https://doi.org/10.1039/c0py00168f>.



- (170) Bellotti, V.; Simonutti, R. New Light in Polymer Science: Photoinduced Reversible Addition-Fragmentation Chain Transfer Polymerization (PET-RAFT) as Innovative Strategy for the Synthesis of Advanced Materials. *Polymers (Basel)* **2021**, *13* (7). <https://doi.org/10.3390/polym13071119>.
- (171) Semsarilar, M.; Perrier, S. "Green" Reversible Addition-Fragmentation Chain-Transfer (RAFT) Polymerization. *Nat Chem* **2010**, *2* (10), 811–820. <https://doi.org/10.1038/nchem.853>.
- (172) Keddie, D. J.; Moad, G.; Rizzardo, E.; Thang, S. H. RAFT Agent Design and Synthesis. *Macromolecules* **2012**, *45* (13), 5321–5342. <https://doi.org/10.1021/ma300410v>.
- (173) Wang, Q.; Hu, L.; Cui, Z.; Fu, P.; Liu, M.; Qiao, X.; Pang, X. Dual Roles of Amino-Functionalized Silicon Quantum Dots (SiQDs) for Visible-Light-Induced Surface-Initiated PET-RAFT Polymerization on Substrates. *ACS Appl Mater Interfaces* **2020**, *12* (37), 42161–42168. <https://doi.org/10.1021/acscami.0c12299>.
- (174) Ng, G.; Li, M.; Yeow, J.; Jung, K.; Pester, C. W.; Boyer, C. Benchtop Preparation of Polymer Brushes by SI-PET-RAFT: The Effect of the Polymer Composition and Structure on Inhibition of a Pseudomonas Biofilm. *ACS Appl Mater Interfaces* **2020**, *12* (49), 55243–55254. <https://doi.org/10.1021/acscami.0c15221>.
- (175) Allegrezza, M. L.; Konkolewicz, D. PET-RAFT Polymerization: Mechanistic Perspectives for Future Materials. *ACS Macro Lett* **2021**, *10* (4), 433–446. <https://doi.org/10.1021/acsmacrolett.1c00046>.
- (176) Xu, J.; Shanmugam, S.; Duong, H. T.; Boyer, C. Organo-Photocatalysts for Photoinduced Electron Transfer-Reversible Addition-Fragmentation Chain Transfer (PET-RAFT) Polymerization. *Polym Chem* **2015**, *6* (31), 5615–5624. <https://doi.org/10.1039/c4py01317d>.
- (177) Kuzmyn, A. R.; Nguyen, A. T.; Teunissen, L. W.; Zuilhof, H.; Baggerman, J. Antifouling Polymer Brushes via Oxygen-Tolerant Surface-Initiated PET-RAFT. *Langmuir* **2020**, *36* (16), 4439–4446. <https://doi.org/10.1021/acs.langmuir.9b03536>.
- (178) Zhu, Y.; Egap, E. PET-RAFT Polymerization Catalyzed by Cadmium Selenide Quantum Dots (Qds):: Grafting-from Qds Photocatalysts to Make Polymer Nanocomposites. *Polym Chem* **2020**, *11* (5), 1018–1024. <https://doi.org/10.1039/c9py01604j>.
- (179) Hu, L.; Hao, Q.; Wang, L.; Cui, Z.; Fu, P.; Liu, M.; Qiao, X.; Pang, X. Thein Situ "Grafting from" Approach for the Synthesis of Polymer Brushes on Upconversion Nanoparticles via NIR-Mediated RAFT Polymerization. *Polym Chem* **2021**, *12* (4), 545–553. <https://doi.org/10.1039/d0py01550d>.
- (180) Wei, Y. Y.; Sun, X. T.; Xu, Z. R. One-Step Synthesis of Bifunctional PEGDA/TiO<sub>2</sub> Composite Film by Photopolymerization for the Removal of Congo Red. *Appl Surf Sci* **2018**, *445*, 437–444. <https://doi.org/10.1016/j.apsusc.2018.03.149>.
- (181) Yang, J.; Hou, L.; Xu, B.; Zhang, N.; Liang, Y.; Tian, W.; Dong, D. Polymer Brushes on Planar TiO<sub>2</sub> Substrates. *Macromol Rapid Commun* **2014**, *35* (13), 1224–1229. <https://doi.org/10.1002/marc.201400068>.
- (182) Pant, B.; Park, M.; Park, S. J. Recent Advances in TiO<sub>2</sub> Films Prepared by Sol-Gel Methods for Photocatalytic Degradation of Organic Pollutants and Antibacterial Activities. *Coatings* **2019**, *9* (10). <https://doi.org/10.3390/coatings9100613>.
- (183) Wang, X.; Lu, Q.; Wang, X.; Joo, J.; Dahl, M.; Liu, B.; Gao, C.; Yin, Y. Photocatalytic Surface-Initiated Polymerization on TiO<sub>2</sub> toward Well-Defined Composite Nanostructures. *ACS Appl Mater Interfaces* **2016**, *8* (1), 538–546. <https://doi.org/10.1021/acscami.5b09551>.

- (184) Zivic, N.; Kuroishi, P. K.; Dumur, F.; Gimes, D.; Dove, A. P.; Sardon, H. Recent Advances and Challenges in the Design of Organic Photoacid and Photobase Generators for Polymerizations. *Angewandte Chemie - International Edition* **2019**, *58* (31), 10410–10422. <https://doi.org/10.1002/anie.201810118>.
- (185) Saway, J.; Salem, Z. M.; Badillo, J. J. Recent Advances in Photoacid Catalysis for Organic Synthesis. *Synthesis (Germany)* **2021**, *53* (3), 489–497. <https://doi.org/10.1055/s-0040-1705952>.
- (186) Dai, J.; Lowes, J.; Jones, C. (54) Bottom-Up Conformal Coating and Photopatterning on PAG-Immobilized Surfaces. **2020**. <https://doi.org/US2020/0142308A1>.
- (187) Kuznetsova, N. A.; Malkov, G. V.; Gribov, B. G. Photoacid Generators. Application and Current State of Development. *Russian Chemical Reviews* **2020**, *89* (2), 173–190. <https://doi.org/10.1070/rcr4899>.
- (188) Burnstine-Townley, A.; Mondal, S.; Agam, Y.; Nandi, R.; Amdursky, N. Light-Modulated Cationic and Anionic Transport across Protein Biopolymers\*\*. *Angewandte Chemie - International Edition* **2021**. <https://doi.org/10.1002/anie.202111024>.
- (189) Tasdelen, M. A.; Yagci, Y. Lichtinduzierte Klickreaktionen. *Angewandte Chemie* **2013**, *125* (23), 6044–6053. <https://doi.org/10.1002/ange.201208741>.
- (190) Chen, R. T.; Marchesan, S.; Evans, R. A.; Styan, K. E.; Such, G. K.; Postma, A.; McLean, K. M.; Muir, B. W.; Caruso, F. Photoinitiated Alkyne-Azide Click and Radical Cross-Linking Reactions for the Patterning of PEG Hydrogels. *Biomacromolecules* **2012**, *13* (3), 889–895. <https://doi.org/10.1021/bm201802w>.
- (191) Chen, R. T.; Muir, B. W.; Such, G. K.; Postma, A.; Evans, R. A.; Pereira, S. M.; McLean, K. M.; Caruso, F. Surface “Click” Chemistry on Brominated Plasma Polymer Thin Films. *Langmuir* **2010**, *26* (5), 3388–3393. <https://doi.org/10.1021/la9031688>.
- (192) Michel, O.; Ravoo, B. J. Carbohydrate Microarrays by Microcontact “Click” Chemistry. *Langmuir* **2008**, *24* (21), 12116–12118. <https://doi.org/10.1021/la802304w>.
- (193) El Zubir, O.; Barlow, I.; Ul-Haq, E.; Tajuddin, H. A.; Williams, N. H.; Leggett, G. J. Generic Methods for Micrometer- and Nanometer-Scale Surface Derivatization Based on Photochemical Coupling of Primary Amines to Monolayers of Aryl Azides on Gold and Aluminum Oxide Surfaces. *Langmuir* **2013**, *29* (4), 1083–1092. <https://doi.org/10.1021/la303746e>.
- (194) Bou-Hamdan, F. R.; Lévesque, F.; O’Brien, A. G.; Seeberger, P. H. Continuous Flow Photolysis of Aryl Azides: Preparation of 3H-Azepinones. *Beilstein Journal of Organic Chemistry* **2011**, *7*, 1124–1129. <https://doi.org/10.3762/bjoc.7.129>.
- (195) Wollmann, E.; Kang, D.; Frisbie, D.; Lorcovic, I.; Wrighton, M. Photosensitive Self-Assembled Monolayers on Gold: Photochemistry of Surface-Confining Aryl Azide and Cyclopentadienylmanganese Tricarbonyl. *American Chemical Society* **1993**. <https://doi.org/10.1021/ja00089a030>.
- (196) Snell, K. E.; Ismaili, H.; Workentin, M. S. Photoactivated Nitrene Chemistry to Prepare Gold Nanoparticle Hybrids with Carbonaceous Materials. *ChemPhysChem* **2012**, *13* (13), 3185–3193. <https://doi.org/10.1002/cphc.201200240>.
- (197) Elender, G.; Kfihner, M.; Sackmann, E. Functionalisation of Si/SiO<sub>2</sub> and Glass Surfaces with Ultrathin Dextran Films and Deposition of Lipid Bilayers. *Biosens Bioelectron* **1996**, *11* (6), 565–577. [https://doi.org/10.1016/0956-5663\(96\)83292-1](https://doi.org/10.1016/0956-5663(96)83292-1).

- (198) Zhao, Y.; Xu, Z.; Wang, X.; Lin, T. Photoreactive Azido-Containing Silica Nanoparticle/Polycation Multilayers: Durable Superhydrophobic Coating on Cotton Fabrics. *Langmuir* **2012**, *28* (15), 6328–6335. <https://doi.org/10.1021/la300281q>.
- (199) Muhr, N.; Puchleitner, R.; Kern, W. Nanoparticles Bearing a Photoreactive Shell: Interaction with Polymers and Polymer Surfaces. *Eur Polym J* **2013**, *49* (10), 3114–3124. <https://doi.org/10.1016/j.eurpolymj.2013.07.010>.
- (200) Picu, C. R.; Krawczyk, K. K.; Wang, Z.; Pishvazadeh-Moghaddam, H.; Sieberer, M.; Lassnig, A.; Kern, W.; Hadar, A.; Constantinescu, D. M. Toughening in Nanosilica-Reinforced Epoxy with Tunable Filler-Matrix Interface Properties. *Compos Sci Technol* **2019**, *183*. <https://doi.org/10.1016/j.compscitech.2019.107799>.
- (201) Liu, L. H.; Yan, M. Perfluorophenyl Azides: New Applications in Surface Functionalization and Nanomaterial Synthesis. *Acc Chem Res* **2010**, *43* (11), 1434–1443. <https://doi.org/10.1021/ar100066t>.
- (202) Bartlett, M.; Yan, M. Fabrication of Polymer Thin Films and Arrays with Spatial and Topographical Controls. *Advanced Materials* **2001**. [https://doi.org/10.1002/1521-4095\(200110\)13:19<1449::AID-ADMA1449>3.0.CO;2-M](https://doi.org/10.1002/1521-4095(200110)13:19<1449::AID-ADMA1449>3.0.CO;2-M).
- (203) Liu, L.; Yan, M. A General Approach to the Covalent Immobilization of Single Polymers. *Angewandte Chemie - International Edition* **2006**, *45* (37), 6207–6210. <https://doi.org/10.1002/anie.200602097>.
- (204) Liu, L.; Engelhard, M. H.; Yan, M. Surface and Interface Control on Photochemically Initiated Immobilization. *J Am Chem Soc* **2006**, *128* (43), 14067–14072. <https://doi.org/10.1021/ja062802l>.
- (205) Yan, M.; Bartlett, M. Polymeric Structures, Particular Microstructures, and Methods for Making Same. **2004**. <https://doi.org/US 2004/0242023 A>.
- (206) Yan, M.; Ren, J. Covalent Immobilization of Polypropylene Thin Films. *J Mater Chem* **2005**, *15* (4), 523–527. <https://doi.org/10.1039/b410972d>.
- (207) Pei, Y.; Yu, H.; Pei, Z.; Theurer, M.; Ammer, C.; André, S.; Gabius, H. J.; Yan, M.; Ramström, O. Photoderivatized Polymer Thin Films at Quartz Crystal Microbalance Surfaces: Sensors for Carbohydrate-Protein Interactions. *Anal Chem* **2007**, *79* (18), 6897–6902. <https://doi.org/10.1021/ac070740r>.
- (208) Wang, X.; Ramström, O.; Yan, M. Quantitative Analysis of Multivalent Ligand Presentation on Gold Glyconanoparticles and the Impact on Lectin Binding. *Anal Chem* **2010**, *82* (21), 9082–9089. <https://doi.org/10.1021/ac102114z>.
- (209) Pei, Z.; Yu, H.; Theurer, M.; Waldén, A.; Nilsson, P.; Yan, M.; Ramström, O. Photogenerated Carbohydrate Microarrays. *ChemBioChem* **2007**, *8* (2), 166–168. <https://doi.org/10.1002/cbic.200600447>.
- (210) Liu, L. H.; Dietsch, H.; Schurtenberger, P.; Yan, M. Photoinitiated Coupling of Unmodified Monosaccharides to Iron Oxide Nanoparticles for Sensing Proteins and Bacteria. *Bioconjug Chem* **2009**, *20* (7), 1349–1355. <https://doi.org/10.1021/bc900110x>.
- (211) Kubo, T.; Wang, X.; Tong, Q.; Yan, M. Polymer-Based Photocoupling Agent for the Efficient Immobilization of Nanomaterials and Small Molecules. *Langmuir* **2011**, *27* (15), 9372–9378. <https://doi.org/10.1021/la201324h>.
- (212) Delaitre, G.; Goldmann, A. S.; Mueller, J. O.; Barner-Kowollik, C. Effiziente Photochemische Verfahren Für Die Räumlich Aufgelöste Oberflächenfunktionalisierung. *Angewandte Chemie* **2015**, *127* (39), 11548–11564. <https://doi.org/10.1002/ange.201504920>.

- (213) Dietrich, M.; Delaittre, G.; Blinco, J. P.; Inglis, A. J.; Bruns, M.; Barner-Kowollik, C. Photoclickable Surfaces for Profluorescent Covalent Polymer Coatings. *Adv Funct Mater* **2012**, *22* (2), 304–312. <https://doi.org/10.1002/adfm.201102068>.
- (214) Rodriguez-Emmenegger, C.; Preuss, C. M.; Yameen, B.; Pop-Georgievski, O.; Bachmann, M.; Mueller, J. O.; Bruns, M.; Goldmann, A. S.; Bastmeyer, M.; Barner-Kowollik, C. Controlled Cell Adhesion on Poly(Dopamine) Interfaces Photopatterned with Non-Fouling Brushes. *Advanced Materials* **2013**, *25* (42), 6123–6127. <https://doi.org/10.1002/adma.201302492>.
- (215) Kotzyba-Hibert, F.; Kapfer, I.; Goeldner, M. Neue Entwicklungen Bei Der Photoaffinitätsmarkierung. *Angewandte Chemie* **1995**, *107*. <https://doi.org/https://doi.org/10.1002/ange.19951071204>.
- (216) Ismaili, H.; Lee, S.; Workentin, M. S. Diazirine-Modified Gold Nanoparticle: Template for Efficient Photoinduced Interfacial Carbene Insertion Reactions. *Langmuir* **2010**, *26* (18), 14958–14964. <https://doi.org/10.1021/la102621h>.
- (217) Ismaili, H.; Workentin, M. S. Covalent Diamond-Gold Nanoparticle Hybrids via Photochemically Generated Carbenes. *Chemical Communications* **2011**, *47* (27), 7788–7790. <https://doi.org/10.1039/c1cc12125a>.
- (218) Ismaili, H.; Lagugné-Labarthe, F.; Workentin, M. S. Covalently Assembled Gold Nanoparticle-Carbon Nanotube Hybrids via a Photoinitiated Carbene Addition Reaction. *Chemistry of Materials* **2011**, *23* (6), 1519–1525. <https://doi.org/10.1021/cm103284g>.
- (219) Ismaili, H.; Geng, D.; Sun, A. X.; Kantzas, T. T.; Workentin, M. S. Light-Activated Covalent Formation of Gold Nanoparticle-Graphene and Gold Nanoparticle-Glass Composites. *Langmuir* **2011**, *27* (21), 13261–13268. <https://doi.org/10.1021/la202815g>.
- (220) Kanoh, N.; Kumashiro, S.; Simizu, S.; Kondoh, Y.; Hatakeyama, S.; Tashiro, H.; Osada, H. Immobilization of Natural Products on Glass Slides by Using a Photoaffinity Reaction and the Detection of Protein–Small-Molecule Interactions. *Angewandte Chemie* **2003**, *115* (45), 5742–5745. <https://doi.org/10.1002/ange.200352164>.
- (221) Meng, Q.; Xiang, S.; Zhang, K.; Wang, M.; Bu, X.; Xue, P.; Liu, L.; Sun, H.; Yang, B. A Facile Two-Step Etching Method to Fabricate Porous Hollow Silica Particles. *J Colloid Interface Sci* **2012**, *384* (1), 22–28. <https://doi.org/10.1016/j.jcis.2012.06.043>.
- (222) Li, W.; Bao, C.; Wright, R. A. E.; Zhao, B. Synthesis of Mixed Poly( $\epsilon$ -Caprolactone)/Polystyrene Brushes from  $\gamma$ -Initiator-Functionalized Silica Particles by Surface-Initiated Ring-Opening Polymerization and Nitroxide-Mediated Radical Polymerization. *RSC Adv* **2014**, *4* (36), 18772–18781. <https://doi.org/10.1039/c4ra02429j>.
- (223) Gann, J. P.; Yan, M. A Versatile Method for Grafting Polymers on Nanoparticles. *Langmuir* **2008**, *24* (10), 5319–5323. <https://doi.org/10.1021/la7029592>.
- (224) Müller, M.; Drusgala, M.; Fischer, R. C.; Torvisco, A.; Kern, W.; Haas, M.; Bandl, C. Surface-Initiated Polymerizations Mediated by Novel Germanium-Based Photoinitiators. *ACS Appl Mater Interfaces* **2023**. <https://doi.org/10.1021/acsami.3c05528>.
- (225) Zefirov, Y. V.; Zorkii, P. M. Van Der Waals Radii and Their Application in Chemistry. *Translated from Uspekhi Khimii* **1989**, *58* (5), 713–746. <https://doi.org/10.1070/RC1989v058n05ABEH003451>.
- (226) Rowland, R. S.; Taylor, R. Intermolecular Nonbonded Contact Distances in Organic Crystal Structures: Comparison with Distances Expected from van Der Waals Radii. *J. Phys. Chem.* **1996**, *100*, *18*, 7384–7391 **1996**. <https://doi.org/https://doi.org/10.1021/jp953141+>.

- (227) Car, J.; Krstulović, N. Fitting Procedure to Reconstruct the Size Distribution and the Concentration of Silver Colloidal Nanoparticles from UV-Vis Spectra. *Nanomaterials* **2022**, *12* (19). <https://doi.org/10.3390/nano12193302>.
- (228) Hwang, H. D.; Kim, H. J. Enhanced Thermal and Surface Properties of Waterborne UV-Curable Polycarbonate-Based Polyurethane (Meth)Acrylate Dispersion by Incorporation of Polydimethylsiloxane. *React Funct Polym* **2011**, *71* (6), 655–665. <https://doi.org/10.1016/j.reactfunctpolym.2011.03.004>.
- (229) Lin, O. H.; Md Akil, H.; Mohd Ishak, Z. A. Characterization and Properties of Activated Nanosilica/Polypropylene Composites with Coupling Agents. *Polym Compos* **2009**, *30* (11), 1693–1700. <https://doi.org/10.1002/pc.20744>.
- (230) Koseki, K.; Arita, T.; Tabata, K.; Nohara, T.; Sato, R.; Nagano, S.; Masuhara, A. Effect of Surface Silanol Density on the Proton Conductivity of Polymer-Surface-Functionalized Silica Nanoparticles. *ACS Sustain Chem Eng* **2021**, *9* (30), 10093–10099. <https://doi.org/10.1021/acssuschemeng.1c01922>.
- (231) Perrin, C. L.; Kim, Y.-J. Symmetry of Metal Chelates. *Inorg. Chem.* **2000**, *39*, *17*, 3902–3910 **2000**. <https://doi.org/10.1021/ic000382>.
- (232) Socrates, G. Infrared and Raman Group -Tables and Charts. *John Wiley & Sons Ltd* **2001**.
- (233) Moulder, J.; Stickle, W.; Sobol, P. Handbook of X-Ray Photoelectron Spectroscopy - A Reference Book of Standard Spectra for Identification and Interpretation of XPS Data. **1992**.
- (234) Perruchot, C.; Khan, M. A.; Kamitsi, A.; Armes, S. P.; Watts, J. F.; Von Werne, T.; Patten, T. E. XPS Characterisation of Core-Shell Silica-Polymer Composite Particles Synthesised by Atom Transfer Radical Polymerisation in Aqueous Media. *Eur Polym J* **2004**, *40* (9), 2129–2141. <https://doi.org/10.1016/j.eurpolymj.2004.02.013>.
- (235) Masotti, A. S.; Onófrío, Á. B.; Conceição, E. N.; Spohr, A. M. Uv-Vis Spectrophotometric Direct Transmittance Analysis of Composite Resins. *Dental Materials* **2007**, *23* (6), 724–730. <https://doi.org/10.1016/j.dental.2006.06.020>.
- (236) Yeap, S. P. Permanent Agglomerates in Powdered Nanoparticles: Formation and Future Prospects. *Powder Technol* **2018**, *323*, 51–59. <https://doi.org/10.1016/j.powtec.2017.09.042>.
- (237) Quercia, G.; Lazaro, A.; Geus, J. W.; Brouwers, H. J. H. Characterization of Morphology and Texture of Several Amorphous Nano-Silica Particles Used in Concrete. *Cem Concr Compos* **2013**, *44*, 77–92. <https://doi.org/10.1016/j.cemconcomp.2013.05.006>.
- (238) Palin, W. M.; Leprince, J. G.; Hadis, M. A. Shining a Light on High Volume Photocurable Materials. *Dental Materials* **2018**, *34* (5), 695–710. <https://doi.org/10.1016/j.dental.2018.02.009>.
- (239) Hoyle, C. E.; Bowman, C. N. Thiol-Ene Click Chemistry. *Angewandte Chemie - International Edition* **2010**, *49* (9), 1540–1573. <https://doi.org/10.1002/anie.200903924>.
- (240) Eibel, A.; Radebner, J.; Haas, M.; Fast, D. E.; Freißmuth, H.; Stadler, E.; Faschauner, P.; Torvisco, A.; Lamparth, I.; Moszner, N.; Stueger, H.; Gescheidt, G. From Mono- to Tetraacylgermanes: Extending the Scope of Visible Light Photoinitiators. *Polym Chem* **2018**, *9* (1), 38–47. <https://doi.org/10.1039/c7py01590a>.
- (241) Weber, M.; Khudyakov, I. V.; Turro, N. J. Electron Spin Resonance and Laser Flash Photolysis Study of Radical Addition to Vinyl Acrylate and Related Alkenes. *Journal of Physical Chemistry A* **2002**, *106* (10), 1938–1945. <https://doi.org/10.1021/jp011813s>.

- (242) Colley, C. S.; Grills, D. C.; Besley, N. A.; Jockusch, S.; Matousek, P.; Parker, A. W.; Towrie, M.; Turro, N. J.; Gill, P. M. W.; George, M. W. Probing the Reactivity of Photoinitiators for Free Radical Polymerization: Time-Resolved Infrared Spectroscopic Study of Benzoyl Radicals. *J Am Chem Soc* **2002**, *124* (50), 14952–14958. <https://doi.org/10.1021/ja026099m>.
- (243) Moulder, J. Handbook of X-Ray Photoelectron Spectroscopy. **1992**.
- (244) Vickerman, J.; Briggs, D. ToF-SIMS: Materials Analysis by Mass Spectrometry. **2013**.
- (245) Fricker, A. L.; McPhail, D. S.; Keneghan, B.; Pretzel, B. Investigating the Impact of Cleaning Treatments on Polystyrene Using SEM, AFM and ToF-SIMS. *Herit Sci* **2017**, *5* (1). <https://doi.org/10.1186/s40494-017-0142-5>.
- (246) Winter, R.; Nixon, P. G.; Terjeson, R. J.; Mohtasham, J.; Holcomb, N. R.; Grainger, D. W.; Graham, D.; Castner, D. G.; Gard, G. L. Perfluorinated Polymer Surfaces Comprising SF 5-Terminated Long-Chain Perfluoroacrylate. *J Fluor Chem* **2002**. [https://doi.org/https://doi.org/10.1016/S0022-1139\(02\)00008-8](https://doi.org/https://doi.org/10.1016/S0022-1139(02)00008-8).
- (247) Kaiser, W. Kunststoffchemie Für Ingenieure. *Carl Hanser Verlag GmbH & Co. KG* **2016**. <https://doi.org/https://doi.org/10.3139/9783446430495>.
- (248) Ek, S.; Root, A.; Peussa, M.; Niinisto, L. Determination of the Hydroxyl Group Content in Silica by Thermogravimetry and a Comparison with  $^1\text{H}$  MAS NMR Results. *Thermochimica Acta Volume 379, Issues 1–2, 22 November 2001, Pages 201–212* **2001**. [https://doi.org/https://doi.org/10.1016/S0040-6031\(01\)00618-9](https://doi.org/https://doi.org/10.1016/S0040-6031(01)00618-9).
- (249) Unsworth, L. D.; Sheardown, H.; Brash, J. L. Protein Resistance of Surfaces Prepared by Sorption of End-Thiolated Poly(Ethylene Glycol) to Gold: Effect of Surface Chain Density. *Langmuir* **2005**, *21* (3), 1036–1041. <https://doi.org/10.1021/la047672d>.
- (250) Feric, T. G.; Hamilton, S. T.; Haque, M. A.; Jeddi, J.; Sangoro, J.; Dadmun, M. D.; Park, A. H. A. Impacts of Bond Type and Grafting Density on the Thermal, Structural, and Transport Behaviors of Nanoparticle Organic Hybrid Materials-Based Electrolytes. *Adv Funct Mater* **2022**, *32* (36). <https://doi.org/10.1002/adfm.202203947>.
- (251) Adumeau, L.; Genevois, C.; Roudier, L.; Schatz, C.; Couillaud, F.; Mornet, S. Impact of Surface Grafting Density of PEG Macromolecules on Dually Fluorescent Silica Nanoparticles Used for the in Vivo Imaging of Subcutaneous Tumors. *Biochim Biophys Acta Gen Subj* **2017**, *1861* (6), 1587–1596. <https://doi.org/10.1016/j.bbagen.2017.01.036>.
- (252) Liangt, C. Y.; Krimm, S. Infrared Spectra of High Polymers. VI. Polystyrene\*. *JOURNAL OF POLYMER SCIENCE* **1958**, *XXVII*, 241–254. <https://doi.org/https://doi.org/10.1002/pol.1958.1202711520>.
- (253) Tsujii, Y.; Ejaz, M.; Sato, K.; Goto, A.; Fukuda, T. Mechanism and Kinetics of RAFT-Mediated Graft Polymerization of Styrene on a Solid Surface. 1. Experimental Evidence of Surface Radical Migration. *Macromolecules* **2001**, *34* (26), 8872–8878. <https://doi.org/10.1021/ma010733j>.
- (254) Gao, X.; Feng, W.; Zhu, S.; Sheardown, H.; Brash, J. L. Kinetic Modeling of Surface-Initiated Atom Transfer Radical Polymerization. *Macromol React Eng* **2010**, *4* (3–4), 235–250. <https://doi.org/10.1002/mren.200900063>.
- (255) Michalek, L.; Barner, L.; Barner-Kowollik, C. Polymer on Top: Current Limits and Future Perspectives of Quantitatively Evaluating Surface Grafting. *Advanced Materials* **2018**, *30* (21). <https://doi.org/10.1002/adma.201706321>.
- (256) Abdelhamid, H. N.; Mathew, A. P. Cellulose-Based Nanomaterials Advance Biomedicine: A Review. *Int J Mol Sci* **2022**, *23* (10). <https://doi.org/10.3390/ijms23105405>.

- (257) Li, Z.; Mu, Y.; Peng, C.; Lavin, M. F.; Shao, H.; Du, Z. Understanding the Mechanisms of Silica Nanoparticles for Nanomedicine. *Wiley Interdiscip Rev Nanomed Nanobiotechnol* **2021**, *13* (1). <https://doi.org/10.1002/wnan.1658>.
- (258) Nikolaidis, A. K.; Koulaouzidou, E. A.; Gogos, C.; Achilias, D. S. Synthesis of Novel Dental Nanocomposite Resins by Incorporating Polymerizable, Quaternary Ammonium Silane-Modified Silica Nanoparticles. *Polymers (Basel)* **2021**, *13* (11). <https://doi.org/10.3390/polym13111682>.
- (259) Wang, Y.; Zhao, Q.; Han, N.; Bai, L.; Li, J.; Liu, J.; Che, E.; Hu, L.; Zhang, Q.; Jiang, T.; Wang, S. Mesoporous Silica Nanoparticles in Drug Delivery and Biomedical Applications. *Nanomedicine* **2015**, *11* (2), 313–327. <https://doi.org/10.1016/j.nano.2014.09.014>.
- (260) Gubala, V.; Giovannini, G.; Kunc, F.; Monopoli, M. P.; Moore, C. J. Dye-Doped Silica Nanoparticles: Synthesis, Surface Chemistry and Bioapplications. *Cancer Nanotechnol* **2020**, *11* (1). <https://doi.org/10.1186/s12645-019-0056-x>.
- (261) Peng, H.; Xu, Z.; Wang, Y.; Feng, N.; Yang, W.; Tang, J. Biomimetic Mesoporous Silica Nanoparticles for Enhanced Blood Circulation and Cancer Therapy. *ACS Appl Bio Mater* **2020**, *3* (11), 7849–7857. <https://doi.org/10.1021/acsabm.0c01014>.
- (262) Pham, X. H.; Park, S. M.; Ham, K. M.; Kyeong, S.; Son, B. S.; Kim, J.; Hahm, E.; Kim, Y. H.; Bock, S.; Kim, W.; Jung, S.; Oh, S.; Lee, S. H.; Hwang, D. W.; Jun, B. H. Synthesis and Application of Silica-Coated Quantum Dots in Biomedicine. *Int J Mol Sci* **2021**, *22* (18). <https://doi.org/10.3390/ijms221810116>.
- (263) Cai, L.; Liu, A.; Yuan, Y.; Dai, L.; Li, Z. Self-Assembled Perfluoroalkylsilane Films on Silicon Substrates for Hydrophobic Coatings. *Prog Org Coat* **2017**, *102*, 247–258. <https://doi.org/10.1016/j.porgcoat.2016.10.022>.
- (264) Wu, L.; Cai, L.; Liu, A.; Wang, W.; Yuan, Y.; Li, Z. Self-Assembled Monolayers of Perfluoroalkylsilane on Plasma-Hydroxylated Silicon Substrates. *Appl Surf Sci* **2015**, *349*, 683–694. <https://doi.org/10.1016/j.apsusc.2015.05.073>.
- (265) Alam, A. U.; Howlader, M. M. R.; Deen, M. J. Oxygen Plasma and Humidity Dependent Surface Analysis of Silicon, Silicon Dioxide and Glass for Direct Wafer Bonding. *ECS Journal of Solid State Science and Technology* **2013**, *2* (12), P515–P523. <https://doi.org/10.1149/2.007312jss>.
- (266) Skeist, I. Handbook of Adhesives. *Van Nostrand Reinhold Company* **1990**.
- (267) Theodor, F.; K, K. Ein Konzentrationsumschlag Der Fluoreszenz Des Pyrens. *Zeitschrift für Elektrochemie, Berichte der Bunsengesellschaft für physikalische Chemie* **1955**.
- (268) Cheng, D. F.; Masheder, B.; Urata, C.; Hozumi, A. Smooth Perfluorinated Surfaces with Different Chemical and Physical Natures: Their Unusual Dynamic Dewetting Behavior toward Polar and Nonpolar Liquids. *Langmuir* **2013**, *29* (36), 11322–11329. <https://doi.org/10.1021/la402398y>.
- (269) Brassard, J. D.; Sarkar, D. K.; Perron, J. Fluorine Based Superhydrophobic Coatings. *Applied Sciences (Switzerland)* **2012**, *2* (2), 453–464. <https://doi.org/10.3390/app2020453>.
- (270) Lalevée, J.; Blanchard, N.; Graff, B.; Allonas, X.; Fouassier, J. P. Tris(Trimethylsilyl)Silyl versus Tris(Trimethylsilyl)Germyl: Radical Reactivity and Oxidation Ability. *J Organomet Chem* **2008**, *693* (24), 3643–3649. <https://doi.org/10.1016/j.jorganchem.2008.08.039>.
- (271) Durmaz, Y. Y.; Kukut, M.; Moszner, N.; Yagci, Y. Sequential Photodecomposition of Bisacylgermane Type Photoinitiator: Synthesis of Block Copolymers by Combination of Free Radical Promoted Cationic and Free Radical Polymerization Mechanisms. *J Polym Sci A Polym Chem* **2009**, *47* (18), 4793–4799. <https://doi.org/10.1002/pola.23533>.

- (272) Lalevée, J.; Dirani, A.; El-Roz, M.; Allonas, X.; Fouassier, J. P. Germanes as Efficient Coinitiators in Radical and Cationic Photopolymerizations. *J Polym Sci A Polym Chem* **2008**, *46* (9), 3042–3047. <https://doi.org/10.1002/pola.22644>.
- (273) Aoshima, S.; Higashimura, T. Vinyl Ether Oligomers with Conjugated-Polyene and Acetal Terminals: A New Chain-Transfer Mechanism for Cationic Polymerization of Vinyl Ethers. *Polym J* **1984**, *16* (3), 249–258.
- (274) Matyjaszewski, K.; Hudgin, D. Cationic Polymerizations. *Marcel Dekker, Inc.* **1996**.
- (275) Thieke, B. Makromolekulare Chemie. *WILEY-VCH Verlag GmbH* **2005**.
- (276) Yahiaoui, A.; Belbachir, M.; Soutif, J. C.; Fontaine, L. Synthesis and Structural Analyses of Poly (1, 2-Cyclohexene Oxide) over Solid Acid Catalyst. *Mater Lett* **2005**, *59* (7), 759–767. <https://doi.org/10.1016/j.matlet.2004.11.017>.
- (277) Chen, Y.; Zhang, L.; Jin, Y.; Lin, X.; Chen, M. Recent Advances in Living Cationic Polymerization with Emerging Initiation/Controlling Systems. *Macromol Rapid Commun* **2021**, *42* (13). <https://doi.org/10.1002/marc.202100148>.
- (278) Miyamoto, M.; Sawamoto, M.; Higashimura, T. Synthesis of Monodisperse Living Poly(Vinyl Ethers) and Block Copolymers by the Hydrogen Iodide/Iodine Initiating System. *Macromolecules* **1984**, *17*, 2228–2230.
- (279) Miyamoto, M.; Sawamoto, M.; Higashimura, T. Living Polymerization of Isobutyl Vinyl Ether with the Hydrogen Iodide/Iodine Initiating System. *Macromolecules* **1984**, *17*.
- (280) Uchiyama, M.; Satoh, K.; Kamigaito, M. Cationic RAFT Polymerization Using Ppm Concentrations of Organic Acid. *Angewandte Chemie* **2015**, *127* (6), 1944–1948. <https://doi.org/10.1002/ange.201410858>.
- (281) Aoshima, S.; Kanaoka, S. A Renaissance in Living Cationic Polymerization. *Chem Rev* **2009**, *109* (11), 5245–5287. <https://doi.org/10.1021/cr900225g>.
- (282) Jordan, R.; Ulman, A. Surface Initiated Living Cationic Polymerization of 2-Oxazolines. **1998**. <https://doi.org/https://doi.org/10.1021/ja973392r>.
- (283) Ingall, M. D. K.; Honeyman, C. H.; Mercure, J. V.; Bianconi, P. A.; Kunz, R. R. Surface Functionalization and Imaging Using Monolayers and Surface- Grafted Polymer Layers. *J Am Chem Soc* **1999**, *121* (15), 3607–3613. <https://doi.org/10.1021/ja9833927>.
- (284) Advincula, R. Polymer Brushes by Anionic and Cationic Surface-Initiated Polymerization (SIP). *Advances in Polymer Science* **2006**, *197* (1), 107–136. [https://doi.org/10.1007/12\\_066](https://doi.org/10.1007/12_066).



## 7 Abbreviations

### Theoretical Part

DMAEMA	2-(dimethylaminoethyl) methacrylate
AIBN	2,2-azobis(2-methylpropionitrile)
Irgacure 2959	2-hydroxy-4-(2-hydroxyethoxy)-2-methylpropiophenone
HEA	2-hydroxyethyl) acrylate
HEMA	2-hydroxyethyl) methacrylate
APTES	3-aminopropyltriethoxysilane
ACPA	4,4'-azobis(4-cyanopentanoic acid)
AAm	acrylamide
AA	acrylic acid
BP	benzophenone
BP-DS	benzophenone diazonium salt
BAPO	bis(acyl)phosphane oxide
CNC	cellulose nanocrystals
DC	dithiocarbamate
DTCA	dithiodiundecane- 11,1 diylbis[4({{(diethylamino) carbonothioyl] thioethyl) phenyl] carbamate}}]
GMA	glycidyl methacrylate
HAp	hydroxyapatite
HPTX	hyperbranched thioxanthone
LDPE	low-density-polyethylene
MAA	methacrylic acid
MMA	methyl methacrylate
SDBC	N-(diethylamino) dithiocarbamoylbenzyl-(trimethoxy)silane
DMAAM	N,N-dimethylacrylamide
NIPAM	N-isopropylacrylamide
NITEC	nitrile imine -mediated tetrazole-ene cycloaddition
PFPA	perfluorophenyl azides
PAH	photoacid
PAG	photoacid generator
PC	photoredox catalyst

PAA	poly (acrylic acid)
PMAA	poly (methacrylic acid)
PMMA	poly (methyl methacrylate)
PAAm	poly acrylamide
PEOX	poly(2-ethyl-2-oxazoline)
PDMAA	poly(dimethylacrylamide)
PEGMA	poly(ethylene glycol) methacrylate
PHEMA	poly(hydroxyethyl methacrylate)
PEI	poly(propyleneimine)
PEG	polyethylene glycol
PEGDA	polyethylene glycol diacrylate
PP	polypropylene
p(St)	polystyrene
DC-H	sodium- N,N diethyldithiocarbamate trihydrate
St	styrene
SI-ATRP	surface initiated atom transfer radical polymerization
SI-PET-RAFT	Surface initiated photoinduced electron/energy transfer reversible addition-fragmentation chain transfer polymerization
SI-PIMP	surface initiated photoiniferter-mediated polymerization
SI-NMP	surface-initiated nitroxide-mediated polymerization
SI-RAFT	surface-initiated reversible addition fragmentation chain transfer
TPA	Two-photon absorption
TPIP	Two-photon induced photopolymerization
TX	thioxanthone

### Experimental Part

AAm	acrylamide
p(AAm)	poly(acrylamide)
BTG	benzoyltrimethylgermane
CHO	cyclohexene oxide
p(CHO)	poly(cyclohexene oxide)
DBC	double bond conversion

## 7. Abbreviations

---

DCM	dichloromethane
DGEBA	Bisphenol-A-diglycidylether
DIPEA	N,N-diisopropylethylamine
DPIHFP	diphenyliodonium-hexafluorophosphat
FTIR	Fourier transform infrared spectroscopy
FIACr	fluorescein-o-acrylate
GeEt	ethyl-tris(2,4,6-trimethylbenzoyl)germane
GeOH	hydroxy-tris(2,4,6-trimethylbenzoyl)germane
p(FIACr)	poly(fluorescein-o-acrylate)
HFIP	hexafluoroisopropanol
HDT	hexanedithiol
MSP	mesoporous silica nanoparticles
nPVE	n-propyl vinylether
p(nPVE)	poly(n-propyl vinylether)
PAG	photo acid generator
PFACr	1H,1H,2H,2H-perfluorodecyl acrylate
photo-DSC	photo differential scanning calorimetry
p(St)	poly(styrene)
p(PFACr)	poly(1H,1H,2H,2H-perfluorodecyl-acrylate)
PyrMAcr	1-pyrenemethyl methacrylate
p(PyrMAcr)	poly(1-pyrenemethyl methacrylate)
RPCP	radical promoted cationic photopolymerization
SEC	size exclusion chromatography
SEM	scanning electron microscopy
SIPP	surface-initiated photopolymerization
SI-ATRP	surface-initiated atom-transfer radical polymerization
SI-PET-RAFT	surface-initiated photoinduced electron/energy transfer reversible addition-fragmentation chain transfer polymerization
SI-PIMP	surface-initiated photoiniferter-mediated polymerization
SI-RPCP	surface-initiated radical promoted cationic photopolymerization
St	styrene
Tetra	tetrakis(2,4,6-trimethylbenzoyl)germane

## 7. Abbreviations

---

TGA	thermogravimetric analysis
THF	tetrahydrofurane
THFA	tetrahydrofurfuryl acrylate
TMS	tetramethylsilane
TTT	1,3,5-triallyl-1,3,5-triazin-2,4,6(1H,3H,5H)-trion

## 8 List of Figures

Figure 1: Schematic illustration of surface modification using “grafting-to” and “grafting-from” techniques .....	2
Figure 2: Radical generation of type I and II photoinitiators upon light irradiation .....	7
Figure 3: Two synthesis pathways to attach type I initiators onto silicon surfaces (slightly modified from ref. 40; the photosensitive moiety is labelled in red) .....	8
Figure 4: Setup for UV interference lithography and resulting polymer (PMMA) gratings (taken from reference [40]) .....	9
Figure 5: Type I photoinitiators (red) bearing a silane coupling unit (blue) for surface tethering.....	10
Figure 6: Photosensitive azo-compounds (red) with anchor moieties (blue).....	13
Figure 7: BP derivatives with different coupling units (photosensitive groups are labelled in red; anchor moieties are labelled in blue) .....	17
Figure 8: Examples for synergists bearing dimethylamine units (orange) and different coupling groups (blue).....	25
Figure 9: Exemplary preparation of copolymer brushes by SI-PIMP from a benzyl-N,N-diethyldithiocarbamate derivatized substrate (photosensitive group is labelled in red)	31
Figure 10: Iniferter compounds (red) bearing different anchor moieties (blue).....	33
Figure 11: ATRP mechanism and “grafting from” photopolymerization of MMA on a silane-functionalized surface. The ATRP initiator is labelled in orange, and the photoredox catalyst ( $Mt^n/L = Ir(ppy)_3$ ) is labelled in red .....	36
Figure 12: Different compounds containing both an ATRP initiator (orange) and a coupling moiety (blue) .....	38
Figure 13: General mechanism of RAFT polymerization.....	40
Figure 14: RAFT agents (green) with organosilane anchor moieties (blue).....	41
Figure 15: Phenyl azides (red) with anchor moieties (blue) .....	48
Figure 16: Perfluorophenyl azides (red) with anchor moieties (blue) .....	51
Figure 17: Tetrazole and diazirine compounds (red) which can be covalently coupled to surfaces using anchor moieties (blue) .....	54
Figure 18: Molecular expansion in x-direction based OTREP of compound 1 (CCDC 2233933). OTREP data was downloaded from the “Cambridge Crystallographic Data Centre” .....	61

Figure 19: Model for the calculation of $\sigma_{PI}$ , theo for the trisacyl germanium photoinitiator (compound 1) .....	62
Figure 20: FTIR spectrum of the side-product (tertiary ammonium salt) during immobilization of compound 1 onto nanoparticle surfaces .....	72
Figure 21: High resolution XPS spectra of germanium (Ge 3p), left) and bromine (Br 3d, right) for pristine and modified silica nanoparticles including the percentage atomic surface composition.....	73
Figure 22: UV-Vis absorption measurements of photoinitiator-modified nanoparticles (Left: 30 nm particles; right: 180 nm particles, $c = 4.7 \text{ mg mL}^{-1}$ ). The red trace was obtained by subtraction of the blue curve from the black curve .....	74
Figure 23: UV-Vis spectra of functionalized nanoparticles (red and blue curve) and the parent initiator (compound 1, black dash-dotted line). Please note that the blue curve refers to the secondary y-axis.....	74
Figure 24: Photo-DSC curves (left) and double-bond conversion plot (right) for photopolymerization of THFA with 0.1 wt.-% of parent initiator (compound 1, black curve) and 3.1 wt.-% of nanoparticles (30 nm diameter) functionalized with compound 1 (red curve). .....	75
Figure 25: Photo-DSC curves (left) and integral plot (right) for photopolymerization of TTT+HDT with 0.1 wt.-% of parent initiator (compound 1, black curve) and 3.1 wt.-% of nanoparticles (30 nm diameter), bearing coupled light-sensitive moieties (red curve). .....	76
Figure 26: XPS survey spectra of p(St) and p(PFAcr) grafted SiO <sub>2</sub> nanoparticles including the atomic surface composition (in at.-%) .....	79
Figure 27: XPS C1s-deconvolution spectra of p(PFAcr) grafted nanoparticles (left: 30 nm particles; right: 180 nm particles) .....	79
Figure 28: FTIR spectra (ATR) of differently sized nanoparticles grafted with p(PFAcr). The spectra are normalized to the -Si-O-Si- stretching vibration at $1060 \text{ cm}^{-1}$ .....	80
Figure 29: Infrared spectra of nanoparticles bearing a p(St) shell, prepared via photopolymerization of styrene using solutions of different concentrations (left: nanoparticles with a diameter of 30 nm; right: nanoparticles with a diameter of 180 nm). The polymer content is compared by relating the peak intensity at $698 \text{ cm}^{-1}$ to the -Si-O-Si- signal at $1060 \text{ cm}^{-1}$ .....	81

Figure 30: FTIR-spectra of homopolymerized p(St) and p(PFAcr) .....	82
Figure 31: Positive secondary ToF-SIMS spectrum of p(St)-grafted nanoparticles (top) in comparison to neat polystyrene (bottom).....	83
Figure 32: Negative secondary ion ToF-SIMS spectrum of p(St)-grafted nanoparticles (top) in comparison to neat polystyrene (bottom).....	84
Figure 33: Positive secondary ion ToF-SIMS spectrum of p(PFAcr) grafted nanoparticles (top) in comparison to neat p(PFAcr) (bottom). Positively charged fragments were assigned as followed: Na <sup>+</sup> (23), C <sub>2</sub> H <sub>3</sub> <sup>+</sup> (27.02), CF <sup>+</sup> (31), C <sub>3</sub> H <sub>5</sub> <sup>+</sup> (41.04), CHF <sub>2</sub> <sup>+</sup> (51), C <sub>3</sub> H <sub>3</sub> O <sup>+</sup> (55.02), CF <sub>3</sub> <sup>+</sup> (69), C <sub>2</sub> F <sub>4</sub> <sup>+</sup> (100.07), C <sub>2</sub> F <sub>5</sub> <sup>+</sup> (119), C <sub>3</sub> F <sub>5</sub> <sup>+</sup> (130.99), C <sub>3</sub> F <sub>7</sub> <sup>+</sup> (169). <sup>246</sup> .....	85
Figure 34: Comparison of the negative secondary ion ToF-SIMS spectrum of p(PFAcr) grafted nanoparticles (top) with that of neat p(PFAcr) (bottom). Negatively charged fragments were assigned as followed: F <sup>-</sup> (19), C <sub>2</sub> H <sup>-</sup> (13.01), F <sub>2</sub> <sup>-</sup> (38), F <sub>2</sub> H <sup>-</sup> (39.01), C <sub>2</sub> H <sub>2</sub> O <sup>-</sup> (42), C <sub>2</sub> F <sup>-</sup> (43), CF <sub>3</sub> <sup>-</sup> (69), C <sub>3</sub> H <sub>3</sub> O <sub>2</sub> <sup>-</sup> (71.01). <sup>246</sup> .....	86
Figure 35: SEM images of pristine and neat nanoparticles (30 nm initial diameter size). The green scale bar is 100 nm.....	87
Figure 36: SEM images of neat (left) and NaOH etched nanoparticles (right). The green scale bar is 100 nm.....	88
Figure 37: SEM images of neat (left) and p(St)-covered nanoparticles (right) .....	88
Figure 38: Pristine and p(St)- modified nanoparticles (30 nm in diameter) dispersed in toluene. Left: 8.8 mg of neat nanoparticles in 20 mL of toluene; right: 12.3 mg of p(St)- modified nanoparticles in 20 mL of toluene. ....	89
Figure 39: SEM images of highly agglomerated nanoparticles bearing a p(PFAcr) shell. Left: 20 K magnification; right: 50 K magnification.....	90
Figure 40: Results of TGA measurements for polymer-covered and neat SiO <sub>2</sub> nanoparticles (left: 30 nm particles; right: 180 nm particles). ....	91
Figure 41: Characterization of de-grafted polystyrene by TGA (left) and FTIR spectroscopy (right).....	93
Figure 42: XPS survey spectra including peak assignments of a neat Si wafer (bottom, black curve), oxygen plasma activated Si wafer (green curve), and Si wafer functionalized with photoinitiator 1 (red curve). ....	99

Figure 43: UV-Vis absorption of neat and modified quartz plates compared with the corresponding monomers in solution (absorption of the modified quartz plates is plotted using the secondary y-axis) .....	101
Figure 44: UV absorption properties of the used fluorescent monomers. Left: FIAcr; Right: PyrMAcr.....	102
Figure 45: Fluorescence emission spectra of quartz plates bearing grafted p(PyrMAcr) (right, 347 nm excitation wavelength) and p(FIAcr) (left, 450 nm excitation wavelength). The visible fluorescence upon excitation of grafted p(PyrMAcr) with 366 nm light is also shown (insert). .....	103
Figure 46: Water contact angles (WCA) on different Si wafers. From left to right: Neat silicon wafer, Si wafer functionalized with photoinitiator 1, Si wafer with photo-grafted p(PFAcr), Si wafer with photo-grafted p(AAm). .....	104
Figure 47: Microscope image of a patterned p(FIAcr) film (coloured areas) grafted on a Si wafer (grey areas are lacking a graft-layer), and corresponding XPS survey spectra. The red curve is assigned to the area bearing a photo-grafted polymer layer, and the black curve is assigned to areas lacking a graft-layer.....	106
Figure 48: XPS C1s-deconvolution spectra of patterned samples (non-polymerized area) ..	106
Figure 49: Achieved resolution derived by procedure A; Left: Imaging via optical microscopy with 10 times magnification; Red: XPS F1s mapping (fluorine atoms are highlighted red); right: Si2p mapping (silicon atoms appear in blue colour) .....	107
Figure 50: Achieved resolution derived by procedure B; Left: Imaging via optical microscopy with 10 times magnification; Red: XPS F1s mapping; right (fluorine atoms are highlighted red): Si2p mapping (silicon atoms appear in blue colour) .....	107
Figure 51: Achieved resolution derived by procedure C; Left: Imaging via optical microscopy with 10 times magnification; Red: XPS F1s mapping (fluorine atoms are highlighted red); right: Si2p mapping (silicon atoms appear in blue colour) .....	108
Figure 52: (a) Schematic representation of the applied photomask to prepare quarter-structured polymer layers on a silicon wafer, and (b) WCA measurements on the structured polymer surface with hydrophobic and hydrophilic areas. ....	109
Figure 53: UV absorption properties of $\text{Ph}_2\text{I}^+\text{PF}_6^-$ (DPIHFP) and emission spectra of the employed light sources .....	112



---

Figure 54: Light absorption properties of bis-, tris-, and tetraacylgermanes .....	113
Figure 55: Photo-DSC traces for different germanium based photoinitiators in combination with DPIHFP .....	114
Figure 56: Photo-bleaching test using GeEt in DCM with (left) and without (right) the addition of DPIHFP; monochromatic illumination with 405 nm .....	116
Figure 57: Results from FTIR spectroscopy (transmission mode) for p(nPVE) grafted nanoparticles, and comparison with the homopolymer p(nPVE).....	118
Figure 58: TGA investigations of SiO <sub>2</sub> nanoparticles with surface grafted p(nPVE) .....	119
Figure 59: Light absorption of p(nPVE) grafted nanoparticles, produced at different temperatures (red: -30°C, black: room temperature) .....	121
Figure 60: TGA results for 30 nm sized nanoparticles with surface-tethered p(nPVE) including weight loss curves of products obtained from control experiments.....	122
Figure 61: ATR-FTIR spectra of nanoparticles bearing p(nPVE) at their surface and products from control experiments .....	123
Figure 62: FTIR-spectra of p(CHO) homopolymer (blue, secondary y-axis), p(CHO)-grafted nanoparticles (red, primary y-axis) and nanoparticles derived from the SI-RPCP procedure without DPIHFP (black dashed curve, primary y-axis) .....	124
Figure 63: TGA measurements of silica nanoparticles bearing immobilized p(CHO). During the photografting experiments, DPIHFP was present (red curve) or absent (black curve).	125
Figure 64: TGA investigation of the living character via monomer-addition experiments. The abbreviations “2”, “3” and “4” are representative for the respective monomer-addition steps .....	127

## 9 List of Tables

Table 1: Summary of surface coupled photoinitiators and co-initiators .....	27
Table 2: Summary of surface coupled photoiniferters .....	35
Table 3: Results of DSC measurements with THFA and comparison of kinetic parameters including maximum reaction rate ( $R_{p,max}$ ) and time to reach 95% of the final conversion ( $t_{95\%}$ ).....	76
Table 4: Results of photo-DSC measurements with TTT+HDT and comparison of the time to reach 95% of the final conversion ( $t_{95\%}$ ) .....	77
Table 5: Calculated polymer content and $\sigma_{mg}$ for the organic-inorganic hybrid materials ...	92
Table 6: Results for average molar masses ( $M_n$ , $M_w$ , $M_w/M_n$ , $M_z/M_w$ ) of de-grafted polystyrene, and calculated grafting density $\sigma_{chains}$ .....	95
Table 7: Relative atomic surface composition of a neat and a functionalized Si wafer (data obtained from high resolution XPS spectra) .....	99
Table 8: Relative atomic surface composition of a neat quartz plate, and of quartz plates after surface modification via photoinduced “grafting from” of poly(fluorescein-o-acrylate) (p(FIAcr)) and poly(pyrene methacrylate) (p(PyrMAcr)).....	101
Table 9: Overview of atomic surface compositions obtained from XPS survey spectra, and water contact angles (WCA) of a neat Si wafer, a Si wafer functionalized with photoinitiator 1, and Si wafers bearing photo-grafted layers of p(PFAcr) and p(AAm).104	
Table 10: Comparison of the polymerization kinetic parameters including the maximum peak height ( $h$ , $W g^{-1}$ ), polymerization heat ( $\Delta H$ , $J g^{-1}$ ) and the time until 95% of the final conversion was reached ( $t_{95\%}$ ) .....	115